ISBN 978-82-326-6622-5 (printed ver.)
ISBN 978-82-326-5515-1 (electronic ver.)
ISSN 1503-8181 (printed ver.)
ISSN 2703-8084 (electronic ver.)

NTNU
Norwegian University of
Science and Technology

Doctoral theses at NTNU, 2022:71

Torbjørn Langedahl Leirmo

Geometric Accuracy in Laser-Based Powder Bed Fusion of Polymers

Tolerance optimization by part build orientation

Doctoral thesis

Torbjørn Langedahl Leirmo

Doctoral theses at NTNU, 2022:71

NTNU

NTNU
Norwegian University of
Science and Technology
Thesis for the degree of
Philosophiae Doctor
Faculty of Engineering
Department of Manufacturing and Civil
Engineering

NTNU
Norwegian University of
Science and Technology

Torbjørn Langedahl Leirmo

Geometric Accuracy in Laser-Based Powder Bed Fusion of Polymers

Tolerance optimization by part build orientation

Thesis for the degree of Philosophiae Doctor

Gjøvik, March 2022

Norwegian University of Science and Technology
Faculty of Engineering
Department of Manufacturing and Civil Engineering

NTNU
Norwegian University of
Science and Technology

NTNU
Norwegian University of Science and Technology

Thesis for the degree of Philosophiae Doctor

Faculty of Engineering
Department of Manufacturing and Civil Engineering

© Torbjørn Langedahl Leirmo

ISBN 978-82-326-6622-5 (printed ver.)
ISBN 978-82-326-5515-1 (electronic ver.)
ISSN 1503-8181 (printed ver.)
ISSN 2703-8084 (electronic ver.)

Doctoral theses at NTNU, 2022:71

PRINTED IN NORWAY
NO - 1598

NORDIC SWAN ECOLABEL
Printed matter
2041 0731

Printed by Skipnes Kommunikasjon AS

Abstract

As Additive Manufacturing (AM) enters the manufacturing industry, the technology must adhere to stringent quality demands in terms of dimensional and geometric accuracy. However, due to substantial differences in how these technologies realize three-dimensional geometries, generalization of phenomena across AM technologies proves to be quite difficult.

Laser-based Powder Bed Fusion (LB-PBF) is an industrialized AM technology capable of producing functional components and end-use parts. However, to ensure consistent quality for larger production volumes in a mass-customization setting, automated optimization methods and process planning must be developed. This requires valid and reliable data to enable the construction of prediction models.

This thesis is centered around the optimization of part build orientation in LB-PBF of polymers (LB-PBF/P) for which a deterministic method is proposed. The proposed method utilize mathematical models for the effect of part build orientation on the accuracy of various geometric features. To this end, an experiment has been conducted to generate data for empirical modeling. Two new models are devised for the prediction of cylindricity and flatness based on the experimental data.

Variations within and between production runs in LB-PBF/P obscures the validity of experiments. The first Research Question (RQ) addresses this issue and aims at generating valid data for the subsequent analysis. A matrix layout in four dimensions is developed that enables the control of experimental variables while gauging the effect of part placement and production run. The experimental plan successfully enables the analysis

of geometric and dimensional properties as a function of part build orientation. Furthermore, the design makes it possible to characterize the variation within and between different builds. The variation is found to be significant in the y-direction of the build chamber, while x- and z-directions appear to be more stable.

The second RQ utilizes the experimental data to reveal the effect of part build orientation on the geometric accuracy of planes and cylinders. First, the data is analyzed, and the conformance of theoretical models is evaluated. This analysis reveals that existing models insufficiently explain the effect of part build orientation on the geometric accuracy of planes and cylinders. Therefore, novel empirical models are proposed to better assimilate the observed behavior. The proposed empirical models differ in shape from the theoretical models which are based on the staircase effect. This indicates that the staircase effect alone cannot precisely predict the accuracy of LB-PBF/P. Moreover, the proposed models may widen the range of allowable orientations while meeting tolerance requirements.

Finally, a third RQ aims at developing a deterministic method for optimizing accuracy by part build orientation. Mathematical foundations are provided, and a method is described for identifying optimal part build orientations given the geometric features of the part. The proposed method relies on basic information about constituent geometric features and can be populated with any differentiable function for each identified feature type. Through the identification of critical points in a continuous solution space, the optimal orientations are obtained.

The main contributions of this thesis concern the modeling accuracy as an effect of part build orientation where the novel model for cylindricity is particularly disruptive. For future work, the effect of part build orientation on other tolerance characteristics should be investigated, and the work should be extended to other materials and AM technologies. Furthermore, the intelligence of such data and models may be integrated into a digital pipeline for quality assurance throughout the value chain, and the product's life cycle.

Acknowledgments

I would like to thank my supervisor Kristian Martinsen for his continuous support throughout the four years it took me to complete this thesis. In him, I have found inspiration and motivation to overcome any challenge I have encountered along the way. I would also like to thank Oleksandr Semeniuta for the inspiring supervision he provided in the period 2019–2021. His dedication and knowledge inspired much of the data analysis, and he also served as a sparring partner in the crucial stages of conceptualization. Big thanks are also due to Niels Peter Østbø for his valuable input as a co-supervisor in the second half of 2021.

My introduction to additive manufacturing was ensured by Ivanna Baturynska who also planted the first seed for me to pursue a PhD. She has had a tremendously positive influence on my work as well as my well-being, and for this, I am truly grateful. I also appreciate the help and guidance of Pål Erik Endrerud for the laboratory activities conducted in connection to this thesis.

Finally, I am forever grateful to my wife Julie Langedahl Leirmo. For lending me some of her courage, for her ruthless constructive criticism, and for not giving up on me even when I doubt myself.

Contents

List of Tables

List of Figures

List of Acronyms

AM	Additive Manufacturing
BJ	Binder Jetting
CAD	Computer-Aided Design
CAM	Computer-Aided Manufacturing
CAPP	Computer-Aided Process Planing
CMM	Coordinate Measuring Machine
CNC	Computer Numerical Control
CSG	Constructive solid geometry
CSV	Comma-Separated Values
DED	Directed Energy Deposition
DOI	Digital Object Identifier
EA	Evolutionary algorithm
EBM	Electron Beam Melting
EB-PBF	Electron Beam Powder Bed Fusion
ED	energy density
EOS	Electro Optical Systems GmbH
FDM	Fused Deposition Modeling
FFF	Fused Filament Fabrication

GA	Genetic Algorithm
GD&T	Geometric Dimensioning and Tolerancing
LB-PBF	Laser-based Powder Bed Fusion
LB-PBF/M	Laser-Based Powder Bed Fusion of Metals
LB-PBF/P	Laser-Based Powder Bed Fusion of Polymers
LOM	Layered Object Manufacturing
MCS	Machine Coordinate System
ML	Machine Learning
NTNU	Norwegian University of Science and Technology
PA12	Polyamide 12
PBF	Powder Bed Fusion
PCS	Part coordinate system
PSO	Particle Swarm Optimization
RQ	Research Question
SLA	StereoLithography apparatus
SLM	Selective Laser Melting
SLS	Selective Laser Sintering
STEP	STandard for the Exchange of Product model data
STL	STereoLithography (file format)

List of Symbols

ξ	Laser angle
θ	Build angle
θ_{cr}	Critical build angle
P	Laser power
v	Scan speed
Δz	Layer height
h	Scan line spacing
p_x	x-coordinate of a part's center point
p_y	y-coordinate of a part's center point
l_x	x-coordinate of the laser's last deflection point
l_y	y-coordinate of the laser's last deflection point
l_z	z-coordinate of the laser's last deflection point
$\vec{n}$	Normal vector
$\vec{l}$	Laser vector
$\lvert\vec{v}\rvert$	Magnitude of vector $\vec{v}$
δ_z	Deviation in z-direction
δ_{xy}	Deviation in the xy-plane
ϵ_{flat}	Flatness error
ϵ_{cyl}	Cylindricity error
n	Sample size
$\bar{x}$	Sample mean
σ	Standard deviation
a	Random variable for modeling
b	Random variable for modeling
abs	Absolute value

Glossary

Notation	Description
Additive Manufacturing	*"Process of joining materials to make parts from 3D model data, usually layer upon layer [...]"* [1, p. 1].
Base alignment	The definition of the part's location and orientation in the Coordinate Measuring Machine (CMM). The base alignment establishes the coordinate frame for the ensuing inspection, i.e. the reference point for all subsequent measurements.
Bounding box	The bounding box of a three-dimensional object is the minimum rectangular cuboid that contains the entire geometry.
Build direction	The direction in which the layers are stacked to form a three-dimensional object in Additive Manufacturing (AM). Consequently, all layers are orthogonal to the build direction. For most AM machines, the build direction is referred to as the z-direction of the machine coordinate system.
Build space	The volume of the Additive Manufacturing (AM) machine where parts can be fabricated.

Notation	**Description**
Constructive Solid Geometry	A solid modeling method for constructing 3D geometries by Boolean set operations.
Down-facing surface	A surface whose normal vector has a negative z-component. In other words, the surface is generally facing downwards.
Energy density	A measure of how much energy is applied to a volume in Powder Bed Fusion (PBF). The energy density (ED) can roughly be calculated as $$ED = \frac{P}{vhw}$$ where P is the laser power, v is the scan speed, h is the scan line spacing, and w is the layer thickness.
Evolutionary algorithm	*"[...] an algorithm that evolves a problem solution over many iterations."* [2, p. 3]
Feature recognition	The process of identifying geometric elements in a digital 3D model.
Geometric primitive	Generally, the simplest shape a system manages. Specifically, in this thesis, all but one of the common primitives from Constructive solid geometry (CSG) are adopted, namely planes, cylinders, cones, spheres, and tori, while pyramids are considered as a set of planes.
Hatch distance	The distance between two parallel scan lines (hatch lines) in Laser-based Powder Bed Fusion (LB-PBF). This distance applies to the hatch pattern of the part interior, not the contour or edge lines.

Notation	**Description**
Initial build orientation	The designed orientation of the part, i.e. the orientation of the part when loaded from the original file. This orientation is the reference point for defining the part build orientation.
Layer thickness	The thickness of one layer of material in Additive Manufacturing (AM), denoted herein as l. In the present work, the layer thickness is 120 µm unless explicitly defined differently.
Machine Coordinate System	The three-dimensional coordinate system of the Additive Manufacturing machine. The origin is typically fixed towards the front at the lower-left corner of the build space.
Magnitude	The length of an n-dimensional vector. In Euclidean space with $\vec{v} = [x, y, z]$, the magnitude is computed as $\|\vec{v}\| = \sqrt{x^2 + y^2 + z^2}$.
Nominal	The designed ("ideal") version of an entity. A nominal dimension is the designed dimension, while the actual dimension may differ due to errors and natural variation.
Normal vector	A normal vector is defined as the vector orthogonal to a surface. In this thesis, all normal vectors are constructs designed to indicate orientation. As such, all normal vectors herein are also unit vectors, and the combined term "*unit* normal vector" is used synonymously with simply "normal vector".
Optimization	*"[A]n act, process, or methodology of making something (such as a design, system, or decision) as fully perfect, functional, or effective as possible"* [3]

Notation	Description
Orthogonal	In linear algebra, two n-dimensional vectors are orthogonal if their dot-product is zero. In this thesis, the term orthogonal is used in 3D-space to describe the relationship between a plane and a vector, while the term *perpendicular* is preferred to describe the relationship between two vectors.
Part build orientation	The orientation in which the part is fabricated. Typically, the orientation is defined as three rotational displacements from the initial build orientation where the axes of the Machine Coordinate System constitute the axes of rotations (i.e. extrinsic rotations). However, the part coordinate system may also be used (i.e. intrinsic rotations).
Part coordinate system	The three-dimensional coordinate system that is defined locally for the part. The origin of this system is typically defined at the design stage and is the reference for the location and orientation of all part features.
Perpendicular	Symbol = $\perp$. Two vectors are perpendicular if their dot-product is zero. In two dimensions, this represents a right angle between two vectors. $(\vec{v_1} \perp \vec{v_2}) \Leftrightarrow (\vec{v_1} \cdot \vec{v_2} = 0)$
Selective Laser Sintering	An AM process where a laser selectively fuses (without fully melting) powder material in a powder bed.
Support structures	Sacrificial structures that are created during an Additive Manufacturing (AM) process to prevent the part from collapsing or warping [4].
Unit vector	An n-dimensional vector with unit magnitude, i.e. $\lvert\vec{v}\rvert = 1$

Notation	Description
Up-facing surface	A surface which normal vector has a positive z-component. In other words, the surface is generally facing upwards.

Part 1: Thesis

Chapter 1

Introduction

1.1 Background

Additive Manufacturing (AM) is increasingly utilized in manufacturing systems alongside conventional manufacturing technologies. This means that the quality requirements of already established processes are inevitably imposed on the newly developed AM technologies. However, the young AM processes are not yet developed to the stage where quality can be guaranteed to be consistent. Therefore, methods are required for predicting, optimizing and verifying the quality of AM products.

AM had its genesis in the 1980s with Charles W. Hull [5] being credited as the first inventor of an AM system, namely the StereoLithography apparatus (SLA). Since then, the technology has been developed from a rapid prototyping technique to a family of manufacturing processes capable of producing functional components [4]. AM enables mass customization and direct digital manufacturing of parametric designs conceived with artificial intelligence. The ability to manufacture topology optimized designs directly from computer models without human interaction may indeed constitute major savings in global emissions – especially in the transportation sector.

According to ISO/ASTM 52900:2015(E) [1], AM is defined as the *"process of joining materials to make parts from 3D model data, usually layer upon layer [...]"*. This definition encompasses many different technologies which generally can be divided into seven distinct process categories as illustrated in figure 1.1. PBF may be regarded as one of the more

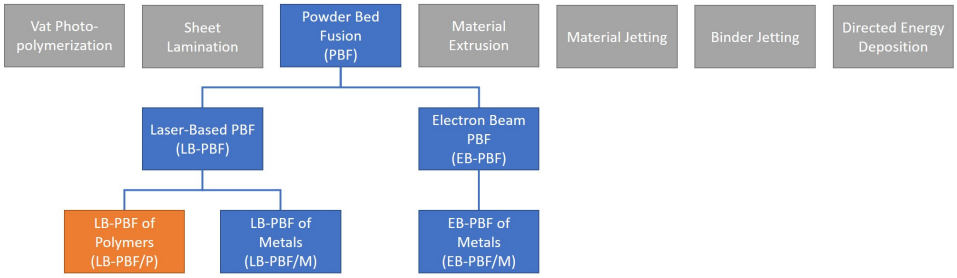

Figure 1.1: Process categories in AM as defined by ISO/ASTM [1], [6]. The technology of interest in the current work, Laser-Based Powder Bed Fusion of Polymers (LB-PBF/P), is highlighted and the relations to similar technologies are visualized.

industrially viable AM technologies due to the ability to produce end-use parts of adequate quality in relevant materials for an array of purposes including the medical, aerospace, and automotive sectors [4]. This category of AM processes can be further divided based on the energy source and material type [6]. The current work is limited to the subcategory using a laser beam as a power source for sintering polymeric powders as highlighted in figure 1.1. While popularly referred to as Selective Laser Sintering (SLS), the term LB-PBF/P is adopted in this thesis for clarity and conformance with ISO/ASTM 52911:2019(E) [6].

Ideal manufacturing systems under the industry 4.0 paradigm should be fully integrated, flexible, and autonomous. AM is considered to be one of the enabling technologies of industry 4.0 [7], yet much effort remains before full integration of AM processes in a digital pipeline is realized. One of the remaining challenges is the qualification and documentation of AM products – especially in a mass customization context. The complexity of standardizing tolerance specifications for AM technologies is highlighted by Ameta, Lipman, Moylan *et al.* [8] who outlines solutions for linking process parameters to tolerance specifications. Yet, the prediction and optimization of achievable tolerances remain a challenge in most AM processes.

AM is largely based on the legacy STL (STereoLithography) file format and related surface representations. However, these file types retain no higher-level information about local topology which makes subsequent optimization and prediction of final geometry difficult. Various operations in AM, therefore, rely on feature recognition algorithms to enable

geometry-based operations, including the optimization of part build orientation. A plethora of algorithms has been developed for partitioning geometries in smaller entities to obtain a better surface finish [9], to fit a large model in a smaller build space [10], or to use the constituent features for Computer-Aided Process Planing (CAPP)/Computer-Aided Manufacturing (CAM) [11]. The proper definition of rules is one of the major challenges of deterministic approaches to feature recognition together with high computational costs [11]. Evolutionary algorithms (EAs) [12] and Machine Learning (ML) methods [11] have been proposed as alternatives to the rule-based algorithms, but the stochastic nature of these approaches renders the results prone to variations. Reliable results are necessary to achieve full integration with downstream processes in an automated fashion.

The optimization of quality in LB-PBF/P is certainly complex with more than 80 identifiable influencing factors [13]. Naturally, only a subset of these are interesting in the context of optimization, and a large number of both technology-specific and general methods have been proposed in the literature. While many optimization methods have been developed for improved mechanical properties [14], dimensional accuracy [15] and surface quality [16], the optimization of geometric accuracy such as flatness and cylindricity is not as heavily researched [17].

Many research efforts on part build orientation in AM utilizes EAs in the search for the optimal orientation due to their ability to traverse multimodal solution spaces [2], [18]. Methods explored in the literature include Genetic Algorithms (GAs) [14], [19]–[24], Particle Swarm Optimization (PSO) [19]–[21], and teaching-learning-based optimization [21] to mention a few – all of which are stochastic methods. Deterministic approaches, on the other hand, either resort to exhaustive searches [25], or rely on gradients to guide the search [26]. While exhaustive searches provide deterministic solutions for multimodal solution spaces, they require discretization of the solution space. Conversely, continuous functions may enable precise determination of local and global optima through mathematical analysis. The potential of efficient deterministic methods motivates more research on the precise identification of global optima in the multimodal solution spaces of the orientation problem.

One of the obstacles on the path to optimization of part quality in AM is the need for prediction models. Theoretical models for single phenomena have been derived [27]–[29], however, these models cannot include all influencing factors of all the different technologies. Consequently, em-

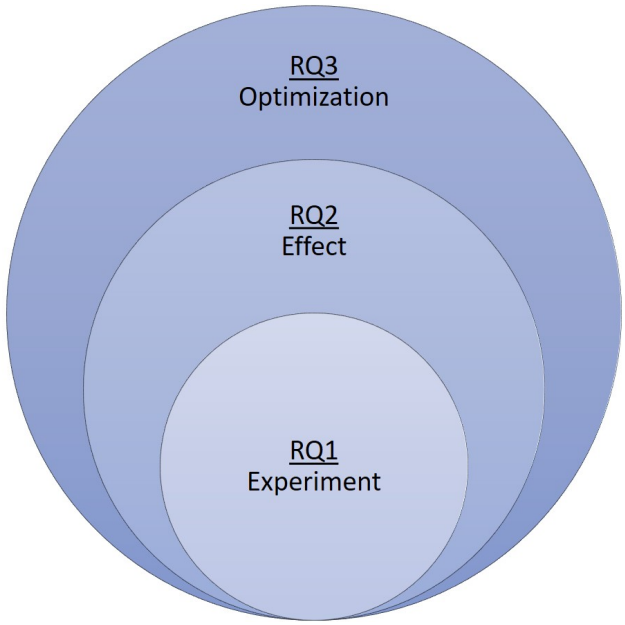

Figure 1.2: Illustration of the hierarchical structure of the RQs where each layer builds on the previous.

pirical models must be constructed for each and every technology. This process is further complicated by the peculiarities of each machine etc. limiting the external utility of the models.

This thesis describes findings, concepts, and methods that contribute towards the optimization of geometric accuracy in LB-PBF/P. While acknowledging the power of randomness when intelligently applied, the approach described herein avoids the use of stochastic tools to enable replication and minimize variation in manufacturing.

1.2 Research questions

A set of RQs is formulated to guide the work presented in this thesis. The RQs are developed with the purpose of contributing towards enhanced knowledge on quality in AM and LB-PBF/P in particular. Figure 1.2 illustrates the hierarchy of research questions where each layer builds on the previous. The RQs are formulated as follows:

RQ1 *How can experiments in LB-PBF/P be designed in a robust manner?*

This RQ tackles the problem of process variation in a scientific setting, i.e. if the process is subject to large random variations, how can experiments be valid? The validity of experiments is pivotal to justify the development of empirical models for optimization purposes. Hence, this RQ is fundamental to later investigations and is situated at the core of figure 1.2.

RQ2 *How does part build orientation affect the geometric accuracy of primitive shapes?*

This RQ aims at exploring the relationship between the build direction and the resulting geometric accuracy of fundamental geometric features. Minor inaccuracies throughout the build process add up to significant inconsistencies between nominal and actual geometries. These inaccuracies may introduce challenges in assembly operations, and can also increase material and energy waste during post-processing. As illustrated in figure 1.2, this RQ benefits from RQ1 and presumes validity to enable experimental inquiries about the relationship between build direction and geometric accuracy.

RQ3 *How can the part build orientation be optimized to meet certain tolerance levels in a deterministic manner?*

This RQ explores the options with regards to optimization techniques and available solutions and also aims at finding a novel solution free from stochastic variables. Output from RQ2 enables intelligent decision-making based on empirical data. In particular, the idea of identifying thresholds of acceptable accuracy is pivotal as no process will ever be completely free from inaccuracies. Managing variations is, therefore, a central task in manufacturing management and operations for ensuring consistent quality and meeting quality requirements.

1.3 Scope of the research

The work presented herein is focused on the AM category LB-PBF/P and the experiments are performed with an EOSINT P395 using Polyamide 12 (PA12) in a 50/50 mix of virgin and recycled powder, and measurements are performed on a Zeiss DuraMax CMM. Other materials and machines are considered out of scope for the current research and thus left for future work. Further details are described in chapter 4.

This PhD thesis focuses on geometric accuracy, and also includes dimensional accuracy to some extent. Although important and interesting, other properties (e.g. mechanical properties) are out of scope and not included in this study. The project is geared towards assembly features of components produced by LB-PBF/P in commercial systems, hence dimensions in the range of 4mm to 24mm are considered. At present, this range is believed to include the critical values between fine and coarse features.

1.4 Contributions of the thesis

This thesis describes five distinct contributions:

1. A robust methodology for experiments in LB-PBF/P with potential utility beyond this technology
2. An open dataset with tolerance characteristics in LB-PBF/P for an array of different shapes and dimensions
3. Improved knowledge on the variations between positions in the build chamber of LB-PBF
4. Empirical models on the effect of part build orientation on geometric accuracy in LB-PBF
5. A novel method for flexible optimization of orientation in LB-PBF/P.

1.5 Thesis outline

The remainder of this thesis is outlined in figure 1.3 with a structure designed to provide the necessary theoretic background before the core of the thesis is presented. Hence, this general introduction is succeeded by an in-depth introduction to AM and LB-PBF/P in particular in chapter 2. Next, related work and state-of-the-art is reviewed in chapter 3 with comments on strengths and shortcomings of previous studies. These chapters provide the theoretical background for the presented work.

In chapter 4, the underlying philosophy of science is discussed before the methodology is presented. A thorough description of the design of experiments is also provided together with the means of data analysis. A brief overview of the experimental results is then presented in section 5.1, before the generated empirical models are described in

Figure 1.3: Outline of the thesis structure. The numbers assigned to each box indicate the chapter number in this thesis.

section 5.2. The main body of the thesis is concluded by a description of a flexible optimization method of part build orientation in section 5.3.

A thorough discussion on implications and shortcomings of the present work is found in chapter 6. This includes remarks on limitations and external validity, as well as relevant avenues of future research. Finally, conclusions are presented in chapter 7 before brief suggestions for future work are presented.

Chapter 2

Introduction to Additive Manufacturing

2.1 Basics of Additive Manufacturing

Additive Manufacturing (AM) is defined by ISO and ASTM as the *"process of joining materials to make parts from 3D model data, usually layer upon layer [...]"* [1, p. 1]. Also, a classification of seven distinct processes is put forward where all processes conform to the definition above while maintaining substantial differences. Table 2.1 showcases these processes with their typical abbreviations and aliases.

The scope of this thesis is limited to a single process category, namely PBF. Furthermore, sub-categories of PBF may be distinguished based on the energy source, and material type. A brief introduction to PBF, the

Table 2.1: Process categories in AM outlined in ISO/ASTM 52900:2015(E) [1]

Process category	Abbreviation	Aliases
Vat Photopolymerization	–	Stereolithography, SLA
Sheet Lamination	–	LOM
Powder Bed Fusion	PBF	SLS, SLM, EBM
Material Extrusion	–	FDM, FFF
Material Jetting	–	Multi-Jet Modeling
Binder Jetting	BJ	3D printing
Directed Energy Deposition	DED	–

sub-categories, and their relation to this thesis is provided in section 2.4. However, the concepts described herein have some applicability beyond this domain under the premise that part build orientation affects final part properties in terms of dimensional and geometric accuracy. At present, this condition holds for any layered approach to AM as illustrated by the vast number of studies that include part build orientation as a factor (see the literature review in chapter 3).

Most AM processes generally follow the same steps to fabricating an object [4]. These steps can be arranged into three distinct phases, namely an input phase, a build phase, and an output phase (see figure 2.1) [30]. The typical steps are as follows:

1. **Geometry acquisition:** A digital 3D model is obtained, generally from Computer-Aided Design (CAD) or 3D-scanning.

2. **Convert to STL:** The 3D model may need to be converted to a different file format, the most common file format in AM is the STL file format [4].

3. **Pre-processing:** AM is a fully automated process, hence all details about the build process must be defined before its initiation.

4. **Transfer to machine:** The process plan is transferred to the AM machine.

5. **Machine setup:** This involves securing a supply of raw material, cleaning equipment, adjusting physical components, etc.

6. **Build process:** The build process may take up to several days to complete depending on AM technology, part volume, layer thickness, etc.

7. **Remove part:** Hot processes generally require a cooling period and cutting tools may be necessary.

8. **Post-processing:** This may involve cleaning, sandblasting, heat treatment, machining, etc.

9. **Application:** AM applications include functional components in medicine, automotive, and aerospace.

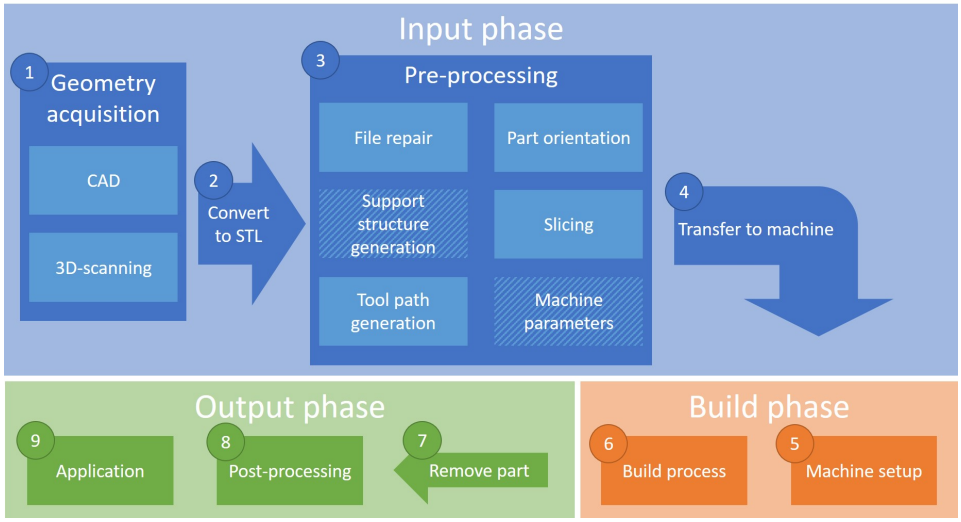

Figure 2.1: Typical workflow of AM processes. The hatched boxes under pre-processing indicate that the operation is not necessary for all AM technologies and machines. Adapted from [30]

2.2 Design for Additive Manufacturing

Additive Manufacturing (AM) constitutes a paradigm shift in engineering design [31]. Not only does AM enable the realization of complex geometries unfeasible with conventional manufacturing, but it opens for mass customization as a viable manufacturing paradigm [32]. On the other hand, a new set of restrictions and challenges are encountered. To unlock the full potential of AM, designers must consider the particular technology from the very beginning of product development. The following subsections are devoted to the descriptions of the possibilities and challenges brought forward by AM.

2.2.1 Design opportunities

AM has gained widespread attention under the catchphrase "complexity for free". While manufacturing an object by conventional means becomes more complex as the geometric complexity of the object increases, this is not generally the case for AM. Contrary to subtractive manufacturing technologies where time and cost is highly dependent on the volume removed from a workpiece, in AM, this relationship is inverted. Consequently, topology optimization has become feasible for widespread adoption, especially in aerospace where the mass of each component is

crucial. The restrictions on geometric complexity have been lifted, and designers are now free to explore intricate geometries without increased manufacturing costs. This provides yet another incentive to minimize material waste and energy consumption.

Because the volume of the object is an important factor in AM, the products are often not solid. To reduce the volume while maintaining the structural integrity of the object, lattice structures are used to fill the interior with the desired ratio of material to void.

The geometric freedom provided by AM enables multiple components to be manufactured in a single process. This also applies to assemblies and moving parts. Consolidating designs reduces the number of manufacturing steps, eliminates dividing lines and welds, and ensures a continuous surface.

As a digital manufacturing technology, automated- and customized designs are possible. The concept of mass customization implies mass production of unique objects – a concept made feasible by AM. Parametric designs enable ergonomically customized products to be mass-produced with minimal human interaction.

2.2.2 Design restrictions

When a three-dimensional geometry is realized layer-by-layer, each layer requires some substrate on which to be deposited. For the first layer, this is trivial as the substrate will be the build platform itself. However, all subsequent layers require support from below which can be achieved by the construction of sacrificial structures to support any overhanging features. These structures, commonly known as support structures, stabilize the part during the build, aid in dispersing thermal energy in hot processes, and may prevent warping. Such structures should be considered at the design stage to optimize their utility, limit negative impacts, and ensure their safe removal. For LB-PBF/P, however, support structures are generally not required.

Due to the layered manner of manufacturing, the thickness of the layers determines the resolution in the build direction. Hence, features smaller than the layer thickness cannot be realized. Additionally, all dimensions in the build direction will be a multiple of the layer thickness. Slicing software tackle this in different ways; some round off to the closest slicing plane, and others simply follow the center plane of the layer. Regardless of how advanced the technology is, some errors will arise if

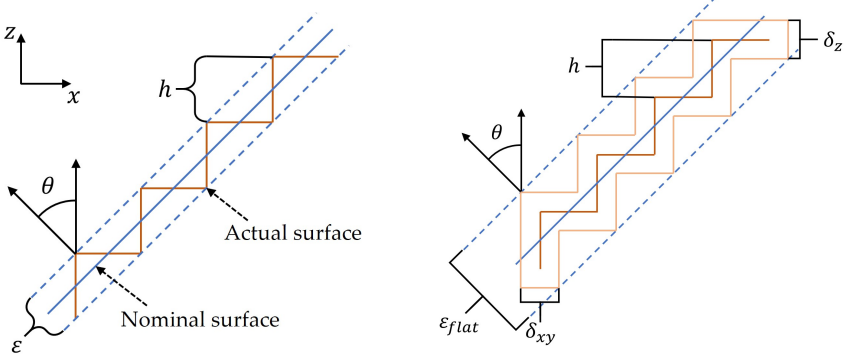

(a) The staircase effect alone

(b) The staircase effect with added in-plane variations, and out-of-plane variations

Figure 2.2: Errors arising from the layered manner of fabrication. Adapted from [33].

the dimensions don't match the layer thickness.

The layer thickness also gives rise to the characteristic staircase effect of AM as displayed in figure 2.2. The deposition of layers in AM technologies is (typically) unidirectional. Any feature that is neither parallel nor perpendicular to the build direction will therefore exhibit a stepped surface. This phenomenon should be considered in the design stage to alleviate downstream processes from counteracting any unwanted effects.

All AM technologies have limitations regarding the resolution in the xy-plane as well. The laser in laser-based technologies has a certain diameter, and so does the nozzle in extrusion-based technologies. Even though a higher resolution can be achieved with SLA or jetting technologies, a certain limit on the resolution – thereby also accuracy – is present for all current technologies also in the xy-plane. Additionally, errors will occur within and between layers which further adds to the inaccuracy of AM products. Figure 2.2 illustrates how these small errors together with the staircase effect add up to significant deviations from the designed (nominal) surface.

Some features may be problematic despite being within the limits of resolution, such as thin walls, narrow slots, etc. Small protrusions may be within the capabilities of the machine but are still unfeasible for

production because they break during the removal- or post-processing step. Narrow and deep holes may be problematic to clean, especially if material adheres inside due to print-through, overcure, etc.

2.2.3 Geometric features in Additive Manufacturing

The term "feature" is rather vague without further introduction as it is used to refer to a variety of different things – from physical entities to abstract constructs. However, in the context of design and manufacturing, a feature is a distinguishable geometric entity constituting a minor part of a larger object. Zhang, Bernard, Gupta *et al.* [34] proposes the following definition for features in the specific context of AM:

> *"An AM feature refers to an identified shape feature representing a certain shape pattern that has some significance or certain functions to a part and carries the information which is important for the pre-processing, processing or post-processing of AM."*

This definition is useful when considering process planning for all stages of the AM process as it concerns the effect of the process on certain geometric shapes and structures. The definition covers thin walls, lattice structures, and geometric primitives. However, for this thesis, the term "geometric feature" is used to cover solely the geometric primitives. This distinction is made to limit the problem to surface types subjected to tolerances for assembly purposes. Moreover, this limitation excludes features that are more likely to yield invalid results and machine failures from the study.

This thesis concerns the part build orientation based on the constituent geometric features. Based on previous studies and geometric primitives from CSG, planes, cylinders, cones, spheres, and tori are considered herein. A clear description of all geometric features, including their orientation, is required for automatic operations. For this purpose, vectorial definitions are adopted as detailed in appendix A.

Some surfaces may, however, be difficult to categorize as any of the above. These surfaces may be partitioned into small patches resembling the surfaces above, but are more effectively handled as free-form surfaces to reduce the number of geometric features. The definition of such surfaces follows no set definition but may be determined from the general direction of the surface, or its boundary.

2.3 Tolerancing in the context of Additive Manufacturing

All manufacturing processes exhibit some degree of variation. Controlling these variations is a matter of process control and optimization. Ensuring the fit and function of products while allowing some variation is however a matter of tolerancing. The Geometric Dimensioning and Tolerancing (GD&T) standards ASME Y14.5 [35] and ISO 1101 [36] are, in the words of Ameta, Lipman, Moylan *et al.* [8, p. 2], *"[...] a language to communicate acceptable 3D variations of geometric elements in a part from design to manufacturing and inspection"*. This section briefly introduces the tolerance characteristics relevant to the current work.

2.3.1 Flatness

The flatness of a surface can according to ISO 1101:2017(E) [36] be measured as the distance between two parallel planes that contain all the points of a surface between them. Because the flatness is a measure typically applied to a larger surface, the sample may involve variations from various sources including warpage, staircase effect, and residue. The flatness of a surface may change due to post-processing activities and comparisons must therefore be made on equal grounds, i.e. after similar treatments.

This measure of flatness is vulnerable to variation in the inspection. Consider for instance an inclined plane manufactured by AM affected by the staircase effect. If the surface is inspected with a CMM one would preferably include the lowest and highest points as depicted in figure 2.3. However, if the machine fails to hit the lowest valley or the highest peak, the recorded flatness will be more accurate than the real value. It is also clear that the probe will act as a mechanical filter due to the inability to reach the deepest corners. Consequently, the probe size should be carefully selected to obtain the desired results.

2.3.2 Cylindricity

Cylindricity error is according to ISO 1101:2017(E) [36] defined as the radial distance between two coaxial cylinders that contain all the measured points on the cylindrical surface. Similar to flatness, the cylindricity characteristic is also susceptible to the staircase effect and the probe size. Minor variations in inspection paths may alter the readings from a CMM, but this measurement uncertainty is countered with a large number of registered points.

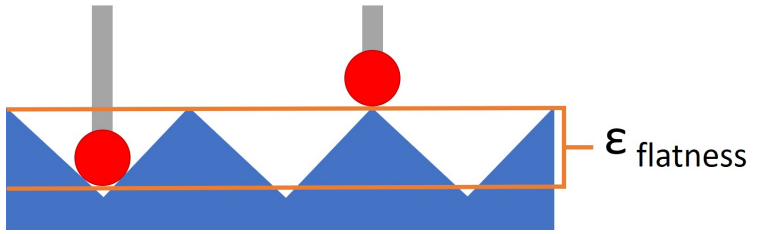

Figure 2.3: Measuring the flatness of a surface affected by the staircase effect with a CMM. $\varepsilon_{flatness}$ indicates the measured flatness.

2.3.3 Diameters

The diameter of a surface can be defined in multiple ways as displayed in figure 2.4. The method selected for defining the diameter is typically based on the function of the feature [37]. The minimum feature method gives the circle with the smallest absolute deviations and is deemed appropriate for estimating the 'true' diameter of the cylinder for the purpose of this work.

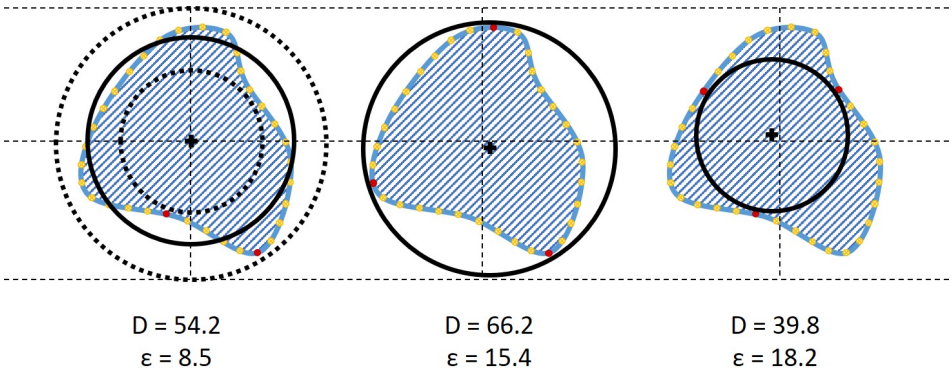

Figure 2.4: Illustration of diameter estimation from measured points and the effect of methodology: From the left: the minimum feature method, the minimum circumscribed circle, and the maximum inscribed circle. Adapted from [37].

2.4 Powder Bed Fusion

Powder Bed Fusion (PBF) had its genesis shortly after SLA [38] and is perhaps the most industrialized technology in the AM family. The technology is relatively stable, energy- and material-efficient, and produces parts of good mechanical and dimensional quality. Predominantly poly-

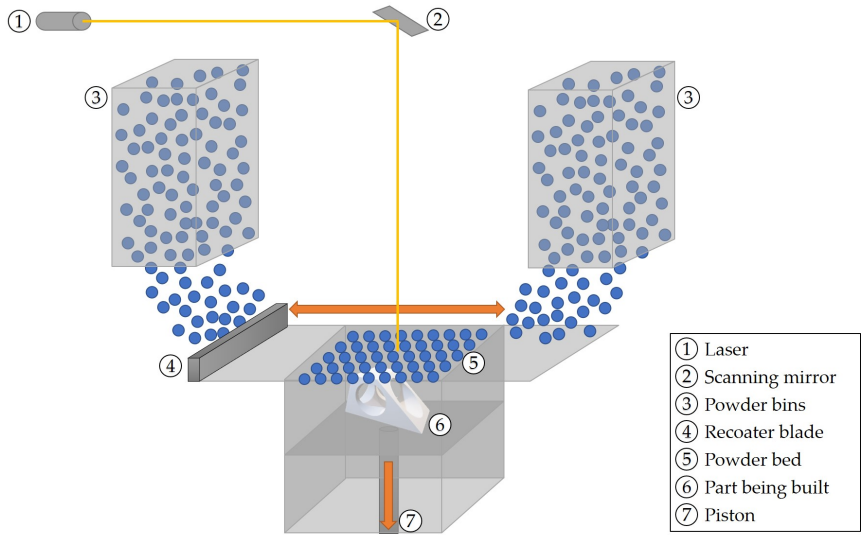

Figure 2.5: General schematic for a LB-PBF machine. The piston lowers the powder bed and the recoater blade distributes powder from the powder bins. Adapted from [41].

mers and metals are used, but applications of ceramics and composites exist to a lesser extent [4], [39], [40].

The process is defined in ISO/ASTM 52900:2015(E) as a *"...process in which thermal energy selectively fuses regions of a powder bed."* [1, p. 2]. Figure 2.5 depicts a general schematic of a LB-PBF machine. The process would begin by distributing a thin layer of powder material on the build platform before the relevant regions are fused. The build platform is then lowered by a distance equivalent to the layer thickness before the process is repeated.

When the build process is complete, the built part will be contained in a bin full of powder – commonly referred to as the 'part cake'. The part cake is allowed to cool before as-built parts may be retrieved, and the excess powder recycled. The material close to the surface of the produced part will be affected by the residual heat from the process. This energy will cause some of the grains to deform or otherwise deteriorate, which renders parts of the part cake less viable for reuse [42]. The aging effect may also influence powder properties within a single build [43]. The as-built parts are typically subject to post-processing to alter mechanical properties and/or to achieve the desired surface quality.

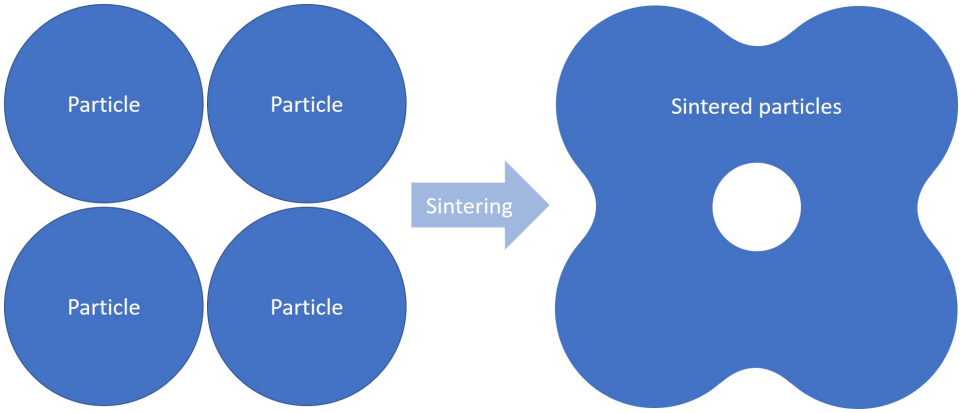

Figure 2.6: Illustration of sintering. From the left, particles are packed closely together. Sintering fuses particles while retaining structural integrity.

Despite their common origins, the PBF-technologies have some fundamental differences that affect how they relate to the contents of this thesis. Most notably, the processing of metals typically requires support structures to help reduce residual stresses and prevent warping during the build [4]. This is not required in LB-PBF/P because the energy levels are much lower than those of the metal counterparts. Nevertheless, all PBF processes will exhibit some degree of staircase effect as a result of the discrete layers of material, thermal gradients impose a risk of warping, and the powder will yield a rough surface on the as-built part.

2.5 Laser-based Powder Bed Fusion of Polymers

The AM technology investigated in this PhD thesis is LB-PBF/P where the particles of a polymeric powder are fused by applying energy with one or more lasers. The technology, typically referred to as sintering, laser sintering, or Selective Laser Sintering (SLS), fuses powder by increasing the temperature just enough for particles to bond without fully melting. This is illustrated in figure 2.6 where the tightly packed powder is sintered to produce a part. As the temperature increases, the particles fuse, and the 'necks' become wider thus reducing the presence of pores [4]. Consequently, higher temperatures are also associated with a higher shrinkage effect. The complexity of this process is significant as it involves porous and brittle inter-layer structures from partial melting and recrystallization [44].

In LB-PBF/P, the build chamber is preheated to a temperature just

below the melting temperature of the powder material. 3D objects are realized through the repetitive process of powder distribution, build chamber heating, and laser sintering. When the process is complete, the part cake is allowed to cool before the finished parts may be removed. The present work follows the rule of thumb stating that the part cake should cool for at least as long as it took to build. Premature removal increases the chances of warping due to rapid cooling upon removal.

2.6 Digital representation of 3D-geometries

In the digital world of today, hardly any product is created without a digital model preceding its manufacture. The old drawing boards are replaced by CAD software that enables the accurate definition and inspection of any geometry. The generated digital models enable simulations of all product life stages from manufacturing to end of life. Most importantly, a digital model facilitates process planning and quality assurance.

In AM, a digital model is necessary for process planning purposes. Before a layer may be deposited, the contour of the layer must be obtained by slicing the CAD model. However, when the first AM systems came to be, the direct slicing of CAD files was infeasible due to the required computational power. Slicing polyhedrons, on the other hand, was within the realm of possibilities. Consequently, the STereoLithography (file format) (STL)[1] was developed as a simple description of the surface part surface to facilitate the slicing procedure.

The STL file format represents the surface of the geometry as a tessellation of triangles. These triangles are defined by three vertices and a unit normal vector pointing towards the exterior of the part as displayed in figure 2.7. This yields a total of 12 floating-point numbers stored for each triangular facet. For redundancy, the vertices of a facet are listed counterclockwise when seen from the outside. This aids in the explicit division of part interior and exterior. The contents of an STL file can either be in ASCII format, which makes it accessible to humans, or a binary format can be used to minimize file size and accelerate loading time at the expense of human readability.

The approximation of curved surfaces to the tessellated surface found

[1] Conveniently, the acronym "STL" can also be described as Standard Tessellation Language, however, STereoLithography (file format) is the original description [45], [46].

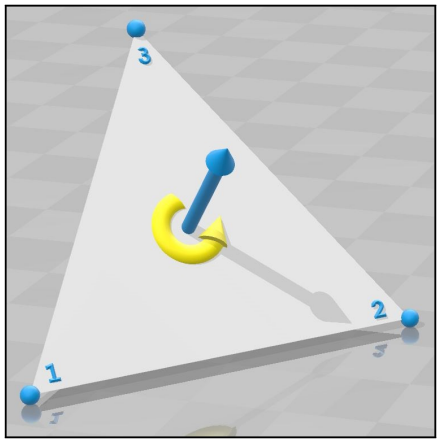

(a) Illustration of a facet in the STL file with vertices and a normal vector.

```
solid <name>
  facet normal <x> <y> <z>
    outer loop
      vertex <x> <y> <z>
      vertex <x> <y> <z>
      vertex <x> <y> <z>
    endloop
  endfacet
.....
(Repeats for each facet)
.....
endsolid <name>
```

(b) Syntax of an STL file in ASCII format.

Figure 2.7: Contents of the STL file.

in STL introduces a certain deviation from the designed surface. Most commercial CAD systems allow the designer to impose tolerances on maximum deviation from the designed surface. Naturally, tighter tolerances require more triangles in the STL file which affects the size and processing time of the file. Nevertheless, the surface will always be an approximation of the surface and errors will arise.

The inability of STL files to accurately represent curved surfaces, together with other desirable capabilities for a digital format for AM, has led to the development of alternative file types in recent years [47]. An effort towards a standard AM file format AMF [48] was initiated, but may have been premature. Inspired by the AMF initiative, a consortium of major corporations from software and AM industry has joined forces in the development of the 3MF file format set to replace the STL file format as the industry standard. 3MF will be based on triangular meshes, but claims to be complete, human readable, simple, extensible, unambiguous and free [49]. This thesis focuses on the STL format due to its widespread use in industry but acknowledges the rise of these formats and their implications are discussed in chapter 6.

2.7 Digital operations in Powder Bed Fusion

When a digital representation of the object is acquired, the process planning may commence with defining the build layout. Typically, the

part build orientation is determined before the geometry is placed in the virtual build space. At this point, multiple objects may be inserted in the build space for simultaneous manufacturing. A separate software may be used for this stage which may include a range of different tools for optimization and automation.

After defining the build layout, the contour of each layer is obtained by slicing the digital model with horizontal planes at intervals equal to the selected layer thickness. The layer thickness is typically constant, but adaptive layer thickness is also possible to mitigate the staircase effect on inclined surfaces [50].

When the geometry is sliced, path planning is performed for each cross-section. For PBF technologies, this entails defining scan paths for the laser to follow, as well as parameters such as laser power, scan speed, and hatch distance. The following sub-sections describe central parameters and concepts for LB-PBF/P.

2.7.1 Contours and edges

To create a solid exterior of the manufactured part, the contour of each layer is normally given a certain thickness before moving to the interior. The contour of a layer constitutes the two-dimensional lines and curves that will make up the part's surface. The scanned contour is slightly offset to account for the diameter of the laser beam, and the surrounding powder being affected by energy dispersion. According to Electro Optical Systems GmbH (EOS), the center of the laser beam will typically trace the contour with a distance of ca. 0.33 mm.

For most layers, the contour offset is unproblematic. However, when a sharp corner or a narrow passage is encountered, the offset will cause a deviation from the nominal to the actual surface. These narrow edges require the system to override the offset and apply a special approach. A common solution is to draw a single line along the center of the edge until it either reaches the exterior or the conditions for contour lines apply again. This can however yield deviations on the final surface as demonstrated in figure 2.8

2.7.2 Raster pattern and hatch distance

While a robust exterior is desired to maintain functionality and to protect the product, the interior of the part is not subject to the same requirements. The density of the interior can be controlled to achieve

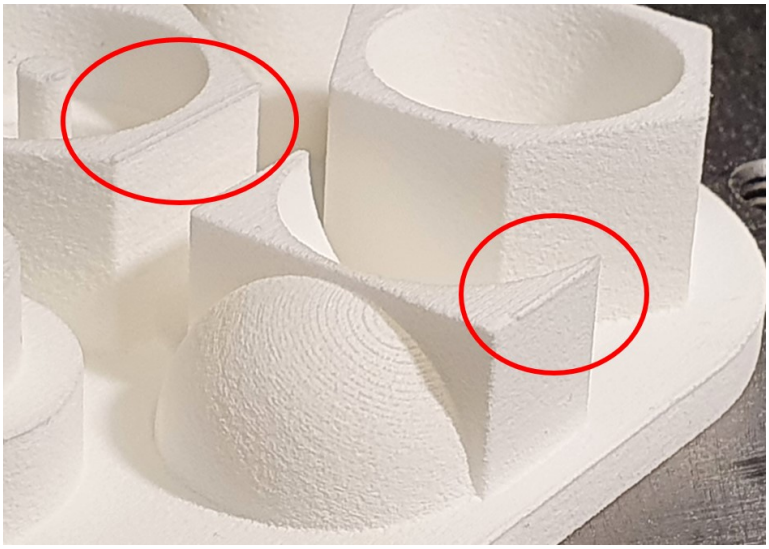

Figure 2.8: Example of edge deviation on a surface. The object is obtained from the experiment of which the details are provided in section 4.4.

the desired weight and weight distribution while withstanding the expected loads and stresses. Typically, the density of the interior is minimized to save material and reduce the weight of the final component.

In LB-PBF/P, the interior of a layer is typically filled with alternating hatching lines. For the AM machine employed in this project (EOSINT P395), these lines follow the x- and y-axis of the Machine Coordinate System (MCS) for every other layer, with a default hatch distance of 0.3 mm. The locations of all hatch lines are preset in the system but only utilized if they fall within the contours of a layer. Consequently, the ith hatching line along the y-axis will be a straight line from x_{min} to x_{max} at $y = 0.3i$ mm. This rigidity results in a different number of hatching lines for a part depending on where in the build space it is placed.

2.7.3 Energy density

The powder material used in PBF is sensitive to changes in temperature (i.e. energy input) [51]. Changes in energy density (ED) influences both mechanical properties and dimensional accuracy [52]. The ED is a measure of how much energy is applied to a certain volume. According to Czelusniak and Amorim [44], the ED can be calculated as:

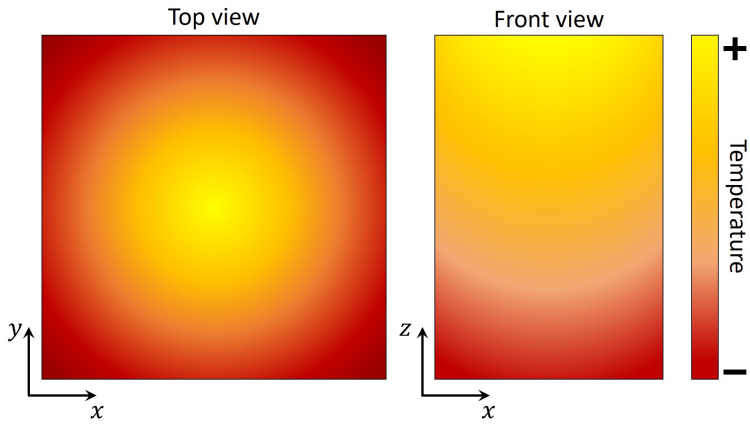

Figure 2.9: Illustration of the temperature distribution in the powder bed (left) and throughout the part cake (right).

$$ED = \frac{P}{\Delta z v h} \tag{2.1}$$

where P is the laser power, v is the laser scan speed, h is the hatch distance, and Δz is the layer thickness. However, note that equation 2.1 takes no regard for the number of hatching lines falling within the contour of the layer, and also disregards any additional settings such as skin thickness and edge parameters. Nevertheless, an estimate can easily be obtained by equation 2.1 without excessive computations.

Because of the iterative process of applying energy to the powder bed and distributing fresh layers of powder, energy accumulates in the part cake. However, due to energy loss to the environment together with internal heat transfer, the temperature distribution is not consistent throughout the part cake [53]. Generally, the center of the build is warmer than the corners as illustrated in figure 2.9 [51]. The temperature distribution can to a certain extent be controlled by part placement and dummy parts may be introduced to ensure an even temperature distribution.

2.7.4 Print-through and laser angle

The laser of LB-PBF machines penetrates more than one layer of material, securing proper bonding between the layers [54]. However, for the first few layers and any down-facing surfaces, the laser will continue through the surface and into the powder bed. This effect is present in

several AM processes and is known as "print-through" or "overcure". Naturally, this will yield larger dimensions in the build direction than what was designed. Some software offers compensation mechanisms to counter this effect by skipping the first few layers of any down-facing surfaces.

The effect of print-through may manifest differently depending on where the part is located in the build space. Because the effect is caused by the laser surpassing the intended volume, the direction of the laser (i.e. the angle between the relevant down-facing surface and the laser) determines the magnitude of the effect. Because the laser beam typically enters the build space through a mirror centered above the powder bed, the laser angle will be higher farther away from the center of the powder bed as illustrated in figure 2.10 This further implies that the effect may appear, not only on down-facing surfaces but also on vertical- and slightly up-facing surfaces.

The laser angle is found to impact surface roughness in Laser-Based Powder Bed Fusion of Metals (LB-PBF/M) [55], and can be calculated as:

$$\xi = \angle(\vec{n}, \vec{l}) = \arccos\left(\frac{\vec{n} \cdot \vec{l}}{|\vec{n}| \cdot |\vec{l}|}\right) \tag{2.2}$$

where ξ is the laser angle, $\vec{n}$ is the surface normal vector, and $\vec{l}$ is the direction vector of the laser. While print-through has received some attention in research efforts, the laser angle is rarely mentioned as a factor for final part properties. Based on recent studies, however, there

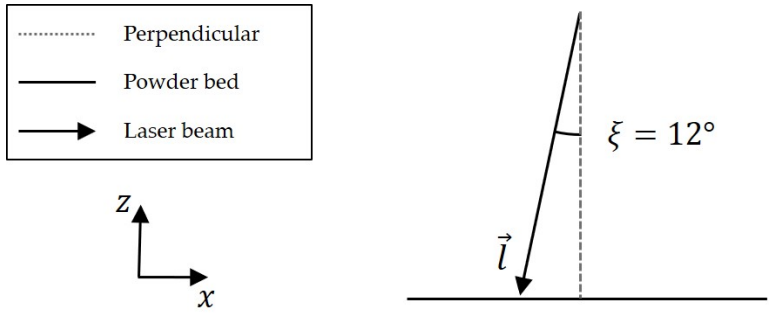

Figure 2.10: Illustration of the laser angle (ξ), here relative to the powder bed.

is reason to believe that the laser angle may have a significant impact on dimensional and geometric accuracy.

Chapter 3

Literature review

This chapter provides an overview of related works in the area of optimization in AM with a particular focus on the optimization of orientation for improved dimensional and geometric accuracy. Optimization is defined by Merriam-Webster [3] as *"an act, process, or methodology of making something (such as a design, system, or decision) as fully perfect, functional, or effective as possible"*.

Optimization schemes in AM concerns all three groups of objectives mentioned in the definition by Merriam-Webster [3]. Certainly, the optimization of product design is obvious in topology optimization where computer-generated designs are produced from parametric models with functional requirements and boundary conditions. System optimization is evident in the continuous improvement of AM systems for consumers and industry alike, including the business models and value chains developed for the new paradigm of manufacturing supported by disruptive technologies. Finally, the optimization of decision-making processes concerns AM at multiple levels from the selection of process parameters to product development and strategy. However, optimization in AM is perhaps most concerned with the improvement of quality, reduction of cost, and elimination of waste.

The present work builds on theory from multiple domains, hence an overview of related work will inevitably touch upon several different fields. The following sections attempt to present relevant research efforts in an orderly manner by roughly categorizing the publications according to topics, aims, and scope.

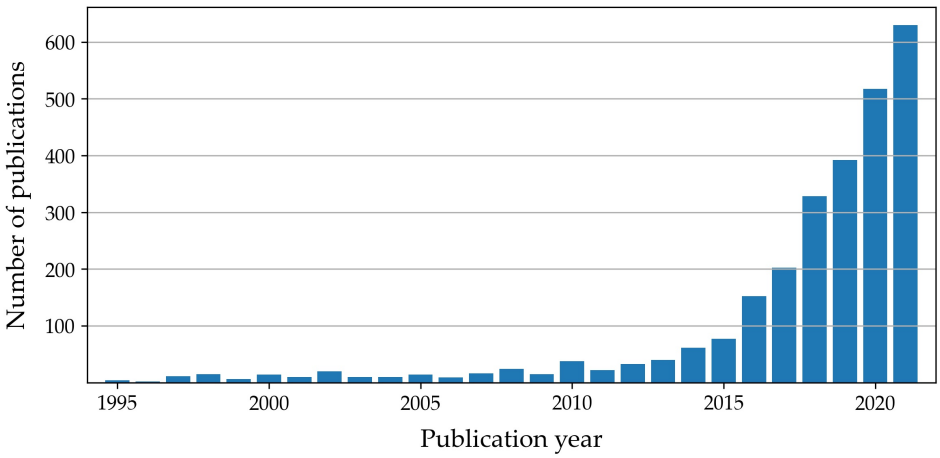

Figure 3.1: Historical view on publications related to part build orientation. The graph is generated from Web of Science[2].

3.1 Related work on part build orientation

The determination of the optimal part build orientation soon became a topic of interest with publications dating back to 1994 [56]. Figure 3.1 displays the results of a query on Web of Science[2] for scientific articles using any synonym for AM and either the word "orientation" or the term "build direction" in the title, abstract, or keywords. A critical point can be identified around the year 2010 after which an exponential growth in research interest can be observed. Note that the work of Allen and Dutta [56] is not present in the graph because it was presented in the Solid Freeform Fabrication Symposium. These proceedings are indexed in neither Scopus nor the Web of Science. Furthermore, papers only mentioning the specific technology and not any of the synonymous terms for AM also suffer the same fate, including the seminal work of Cheng, Fuh, Nee *et al.* [57].

Di Angelo, Di Stefano and Guardiani [58] recently reviewed the literature on the optimization of part build orientation in AM with a particular focus on the objective functions used for the optimization schemes. The authors proclaim in their introduction that *"[d]espite the large number of methods to search for the best build direction published in the related literature, it remains an open issue."* [58, p. 2]. As the AM technologies become increasingly sophisticated, the peculiarities will become more

[2]Web of Science is available from https://www.webofscience.com/.

Table 3.1: Categories of optimization methods reviewed by Di Angelo, Di Stefano and Guardiani [58].

Method	Papers
Weighted sum	15
Primary and secondary objectives	10
Pareto front	9
Others	7
Total	41

Table 3.2: Categories of optimization methods reviewed by Qin, Qi, Shi *et al.* [59].

Method	One-step	Two-step
Weighted sum	21	8
Min-max functions	29	3
Pareto front	7	0
Deviation function	0	1
Ordered weighted averaging operator	0	1
Fuzzy aggregation operators	0	1
Total	57	14

prominent and general applicability will no longer be feasible. The authors divided the reviewed optimization methods into four categories as displayed in table 3.1.

Qin, Qi, Shi *et al.* [59] also performed a recent review on "computer-aided part orientation" where the focus is on the automatic methods for optimizing part build orientation. The review distinguishes between one- and two-step methods and continues to present the different applications based on technology and implementation. The categories of methods reviewed in [59] are tabulated in table 3.2 where the reviewed literature is categorized as either one-step or two-step methods. This separates the methods for direct optimization based on the input geometry from the methods where higher-level information is derived before the optimization process. Evidently, the second review ([59]) is more comprehensive, yet the authors outlines nine directions of future research, ultimately emphasizing the continued need for research on part build orientation.

Early efforts on optimizing the part build orientation were primarily directed towards SLA. At the time, finding a stable orientation where support structures could be easily produced and removed was of high importance [56], [57]. The scope of the research efforts soon extended to build time and surface quality [60], [61], and the cost inferred by build time, pre-processing, and post-processing [62]. Later efforts have included mechanical properties [63], functionally graded materials [64], and lately also sustainability aspects [65].

Recent research efforts are predominantly aimed at specific applications and technologies [66]–[69]. The following subsections elaborate on the existing literature on the effect of part build orientation on tolerance characteristics. Flatness and cylindricity are emphasized as these characteristics constitute the main contributions of the current work. Nevertheless, additional characteristics are included to provide context and facilitate discussion on future prospects.

3.1.1 Part build orientation and flatness

The first model of accuracy in AM as a function of orientation was presented by Arni and Gupta [27] who derived the theoretical model in equation 3.1 for flatness error based on the staircase effect. The authors employ a critical angle θ_{cr} below which the entire surface will be contained within a single layer of material, hence, no steps are produced on the surface (see figure 3.2). The model can be expressed as:

$$\varepsilon_{flat} = \begin{cases} (\Delta z + \delta_z)\cos\theta + (\delta_{xy})\sin\theta & \text{if } \theta_{cr} < \theta \leq \frac{\pi}{2} \\ -(\Delta z + \delta_z)\cos\theta + (\delta_{xy})\sin\theta & \text{if } \frac{\pi}{2} < \theta < \pi - \theta_{cr} \end{cases} \tag{3.1}$$

where Δz is the layer thickness, θ is the angle between the surface normal and the build direction, δ_z is the general deviation in the z-direction, and δ_{xy} is the general deviation in the xy-plane.

3.1.2 Part build orientation and cylindricity

Similar to the work of Arni and Gupta [27] on flatness, Paul and Anand [29] developed a theoretical model for cylindricity as a function of part build orientation as displayed in equation 3.2.

$$\varepsilon_{cyl} = \Delta z \cdot \sin(\theta) \tag{3.2}$$

where Δz is the layer thickness and θ is the angle between the cylinder

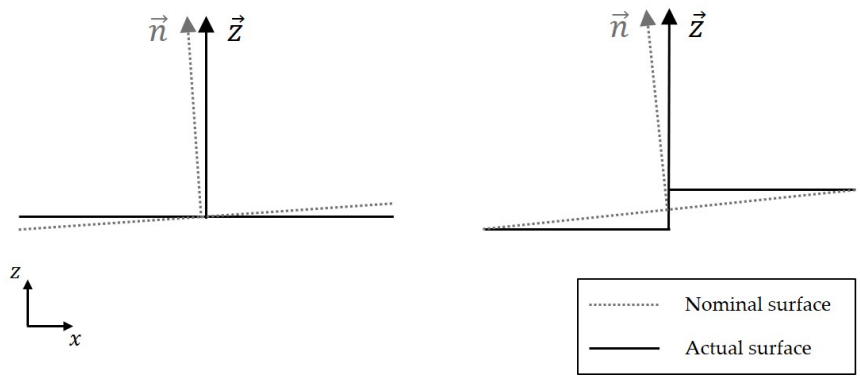

Figure 3.2: Illustration of how steps are introduced on close to horizontal surfaces. Adapted from [27].

axis and the build direction.

Senthilkumaran, Pandey and Rao [70] performed a central composite design experiment to model the effect of multiple factors in LB-PBF/P on form errors, one of the factors being the part build orientation. The authors developed the following model for cylindricity [70]:

$$\begin{aligned}\varepsilon_{cyl} =& 0.10874 + 0.0113P + 2.606 \times 10^{-4}v - 0.0349D + 0.0349\theta \\ & - 3.3833 \times 10^{-4}P\theta - 6.61 \times 10^{-6}v\theta + 3.3466 \times 10^{-4}D^2\end{aligned} \tag{3.3}$$

where P is the laser power, v is the scan speed, θ is the angle between the surface normal and the build direction, D is the diameter of the cylinder. Notably, the authors developed a similar model for flatness but discarded the term with build direction due to the low significance level. In other words, the models of Senthilkumaran, Pandey and Rao [70] consider the build direction to be a significant factor for cylindricity, but not for flatness. The experiment involved five levels for orientation, i.e. $\{0°, 22.5°, 45°, 67.5°, 90°\}$.

Another study was conducted by Ollison and Berisso [71] for Binder Jetting (BJ) at three levels for orientation, i.e. $\{0°, 45°, 90°\}$. The results from this study indicated comparable cylindricity at $0°$ and $45°$, but significantly larger errors for the horizontal orientation.

3.1.3 The effect of part build orientation on other characteristics

Das, Chandran, Samant *et al.* [26] extended the work of Arni and Gupta [27] and Paul and Anand [29] by also developing theoretical models for perpendicularity, parallelism, angularity, conicity and runout errors. Like their inspirations, these models are solely derived from the theoretical staircase effect and therefore do not consider shrinkage, warping, etc.

A great deal of work has been done to determine the relationship between the part build orientation and the surface roughness. The first investigations were performed for SLA [72], [73]. Experiments have later confirmed similar behavior in LB-PBF/P [74].

While the studies on surface roughness involve a large number of orientations, this is not the case for research on geometric and dimensional accuracy where typically only 2–5 orientations are investigated (see e.g. [70], [71], [75]). This constitutes a research gap where a more complex relationship between part build orientation and final part properties may be identified.

3.2 Variation and deviations in AM

Naturally, there are other sources of variations and deviations in AM other than the part build orientation. Certainly, the part build orientation is merely one of many parameters that cause variations in final part quality. Similarly, tolerance characteristics are not the only way to characterize form deviations. The following subsections provide a brief overview of related subjects and associated quality measures.

3.2.1 Variations within and between builds

Despite the continuous efforts to develop a stable process, LB-PBF remains prone to variation within and between builds [76]. Senthilkumaran, Pandey and Rao [77] investigated the shrinkage effect in LB-PBF/P and found larger variations in the y-direction than in the x-direction within the build chamber. Similar results are reported by Gazzerro, Polini and Sorrentino [78] who adds that the accuracy in z-direction appears to be rather stable. The latter study also observed better mechanical properties towards the center of the build compared to the edges of the powder bed. This complies with previous studies where the variation is attributed to uneven temperature distributions [51]. Wang, Wang, Zhao *et al.* [79] investigated the influence of other parameters on the

shrinkage effect in LB-PBF/P using a neural network model, but part build orientation was not part of the study.

Rüsenberg, Josupeit and Schmid [13] performed two builds to characterize the quality in LB-PBF/P, but no dimensions were measured. Nevertheless, the study found minor deviations between the two builds in terms of mechanical properties and argues for good repeatability. Furthermore, the authors mention variations in material properties between positions in the build chamber but do not go into detail.

3.2.2 Compensating deviations in AM

Geometric deviations in layered manufacturing technologies can be thought of as the sum of in-plane deviations and out-of-plane deviations. In-plane deviations are those deviations that can be observed in a single layer of material [80]. Conversely, out-of-plane deviations are deviations observed across layers [81].

Modeling the various failure modes in AM enables the prediction of actual geometry [31]. Consequently, if deviations can be predicted, they can also be mitigated. Compensation of geometric deviations has been proposed both for in-plane deviations [80], [82], [83] and out-of-plane deviations [81], [84]. Skin model shapes have been proposed as a means for modeling final shape deviations which enables simulation and verification of assembly operations [85].

Machine Learning (ML) methods have been proposed to predict and compensate geometric deviations [84], [86] as well as dimensional deviations [87], [88]. By exposing the ML models to a certain number of training geometries, they should be able to produce accurate predictions for any future geometry. A major benefit from this approach is the ability to handle free-form surfaces without explicit knowledge of shape features. However, these methods require correct training reliable results and must be validated carefully.

3.3 Other relevant work

For the problem of part build orientation in AM, a distinction can be made between those who utilize the shape features of the part (e.g. [34], [57], [89], [90]), and those who consider every single facet of the STL file (e.g. [91]–[94]). The latter methods are greatly affected by the number of facets in the STL file, and simplifications of the surface mesh is proposed to reduce the computational cost [65]. However, the computational

burden can be alleviated by handling features rather than single facets. This can be accomplished either by using the native CAD file as basis for optimization [95], [96], or the STL file may be pre-processed by feature recognition to extract relevant geometric features from the surface mesh [97], [98].

Chapter 4

Methodology

The validity of any research effort is determined by the methodology behind it. For any research endeavor to produce valid and reliable results, the methods and epistemological foundations should be carefully and precisely described. This chapter presents the underlying philosophy of science including the context and academic environment in which the project was situated. The first subsection lays out the backdrop for the selected methods which are described in detail thereafter. A separate section is devoted to the description of the experimental work that was conducted which includes an elaborate design of the experiment. Finally, data exploration and -analysis are described before a brief disclosure of limiting factors.

4.1 Transparency and open science

With the risk of repeating the philosophies of Descartes, the question *"how do we know that we know?"* is relevant to any researcher when disseminating their findings. Any research endeavor takes place in a very specific environment, not only with regards to physical installations or the geographical location, but also the academic environment with its culture and traditions. Moreover, the time period with technical developments and state-of-the-art, and maybe even the geopolitical climate, can influence the significance of research results. A researcher should therefore strive to disclose any relevant details about the context of the research to improve the reliability and validity of the results.

In the digital world of today, where the scientific community is fragmen-

ted and scattered throughout the world, the concept of open science is on the rise. Making knowledge available to all – not just for the individual enlightenment, but for others to validate, challenge, and oppose – contributes towards an inclusive yet rigorous scientific community. The availability of research regardless of circumstance remains a core value in modern scientific discourse.

Digitization offers many opportunities along with at least as many challenges. Privacy and intellectual rights are tested in open science, and the FAIR principles for scientific data [99] provide guidelines for how scientific data is treated to maximize findability, accessibility, interoperability and reuse. In the guidelines from the European Research Council Horizon2020 program, it is stated that FAIR data should be "as open as possible, as closed as necessary" [100]. The present work is conducted in line with open science philosophy, and an effort has been made to comply with the FAIR principles[3].

The Norwegian University of Science and Technology (NTNU) slogan *"Knowledge for a better world"* inspires the wide dissemination of research for the good of all humanity. The current work is in its entirety made publicly available through online data repositories, open-source code, and open publications. Every step in the process has been scrutinized for validity, and actions have been made accordingly to maximize validity within the limitations of the project. By disclosing all details pertaining to data generation, adopting the FAIR principles, and disseminating results open access, the current work certainly contributes with knowledge for a better world.

4.2 Contributions of papers

This thesis builds on six (6) papers, denoted P1–P6, written throughout the PhD-work – five of which are published already, and the final paper is accepted for publication. The thesis ties the papers together towards a method for optimizing part build orientation. Figure 4.1 illustrates how the papers address the various RQs posed in section 1.2.

The papers are summarized in table 4.1 and the individual contributions are outlined in the subsequent paragraphs.

[3]The FAIR principles are available from https://www.go-fair.org/fair-principles/

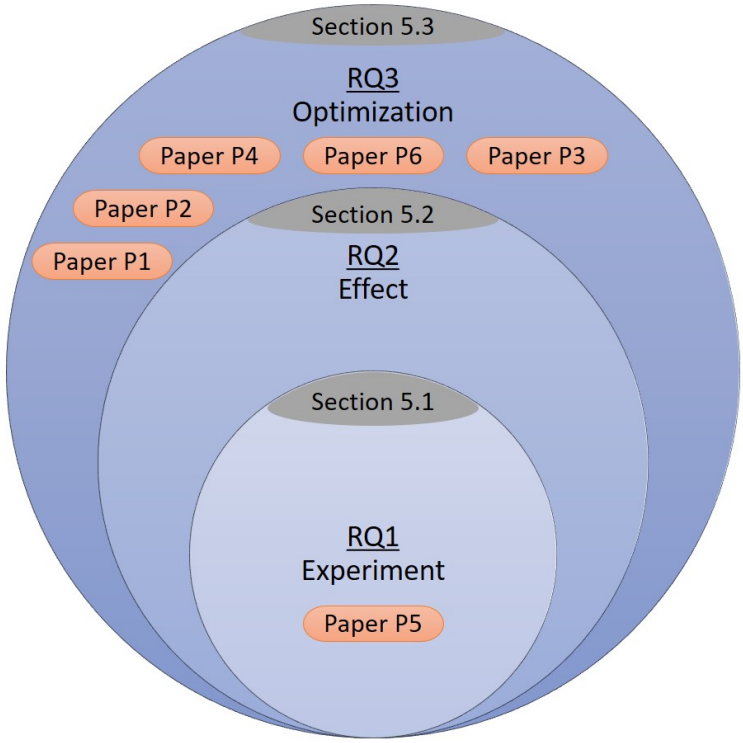

Figure 4.1: Relationship between papers and RQs.

Table 4.1: Overview of articles published in connection with this PhD project.

Number	Year	Main author	Co-author(s)	Journal
P1	2019	Leirmo, T.S.	Martinsen, K.	Procedia CIRP
P2	2020	Leirmo, T.S.	Martinsen, K.	Procedia CIRP
P3	2020	Leirmo, T.L.	Semeniuta, O. Martinsen, K.	Procedia CIRP
P4	2020	Leirmo, T.L.	Semeniuta, O. Baturynska, I. Martinsen, K.	Procedia CIRP
P5	2021	Leirmo, T.L.	Semeniuta, O.	Applied Sciences
P6	—	Leirmo, T.L.	Semeniuta, O.	Open Engineering

P1. Evolutionary algorithms in additive manufacturing systems

Background

The problem of determining a suitable part build orientation in AM is an elusive problem in the sense that it may take many forms depending on the context. Consequently, solutions have been proposed using a plethora of different methods and tools. One group of particularly popular methods is the EAs – a subclass of artificial intelligence – where the solution space is randomly sampled to converge towards the optimal solution. This paper explores the existing alternative solutions to the deterministic demand of RQ3.

Contributions

- Overview of past and current EAs in AM through a literature review
- A discussion on the prospects of EAs in AM projecting increased variation in method types – especially in the sources of inspiration for EAs

P2. Deterministic part orientation in additive manufacturing using feature recognition

Background

For AM to be viable in mass production, a certain level of predictability is necessary. Existing methods for automatic determination of part build orientation in AM typically include a stochastic component which ultimately introduces variations into the production system. Automation of this process is further hampered by the low level of information available in the tessellated STL files which are used for file transfer in AM. This paper address RQ3 and proposes a solution.

Contributions

- A deterministic method for finding a feasible part build orientation in AM
- Demonstration of the efficiency gained from considering features rather than triangles of the STL file.
- Execution times for a C++ implementation of exhaustive search using feature recognition.

P3. Tolerancing from STL data

Background

The conception of AM introduced a need for slicing digital models – a task too complex for the computational power available at the time. The solution was the STL file which represented the geometry as a tessellation of triangles which made slicing much easier. However, the file format remains and is to this day the most common file format in AM. The determination and communication of tolerances are problematic due to the limited information available in the primitive file format. This paper relates to RQ2 and RQ3 and outlines a method for integrating STL files in a digital pipeline for AM.

Contributions

- A method for applying tolerances to STL-models by vectorial tolerancing
- The concept of a digital pipeline for quality assurance in AM
- A simple case study demonstrating the application of the proposed method

P4. Extracting shape features from a surface mesh using geometric reasoning

Background

Many applications benefit from higher-level information regarding the geometry to be fabricated by AM. It is therefore valuable to develop intelligent methods for reconstructing higher-level information from STL files. The extracted information can be used for process planning, file modification, prediction and analysis of mechanical behavior, etc. This paper is closely related to papers P2 and P3, and contributes towards RQ3

Contributions

- An analytic method for feature recognition from STL-files
- A classification of local topology in STL-files

P5. Investigating the dimensional and geometric accuracy of laser-based powder bed fusion of PA2200 (PA12)

Background

AM is increasingly used in the manufacturing industry for manufacturing end-use parts as well as prototypes, however, consistent part quality remains an issue for all AM technologies. For LB-PBF/P, the orientation and placement in the build chamber is known to affect final part properties, however, conducting experiments that account for all possible variations are both difficult and expensive.

The underlying assumption of previous works is that the effect of orientation on accuracy can be inferred from an experiment with a small number of orientations (typically 3–5 orientations). However, the hypothesis of this work is that the relationship is more complex than what such experiments could reveal, and that previous experiments may be compromised due to insufficient control of auxiliary variables. Hence, a robust experiment was designed and conducted to explore this relationship in further detail. This paper describes the design and execution of the experiment in detail and presents results to affirm the validity of the results. Hence, this paper targets RQ1, and provides the foundations for answering RQ2.

Contributions

- A robust experiment design and methodology for LB-PBF/P that enables valid comparisons between different positions in the build chamber. This can further be used for the construction of prediction models.

- A novel test artifact with elements comparable to an existing artifact for external validity

- An open data set available to the research community and the public in the spirit of open research

- Evidence of variations between different positions in a single build

P6. Minimizing form errors in additive manufacturing with part build orientation – An optimization method for continuous solution spaces

Background

The part build orientation in AM is a decisive factor for the final quality, both in terms of dimensional and geometrical accuracy, and surface roughness. Consequently, part build orientation has been subject to optimization schemes for decades with varying scopes, objectives, and complexities. Theoretically, the solution space for this problem is bound to the surface of a unit sphere, however, this space holds an infinite number of unique solutions due to the continuous space. Optimization of part build orientation is therefore accomplished in one of two ways: (i) a finite set of candidate orientations are derived from the solution space by discretization or from the geometry by intelligent methods, or (ii) the continuous solution space is traversed by evolutionary algorithms or other stochastic methods.

This paper describes a method where the geometry defines a continuous solution space where the critical points are derived mathematically. Consequently, a solution to RQ3 is provided in this paper.

Contributions

- Strong mathematical foundations for part build orientation including relevant formalizations
- A novel method for optimizing part build orientation from a continuous solution space
- Generic mathematical models aggregating objective functions for separate feature types
- Validation of said method through two case studies

4.3 Research methods

Although being tightly connected in this thesis, the research questions warrant the application of diverse research methods. RQ2 requires investigation of literature, but benefit more from experimental work that generates valid primary data for creating models that describe the relationship between part build orientation and geometric accuracy. RQ3 is addressed by building on the data from RQ2 to develop an approach for optimizing the part build orientation to meet tolerance requirements.

Table 4.2: Overview of hardware and software used for various research activities.

Activity	Hardware	Software
Design of experiments	Computer	MS Excel, Magics 23.01
Design of specimens	Computer	Solidworks 2018, MS 3D Builder
Manufacturing specimens	EOSINT P395	Magics 23.01, EOS PSW
Measurements	Zeiss Duramax	Calypso
Data analysis	Computer	Python 3, Jupyter Notebook

RQ1 is a question of experiment design and is tightly connected to RQ2, but requires further analysis and discussion around the applicability of the design to other technologies and purposes.

The experimental work constitutes a major part of the project – especially in terms of research methods and tools. An overview of the hardware and software utilized in the various activities connected to the experimental work is presented in table 4.2. Details on the experiment are also allotted a separate section (section 4.4) where the characteristics are outlined.

4.3.1 Literature review

When the project was initiated in 2017, the topic was fuzzy and the problem was not yet defined. However, with progress comes enlightenment, and the topic was funneled into the problem defined in this thesis. This journey is reflected in the keywords used to scrutinize databases throughout the project. Writing papers along the way assisted in focusing the effort on sub-problems, and – to some extent – contain the exploration of a vast ocean of available literature on related subjects.

The literature has been collected by various methods along the way; Structured and unstructured literature searches in academic databases and search engines, e-mail alerts from relevant journals, social network recommendations (i.e. ResearchGate), literature from colleagues and students, and attendance at scientific conferences. Finally, backward- and forward snowballing has been done, starting from literature acquired from the aforementioned methods.

The plethora of terms and phrases surrounding AM complicate the queries necessary to include all relevant literature. For instance, the following string was used to obtain results pertaining to AM in a wide sense:

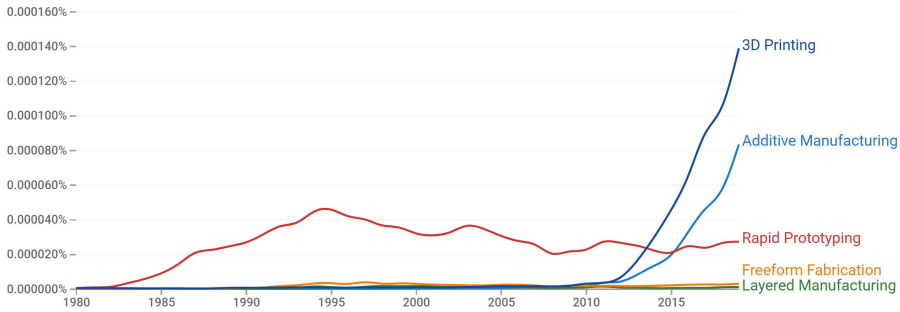

Figure 4.2: The popularity of different synonyms for Additive Manufacturing (AM) from 1980 to 2019. The graph is produced by Google Books Ngram Viwer[4] based on the number of appearances in both popular and scholarly books.

"Additive Manufacturing" OR "Rapid Prototyping" OR "Layered Manufacturing" OR "3D printing" OR "Freeform Fabrication"

All of these terms and more have been used somewhat synonymously over the last decades, and more exist for specific applications of AM technologies, e.g. rapid tooling. Figure 4.2 displays how the popularity of the different terms has developed over time. "Rapid Prototyping" was the term initially used for the concept. However, as more technologies were developed with more use cases, other terms became popularized. The recent shift towards the term "Additive Manufacturing" is mainly due to the standardization efforts in industry and academia, while "3D printing" continues to be the preferred layman's term.

4.3.2 Experiment planning

Based on experience from related works (such as the PhD project of Ivanna Baturynska [41]), the build layout cannot be neglected in the experiment planning. Furthermore, the relatively high cost of experiments leave little room for errors in the planning process. Precautions was therefore taken to minimize risk, and maximize the utility of experiments. Together with the outbreak of the global COVID-19 pandemic, the meticulousness of the experiment planning prolonged this process significantly. The experiment was eventually conducted in May/June of 2020, approximately one year after the first layout was sketched. Details on the experiment planning is presented in section 4.4.

[4]Google Books Ngram Viewer is available from https://books.google.com/ngrams.

4.3.3 Analysis and modeling

The data acquired from the experiment enables the modeling of the effect of part build orientation on select response variables. Initial analysis of the data was aimed at characterizing the variation, and furthermore, to investigate the validity of the generated dataset (as published in paper P5 [101]). The next phase entails the development of empirical models from the experiment data (see section 5.2). This was achieved using Python programming language and is elaborated in section 4.5.

4.4 Experimental work

A detailed description of the experiment is available in paper P5 (Leirmo and Semeniuta [101]) where the validity of the data also is analyzed and discussed. This section is dedicated to reporting and accounting for the decisions made in the experiment design and underlining the main characteristics of the experiment.

4.4.1 Artifact design

A plethora of benchmark artifacts already exists in literature [102], with both NIST [103] and ISO/ASTM [104] contributing with geometries. Nevertheless, every artifact is designed for a particular purpose, and with the relatively large cost of AM, tailoring an artifact to maximize utility while minimizing cost is justified. Hence, inspiration was drawn from the artifact proposed by Minetola, Iuliano and Marchiandi [105] in the design of a new test artifact that enables comparison with related work.

The designed artifact collects multiple geometric features on a base plate which facilitates inspection by CMM. The desire to incorporate multiple dimensions in concave and convex versions inevitably yields a relatively large artifact. The final design was only completed after the feasibility of the total dimensions was confirmed in the build space segmentation phase outlined in subsection 4.4.2. A concurrent process of artifact design and build layout design maximizes the utility of the experiment by allowing adjustments to be made in both regards before arriving at a final solution. Moreover, a prototype was produced using a Prusa i3 MK2.5 Fused Filament Fabrication (FFF) machine which enabled details in the inspection stage to be considered in the final design, including the fixture which is further detailed in subsection 4.4.3. Details on the artifact design are available in appendix C.

4.4.2 Build layout

Large variations have been observed in PBF from one build to the next, and even within a single build [75], [77], [106]. Wu and Hamada advises to *"block what you can and randomize what you cannot"* [107, p. 9]. Consequently, the experiment incorporated blocking strategies to enable comparisons between builds, and between different positions within the same build. The solution was a grid-like structure where 45 discrete positions were defined in the build space. In this context, a position is a point in the build space defined by Cartesian coordinates $\begin{bmatrix} x & y & z \end{bmatrix}$ defined in millimeters relative to the machine coordinate system. This point describes a fixed position in the build space where parts can be fabricated under identical circumstances, i.e. the point is fixed relative to layer thickness and hatch distance. While the purpose was to improve the validity of the results, it also enables a rough analysis of the effect of part location for these discrete positions.

Number of specimens

Previous studies typically consider 2–5 orientations when investigating the effect of orientation on accuracy (see e.g. [70], [71], [75]). This, however, appears to be insufficient for creating an accurate model of the relationship. To enable a complex relationship to manifest, it is desired to produce specimens at five-degree intervals.

Because LB-PBF/P does not require any support structuress, the results may be expected to be symmetrical about the horizontal, i.e. up-facing and down-facing surfaces may be evaluated identically as a function of their offset from the horizontal orientation. However, due to print-through, the bottom side may have a higher surface roughness than the top. Similarly, the actual surface may also be slightly offset and impact tolerance characteristics. It is therefore necessary to investigate the full range of orientations from zero- to 180-degrees. With five-degree intervals, this yields a total of 37 orientations.

Finally, three replications of each orientation are desired to enable the analysis and characterization of variation. Consequently, 111 specimens must be produced to realize the desired resolution of investigated orientations, and also meet the demand for replication.

Build space segmentation

The build volume of the EOSINT 395 is finite with fixed dimensions 340 $\times$ 340 $\times$ 620 mm in x-, y-, and z-direction respectively. Additionally, it is advised to keep a certain distance from the edges (20 mm), as well as the build platform (6 mm). This further decreases the available build space to 300 $\times$ 300 $\times$ 614 mm.

The combination of available space and desired elements of the artifact converged towards a 3 $\times$ 3 grid of fixed positions in the xy-plane of the build space. Because there is no need for support structures in LB-PBF/P, parts can be fabricated on top of each other without compromising the quality of already manufactured products. Consequently, the 3 $\times$3 grid of positions can be repeated in the build direction to yield additional specimens from a single build.

To accommodate the designed artifact in any orientation in any position, the distance between the centerline of each layer of parts must also be roughly 100 mm. The thickness of the layers must be considered to mitigate any variation arising from part placement with regards to the layers. Therefore, the distance between the centerline of each layer is set to a multiple of the layer thickness (120 µm). Considering the restrictions above, three builds are necessary to fabricate 111 specimens).

The build space segmentation described above yields 135 positions over three builds. Because the experiment requires 111 specimens to produce three replications of each orientation, there are 24 positions more than what is strictly required. These additional positions offer a few challenges and opportunities. Firstly, leaving the positions empty would affect the temperature distribution in the vicinity by reducing the ED. Similarly, utilizing this space to manufacture something else may also distort the ED. Hence, the same geometry should be fabricated in all positions of the build space to ensure an even temperature distribution and avoid major differences in ED.

When it is clear that eight additional copies of the same geometry will be fabricated in each build, it is desirable to make these specimens useful. One approach would be to create multiple replications of central orientations. However, this could introduce inconvenient variation in input data for statistical analysis in later stages. Another utility of these extra specimens is to use them to analyze and characterize variation between- and within builds with higher accuracy than what the experi-

ment initially would accommodate. This is achieved by reserving some of the fixed positions for these additional specimens. By reserving corresponding positions at every level in every build, the effect of build and position can be analyzed separately from part build orientation. With eight extra specimens in each build, one position in each level may be reserved. The remaining three positions are reserved at levels 1, 3 and 5 for even distribution. Because these positions can be used as reference points for the experiment, these are referred to as 'anchor positions' and 'anchor specimens' in this work.

Assigning orientations to positions

The experiment is designed based on the presumption that the variation between- and within builds is non-negligible. Randomization is therefore employed as a tool to avoid systematical variation. A spreadsheet in MS Excel allowed the random assignment of part build orientations to the defined positions in the build space. This was achieved as follows:

1. Compile the list of all non-anchor positions
2. Give all positions in the build space a number (1–45)[5]
3. Randomly assign each part build orientation a number $[0, 1)$
4. Sort the part build orientations based on the random number
5. The position of the part build orientation in the list correspond to the position defined under item 1

This process was repeated separately for each build, and the layout was implemented in Magics where the parts were first moved to their respective positions before they were rotated according to the randomized scheme above. The position of a part in the build space is defined by the central point of the part's bounding box in its initial orientation as illustrated in figure 4.3. The bounding box of a three-dimensional object is the minimum rectangular cuboid that contains the entire geometry. In the present work, the edges of the bounding box are parallel to the axes of the machine coordinate system.

The anchor specimens were rotated 90° to minimize the sintered area of the relevant layers, and to contribute towards an even slice distribution.

[5]Anchor positions follow the same numbering scheme but are excluded from the random orientation assignment scheme.

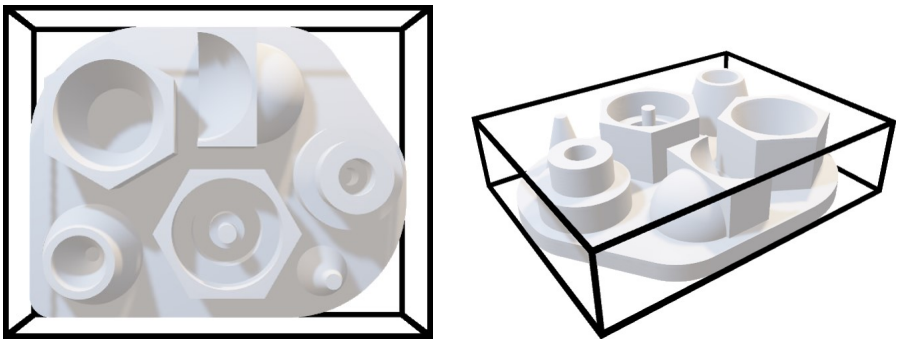

(a) Top view **(b)** Above right back view

Figure 4.3: The bounding box of the test artifact.

The anchor specimens are rotated about the x-axis in the opposite direction to differentiate them from the main specimens of the experiment. Specifics of the layout are available in appendix B, table B.1.

Additional objects

When all 135 specimens are placed in the build space, the slice distribution exhibits large fluctuations in input energy between the layers of specimens. To flatten this curve, additional objects were inserted in the build chamber. Once again, an opportunity reveals itself to enrich the experiment with additional data.

For the first iteration, two sample types were adopted. Firstly, the fabrication of hollow boxes is an elegant solution for retrieving powder samples from within the build. With this in mind, four boxes were inserted between the part layers. Secondly, because cylinders were of particular interest, the fine cylindrical geometry (CA_F) of ISO/ASTM 52902:2019(E) [104] was utilized. Clusters of six specimens in orthogonal directions were replicated 12 times in each build to produce a total of 216 additional parts.

Furthermore, 32 replications were produced along the edges of each build to enable the investigation of how the laser angle affects cylindricity. 50% of these specimens were fabricated with the axis parallel to the build direction, while the remaining 50% was re-oriented to align with the laser angle. The alignment was achieved by rotations R_x and R_y about the x- and y-axes of the part's bounding box. The magnitudes for rotations R_x and R_y was derived from the part coordinates as follows:

$$R_x = \arctan\left(\frac{p_y - l_y}{l_z}\right) \tag{4.1}$$

$$R_y = \arctan\left(\frac{p_x - l_x}{l_z}\right) \tag{4.2}$$

where p_x and p_y are the x- and y-coordinates of the part's center point, and l_x, l_y and l_z are the x,- y-, and z-coordinates of the last deflection point of the laser beam before entering the build space. While the position of the part relative to the machine coordinate system is set by the user and therefore readily available, the position of the last deflection point is unfortunately confidential and unavailable. Consequently, this location is estimated based on external measurements and best guesses to be centered above the build space with respect to the x-y plane at a height of approximately 600 mm.

The introduction of these additional objects improved the slice distribution, but there was still room for improvement. A third object was designed specifically to fit in the corners of the build space without entering the buffer zone around each position. This object was designed by CSG using Microsoft 3D Builder in three steps; (i) the shape and size of the available space were estimated and created as a solid part, (ii) the linear artifact (LA) of ISO/ASTM 52902:2019(E) [104] was used to make imprints in the geometry, and (iii) the larger open areas were used to create small cylindrical imprints. This corner geometry's main purpose is to even out the slice distribution for better temperature distribution. However, the imprinted geometries enable inspection of linear accuracy in x-, y-, and z-direction in all corners of each build, as well as roundness errors.

4.4.3 Data collection

An inspection strategy was developed for a Zeiss Duramax CMM, and a fixture was designed specifically for the experimental artifact (see appendix D). The CMM ensures accurate measurements by Computer Numerical Control (CNC) which minimizes measurement uncertainty. The fixture is a clamping device that holds the specimen in place during the inspection, and also ensures close to identical placement of all specimens in the CMM. A 3 mm ruby probe was used to perform the inspections. This dimension act as a mechanical filter that reduces the noise from surface roughness which is not the focus of this study.

Before the CMM can run an inspection in CNC mode (i.e. fully automatic), a base alignment must be established. This alignment allows the machine to know where the specimen is located in the measurement volume, and how it is oriented. Because the Duramax CMM does not employ any sensors apart from the inspection probe, the position and orientation are communicated to the machine by manually measuring a set of points on the specimen. This process, referred to as manual alignment, was in this experiment performed for every single inspection. Note that the same position and orientation could be assumed for every specimen because the fixture would eliminate most variation in this regard. After all, form features are approximated, and form deviations are computed relative to the fitted feature – not its nominal position.

All inspections were repeated thrice to counter measuring uncertainty. This repetition included re-mounting the specimen in the fixture and the subsequent establishment of a base alignment to incorporate natural variation from this procedure.

4.5 Data processing and analysis

The data collected from the CMM was aggregated in a Zeiss proprietary database as tolerance characteristics. The data was exported from this database as Comma-Separated Values (CSV) files that are compatible with third-party software. This raw data was made available through the open repository together with supporting information about experiment execution and meta data[6].

The collected data was cleaned and analyzed with Python programming language in a Jupyter Notebook environment. The generated code was made accessible through GitHub repositories linked to the relevant publications. Several analyses were performed to explore the dataset and to perform statistical tests. Figure 4.4 give an overview of the information flow in the experiments. The icons associated with each python package symbolize their utility in the project. Starting at the top of the python packages in figure 4.4, pandas [109] is used to store and manipulate tabular data, i.e. import and filter the experiment data. Continuing clockwise, NumPy [110] is used for heavy lifting in computations, especially matrix and vector operations. Matplotlib [111] and seaborn [112] are both used for exploring and visualizing data, however, seaborn offer some additional functionality for statistical

[6]The data is made available through the open repository DataverseNO [108].

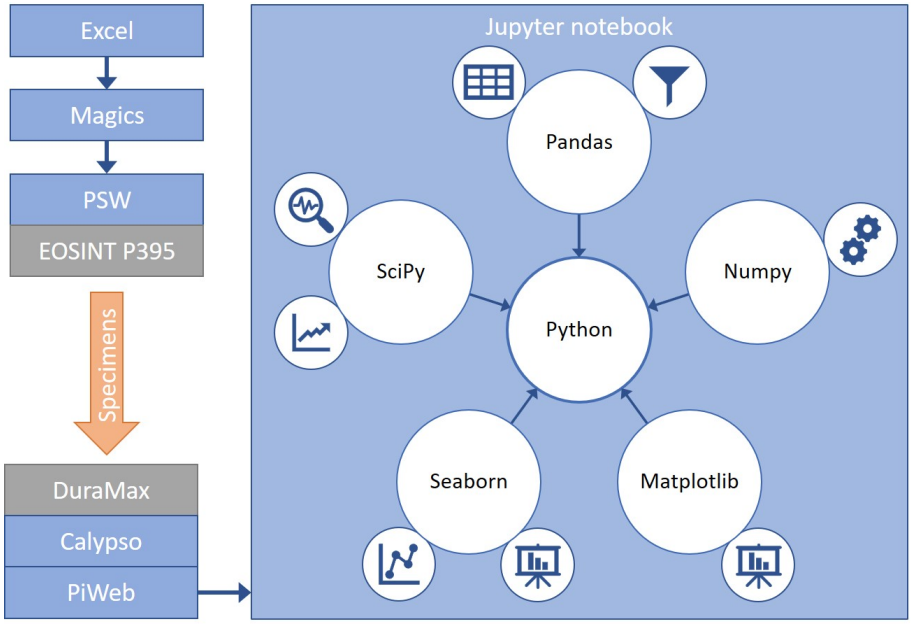

Figure 4.4: Information flow in the experiment from layout planning to model development.

analysis [112]. Finally, SciPy [113] is used for statistical analysis and curve fitting in the modeling stage.

In addition to the packages directly related to the analysis of experimental data, the python package SymPy [114] has been utilized as a symbolic solver for performing mathematical operations – especially in the context of paper P5. Naturally, many tools and methods have been explored and discarded throughout the PhD project. Remnants of this may have a certain influence on the results, but the tools and methods presented above are responsible for the main contributions towards this thesis.

Chapter 5

Results

This chapter summarizes all the results through three sections – one for each RQ as illustrated in figure 4.1. The first section describes the results from the experiment, and more importantly, the findings related to the robustness of the experiment in terms of variation within and between the builds. The second section develops empirical models based on the experimental data, and the third section describes a deterministic method for the optimization of part build orientation in a continuous solution space.

5.1 Experimental results

The experiment successfully generated a large amount of data as made available through an open repository [108][7]. This section presents these data through five sections; Firstly, the validity of the acquired data is analyzed and commented to give a solid foundation for the following sections, subsequently, the central characteristics are investigated in separate sections, before the final section describes other data obtained from the experiment. This section forms the basis for answering RQ1 with support from paper P5 [101], and further provides the foundation for later sections.

[7]The dataset is available in the open repository DataverseNO with DOI 10.18710/DHACHZ [108]. The interested reader is referred to the article by Conzett [115] for more information on the repository and its relation to the FAIR principles.

5.1.1 Variations in the experiment data

All manufacturing processes, as well as inspection methods, are inherently prone to variations [116]. Despite the measures taken in the experiment design to reduce variation, some discrepancies are to be expected. Full disclosure and a thorough analysis of observed variation is necessary to establish a good foundation for data analysis. A full analysis of variations in the dataset is presented in paper P5 [101], but is also repeated here for coherence.

Firstly, the validity of the measurements is verified by analysis of variation between repeated measurements. When the validity of measurements is confirmed, the variation between the different builds is investigated. Comparable results between the builds are fundamental for the validity of the experiment and are required for the subsequent analysis of variation between positions in the builds as presented in the final subsection.

Variation between repeated measurements

Each specimen was inspected thrice, including mounting and dismounting of the specimen in the fixture. This means measurement uncertainty is also included in the analysis of variation between repeated measurements. Figure 5.1 compares the three repeated inspections of `HX1_Plane1` from a randomly selected specimen, i.e. specimen number 6 from build 3 (i.e. `Build3_#6_HX1_Plane1`). Each green line in figure 5.1 corresponds to the measured deviation from the ideal plane with the minimal and maximal points indicated with red circles. The plots display minor variations between the inspections, but the location and magnitude of the hills and valleys are close to identical. The measured error values for flatness are 0.062, 0.058, and 0.059 mm for the respective repetitions.

Table 5.1 displays a statistical description of the variation between repeated measurements of flatness, cylindricity, and diameter aggregated for all specimens where Rep 1–3 corresponds to the first, second, and third repeated inspections respectively. The column Mean contains the data for the mean of the three repeated measurements of each characteristic. Finally, Δ is the difference between the smallest and the largest value among the three repeated measurements.

A slight decrease in the observed error can be observed through the repeated inspections as evident in table 5.1. This may be attributed to

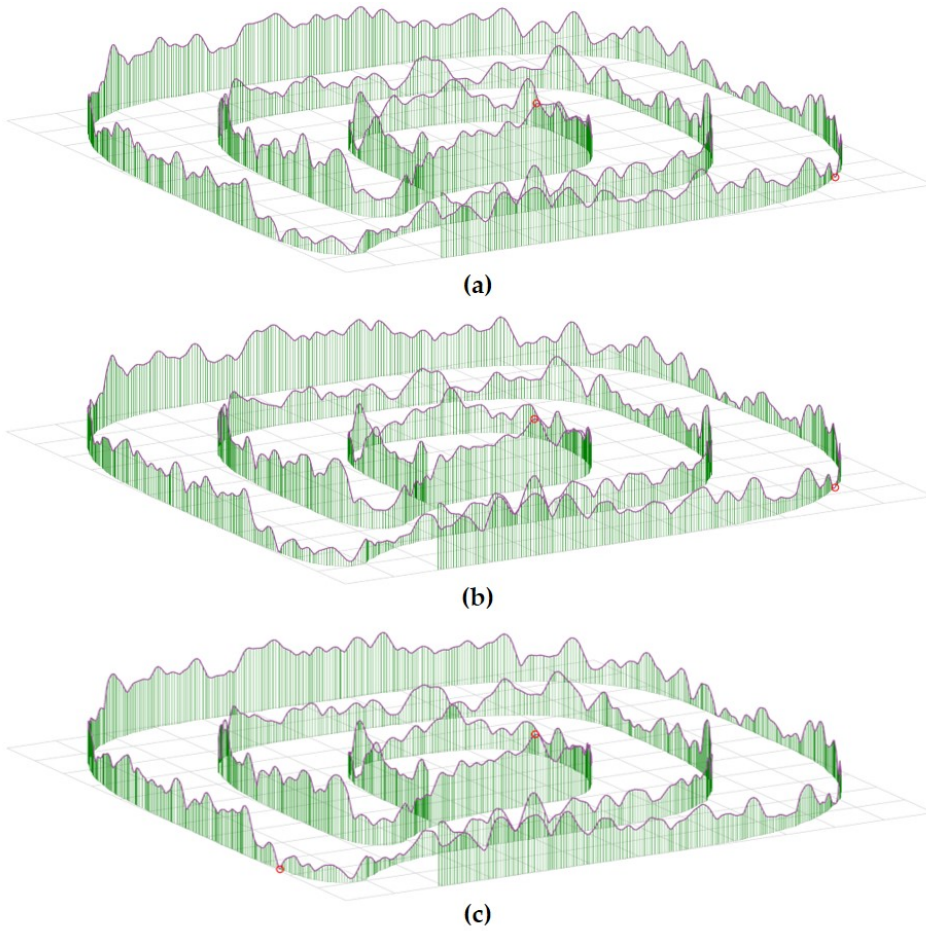

Figure 5.1: Measured flatness for three repeated measurements for specimen `Build3_#6_HX1_Plane1`. (a) 1st inspection: 0.062 mm; (b) 2nd inspection: 0.058 mm; (c) 3rd inspection: 0.059 mm.

Table 5.1: Statistical data for repeated measurements.

	Rep 1	Rep 2	Rep 3	Mean	Δ
n	3510	3510	3510	–	–
$\bar{x}$	0.088577	0.084998	0.083011	0.085529	0.008634
σ	0.122123	0.118936	0.117179	0.119282	0.011865
Min	−0.544659	−0.540020	−0.537463	−0.540714	0.000022
25%	0.068541	0.066567	0.065653	0.066977	0.002682
50%	0.090128	0.087218	0.086086	0.087838	0.005521
75%	0.132110	0.127516	0.124374	0.127606	0.009823
Max	0.626687	0.576267	0.542467	0.559931	0.256032

any residual powder being brushed off between the inspections. Regardless, the variations observed between the repeated inspections of table 5.1 appear to be minimal. Figure 5.2 displays normalized histograms for these characteristics individually, and in concert. The plots seem to generally follow a log-normal distribution where a high share of the data points are located close to zero. Hence, a log-normal curve is fitted to the data and plotted together with the histograms, and the final panel compares these log-normal distributions. Among these characteristics, diameter stands out as slightly less repeatable.

Looking at the Δ column from table 5.1, it may be observed that the standard deviation of Δ values is approximately ten percent of the layer thickness. This is probably coincidental, but nevertheless illustrates the magnitude of measurement error. The analysis from figure 5.2 indicates a smaller variation in the measured values for flatness and cylindricity compared to diameter. Consequently, these characteristics are better suited for the development of precise empirical models in later stages (see section 5.2). The analysis of measurement variation however indicates that the measurements are valid, and the mean value of the three repeated measurements can be used as an estimation of the true value.

Variation between the builds

Three builds were necessary to create three replications of each part build orientation. However, the variation between these three builds must be investigated to ensure a valid comparison between them. The variation between the builds can be analyzed by comparing the anchor specimens from each build. However, this would only compare the variation at the anchor positions between the builds. Another opportunity presents itself in planes 2 and 5 from HX2 which are vertical for all orientations. This enables a much more robust analysis because all specimens can be included in the sample.

A statistical description of the variation in measured flatness between the builds is presented table 5.2. The builds display comparable results as further substantiated in figure 5.3 where the distributions are compared. The distributions are highly uniform with a few outliers clearly visible in the boxplot.

Figure 5.2: Log-normal probability distributions fitted to the difference in repeated measurements. Each panel displays the distribution of Δ values for a characteristic, and the final panel compares the fitted log-normal probability distributions.

Table 5.2: Statistical data for different builds.

	Build 1	Build 3	Build 3	Mean	Diff
n	90	90	90	–	–
$\bar{x}$	0.100579	0.091916	0.091149	0.094548	0.040117
σ	0.049281	0.028711	0.025326	0.026291	0.040889
Min	0.058330	0.052950	0.054538	0.065753	0.002214
25%	0.074281	0.072488	0.070237	0.075634	0.019272
50%	0.084530	0.083260	0.085130	0.086795	0.027337
75%	0.105167	0.103796	0.107094	0.103580	0.049757
Max	0.400476	0.193571	0.162345	0.211045	0.301388

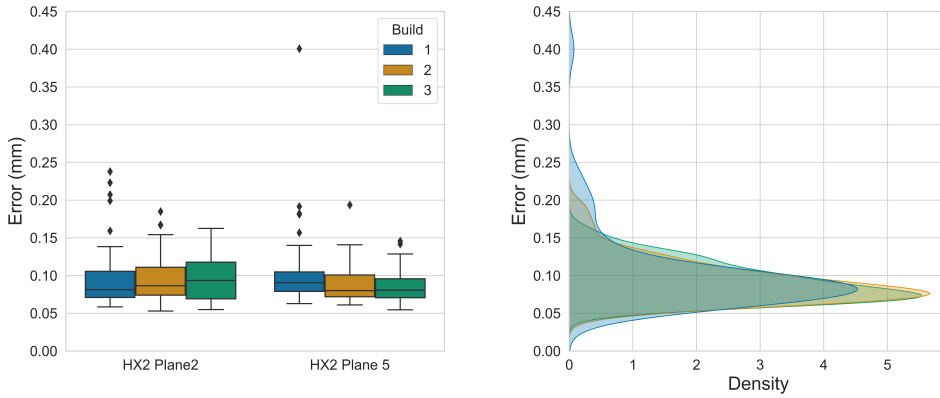

Figure 5.3: Variation in measured flatness error for vertical planes between the three builds. Boxplot (left) and kernel density estimation (right) illustrates the variation in measured error between builds and surfaces.

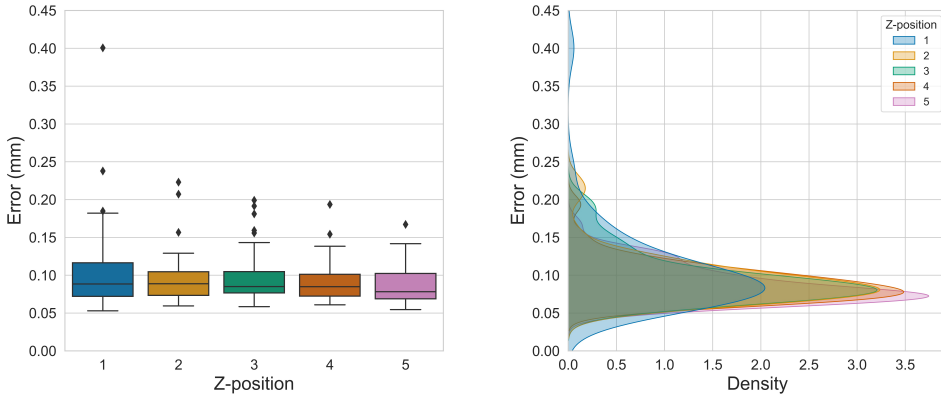

Figure 5.4: Variation in measured flatness error for vertical planes with z-position. Boxplot (left) and kernel density estimation (right) illustrate the variation in measured error between layers in the z-direction.

Table 5.3: Statistical data for part layers the in z-direction of the build space.

	Layer 1	Layer 2	Layer 3	Layer 4	Layer 5	Mean	Diff
n	54	54	54	54	54	–	–
$\bar{x}$	0.104644	0.093710	0.096776	0.089911	0.087698	0.094548	0.054769
σ	0.055572	0.031782	0.033028	0.025317	0.024961	0.024226	0.050230
Min	0.052950	0.059441	0.058330	0.060803	0.054538	0.063893	0.011309
25%	0.071951	0.073234	0.076536	0.072325	0.068809	0.078640	0.025433
50%	0.088348	0.088711	0.084912	0.084803	0.078242	0.087961	0.041132
75%	0.116436	0.104522	0.104658	0.101218	0.102372	0.110861	0.063584
Max	0.400476	0.222995	0.199056	0.193571	0.167091	0.176043	0.328619

Variation between positions

The experiment design enables the investigation of variation within the build space by analyzing the effect of position on the flatness of the vertical planes (planes 2 and 5 from HX2). The build layout is a matrix where a 3×3 grid is repeated in five layers in the build direction (see appendix B for details). A slight reduction in variation is observed with a higher z-position as visualized in figure 5.4. Table 5.3 tabulates the statistical data for the vertical planes at different layers in the z-direction.

The distributions appear to be comparable despite a minor reduction in variation in the z-direction. The situation is however rather different in the xy-plane. While the variation along the x-axis is relatively stable,

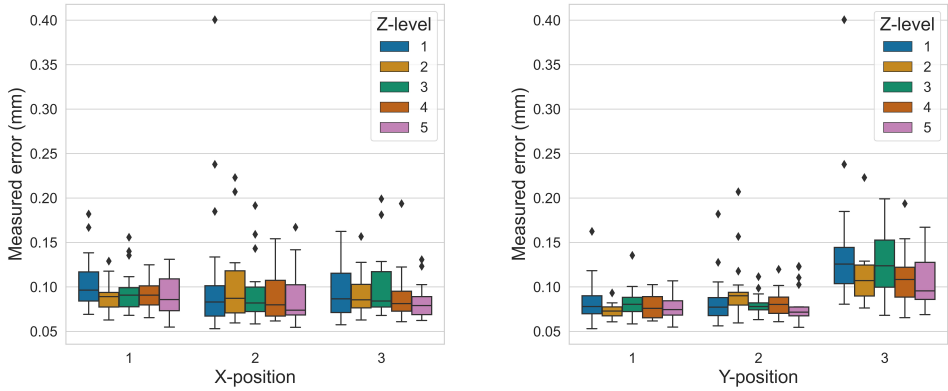

Figure 5.5: Variation in measured flatness error for vertical planes in the xy-plane. The left panel illustrates the variation along the x-axis of the build space, and the right panel visualizes the variation along the y-axis of the build space.

a clear difference is observed in variation along the y-axis as displayed in figure 5.5. Apparently, the rear of the machine experiences larger variations and generally poorer accuracy. This variation may constitute a significant noise factor for model creation and cannot be neglected. This variation along the y-axis can be verified with a T-test which confirms that the distributions are dissimilar with a probability of >99.9%.

5.1.2 Flatness

With 12 planes on 111 specimens, a total of 1332 flatness measurements was obtained. Because the 12 planes are designed as two hexagonal protrusions, their angle to the build direction takes many values. Figure 5.6 displays the unfiltered data for all orientations.

The results indicate major variations in achievable flatness with values ranging from 0.05 to 0.32 mm. However, closer examination of figure 5.6 reveals that there are orientations in which the flatness is bound to exceed 0.10 mm, while other orientations have a high certainty of obtaining values below 0.10 mm. By analyzing the data to determine achievable tolerances as best-case scenarios, orientations close to horizontal (both up-facing and down-facing) yield higher deviations and lower quality surfaces.

The plot in figure 5.6 exhibit close to symmetric results about the 90-degree mark. This indicates that up-facing and down-facing surfaces

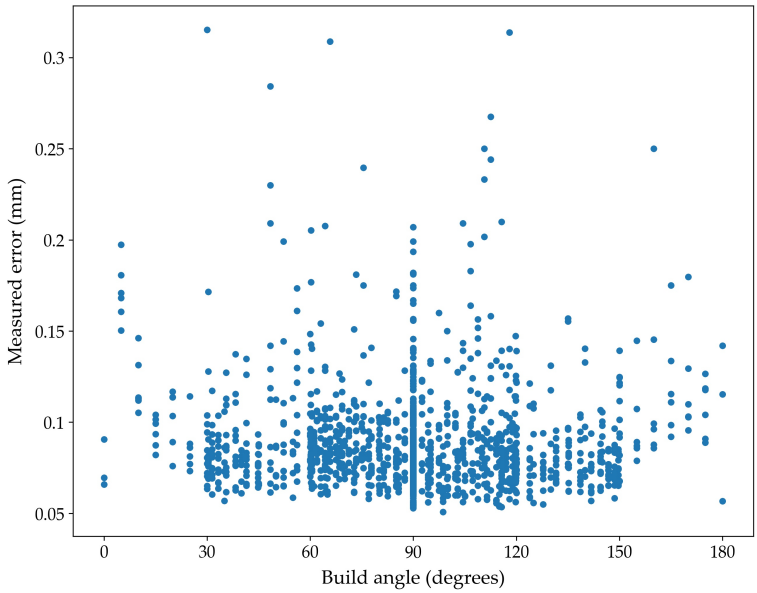

Figure 5.6: Measured flatness error for all orientations

are relatively similar in this context. However, a deviation from this pattern may be observed for orientations close to the horizontal where down-facing surfaces appear to achieve slightly better results on average.

5.1.3 Cylindricity

Valid data on cylindricity was obtained for all but one cylindrical feature, namely the cylindrical hole of 4 mm diameter. The results indicate variation between the different cylindrical features with some exhibiting a more clear trend than others. Figure 5.7 visualizes the results for each feature separately where the points indicate the measured error and the solid line indicates the mean value of the three replications. All plots exhibit symmetric behavior about the 90-degree mark where the cylinders are oriented perpendicular to the build direction.

A clear trend is visible in figure 5.7 where the cylindricity deteriorates as the cylinder rotates away from the build direction. Moreover, values below 0.10 mm are for most dimensions unrealistic for orientations above 60 degrees.

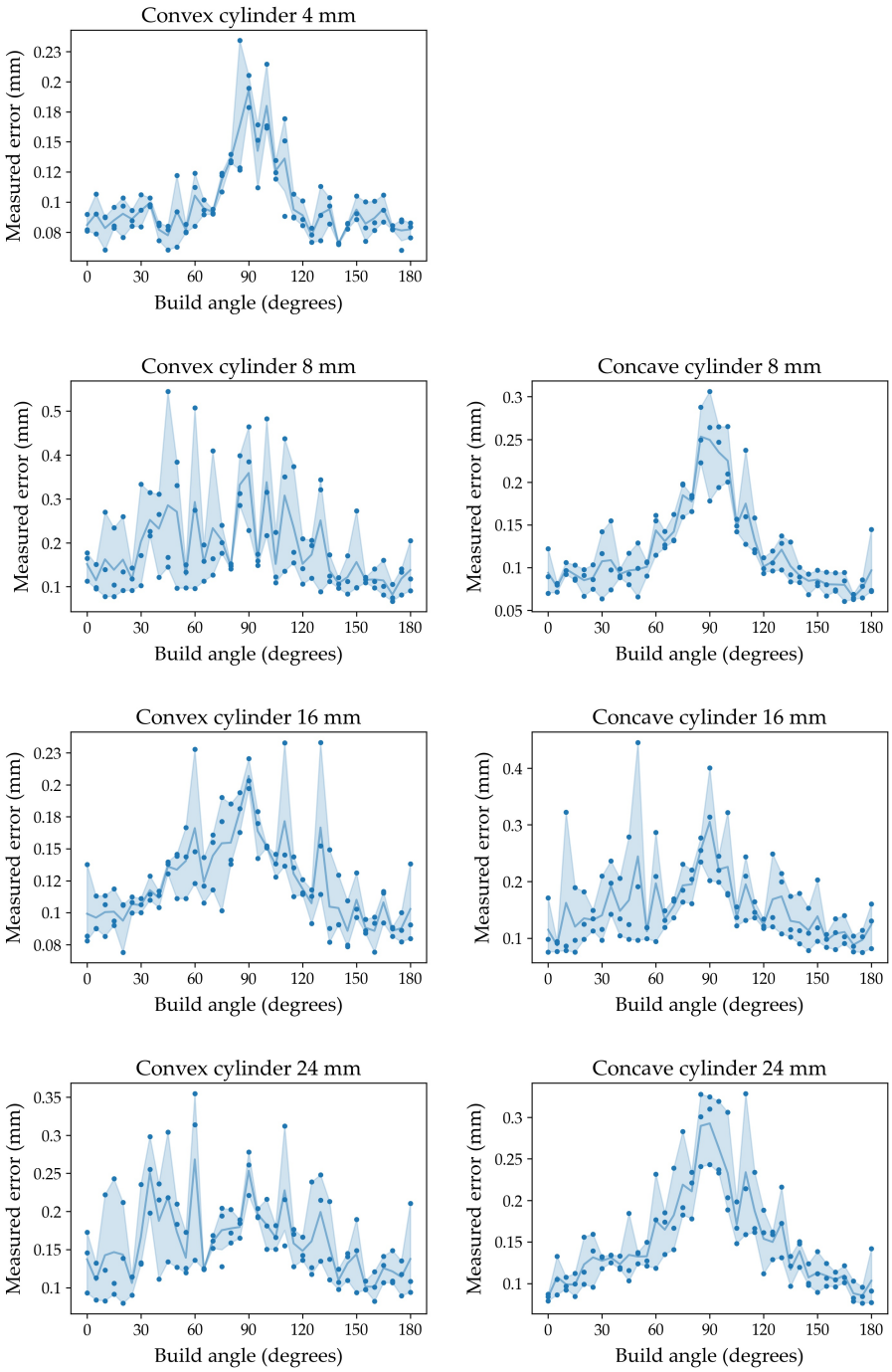

Figure 5.7: Measured cylindricity error for different cylinder types in all orientations.

5.1.4 Diameters

Similar to the data on cylindricity, measured diameters also vary between the different features as evident in figure 5.8. The clearest correlation between orientation and diameter can be observed for the 4 mm convex cylinder where the dimensions seem to increase when the cylinder is oriented perpendicular to the build direction. Generally, the convex cylinders appear to be larger than nominal dimensions, while the concave cylinders (holes) are smaller than designed. This effect may be caused by residual powder that ultimately causes measurements to yield larger dimensions than the actual geometry.

All but one dimension exhibit some correlation between orientation and dimensional deviations, namely the 16 mm diameter concave cylinder. This feature appears to have little to no effect from orientation but is also subject to large variations that could diffuse any underlying patterns. The plots in figure 5.8 indicates that orientation may cause deviations up to 0.3 mm from vertical to horizontal orientation.

5.1.5 Other data

The experiment was designed to generate a large amount of data on all the relevant AM features (as introduced in subsection 2.2.3). Flatness and cylindricity errors were of primary interest, and diameters were also readily available from these inspections as detailed above. However, the experiment included many other characteristics evaluated with varying success. The following subsections describe the additional data retrieved from the experiment and discuss the validity of the data.

Cones

Four conic shapes were inspected; two concave and two convex. The apex angles were estimated from the measured points, but the software consistently evaluated to zero deviation between nominal and actual value. This is obviously incorrect and data regarding cones are invalid. This error may be due to inadequate or unsuitable inspection strategy, or that the software for any other reason is unable to calculate the apex angle from the available data. Regardless, this data is not further considered in this study.

Spheres

One convex- and one concave quarter-sphere was included in the experiment. These spheres were evaluated for roundness and diameter by

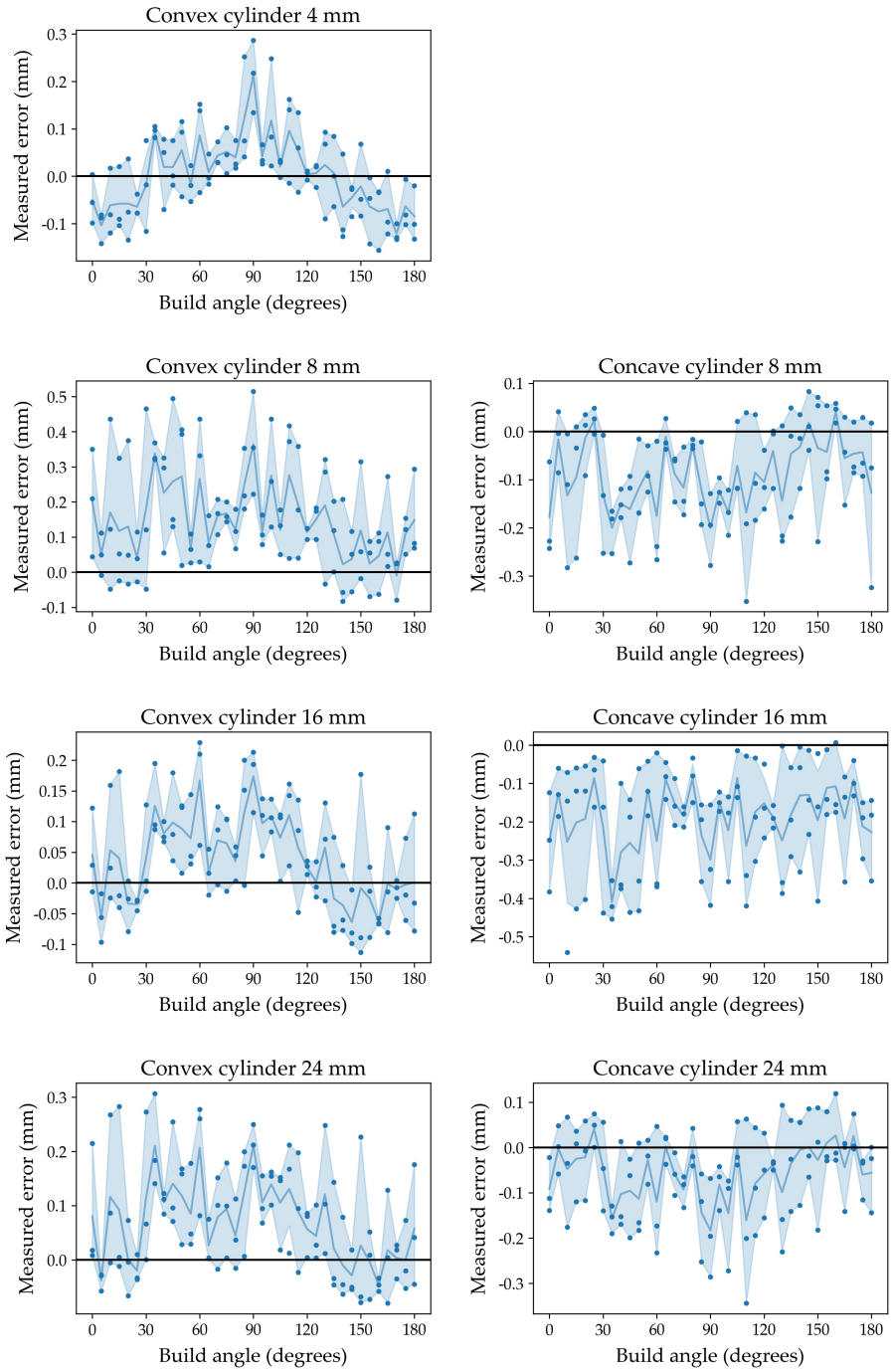

Figure 5.8: Measured diametrical error for different cylinder types in all orientations

inspecting three meridian paths. However, these data were also free from errors and therefore rendered invalid for the present study.

Positions

The positions of the various features on each specimen were recorded. This was intended to enable an analysis of positional accuracy. However, due to difficulties in defining a stable origin in the base alignment, the positional data for a single feature cannot directly be compared between specimens. This is because the coordinates of the positions are defined relative to an origin that may move from one specimen to the next. On the other hand, all positions on one specimen are recorded relative to the same origin. Hence, relative positions are still valid but require some further data processing before analysis is meaningful.

Parallelism

Parallelism is a measure of how surfaces are oriented relative to each other. This characteristic was pairwise applied to the planes of the hexagonal protrusions. The data for parallelism has however not yet been analyzed but appears to have yielded valid results.

Coaxiality

Cylinders that share the same axis may be inspected for coaxiality, i.e. the extent to which they share the same axis. For this characteristic, the axis of one cylinder is used as the datum to which the other axis is compared. This characteristic has been applied pairwise to the cylinders of the artifact. Concave and convex cylinders are kept separate and characteristics involving the smallest concave cylinder were rendered invalid because inspections could not be performed in a consistent manner.

5.2 Empirical models

Optimization of part build orientation is based on the idea that the build direction is detrimental to the end result. The analysis in section 5.1 indicates a clear correlation between the two, however, details on *how* the accuracy is affected by part build orientation require further investigation. In order to predict the result, one can apply theoretically derived models such as the ones developed by Paul and Anand [29], [117] or Arni and Gupta [27]. However, just as all models are wrong [118], so are these theoretical models. More precise predictions may be acquired from experimental data if modeled appropriately [70], but these must also be verified. This section is dedicated to the development of empirical

models from the experimental data.

Because the characteristics are affected differently by part build orientation, this section contains separate sections for each relevant characteristic, i.e. subsection 5.2.1 concerns the modeling of cylindricity, and subsection 5.2.2 is devoted to the modeling of flatness. Each section contains the entire procedure for developing and validating the models separately, including concluding remarks on their viability.

The Python ecosystem is utilized to analyze the data and evaluate the fitness of models from the literature. The models are created through four phases:

1. Visualize and filter data
2. Compare data to existing models
3. Fit new expression to data
4. Evaluate the new model

The actual implementation is of course more organic than what the list above implies. Iterating between filtering and visualization is necessary to evaluate the appropriateness of filter parameters. These parameters may also have to be re-visited at later stages for sensitivity analysis etc. Furthermore, the exact route may differ from one model to the next depending on the intricacy of the phenomenon and the correctness of initial assumptions. The following sections reflect this exploratory approach and describe the journey from initial analysis through observations to enlightenment.

5.2.1 Modeling cylindricity

This section describes the modeling of cylindricity in detail. The following subsections deal with each of the phases outlined above successively.

Visualize and filter cylindricity data

Following the outlined progression, the first step is to visualize and filter data. Figure 5.9 contain a plot of unfiltered data for cylindricity, i.e. both convex and concave cylinders in all dimensions.

Even though a clear trend is observed in the cylindricity data, the noise imposed by outliers can disrupt the modeling process. Closer examination reveals that the deviation observed in these points is a systematic

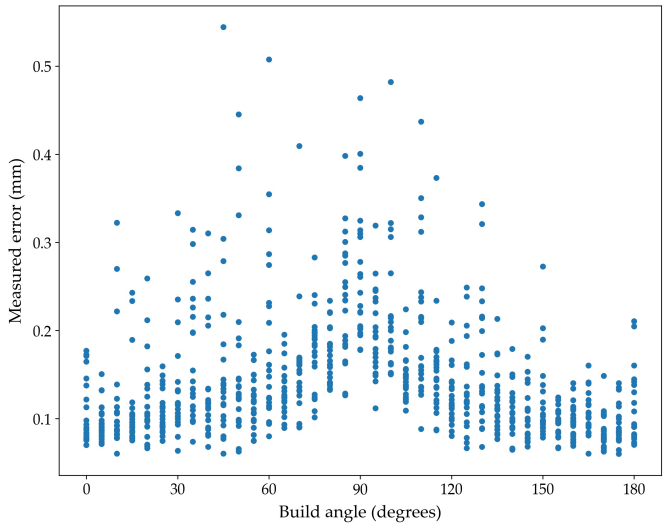

Figure 5.9: Measured cylindricity error for all orientations.

deviation, and the product of two factors: (i) the cylinders closest to the base plate of the artifact, and (ii) the rear of the machine. This is visualized in figure 5.10 where data from these particular cylinders are highlighted and clearly stand out from the overall population. A possible explanation for this deviation is that powder adheres more to these cylinders, making the powder harder to remove. The increased adherence may be due to higher surface roughness in the rear of the machine or other factors influencing powder adherence. The reason remains to be investigated, but regardless, results in larger deviations in these cylinders, warranting their exclusion.

After the systematic sources of error have been eliminated, the random sources of error may be addressed. The symmetry about the $90°$ mark is exploited to obtain a better foundation for calculating means and standard deviations. The filter eliminates data points that exceed three standard deviations (3σ) for each orientation when mirrored about the $90°$ mark (e.g. $45°$ and $135°$ are considered as one orientation). The application of this filter eliminates another two data points from the dataset as illustrated in figure 5.11 which is now cleaned and ready for the next phase.

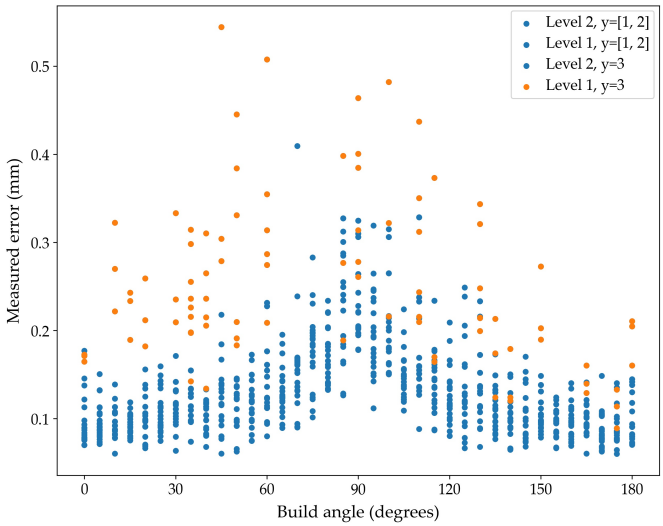

Figure 5.10: Cylindricity data when filtering for systematic sources of error. The orange points indicate the cylinders close to the build plate of artifacts fabricated in the rear of the build space (y-position = 3).

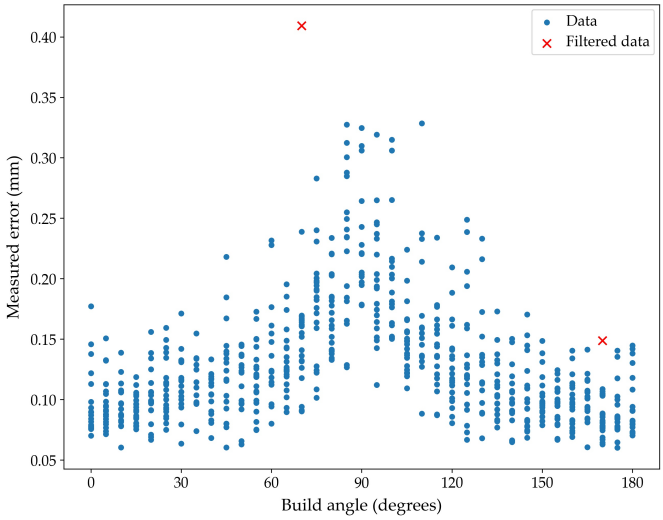

Figure 5.11: Cylindricity data when filtering for random sources of error. The threshold is 3σ in both directions for each orientation. Red crosses indicate data points that are filtered out,

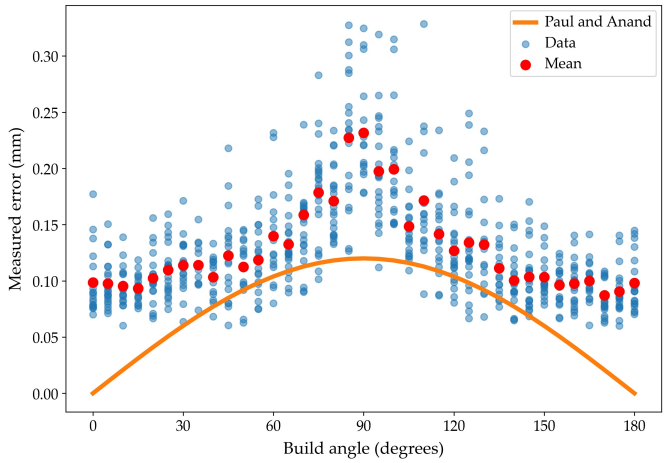

Figure 5.12: Theoretical model from [29] relative to experimental data.

Compare existing models to cylindricity data

The second step is to compare existing models to the experimental data. Paul and Anand [29] theoretically derived the cylindricity error ε_{cyl} from the staircase effect. They modeled the staircase effect as a function of the layer thickness Δz and the angle θ to the build direction as follows:

$$\varepsilon_{cyl} = \Delta z \cdot \sin(\theta) \tag{5.1}$$

By inserting 0.12 mm for Δz (the layer thickness employed for the experiment), the curve of figure 5.12 is produced. It is clear that the model is – at least in its original form – ill-suited for this experimental data. However, because the theoretical model is general in the sense that the peculiarities of specific applications are neglected, a closer investigation of equation 5.1 is necessary before the model can be disregarded.

A parameterized version of equation 5.1 can be written as

$$\varepsilon_{cyl} = a \cdot \sin(\theta) + b \tag{5.2}$$

where a and b are parameters that can be used for curve fitting with SciPy [113]. For this purpose, the data is first filtered by 3σ for each orientation before fitting equation 5.2. This yields an approximate value of 0.096 for a and 0.081 for b, and is displayed in figure 5.13.

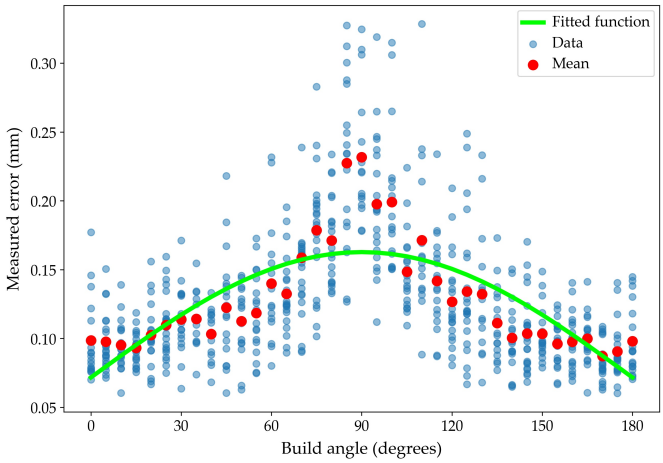

Figure 5.13: Equation 5.2 fitted to experimental data.

The fitted line in figure 5.13 however still exhibits a poor fit as the general shape of the line doesn't seem to follow the data. This is also clear from the R^2 value of 0.614, and the shape misfit is also clear from figure 5.14(b).

Another model for cylindricity was presented by Senthilkumaran, Pandey and Rao [70] (see equation 3.3). This model is experimentally derived, but yet it fails in predicting the cylindricity. Despite the high effort in fitting the model to the experimental data, no version appears to come close to the observed deviations as displayed in figure 5.15.

Fit new model to cylindricity data

At this point, we reject the existing models and venture to develop a new model to better assimilate the experimental data. An observation can be made that the data seem to follow an altered sine curve. A sine curve can be parameterized for curve fitting as follows:

$$\varepsilon_{cyl} = a \cdot \sin^b(\theta) + c \tag{5.3}$$

Curve fitting with SciPy is once again performed, this time on equation 5.3 by inserting 0.1 for c as an initial estimate based on the earlier plots. The curve fitting estimates a to 0.101 and b to 3.637 which yields the curve displayed in figure 5.16.

The result is much more satisfactory, but it appears that a more steep

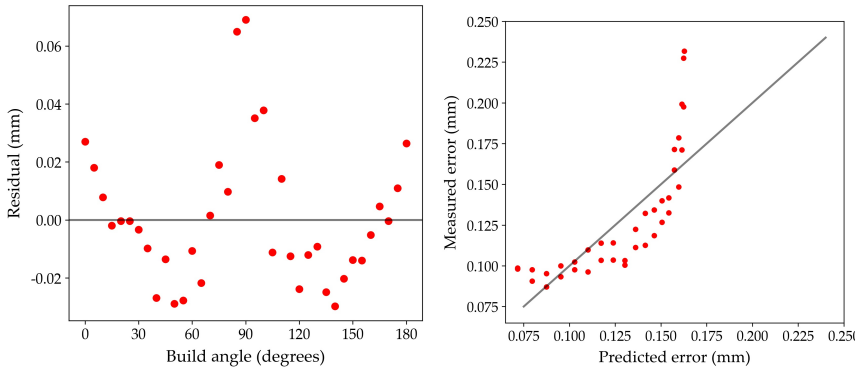

(a) Residual plot **(b)** R^2 plot

Figure 5.14: Plots for evaluating the fitted version of equation 5.2.

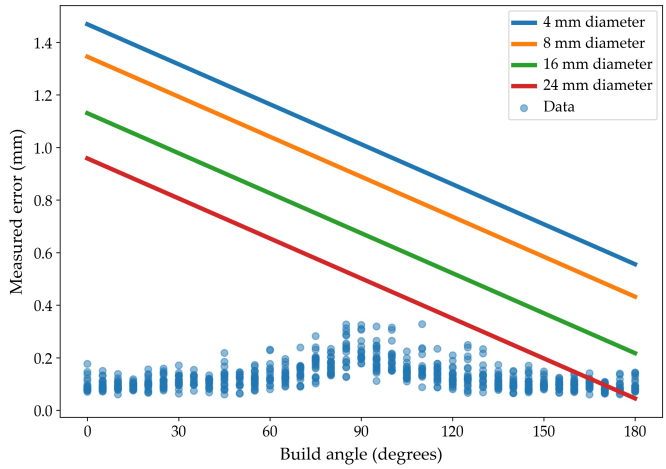

Figure 5.15: The model proposed in [70] (equation 3.3) for the relevant dimensions.

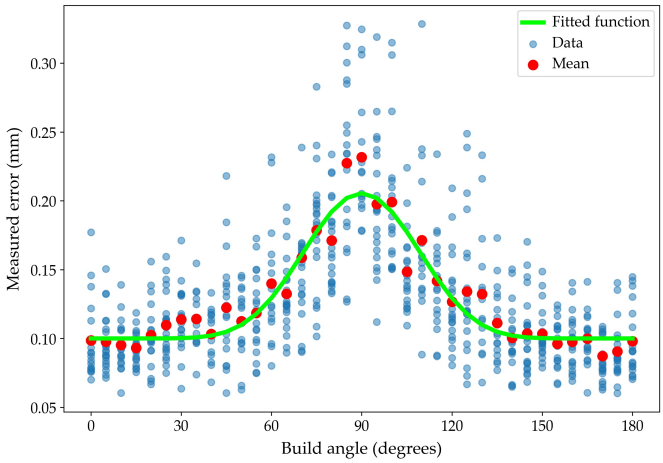

Figure 5.16: Equation 5.3 fitted to experimental data.

top at 90 degrees should be achieved. The R^2 value is also slightly better at 0.910, but the shape of the curve is still not entirely correct as visible in the R^2 plot of figure 5.17(b).

One method for achieving the steep top required to assimilate the data around 90 degrees is to formulate the expression as a quotient. The following parameterized quotient is developed for curve fitting:

$$\varepsilon_{cyl} = \frac{a}{\text{abs}\left(\theta - \frac{\pi}{2}\right) + b} + \frac{\Delta z}{2} \tag{5.4}$$

where Δz is the layer thickness which for the experimental data is 0.12 mm. With this formulation, the curve fitting of SciPy arrives at the approximate values of 0.063 and 0.347 for a and b respectively. The curve for equation 5.4 is plotted in figure 5.18.

Evaluate the proposed cylindricity model

The final step involves the evaluation of the proposed model. This entails both a qualitative assessment of the curve shape and assimilation of the model and also a quantitative evaluation of the model's fitness. The developed model for cylindricity achieves an R^2 value of 0.943 which is a significant improvement from the other evaluated models as compared in table 5.4.

Note that a relatively small improvement is observed from the sine model

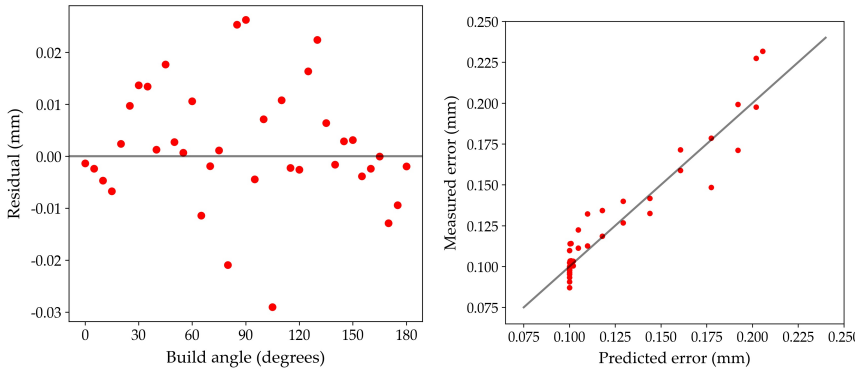

(a) Residual plot **(b)** R^2 plot

Figure 5.17: Plots for evaluating the fitted version of equation 5.3.

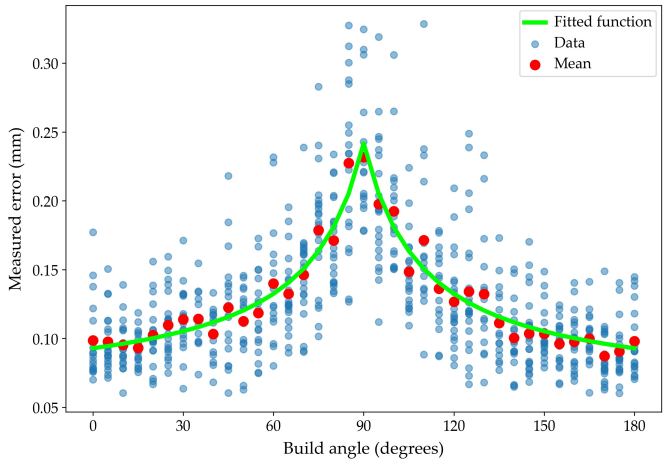

Figure 5.18: Equation 5.4 fitted to experimental data.

Table 5.4: Comparison of R^2 values for the evaluated cylindricity models.

Model	R^2
Senthilkumaran, Pandey and Rao [70]	0.001
Paul and Anand [29]	0.614
Sine curve (equation 5.3	0.910
Quotient curve (equation 5.4)	0.943

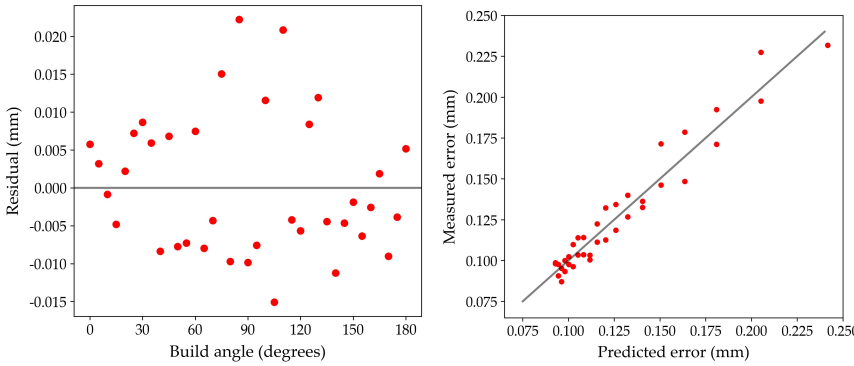

(a) Residual plot **(b)** R^2 plot

Figure 5.19: Plots for evaluating the fitted version of equation 5.4.

to the final quotient model. These models are relatively similar in shape which may explain similar R^2 values. The largest differences between the two models relate to the shape of the curve around the vertical and horizontal orientations where the sine model yields a flat curve at these orientations, whereas the quotient curve is steep at the horizontal orientation, and also slightly inclined even close to vertical orientations. Apparently, this minor difference does assimilate the experimental data slightly better.

Figure 5.19(b) displays the R^2 plot for the proposed model with respect to the mean values from each orientation. This visualization shows two important characteristics of the proposed model:

1. There are no apparent patterns in the deviations between predicted and observed values; and

2. The magnitude of the deviations are comparable regardless of the magnitude of the predicted values.

These characteristics are hallmarks of good fitness, and the model may be considered appropriate. Higher R^2 values may be attainable, but could also risk over-fitting as random variations always will be present in real data.

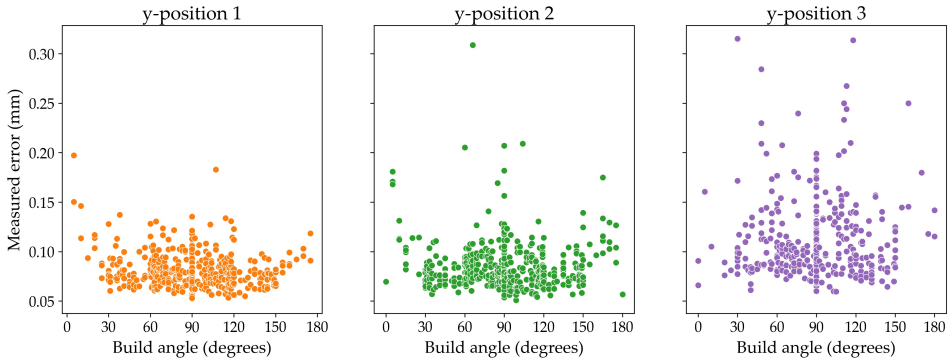

Figure 5.20: Flatness data at different y-positions. y-position 3 exhibit substantially larger variations compared to positions 1 and 2.

5.2.2 Modeling flatness

The modeling of flatness may be conducted following the same procedure as for cylindricity. The following sections detail the evaluation of existing models, and the creation of a new empirical model for flatness in LB-PBF/P.

Visualize and filter flatness data

As described in section 5.1, the test artifact contains twelve planes in different orientations. As the artifact is rotated about the x-axis, these planes will give data pertaining to many more than just the 37 orientations of the artifact, but rather a total of 85 different orientations. This results in a rather dense population of data points around the 90° mark, and more sparsely populated areas around the horizontal orientation which is only covered by two planes (one up-facing and one down-facing surface). This is apparent in figure 5.6 where the flatness of all planes is plotted without any filtering.

It is clear from the modeling of cylindricity that the rear positions may be subject to larger variations compared to the center and front. Contrary to the cylinders, however, all the planes extend from the base plate of the artifact and, therefore, no discrimination can be made between the planes in this regard. Figure 5.20 show that the rear of the machine does indeed yield larger variations than the front. These data points are therefore excluded from further analysis to facilitate the creation of clear models. This reduces the population by 27%, leaving 972 data points after this initial filtering.

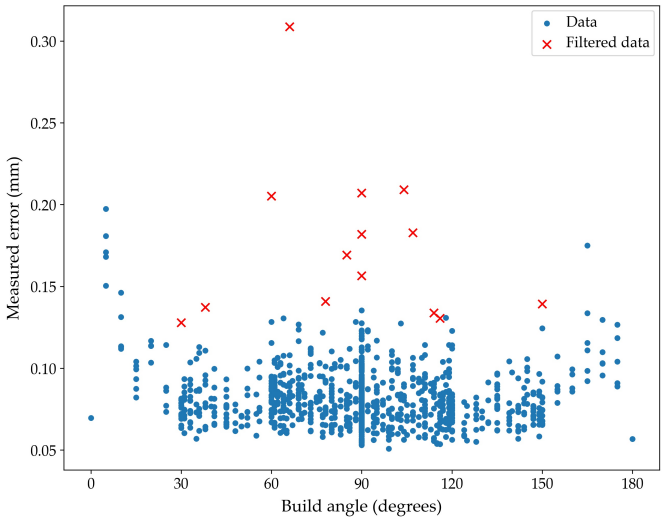

Figure 5.21: Filtered flatness data. The red crosses (n=14) indicates the eliminated data points, whereas the blue points (n=958) constitutes the remaining data points.

The same filtering strategy from cylinders is applied also to the flatness data, i.e. eliminating observations exceeding 3σ. As this filtering is more effective with larger populations, the assumption is made that orientations within five-degree intervals have a comparable effect on flatness. This results in the elimination of 14 data points from the population of 972 as displayed in figure 5.21.

Compare existing models to flatness data

Arni and Gupta [27] derived a conditional expression for flatness error based on the theoretical staircase effect (see equation 3.1). Initially, no data is available for δz nor δxy. Nevertheless, by assuming a perfect process with a layer thickness of 0.12 mm, figure 5.22 is produced.

The model appears not to assimilate the data very well without the terms for δz and δxy. Since these error terms are unknown for the machine used in the experiment, these terms are used for the curve fitting procedure in SciPy which yields the approximate values of -0.07 and 0.07 for δz and δxy respectively. This yields the curve in figure 5.23 which appears to follow the data more closely, but still fails to capture the true form of the data and achieves an R^2 value of 0.188.

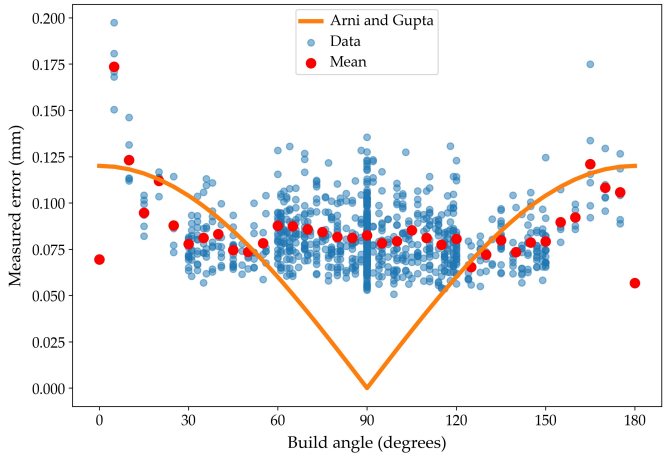

Figure 5.22: Theoretical model from [27] relative to experimental data.

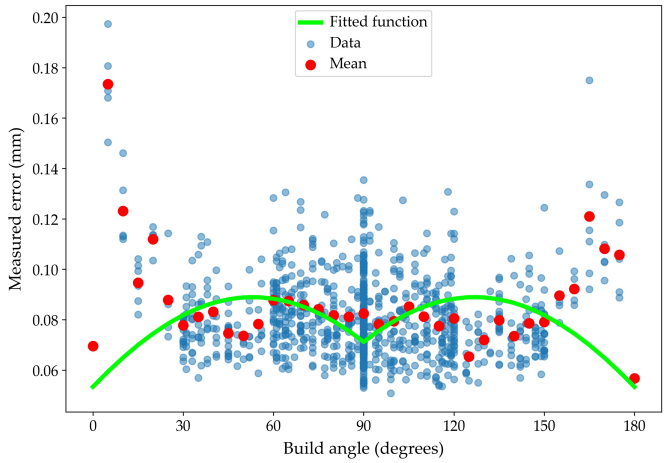

Figure 5.23: Equation 3.1 fitted to experimental data.

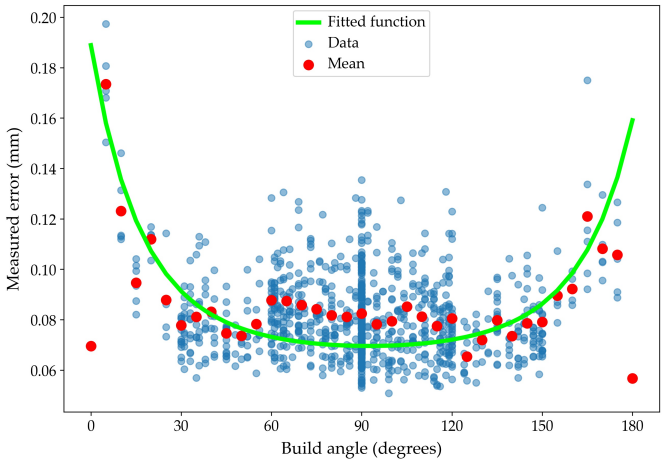

Figure 5.24: First curve fitted to data

Fit new model to flatness data

Visual inspection of the mean values indicate a relatively symmetric curve about the $90°$ mark with exponential growth towards the horizontal orientations. Based on this observation, the following expression can be used as a starting point:

$$\varepsilon_{flatness} = b \cdot e^{\theta - \frac{\pi}{a}} + \frac{\Delta z}{2} \tag{5.5}$$

where a and b are parameters for curve fitting, Δz is the layer thickness, and θ is the build angle. This yields the curve in figure 5.24. However, this curve achieves an R^2 value of 0.175 which is lower than the theoretical model of Arni and Gupta [27] as displayed in figure 5.23. This may be explained by the large predictive errors of equation 5.5 at horizontal orientations where the measured flatness error is low. This can be mitigated by a conditional statement to yield different results at these orientations as:

$$\varepsilon_{flatness} = \begin{cases} \frac{c}{2} & \text{if } \theta = 0 \text{ or } \pi \\ b \cdot e^{(\theta - \frac{\pi}{a})} + \frac{c}{2} & \text{if } 0 < \theta < \pi \end{cases} \tag{5.6}$$

where a and b are parameters for curve fitting, c is the layer thickness, and θ is the build angle. The predictions from equation 5.6 is plotted

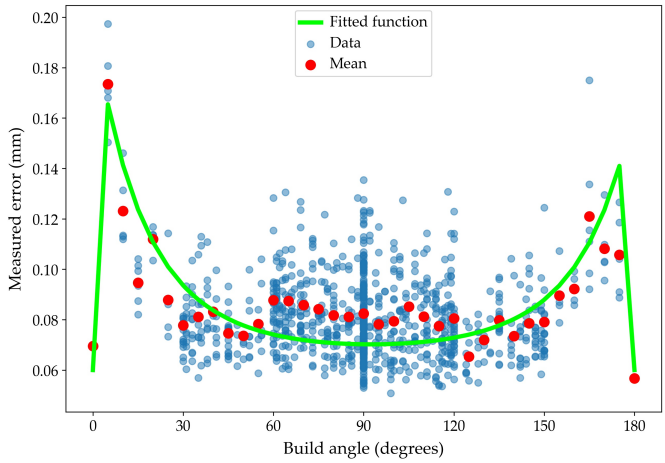

Figure 5.25: Second curve fitted to data

in figure 5.25 together with the filtered experimental data. The minor change from equation 5.5 to 5.6 results in a drastic increase in R^2 from 0.175 to 0.749. However, there are still some deviations between predicted and measured values, particularly in the region from $60°$ to $120°$, and in the values close to $180°$.

Equation 5.6 can be further adapted to the experimental data by introducing additional conditions. This is explored in the following expression where the orientation space is segmented into five regions:

$$\varepsilon_{flatness} = \begin{cases} a & \text{if } \theta = 0° \\ a + \frac{b}{\theta} & \text{if } 0° < \theta < 60° \\ 1.5a & \text{if } 60° < \theta < 120° \\ a \cdot e^{b(\theta - 120°)} & \text{if } 120° < \theta < 180° \\ a & \text{if } \theta = 180° \end{cases} \tag{5.7}$$

This expression is fitted to the experimental data with SciPy, and the resulting curve is plotted in figure 5.26. Evidently, the curve assimilates the data much better and an R^2 value of 0.893 is achieved.

Evaluate the proposed flatness model

The previous subsection successively devises three new models for flatness error based on the experimental data. Table 5.5 compares the

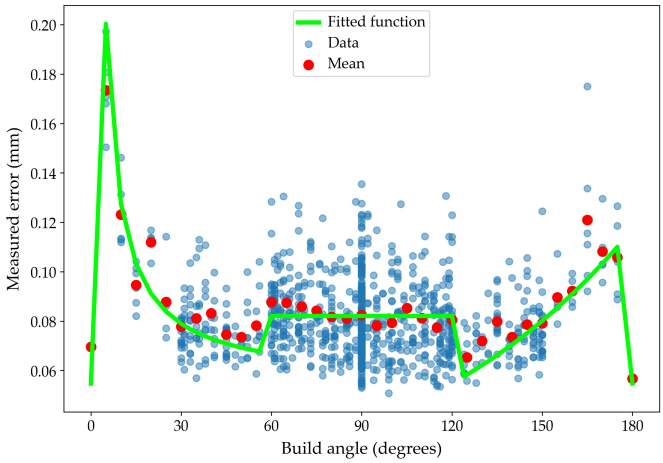

Figure 5.26: Third curve fitted to data

Table 5.5: Comparison of R^2 values for the evaluated flatness models.

Model	R^2
Arni and Gupta [27] (fitted)	0.188
1st fitted model (equation 5.5)	0.175
2nd fitted model (equation 5.6)	0.749
3rd fitted model (equation 5.7)	0.893

performance of the three proposed flatness models and the one theoretical model found in the literature.

The theoretical model of Arni and Gupta [27] displays poor fitness to the data even after curve fitting. The residual plot in figure 5.27(a) displays large fluctuations with increasing build angle, indicating disharmony between the shape of the predicted curve and the measured values. The accompanying R^2 plot in figure 5.27(b) also reveals large deviations between predicted and measured values.

The proposed model in equation 5.6 exhibit much better performance in terms of deviations between predicted and measured values. The residual plot in figure 5.28(a) display not only closer similarity to the curve of the data but also smaller absolute deviations compared to those in figure 5.27(a). This is reflected in a much improved R^2 value, and an R^2 plot where the predicted values follow the diagonal more closely (see figure 5.28(b)).

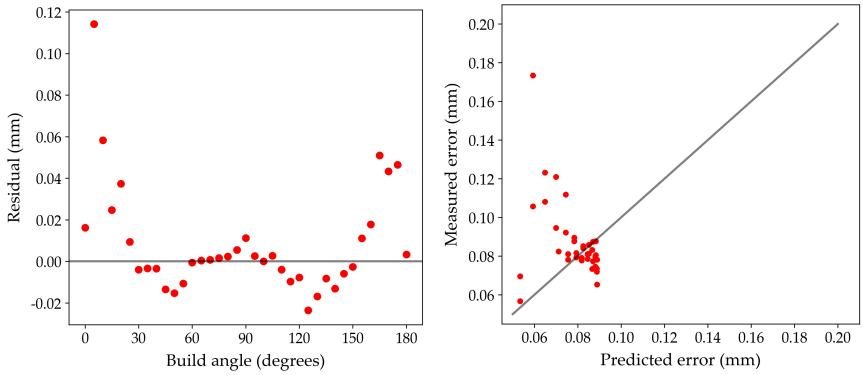

(a) Residual plot **(b)** R^2 plot

Figure 5.27: Plots for evaluating the fitted version of equation 3.1.

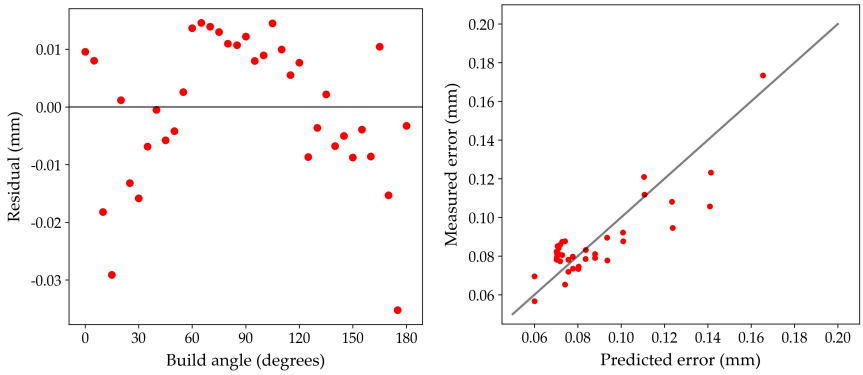

(a) Residual plot **(b)** R^2 plot

Figure 5.28: Plots for evaluating the fitted version of equation 5.6.

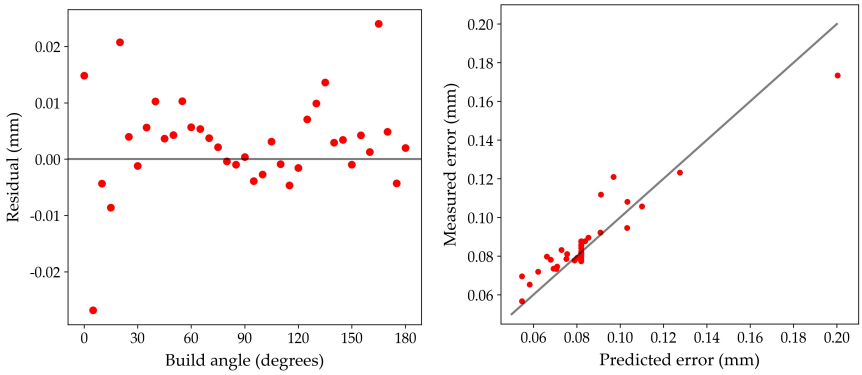

(a) Residual plot **(b)** R^2 plot

Figure 5.29: Plots for evaluating the fitted version of equation 5.7.

Finally, the model in equation 5.7 seems to assimilate the experimental data better than both of the previously assessed models. The residual plot in figure 5.29(a)shows no clear patterns with small absolute deviations from measured data, and the accompanying R^2 plot in figure 5.29(b)follows the diagonal line closely. While these results may indicate good model fitness, they can also be a sign of overfitting. As the models become increasingly complex, and more effort is put into fitting the curve to experimental data, the more tailored the model becomes. Consequently, the resulting model may prove invalid for later data and be rendered useless in practical applications. This is further discussed in chapter 6.

5.3 A flexible method for optimizing part build orientation

This section investigates RQ3 and proposes a deterministic method for optimizing part build orientation as described in paper P6. The investigation of RQ3 as presented in this thesis is supported by the four papers P1–P4 that shed light on various aspects of the problem. The following sections first describe the background and fundamentals before the proposed optimization method is presented. Finally, the method is placed in a larger context where its implementation in a digital pipeline is outlined with accompanying implications for a real-world application.

5.3.1 Preliminaries

The optimization of part build orientation is necessarily based on the geometry of the part to be produced. However, as this geometry oftentimes

is only available in the rather primitive STL file format, the deduction of local topology provides crucial information for any optimization scheme. Paper P4 proposes a rule-based approach to the problem by geometric reasoning. This approach provides a deterministic solution to the feature recognition problem and enables the vectorial definition of part features.

Without the knowledge of part features, every single facet of the STL file must be considered for optimization. This is both cumbersome and time-consuming as the number of facets may exceed 10,000 even for simple geometries. Conversely, the facets can effectively be bundled together to form geometric primitives with known behavior for all build directions. In this way, the 10,000 variables are reduced to only a fraction without compromising the reliability of the method. The evaluation of geometric primitives may improve the effectiveness compared to the direct method as better informed and more nuanced decisions can be made.

Deterministic optimization of part build orientation can be achieved in several ways. The most primitive way is perhaps the exhaustive search in which the geometry is rotated in fixed intervals about predetermined axes. The solution is then evaluated according to an objective function for each incremental rotation and compared to the current best solution. This procedure is demonstrated in paper P2 where intervals of 1° about both the x- and y-axis are used, resulting in a total of 64,800 function evaluations for each feature.

The exhaustive search method described in paper P2 suffer from three distinct shortcomings: (i) the magnitude of intervals determine the accuracy of the results; (ii) only orientations at certain intervals from the initial part build orientation is evaluated; and (iii) the number of function evaluations increases drastically with increased geometric complexity and resolution of the search grid.

5.3.2 Proposed optimization method

When the effect of part build orientation on quality is mathematically described, this can be used as input in an optimization scheme. Paper P6 [119] presents a flexible method for optimizing part build orientation based on mathematical models. The progression of the method is illustrated in figure 5.30 where two inputs are required: (i) vectorial representations of part features, and (ii) mathematical models describing the impact of part build orientation on these features. Consequently, this approach enables the deterministic optimization of part build orientation

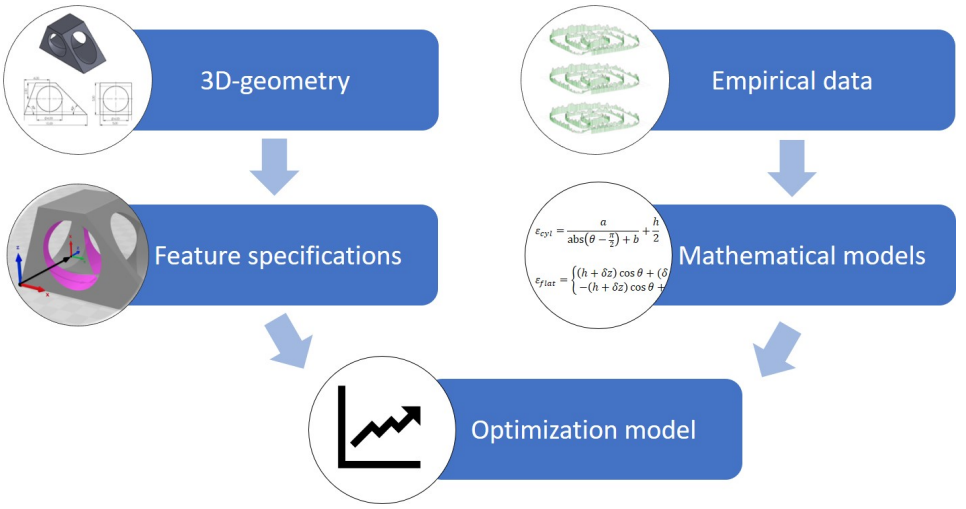

Figure 5.30: Illustration of the proposed method for part build optimization.

in an automated fashion.

The presented method can be applied for a multitude of different objectives but is here demonstrated for the optimization of part build orientation for improved geometric accuracy using vectorial definitions of features. Such representations of part features are readily available in CAD models, but can also be extracted from a surface mesh as described in paper P4 [120]. Generally, the method can be applied to any 3D geometry of any origin as long as the mathematical models are constructed to handle the data type.

The mathematical models can be theoretically derived such as those found in the literature (e.g. [26], [27], [29]), or they can be developed from empirical data as described in section 5.2 and [70]. How the models are acquired is of no importance, but will determine the validity of the model and consequently the validity of the optimization scheme. The case studies presented in paper P6 make use of theoretically derived models based on the orientation rules defined by Frank and Fadel [61] which coincidentally yield a model similar to that of Paul and Anand [29] for cylindricity.

When feature specifications have been acquired, and mathematical models for these geometric features are available, an aggregated mathematical model can be constructed. Consider for instance a part P consisting of a finite set of features $P = \{F_1, F_2, \ldots, F_n\}$ where each feature may be

a different type and size. If a mathematical description of the relationship between feature quality and build direction is available, the quality of the entire part can be expressed as a function of part build orientation as follows:

$$Q_{part} = \frac{\sum_{i=1}^{n} Q_i A_i}{A_{part}} \tag{5.8}$$

where n is the number of features, Q_i and A_i is the quality and area of the ith feature respectively, and A_{part} is the total surface area of the part.

This particular formulation prescribes a weight factor to each feature relative to the surface area of that feature. This can naturally be adjusted for particular applications – perhaps equal weights are more appropriate, or a manual priority should be implemented. Nevertheless, this allows for deterministic, robust optimization of part build orientation in a continuous solution space by identification of critical points where

$$\frac{\partial f}{\partial x} = \frac{\partial f}{\partial y} = 0 \text{ or undefined} \tag{5.9}$$

Each critical point will in this case constitute a candidate orientation that is evaluated relative to the objective function for identification of maximum and/or minimum. This mathematical approach also enables the identification of feasible regions for subsequent optimization of secondary objectives such as mechanical properties or packing density of the build space. The method is demonstrated on two case studies in paper P6 where simple mathematical functions are derived from literature. Naturally, more reliable results are obtained by utilizing empirical models such as those developed in section 5.2. This is, however, left for future work and further discussed in chapter 6.

5.3.3 Optimization of part build orientation in a larger context

The proposed method for the optimization of part build orientation can be implemented in a digital pipeline for quality assurance in AM. The method offers flexibility in terms of input geometry and evaluation of quality which grants applicability beyond LB-PBF/P given the right mathematical formulations. Moreover, the traceability to part features can extend to tolerancing either in input as requirements, or output as

feasible orientation zones. The application of tolerances to STL files has been discussed in paper P3 where the possibility of an uninterrupted digital pipeline from CAD model to part qualification is outlined.

The automation of processing stages is an important step towards mass customization and large-scale production in AM. The proposed method provides a deterministic method for identifying the optimum in a continuous solution space.

Chapter 6

Discussion

This chapter aims to give explicit answers to the RQs posed in section 1.2 and to discuss the implications of the findings. To this end, one section is dedicated to each of the RQs. Finally, the external validity and relevance are discussed in section 6.4.

6.1 Discussion on RQ1

RQ1 *How can experiments in LB-PBF/P be designed in a robust manner?*

Variation control is complicated enough in a manufacturing setting, much more so in research experiments. This project involves a carefully planned and executed experiment with a particular focus on dealing with the inevitable inherent variation of LB-PBF/P. Valid results are achieved by employing blocking and randomization strategies as described in section 4.4. These strategies enable the characterization of variation within and between builds as detailed in paper P5 [101].

The orientation of the manufactured artifacts was the only independent variable in the experiment. The decision to keep all other parameters constant was made to maximize the probability of generating reproducible results that could yield valid empirical models. This greatly improves the reliability of the results and facilitates the subsequent data analysis and model development. This decision constitutes a trade-off between experiment utility and -reliability where a decision was made to rather get small amounts of valid data rather than large amounts of invalid data.

Three builds were required to achieve the desired robustness of the experiment. Variation between builds introduces noise in the generated data. The analysis of variation between the builds is therefore crucial to account for this variation and argue for the valid comparison of builds. However, this robustness comes at a cost. The realization of three full builds is relatively expensive in terms of the required material, energy, and the depreciation of the machine. Alternatively, the extra space spent on keeping all three builds as identical as possible could have been used to produce additional specimens which would have increased the utility of the builds. Again, this decision is made on the grounds that small amounts of valid data are far more valuable than large amounts of invalid data.

The analysis is provided in paper P5 [101] confirms that the experiment design has generated valid data from which the effect if part build orientation can be determined. Not only does this experimental setup allow variations to be characterized, but it also allows for variations within and between builds to be captured and accounted for. The results indicates that the characterization is indeed warranted as variations was observed in the xy-plane while the z-direction was rather stable. This observation is in line with previous research [51], [77], [78]. The large number of levels utilized in this experiment may be overly cautious, but revealed behaviors not included in previous models. The proposed method for robust experiment design in LB-PBF/P is a contribution towards valid experiments in AM, and further work is required to develop general rules for experimental design.

6.2 Discussion on RQ2

RQ2 *How does part build orientation affect the geometric accuracy of primitive shapes?*

This RQ concerns several different shapes as described in appendix A, hence separate discussions are warranted. The following subsections discuss the findings for cylinders and planes separately before additional findings are discussed in subsection 6.2.3.

6.2.1 Cylindricity

Previous studies on the effect of part build orientation on cylindricity have presumed a certain relationship between the two. However, the analysis presented in section 5.2 reveals a rather different pattern. This

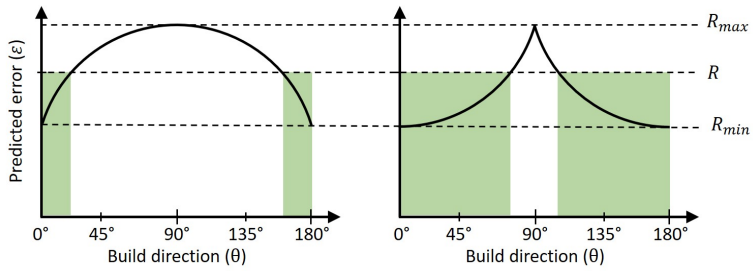

Figure 6.1: Comparison of acceptable orientations according to two different model types: A parabola similar to the cylindricity model from [29] (left) and a model similar to that from experimental data (right).

revelation may widen the range of acceptable orientations relative to the existing models as outlined in figure 6.1 where the two model types are compared, both with the same maximum and minimum values, and equal but opposite (exaggerated) curvatures. With the target value R, the ranges of acceptable orientations are illustrated by the green areas. The larger green areas observed in the right figure directly translate to the range available for later optimization of part build orientation.

The two models in figure 6.1 exhibit equally sensitive responses in predicted accuracy depending on part build orientation, but this sensitivity is not equally distributed. Consider gradually increasing the required accuracy R from R_{min} to R_{max}. At R_{min}, the only viable orientation is at $0°$. As R increases from R_{min}, the range of allowable orientations will increase slowly in the first model, while a rapid increase will be observed for the second model. This rapid increase translates to the second model allowing a larger range of orientations for tighter tolerances compared to the first model. Note, however, that the actual accuracy does not depend on the model – regardless of which assumption is made, the measured cylindricity at orientation θ will be the same. The only difference is the underlying assumption of the relationship between part build orientation and resulting cylindricity.

Clearly, the underlying assumptions that define the choice of model type are crucial for the accuracy of the developed model, and in consequence, the boundaries imposed on the optimization of part build orientation. By opening up larger areas of the solution space to subsequent optimization processes, more objectives may be successfully addressed and a higher quality product may be accomplished.

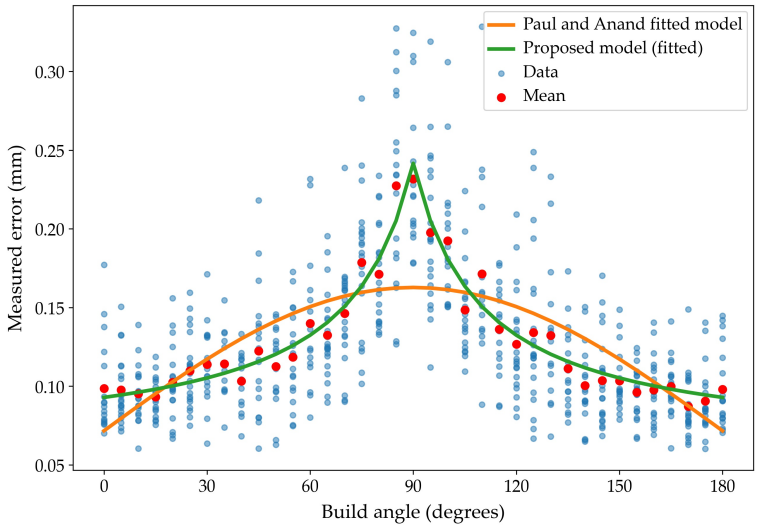

Figure 6.2: Comparison of a theoretical and an empirical model when fitted to experimental data.

Nevertheless, the curves in figure 6.1 deviates from the findings in section 5.2 where the fitted model of Paul and Anand [29] predicts smaller deviations at horizontal orientations than what the proposed model does (0.18 mm vs 0.25 mm), i.e. the minimal and maximal predicted values are not equal between the models. This is displayed in figure 6.2 where the predictions of the two models are compared to experimental data.

Figure 6.2 show how the theoretically derived model predicts smaller deviations both for vertical and horizontal orientations compared to the proposed model. While the discrepancy at vertical orientations is relatively insignificant, the difference in predicted value at horizontal orientations are quite large both in magnitude and range. Consequently, the choice of model is detrimental to the availability of this area in later processing.

The modeling efforts presented in section 5.2 reveals that the staircase effect alone cannot fully explain the observed deviations from nominal geometry. Firstly, this fails to consider a general baseline of inaccuracy such as the imperfections imposed by adhering powder, etc. Secondly, the observed curve in the experimental data implies a rapid increase in deviations when the cylinder was close to horizontal, culminating at the horizontal orientation before decreasing identically on the negative side.

The symmetry about the 90° mark is easily explained by the symmetry of the cylinder, ultimately yielding repeated results about the horizontal line. However, the results obtained between 0° and 90° require more attention and cannot be explained from these results alone.

6.2.2 Flatness

The effect of part build orientation on flatness appears to be more complex than the behavior of cylindricity. The analysis revealed large variations and slightly different behavior of up-facing and down-facing surfaces. A more staggering observation is perhaps the relatively good quality achieved around the 45° mark. According to the experiments reported herein, the flatness at this orientation is actually comparable to that of horizontal and vertical orientations.

The theoretical model of Arni and Gupta [27] which solely considers the staircase effect is found not to follow the trend observed in the experimental data, not even after the curve fitting procedure. Unlike cylindricity, no empirical models for flatness have been found in the literature to which the experimental data can be compared. Therefore, the empirical models for flatness are a first attempt at modeling this rather complex behavior. Due to this complexity, the empirical models were developed in three successive stages to assimilate the data.

As the model complexity increases, the predictions more closely follow the experimental data. However, this conformance comes at the cost of validity as the model may not have any utility beyond this dataset. The third and final model presented in subsection 5.2.2 involve 'hard' definitions of critical angles along the lines of Arni and Gupta [27], and is very likely to be over-fitted.

While the symmetry of the cylindrical data could be utilized to simplify the corresponding model, this will not yield adequate results for flatness as up-facing and down-facing surfaces appear to be affected differently by part build orientation. Nevertheless, the second model where some symmetry is retained may perform better on new data and is perhaps more flexible to be adapted to new data.

The shape of the curve for flatness resembles that of surface roughness as reported in the literature [72], [73], however, the curve appears to be somewhat distorted. The similarity may not be coincidental as the relatively small area of these planes may prevent the manifestation of warping effects, rendering the surface roughness as a primary driver of

flatness error on these surfaces.

Another effect of the small surface area of the planes is the magnitude of the measured error. Larger surfaces are likely to yield larger absolute deviations as effects other than surface roughness become more prominent. Although not included in the study, data is obtained for the flatness of the artifact's base plate. This data generally displays larger deviations across all orientations. Comparison is however invalid because of the major area difference, and also the force from the fixture being applied directly on the base plate during the inspection which may affect the measurements.

6.2.3 Other findings related to RQ2

The diameters of all cylinders have been measured and are included in the dataset, but is not a geometric tolerance and has not been subject to modeling. However, two observations can be made regarding the dimensional accuracy of cylinders: (i) convex cylinders are generally larger than nominal values while concave cylinders are smaller; and (ii) deviations from nominal dimensions increase as the cylinder is rotated towards the horizontal orientation. The first observation may be expected as the dimension of the probe acts as a mechanical filter that inhibits its entry into the smallest cracks and creases. Due to the surface roughness, some irregularities are to be expected. Conversely, the trend for 4mm convex cylinder transcends the zero-line which defies the general observation of positive versus negative deviations. The larger dimensions observed for convex cylinders at horizontal orientations may be attributed to powder adhesion as discussed by Launhardt and Drummer [54]. Theoretically, this should have an opposite effect of equal magnitude on concave cylinders, however, this cannot be clearly observed in the acquired data.

6.3 Discussion on RQ3

RQ3 *How can the part build orientation be optimized to meet certain tolerance levels in a deterministic manner?*

This RQ requires three choices to be made: Firstly, as implicit from the topic of this thesis and previous RQs, the question relates to the part build orientation in LB-PBF/P specifically. Any external validity to other problems and technologies will be discussed in section 6.4. Secondly, accuracy may be of either primary or secondary interest. A distinction

must be made between finding the globally optimal orientation(s), and identifying regions in which a certain tolerance requirement can be met – regions from which the final part build orientation may be selected based on other considerations such as mechanical properties, build space utilization, etc. And finally, the geometry could be partitioned into smaller pieces for their individual fabrication in each of their own optimal orientations before the parts are finally assembled to make up the final product (as exemplified in [121]). While the proposed method can be applied to each of the constituent parts, the method is intended for geometries containing more than one surface of interest without splitting into smaller components.

Paper P6 [119] presents the foundations for the mathematical description of entire solution spaces, and continues with the identification of the optimal orientation in a continuous solution space. This approach constitutes a deterministic solution to the part build orientation problem and can be extended to comprise many more objectives and variables. Both of these alternatives constitutes interesting avenues of future work, and directions are discussed further in section 7.1.

The proposed method is based on the geometry of the part to be produced and offers some possibilities with the relative significance of each feature, or each feature type. The examples in paper P6 consider every surface of the parts when constructing the solution spaces, but implementations of the method may opt to leave some surfaces out of the equation or to assign weight factors to the different features. How the features are obtained is not within the scope of this research although one approach is presented in paper P4 [120]. Nevertheless, to maintain a deterministic pipeline, the manner in which these features are obtained naturally also has to be deterministic. Hence, direct import from native CAD files, or STandard for the Exchange of Product model data (STEP) files would be advantageous.

If a continuous solution space is obtained, the definition of feasible orientation regions can also be defined in a similar fashion. These regions may then constitute the boundaries for subsequent optimization schemes for multi-objective optimization. Alternatively, the feasible regions can be visualized similar to the approach of Budinoff and McMains [122] for the manual determination of part build orientation based on implicit knowledge and experience.

The method described in paper P6 [119] is based on continuous solution

spaces. Conditional statements are common place in existing literature including the models proposed in section 5.2. These statements are necessary to incorporate different behavior on either side of a critical angle (i.e. a threshold), e.g. for distinguishing the quality of an up-facing surface from that of a down-facing surface. While conditional statements complicate the mathematical approach described in paper P6, they merely introduce edges in the solution space that require additional attention and prolong the execution time of the algorithm. Certainly, at some point, the solution space will have reached a complexity where mathematical methods may be infeasible. However, as the solution space becomes more complex, the chances of other methods (e.g. gradient-based methods and EAs) getting stuck in local optima increases.

6.4 External validity and relevance

As all PhD projects should be, the present thesis is focused on a particular domain. However, the findings will have a utility beyond the scope of this thesis. The following subsections discuss and describe the utility and validity of the current work outside the narrow scope defined as limitations to this thesis.

6.4.1 Validity versus other systems for LB-PBF/P

The experiment is central to this thesis and was performed in the EOS-INT P395 LB-PBF machine at NTNU in Gjøvik, Norway. However, because a fundamental assumption of the current work is that large variations exist within and between builds of a single machine, why would the results have any validity beyond this particular machine? The answer to this lies both in the analysis performed in this thesis, and in the bigger epistemological picture.

The analysis performed in section 5.1 reveals that despite variations between various positions in the build space, the three performed builds are indeed comparable. This indicates that – given identical circumstances and parameter settings – another AM machine should be able to replicate the results. However, there are numerous obstacles that hinder the direct comparison between machines, including different hardware, firmware, and software. Most notably is perhaps the unknown parameters wrapped inside the 'balanced' process parameters of EOS that were used for the experiment.

Similarly, the material is an important factor in the determination of final part properties. While different mechanical properties are to be

expected, the effect of material on geometric accuracy is less certain [51]. Different particle sizes and melting temperatures are bound to influence the achievable accuracy as well as the observed variation. Investigating the role of material in the context of geometric accuracy and variations is beyond the scope of this thesis and is left for future work.

In the larger picture, one may argue that all systems for LB-PBF/P have the same general mechanics and that the behavior is comparable between the different vendors. Despite different solutions for feeding and spreading the powder in the build space, the material should behave similarly when exposed to a laser beam. This means that even though the measured values may differ, the general behavior should be similar and the base (un-fitted) model should have external validity. Replicating the experiment to validate the developed models on other LB-PBF/P systems is left for future work and would significantly elevate the validity of the devised models.

6.4.2 Validity versus other PBF technologies

While LB-PBF/P systems are fairly similar, one would also expect that some of this behavior could be transferred to other materials and other energy sources. Polymers and metals retain quite dissimilar material properties and behave rather differently from each other. Still, the general influence of part build orientation on part properties may be quite similar. Moreover, the adopted methodology for developing mathematical models may be applicable beyond the realm of polymers and lasers.

6.4.3 Validity versus other AM technologies

The study performed in the current work has confirmed that the staircase effect alone is insufficient to predict the geometric accuracy. While the layered manner of fabrication is a central characteristic of AM [1], other factors beyond the staircase effect should be considered regardless of AM technology.

Closely related technologies (i.e. powder-based technologies) benefit more directly from the presented thesis relative to technologies of larger fundamental differences. Theory states for instance that the melt flow index of the powder may influence the quality of the final product [123]. This index is naturally not applicable in Layered Object Manufacturing (LOM) and demonstrates the dissimilarity of the two technologies. Consequently, the methodological approaches described herein are ap-

plicable outside the domain of PBF, but the practical aspect is rather technology-specific, including the models derived from the experimental data. However, the adopted approach to developing mathematical models may be used for other processes under the AM umbrella.

The optimization method proposed herein does indeed have utility beyond PBF as it merely requires the input to be changed accordingly. With models developed specifically for the technology in question, the method can theoretically be applied to any AM technology. Certainly, as the models become more specific, the accuracy may increase, but the external validity will suffer. With the words of George E. P. Box in mind [118], this trade-off is necessary to ensure the usefulness of the developed model.

6.4.4 Utility beyond AM

This thesis is founded on the layered manner of fabrication used in most AM technologies, and not so many others. However, there are some areas where the described concepts may have some use.

Firstly, a large portion of this work has revolved around the issue of STL files and the interpretations of their contents. This and similar file types are also used in other domains ranging from computer graphics to CAM applications. The ability to derive higher-level information from a surface mesh is valuable beyond AM. This topic is considered in paper P4 [120] where features are extracted from STL files, and in paper P3 [124] where the problem of applying tolerances to STL files is discussed.

Secondly, other manufacturing technologies also face problems related to generating valid data from processes where variations are commonplace. The approach used for the experiments as elaborated in paper P5 [101] can be adapted to handle uncertain conditions also in other manufacturing processes. Moreover, the subsequent data treatment may serve as an example of how empirical models can be developed from noisy experimental data.

Chapter 7

Conclusions

This PhD work has developed experimental and optimization methodology to minimize form errors by optimizing part build orientation. An elaborate experiment was conducted to generate data for the creation of empirical models, and a method for extracting geometric features from STL files was presented to enable flexible optimization based on the part geometry. These elements can be used to construct a digital pipeline for the processing of additively manufactured components with minimal human interaction.

The presented methodology for planning and executing experiments in LB-PBF/P enables the characterization of variation within and between builds. This facilitates the construction of empirical models from the generated data and further enables the modeling of uncertainty.

This study shows that the staircase effect alone is insufficient in predicting neither cylindricity nor flatness. Consequently, new models for both of these characteristics are proposed which better assimilate the experimental data. The fitness of the models is evaluated by R^2 values where the novel model for cylindricity achieves a value of 0.943. The effect of part build orientation on flatness appears to be more complex and may require conditional statements to achieve better fitness. A single expression is presented that achieves an R^2 value of 0.749.

A number of optimization strategies have been investigated, and a deterministic method is presented for continuous solution spaces. The integrated method enables automatic optimization of part build orientation based on the geometric primitives of the part by employing

mathematical models.

7.1 Future work

Several avenues of future work have been discovered during the PhD work, and some developed concepts do require further work. The following directions remain for future work:

- The current work developed empirical models for flatness and cylindricity, but other tolerance characteristics remain (most notably conicity).
- The proposed optimization method assumed a full revolution of revolved surfaces. Developing models for partially revolved surfaces (e.g. quarter of a cylinder) is of interest in future work.
- The elements of this thesis fit well into the industry 4.0 paradigm, and a promising direction of future work is the design of a complete digital pipeline for quality assurance in AM from CAD to qualification. This problem can also be elevated to the value chain level where the digital pipeline extends upstream to material suppliers and machine vendors and downstream to clients and customers.
- The experiment was conducted on a single machine, and due to cost- and time restrictions, a separate build for verification was not possible. Replication of one or more builds would improve the validity of the current work by enabling verification and validation. This should primarily be done on a comparable machine (i.e. LB-PBF/P), but the replication on other systems and materials would also be interesting.
- The experiment yielded a large body of data, of which only a small portion has been analyzed. The data is made publicly available through an open repository [108] for anyone who would like to make use of it.
- Only the main specimens of the experiment have been inspected, and an immense source of data remains untouched. The inspection of the additional specimens is a natural path of future work.

List of publications

1. T. S. Leirmo and K. Martinsen, 'Evolutionary algorithms in additive manufacturing systems: Discussion of future prospects,' *Procedia CIRP*, vol. 81, pp. 671–676, 2019, ISSN: 2212-8271. DOI: 10.1016/j.procir.2019.03.174. [Online]. Available: http://www.sciencedirect.com/science/article/pii/S2212827119304792

2. T. S. Leirmo and K. Martinsen, 'Deterministic part orientation in additive manufacturing using feature recognition,' *Procedia CIRP*, vol. 88, pp. 405–410, 2020, ISSN: 2212-8271. DOI: 10.1016/j.procir.2020.05.070. [Online]. Available: http://www.sciencedirect.com/science/article/pii/S2212827120303899

3. T. L. Leirmo, O. Semeniuta and K. Martinsen, 'Tolerancing from STL data: A Legacy Challenge,' *Procedia CIRP*, vol. 92, pp. 218–223, 2020, ISSN: 2212-8271. DOI: 10.1016/j.procir.2020.05.180. [Online]. Available: http://www.sciencedirect.com/science/article/pii/S221282712030946X

4. T. L. Leirmo, O. Semeniuta, I. Baturynska *et al.*, 'Extracting shape features from a surface mesh using geometric reasoning,' *Procedia CIRP*, vol. 93, pp. 544–549, 2020, ISSN: 2212-8271. DOI: 10.1016/j.procir.2020.02.142. [Online]. Available: http://www.sciencedirect.com/science/article/pii/S2212827120306788

5. T. L. Leirmo and O. Semeniuta, 'Investigating the Dimensional and Geometric Accuracy of Laser-Based Powder Bed Fusion of PA2200 (PA12): Experiment Design and Execution,' *Applied Sciences*, vol. 11, no. 5, p. 2031, 2021, ISSN: 2076-3417. DOI: 10.3390/

app11052031. [Online]. Available: https://www.mdpi.com/2076-3417/11/5/2031

6. T. L. Leirmo and O. Semeniuta, 'Minimizing form errors in additive manufacturing with part build orientation - An optimization method for continuous solution spaces,' *Open Engineering*, vol. (Accepted),

Bibliography

[1] ISO/ASTM 52900:2015(E), *Standard Terminology for Additive Manufacturing – General Principles – Terminology*, West Conshohocken, 2015.

[2] D. Simon, *Evolutionary optimization algorithms*, English. Hoboken, New Jersey: John Wiley & Sons, 2013, p. 776, ISBN: 978-0-470-93741-9.

[3] Merriam-Webster, *Optimization*, Mar. 2021. [Online]. Available: https://www.merriam-webster.com/dictionary/optimization.

[4] I. Gibson, D. Rosen, B. Stucker and M. Khorasani, *Additive Manufacturing Technologies*, 3rd ed. Cham: Springer Nature Switzerland AG, 2021, ISBN: 978-3-030-56127-7. DOI: 10.1007/978-3-030-56127-7.

[5] C. W. Hull, *Apparatus for production of three-dimensional objects by stereolithography*, English, U. S. P. (USPTO) and T. Office, Eds., US, 1986. [Online]. Available: https://www.google.com/patents/US4575330.

[6] ISO/ASTM 52911:2019(E), *Additive manufacturing – Design – Part 2: Laser-based powder bed fusion of polymers*, 2019.

[7] J. Butt, 'Exploring the Interrelationship between Additive Manufacturing and Industry 4.0,' *Designs*, vol. 4, no. 2, 2020, ISSN: 2411-9660. DOI: 10.3390/designs4020013. [Online]. Available: https://www.mdpi.com/2411-9660/4/2/13.

[8] G. Ameta, R. Lipman, S. Moylan and P. Witherell, 'Investigating the Role of Geometric Dimensioning and Tolerancing in Additive Manufacturing,' *Journal of Mechanical Design*, vol. 137, no. 11, pp. 111 401–111 401, 2015, ISSN: 1050-0472. DOI: 10.1115/1.4031296. [Online]. Available: http://dx.doi.org/10.1115/1.4031296.

[9] K. Hildebrand, B. Bickel and M. Alexa, 'Orthogonal slicing for additive manufacturing,' *Computers and Graphics (Pergamon)*, vol. 37, no. 6, pp. 669–675, 2013, ISSN: 0097-8493. DOI: 10.1016/j.cag.2013.05.011.

[10] J. Hao, L. Fang and R. E. Williams, 'An efficient curvature-based partitioning of large-scale STL models,' *Rapid Prototyping Journal*, vol. 17, no. 2, L. Fang, Ed., pp. 116–127, 2011, ISSN: 1355-2546. DOI: 10.1108/13552541111113862. [Online]. Available: https://doi.org/10.1108/13552541111113862.

[11] P. Shi, Q. Qi, Y. Qin, P. J. Scott and X. Jiang, 'A novel learning-based feature recognition method using multiple sectional view representation,' *Journal of Intelligent Manufacturing*, vol. 31, no. 5, pp. 1291–1309, 2020, ISSN: 1572-8145. DOI: 10.1007/s10845-020-01533-w. [Online]. Available: https://doi.org/10.1007/s10845-020-01533-w.

[12] J. Hao, L. Fang and H. Yang, 'An improved boundary extraction method of STL model based on edge curvature estimation,' *Computer Modelling and New Technologies*, vol. 18, no. 10, pp. 252–258, 2014. [Online]. Available: http://www.cmnt.lv/en/on-line-journal/2014/2014-volume-18-10.

[13] S. Rüsenberg, S. Josupeit and H. J. Schmid, 'A Method to Characterize the Quality of a Polymer Laser Sintering Process,' *Advances in Mechanical Engineering*, vol. 2014, 2014, ISSN: 1687-8140. DOI: 10.1155/2014/185374.

[14] S. E. Brika, Y. F. Zhao, M. Brochu and J. Mezzetta, 'Multi-Objective Build Orientation Optimization for Powder Bed Fusion by Laser,' *Journal of Manufacturing Science and Engineering*, vol. 139, no. 11, p. 111 011, 2017, ISSN: 1087-1357. DOI: 10.1115/1.4037570. [Online]. Available: http://dx.doi.org/10.1115/1.4037570.

[15] W. Rong-Ji, L. Xin-hua, W. Qing-ding and W. Lingling, 'Optimizing process parameters for selective laser sintering based on neural network and genetic algorithm,' *The International Journal of Advanced Manufacturing Technology*, vol. 42, no. 11, pp. 1035–

1042, 2009, ISSN: 1433-3015. DOI: 10.1007/s00170-008-1669-0. [Online]. Available: https://doi.org/10.1007/s00170-008-1669-0.

[16] S.-M. Hur, K.-H. Choi, S.-H. Lee and P.-K. Chang, 'Determination of fabricating orientation and packing in SLS process,' *Journal of Materials Processing Technology*, vol. 112, no. 2–3, pp. 236–243, 2001, ISSN: 0924-0136. DOI: 10.1016/S0924-0136(01)00581-7. [Online]. Available: //www.sciencedirect.com/science/article/pii/S0924013601005817.

[17] N. K. Maurya, V. Rastogi and P. Singh, 'An overview of mechanical properties and form error for rapid prototyping,' *CIRP Journal of Manufacturing Science and Technology*, vol. 29, pp. 53–70, 2020, ISSN: 1755-5817. DOI: 10.1016/j.cirpj.2020.02.003. [Online]. Available: http://www.sciencedirect.com/science/article/pii/S1755581720300122.

[18] T. S. Leirmo and K. Martinsen, 'Evolutionary algorithms in additive manufacturing systems: Discussion of future prospects,' *Procedia CIRP*, vol. 81, pp. 671–676, 2019, ISSN: 2212-8271. DOI: 10.1016/j.procir.2019.03.174. [Online]. Available: http://www.sciencedirect.com/science/article/pii/S2212827119304792.

[19] N. Padhye and K. Deb, 'Multi-objective optimisation and multi-criteria decision making in SLS using evolutionary approaches,' *Rapid Prototyping Journal*, vol. 17, no. 6, pp. 458–478, 2011, ISSN: 1355-2546. DOI: 10.1108/13552541111184198. [Online]. Available: http://www.emeraldinsight.com/doi/abs/10.1108/13552541111184198.

[20] A. Ghorpade, Y. Dashroa, M. K. Tiwari and K. P. Karunakaran, 'Introducing Hierarchical Particle Swarm Optimization to Optimal Part Orientation in Fused Deposition Modeling,' in *ASME 2006 International Design Engineering Technical Conferences and Computers and Information in Engineering Conference*, 2006, pp. 233–240, ISBN: 0-7918-4255-X. DOI: 10.1115/DETC2006-99534. [Online]. Available: http://dx.doi.org/10.1115/DETC2006-99534.

[21] R. V. Rao and D. P. Rai, 'Optimization of fused deposition modeling process using teaching-learning-based optimization algorithm,' *Engineering Science and Technology, an International Journal*, vol. 19, no. 1, pp. 587–603, 2016, ISSN: 2215-0986. DOI: 10.1016/j.jestch.2015.09.008. [Online]. Available: http://www.sciencedirect.com/science/article/pii/S2215098615001536.

[22] A. S. Nezhad, F. Barazandeh, A. R. Rahimi and M. Vatani, 'Pareto-Based Optimization of Part Orientation in Stereolithography,' *Proceedings of the Institution of Mechanical Engineers, Part B: Journal of Engineering Manufacture*, vol. 224, no. 10, pp. 1591–1598, 2010. DOI: 10.1243/09544054jem1842. [Online]. Available: http://journals.sagepub.com/doi/abs/10.1243/09544054JEM1842.

[23] V. Canellidis, J. Giannatsis and V. Dedoussis, 'Genetic-algorithm-based multi-objective optimization of the build orientation in stereolithography,' *The International Journal of Advanced Manufacturing Technology*, vol. 45, no. 7, pp. 714–730, 2009, ISSN: 1433-3015. DOI: 10.1007/s00170-009-2006-y. [Online]. Available: https://doi.org/10.1007/s00170-009-2006-y.

[24] P. M. Pandey, K. Thrimurthulu and N. V. Reddy, 'Optimal part deposition orientation in FDM by using a multicriteria genetic algorithm,' *International Journal of Production Research*, vol. 42, no. 19, pp. 4069–4089, 2004, ISSN: 0020-7543. DOI: 10.1080/00207540410001708470. [Online]. Available: http://dx.doi.org/10.1080/00207540410001708470.

[25] G. Strano, L. Hao, R. M. Everson and K. E. Evans, 'Multi-objective optimization of selective laser sintering processes for surface quality and energy saving,' *Proceedings of the Institution of Mechanical Engineers, Part B: Journal of Engineering Manufacture*, vol. 225, no. 9, pp. 1673–1682, 2011. DOI: 10.1177/0954405411402925. [Online]. Available: http://journals.sagepub.com/doi/abs/10.1177/0954405411402925.

[26] P. Das, R. Chandran, R. Samant and S. Anand, 'Optimum Part Build Orientation in Additive Manufacturing for Minimizing Part Errors and Support Structures,' *Procedia Manufacturing*, vol. 1, pp. 343–354, 2015, ISSN: 2351-9789. DOI: 10.1016/j.promfg.2015.09.041. [Online]. Available: http://www.sciencedirect.com/science/article/pii/S2351978915010410.

[27] R. Arni and S. K. Gupta, 'Manufacturability analysis of flatness tolerances in solid freeform fabrication,' *Journal of Mechanical Design*, vol. 123, no. 1, pp. 148–156, 2001, ISSN: 1050-0472. DOI: 10.1115/1.1326439.

[28] S. H. Masood, W. Rattanawong and P. Iovenitti, 'Part Build Orientations Based on Volumetric Error in Fused Deposition Modelling,' *The International Journal of Advanced Manufacturing*

Technology, vol. 16, no. 3, pp. 162–168, 2000, ISSN: 1433-3015. DOI: 10.1007/s001700050022. [Online]. Available: https://doi.org/10.1007/s001700050022.

[29] R. Paul and S. Anand, 'Optimal part orientation in Rapid Manufacturing process for achieving geometric tolerances,' *Journal of Manufacturing Systems*, vol. 30, no. 4, pp. 214–222, 2011, ISSN: 0278-6125. DOI: 10.1016/j.jmsy.2011.07.010. [Online]. Available: http://www.sciencedirect.com/science/article/pii/S0278612511000665.

[30] Z. Zhu, 'Modèles géométriques avec defauts pour la fabrication additive,' Ph.D. dissertation, Université Paris-Saclay, 2019. [Online]. Available: https://hal.inria.fr/tel-02390292v1.

[31] J.-Y. Dantan, Z. Huang, E. Goka, L. Homri, A. Etienne, N. Bonnet and M. Rivette, 'Geometrical variations management for additive manufactured product,' *CIRP Annals*, vol. 66, no. 1, pp. 161–164, 2017, ISSN: 0007-8506. DOI: 10.1016/j.cirp.2017.04.034. [Online]. Available: http://www.sciencedirect.com/science/article/pii/S0007850617300343.

[32] M. K. Thompson, G. Moroni, T. Vaneker, G. Fadel, R. I. Campbell, I. Gibson, A. Bernard, J. Schulz, P. Graf, B. Ahuja and F. Martina, 'Design for Additive Manufacturing: Trends, opportunities, considerations, and constraints,' *CIRP Annals*, vol. 65, no. 2, pp. 737–760, 2016, ISSN: 0007-8506. DOI: 10.1016/j.cirp.2016.05.004. [Online]. Available: http://www.sciencedirect.com/science/article/pii/S0007850616301913.

[33] C. Yu, L. Qie, S. Jing and Y. Yan, 'Personalized design of part orientation in additive manufacturing,' *Rapid Prototyping Journal*, vol. 25, no. 10, pp. 1647–1660, Jan. 2019, ISSN: 1355-2546. DOI: 10.1108/RPJ-12-2018-0309. [Online]. Available: https://doi.org/10.1108/RPJ-12-2018-0309.

[34] Y. Zhang, A. Bernard, R. K. Gupta and R. Harik, 'Feature based building orientation optimization for additive manufacturing,' *Rapid Prototyping Journal*, vol. 22, no. 2, pp. 358–376, 2016, ISSN: 1355-2546. DOI: 10.1108/rpj-03-2014-0037.

[35] ASME Y14.5M-2018, *Dimensioning and Tolerancing*, English, New York, USA, 2018.

[36] ISO 1101:2017(E), *Geometrical product specifications (GPS) – Geometrical tolerancing – Tolerances of form, orientation, location and run-out*, Geneva, 2017.

[37] A. A. Weckenmann, 'Form Error,' in *CIRP Encyclopedia of Production Engineering*, Berlin, Heidelberg: Springer Berlin Heidelberg, 2014, pp. 535–539, ISBN: 978-3-642-20617-7. DOI: 10.1007/978-3-642-20617-7{_}6683. [Online]. Available: https://doi.org/10.1007/978-3-642-20617-7_6683.

[38] C. R. Deckard, *Method and Apparatus for Producing Parts by Selective Sintering*, 1989. [Online]. Available: https://patents.google.com/patent/US4863538.

[39] F. Calignano, D. Manfredi, E. P. Ambrosio, S. Biamino, M. Lombardi, E. Atzeni, A. Salmi, P. Minetola, L. Iuliano and P. Fino, 'Overview on Additive Manufacturing Technologies,' *Proceedings of the IEEE*, vol. 105, no. 4, pp. 593–612, 2017, ISSN: 1558-2256. DOI: 10.1109/JPROC.2016.2625098.

[40] A. Zocca, P. Colombo, C. M. Gomes and J. Günster, 'Additive Manufacturing of Ceramics: Issues, Potentialities, and Opportunities,' *Journal of the American Ceramic Society*, vol. 98, no. 7, pp. 1983–2001, Jul. 2015, ISSN: 0002-7820. DOI: 10.1111/jace.13700. [Online]. Available: https://doi.org/10.1111/jace.13700.

[41] I. Baturynska, 'Machine Learning of Quality Assurance in Polymer Powder Bed Fusion Additive Manufacturing,' Ph.D. dissertation, NTNU - Norwegian University of Science and Technology, Gjøvik, Apr. 2020, ISBN: 978-82-326-4589-3. [Online]. Available: https://hdl.handle.net/11250/2649915.

[42] K. Dotchev and W. Yusoff, 'Recycling of polyamide 12 based powders in the laser sintering process,' *Rapid Prototyping Journal*, vol. 15, no. 3, pp. 192–203, 2009, ISSN: 1355-2546. DOI: 10.1108/13552540910960299. [Online]. Available: https://doi.org/10.1108/13552540910960299.

[43] K. Wudy and D. Drummer, 'Aging effects of polyamide 12 in selective laser sintering: Molecular weight distribution and thermal properties,' *Additive Manufacturing*, vol. 25, pp. 1–9, 2019, ISSN: 2214-8604. DOI: 10.1016/j.addma.2018.11.007. [Online]. Available: http://www.sciencedirect.com/science/article/pii/S2214860418307024.

[44] T. Czelusniak and F. L. Amorim, 'Influence of energy density on polyamide 12 processed by SLS: from physical and mechanical properties to microstructural and crystallization evolution,' *Rapid Prototyping Journal*, 2021, ISSN: 1355-2546. DOI: 10.1108/RPJ-02-2020-0027.

[45] C. W. Hull, S. T. Spence, D. J. Albert, D. R. Smally, R. A. Harlow, P. Steinberg, H. L. Tarnoff, H. D. Nguyen, C. W. Lewis, T. J. Vorgitch and D. Z. Remba, *Cad/cam stereolithographic data conversion*, English / French, US, 1989. [Online]. Available: https://www.google.com/patents/WO1989010256A1?cl=en.

[46] Digital Preservation at the Library of Congress, *STL (STereo-Lithography) File Format Family*, Sep. 2019. [Online]. Available: https://www.loc.gov/preservation/digital/formats/fdd/fdd000504.shtml.

[47] Y. Qin, Q. Qi, P. J. Scott and X. Jiang, 'Status, comparison, and future of the representations of additive manufacturing data,' *Computer-Aided Design*, vol. 111, pp. 44–64, 2019, ISSN: 0010-4485. DOI: 10.1016/j.cad.2019.02.004. [Online]. Available: https://www.sciencedirect.com/science/article/pii/S0010448518304202.

[48] ISO/ASTM 52915:2016(E), *Specification for Additive Manufacturing File Format (AMF) Version 1.2*, Geneva, 2016.

[49] The 3MF Consortium, *3MF Consortium*, 2020. [Online]. Available: https://3mf.io/.

[50] Q. Chen, J. Xu and S. Zhang, 'Cylindricity and flatness optimization for mechanical parts in additive manufacturing based on tolerance adaptive slicing,' *International Journal of Advanced Manufacturing Technology*, vol. 115, no. 11-12, pp. 3839–3857, Aug. 2021, ISSN: 14333015. DOI: 10.1007/s00170-021-07271-4.

[51] R. D. Goodridge, C. J. Tuck and R. J. M. Hague, 'Laser sintering of polyamides and other polymers,' *Progress in Materials Science*, vol. 57, no. 2, pp. 229–267, 2012, ISSN: 0079-6425. DOI: 10.1016/j.pmatsci.2011.04.001. [Online]. Available: http://www.sciencedirect.com/science/article/pii/S0079642511000648.

[52] M. Pavan, M. Faes, D. Strobbe, B. Van Hooreweder, T. Craeghs, D. Moens and W. Dewulf, 'On the influence of inter-layer time and energy density on selected critical-to-quality properties of PA12 parts produced via laser sintering,' *Polymer Testing*, vol. 61, pp. 386–395, 2017, ISSN: 0142-9418. DOI: 10.1016/j.

polymertesting.2017.05.027. [Online]. Available: http://www.sciencedirect.com/science/article/pii/S0142941817303306.

[53] D. L. Bourell, T. J. Watt, D. K. Leigh and B. Fulcher, 'Performance Limitations in Polymer Laser Sintering,' *Physics Procedia*, vol. 56, pp. 147–156, 2014, ISSN: 1875-3892. DOI: 10.1016/j.phpro.2014.08.157. [Online]. Available: http://www.sciencedirect.com/science/article/pii/S1875389214003022.

[54] M. Launhardt and D. Drummer, 'Determination of the fundamental dimension development in building direction for laser-sintered parts,' *Journal of Polymer Engineering*, vol. 39, no. 2, pp. 197–206, Feb. 2019, ISSN: 0334-6447. DOI: 10.1515/polyeng-2018-0204.

[55] S. Rott, A. Ladewig, K. Friedberger, J. Casper, M. Full and J. H. Schleifenbaum, 'Surface roughness in laser powder bed fusion – Interdependency of surface orientation and laser incidence,' *Additive Manufacturing*, vol. 36, p. 101 437, 2020, ISSN: 2214-8604. DOI: 10.1016/j.addma.2020.101437. [Online]. Available: http://www.sciencedirect.com/science/article/pii/S2214860420308095.

[56] S. Allen and D. Dutta, 'On the computation of part orientation using support structures in layered manufacturing,' in *Proceedings of Solid Freeform Fabrication Symposium*, University of Texas at Austin, Austin, TX, 1994, pp. 259–269.

[57] W. Cheng, J. Y. H. Fuh, A. Y. C. Nee, Y. S. Wong, H. T. Loh and T. Miyazawa, 'Multi-objective optimization of part-building orientation in stereolithography,' *Rapid Prototyping Journal*, vol. 1, no. 4, pp. 12–23, 1995, ISSN: 1355-2546. DOI: 10.1108/13552549510104429.

[58] L. Di Angelo, P. Di Stefano and E. Guardiani, 'Search for the Optimal Build Direction in Additive Manufacturing Technologies: A Review,' *Journal of Manufacturing and Materials Processing*, vol. 4, no. 3, p. 71, 2020, ISSN: 2504-4494. DOI: 10.3390/jmmp4030071. [Online]. Available: https://www.mdpi.com/2504-4494/4/3/71.

[59] Y. Qin, Q. Qi, P. Shi, P. J. Scott and X. Jiang, 'Status, issues, and future of computer-aided part orientation for additive manufacturing,' *The International Journal of Advanced Manufacturing Technology*, May 2021, ISSN: 0268-3768. DOI: 10.1007/s00170-021-06996-6.

[60] P.-T. Lan, S.-Y. Chou, L.-L. Chen and D. Gemmill, 'Determining fabrication orientations for rapid prototyping with Stereolithography apparatus,' *Computer-Aided Design*, vol. 29, no. 1, pp. 53–62, 1997, ISSN: 0010-4485. DOI: 10.1016/S0010-4485(96)00049-8. [Online]. Available: http://www.sciencedirect.com/science/article/pii/S0010448596000498.

[61] D. Frank and G. Fadel, 'Expert system-based selection of the preferred direction of build for rapid prototyping processes,' *Journal of Intelligent Manufacturing*, vol. 6, no. 5, pp. 339–345, 1995, ISSN: 1572-8145. DOI: 10.1007/bf00124677. [Online]. Available: http://dx.doi.org/10.1007/BF00124677.

[62] P. Alexander, S. Allen and D. Dutta, 'Part orientation and build cost determination in layered manufacturing,' *Computer-Aided Design*, vol. 30, no. 5, pp. 343–356, 1998, ISSN: 0010-4485. DOI: 10.1016/S0010-4485(97)00083-3. [Online]. Available: http://www.sciencedirect.com/science/article/pii/S0010448597000833.

[63] S. Beitz, R. Uerlich, T. Bokelmann, A. Diener, T. Vietor and A. Kwade, 'Influence of Powder Deposition on Powder Bed and Specimen Properties,' *Materials*, vol. 12, no. 2, 2019, ISSN: 1996-1944. DOI: 10.3390/ma12020297.

[64] P. Jaiswal, J. Patel and R. Rai, 'Build orientation optimization for additive manufacturing of functionally graded material objects,' *The International Journal of Advanced Manufacturing Technology*, 2018, ISSN: 1433-3015. DOI: 10.1007/s00170-018-1586-9. [Online]. Available: https://doi.org/10.1007/s00170-018-1586-9.

[65] M. Mele and G. Campana, 'Sustainability-driven multi-objective evolutionary orienting in additive manufacturing,' *Sustainable Production and Consumption*, vol. 23, pp. 138–147, 2020, ISSN: 2352-5509. DOI: 10.1016/j.spc.2020.05.004. [Online]. Available: http://www.sciencedirect.com/science/article/pii/S2352550920300762.

[66] J. Villacres, D. Nobes and C. Ayranci, 'Additive manufacturing of shape memory polymers: effects of print orientation and infill percentage on shape memory recovery properties,' *Rapid Prototyping Journal*, vol. 26, no. 9, pp. 1593–1602, 2020, ISSN: 1355-2546. DOI: 10.1108/RPJ-09-2019-0239. [Online]. Available: https://doi.org/10.1108/RPJ-09-2019-0239.

[67] M. Zago, N. F. M. Lecis, M. Vedani and I. Cristofolini, 'Dimensional and geometrical precision of parts produced by binder jetting process as affected by the anisotropic shrinkage on sintering,' *Additive Manufacturing*, vol. 43, Jul. 2021, ISSN: 2214-8604. DOI: 10.1016/j.addma.2021.102007.

[68] A. Liebrich, H. C. Langowski, R. Schreiber and B. R. Pinzer, 'Effect of thickness and build orientation on the water vapor and oxygen permeation properties of laser-sintered polyamide 12 sheets,' *Rapid Prototyping Journal*, vol. 27, no. 5, pp. 1030–1040, 2021, ISSN: 13552546. DOI: 10.1108/RPJ-05-2020-0101.

[69] H. Shen, X. Ye, G. Xu, L. Zhang, J. Qian and J. Fu, '3D printing build orientation optimization for flexible support platform,' *Rapid Prototyping Journal*, vol. 26, no. 1, pp. 59–72, Jan. 2020, ISSN: 1355-2546. DOI: 10.1108/RPJ-09-2018-0252.

[70] K. Senthilkumaran, P. M. Pandey and P. V. M. Rao, 'Statistical modeling and minimization of form error in SLS prototyping,' *Rapid Prototyping Journal*, vol. 18, no. 1, pp. 38–48, 2012, ISSN: 1355-2546. DOI: 10.1108/13552541211193485. [Online]. Available: https://doi.org/10.1108/13552541211193485.

[71] T. Ollison and K. Berisso, 'Three-Dimensional Printing Build Variables That Impact Cylindricity,' *Journal of Industrial Technology*, vol. 26, no. 1, 2010, ISSN: 1537-0429. [Online]. Available: https://cdn.ymaws.com/www.atmae.org/resource/resmgr/JIT/ollison010510.pdf.

[72] P. E. Reeves and R. C. Cobb, 'Reducing the surface deviation of stereolithography using in-process techniques,' *Rapid Prototyping Journal*, vol. 3, no. 1, pp. 20–31, 1997, ISSN: 1355-2546. DOI: 10.1108/13552549710169255. [Online]. Available: http://www.emeraldinsight.com/doi/abs/10.1108/13552549710169255.

[73] H.-C. Kim and S.-H. Lee, 'Reduction of post-processing for stereolithography systems by fabrication-direction optimization,' *Computer-Aided Design*, vol. 37, no. 7, pp. 711–725, 2005, ISSN: 0010-4485. DOI: 10.1016/j.cad.2004.08.009. [Online]. Available: http://www.sciencedirect.com/science/article/pii/S0010448504001836.

[74] P. B. Bacchewar, S. K. Singhal and P. M. Pandey, 'Statistical modelling and optimization of surface roughness in the selective laser sintering process,' *Proceedings of the Institution of Mechanical Engineers, Part B: Journal of Engineering Manufacture*,

vol. 221, no. 1, pp. 35–52, 2007, ISSN: 0954-4054. DOI: 10.1243/09544054jem670. [Online]. Available: http://journals.sagepub.com/doi/abs/10.1243/09544054JEM670.

[75] I. Baturynska, 'Statistical analysis of dimensional accuracy in additive manufacturing considering STL model properties,' *The International Journal of Advanced Manufacturing Technology*, no. 97, pp. 2835–2849, 2018, ISSN: 1433-3015. DOI: 10.1007/s00170-018-2117-4. [Online]. Available: https://doi.org/10.1007/s00170-018-2117-4.

[76] M. Schmidt, M. Merklein, D. Bourell, D. Dimitrov, T. Hausotte, K. Wegener, L. Overmeyer, F. Vollertsen and G. N. Levy, 'Laser based additive manufacturing in industry and academia,' *CIRP Annals*, vol. 66, no. 2, pp. 561–583, 2017, ISSN: 0007-8506. DOI: 10.1016/j.cirp.2017.05.011. [Online]. Available: http://www.sciencedirect.com/science/article/pii/S0007850617301506.

[77] K. Senthilkumaran, P. M. Pandey and P. V. M. Rao, 'Influence of building strategies on the accuracy of parts in selective laser sintering,' *Materials & Design*, vol. 30, no. 8, pp. 2946–2954, 2009, ISSN: 0261-3069. DOI: 10.1016/j.matdes.2009.01.009. [Online]. Available: http://www.sciencedirect.com/science/article/pii/S0261306909000028.

[78] A. Gazzerro, W. Polini and L. Sorrentino, 'Investigation on selective laser sintering of PA12: dimensional accuracy and mechanical performance,' *Rapid Prototyping Journal*, vol. 27, no. 5, pp. 1010–1019, 2021, ISSN: 1355-2546. DOI: 10.1108/RPJ-06-2020-0125.

[79] R. J. Wang, L. Wang, L. Zhao and Z. Liu, 'Influence of process parameters on part shrinkage in SLS,' *International Journal of Advanced Manufacturing Technology*, vol. 33, no. 5-6, pp. 498–504, Jun. 2007, ISSN: 0268-3768. DOI: 10.1007/s00170-006-0490-x.

[80] Q. Huang, H. Nouri, K. Xu, Y. Chen, S. Sosina and T. Dasgupta, 'Statistical Predictive Modeling and Compensation of Geometric Deviations of Three-Dimensional Printed Products,' *Journal of Manufacturing Science and Engineering*, vol. 136, no. 6, p. 061 008, 2014, ISSN: 1087-1357. DOI: 10.1115/1.4028510. [Online]. Available: http://dx.doi.org/10.1115/1.4028510.

[81] Y. Jin, S. J. Qin and Q. Huang, 'Modeling inter-layer interactions for out-of-plane shape deviation reduction in additive manufacturing,' *IISE Transactions*, vol. 52, no. 7, pp. 721–731, Jul. 2020, ISSN: 2472-5854. DOI: 10.1080/24725854.2019.1676936. [Online]. Available: https://doi.org/10.1080/24725854.2019.1676936.

[82] A. Wang, S. Song, Q. Huang and F. Tsung, 'In-Plane Shape-Deviation Modeling and Compensation for Fused Deposition Modeling Processes,' *IEEE Transactions on Automation Science and Engineering*, vol. 14, no. 2, pp. 968–976, 2017, ISSN: 1558-3783. DOI: 10.1109/TASE.2016.2544941.

[83] L. Cheng, A. Wang and F. Tsung, 'A prediction and compensation scheme for in-plane shape deviation of additive manufacturing with information on process parameters,' *IISE Transactions*, vol. 50, no. 5, pp. 394–406, 2018, ISSN: 2472-5854. DOI: 10.1080/24725854.2017.1402224. [Online]. Available: https://doi.org/10.1080/24725854.2017.1402224.

[84] N. Decker, M. Lyu, Y. Wang and Q. Huang, 'Geometric Accuracy Prediction and Improvement for Additive Manufacturing Using Triangular Mesh Shape Data,' *Journal of Manufacturing Science and Engineering*, vol. 143, no. 6, Dec. 2020, ISSN: 1087-1357. DOI: 10.1115/1.4049089. [Online]. Available: https://doi.org/10.1115/1.4049089.

[85] B. Schleich, N. Anwer, L. Mathieu and S. Wartzack, 'Skin Model Shapes: A new paradigm shift for geometric variations modelling in mechanical engineering,' *Computer-Aided Design*, vol. 50, pp. 1–15, 2014, ISSN: 0010-4485. DOI: 10.1016/j.cad.2014.01.001. [Online]. Available: https://www.sciencedirect.com/science/article/pii/S0010448514000025.

[86] R. d. S. B. Ferreira, A. Sabbaghi and Q. Huang, 'Automated Geometric Shape Deviation Modeling for Additive Manufacturing Systems via Bayesian Neural Networks,' *IEEE Transactions on Automation Science and Engineering*, vol. 17, no. 2, pp. 584–598, 2020. DOI: 10.1109/TASE.2019.2936821.

[87] I. Baturynska and K. Martinsen, 'Prediction of geometry deviations in additive manufactured parts: comparison of linear regression with machine learning algorithms,' *Journal of Intelligent Manufacturing*, 2020, ISSN: 1572-8145. DOI: 10.1007/s10845-020-01567-0. [Online]. Available: https://doi.org/10.1007/s10845-020-01567-0.

[88] S. Chowdhury, K. Mhapsekar and S. Anand, 'Part Build Orientation Optimization and Neural Network-Based Geometry Compensation for Additive Manufacturing Process,' English, *Journal of Manufacturing Science and Engineering*, vol. 140, no. 3, p. 031 009, 2018, ISSN: 1087-1357. DOI: 10.1115/1.4038293.

[89] W. Rattanawong, S. H. Masood and P. Iovenitti, 'A volumetric approach to part-build orientations in rapid prototyping,' *Journal of Materials Processing Technology*, vol. 119, no. 1, pp. 348–353, 2001, ISSN: 0924-0136. DOI: 10.1016/S0924-0136(01)00924-4. [Online]. Available: http://www.sciencedirect.com/science/article/pii/S0924013601009244.

[90] R. Huang, N. Dai, D. Li, X. Cheng, H. Liu and D. Sun, 'Parallel non-dominated sorting genetic algorithm-II for optimal part deposition orientation in additive manufacturing based on functional features,' *Proceedings of the Institution of Mechanical Engineers, Part C: Journal of Mechanical Engineering Science*, vol. 232, no. 19, pp. 3384–3395, 2018. DOI: 10.1177/0954406217737105. [Online]. Available: http://journals.sagepub.com/doi/abs/10.1177/0954406217737105.

[91] L. Di Angelo, P. Di Stefano, A. Dolatnezhadsomarin, E. Guardiani and E. Khorram, 'A reliable build orientation optimization method in additive manufacturing: the application to FDM technology,' *The International Journal of Advanced Manufacturing Technology*, vol. 108, no. 1, pp. 263–276, 2020, ISSN: 1433-3015. DOI: 10.1007/s00170-020-05359-x. [Online]. Available: https://doi.org/10.1007/s00170-020-05359-x.

[92] M. A. Matos, A. M. A. C. Rocha and A. I. Pereira, 'Improving additive manufacturing performance by build orientation optimization,' *The International Journal of Advanced Manufacturing Technology*, 2020, ISSN: 1433-3015. DOI: 10.1007/s00170-020-04942-6. [Online]. Available: https://doi.org/10.1007/s00170-020-04942-6.

[93] M. A. Matos, A. M. A. C. Rocha and L. A. Costa, 'Many-objective optimization of build part orientation in additive manufacturing,' *The International Journal of Advanced Manufacturing Technology*, 2020, ISSN: 1433-3015. DOI: 10.1007/s00170-020-06369-5. [Online]. Available: https://doi.org/10.1007/s00170-020-06369-5.

[94] S. Pereira, A. I. F. Vaz and L. N. Vicente, 'On the optimal object orientation in additive manufacturing,' *The International Journal of Advanced Manufacturing Technology*, vol. 98, no. 5, pp. 1685–1694, 2018, ISSN: 1433-3015. DOI: 10.1007/s00170-018-2218-0. [Online]. Available: https://doi.org/10.1007/s00170-018-2218-0.

[95] B. Zhang, A. Goel, O. Ghalsasi and S. Anand, 'CAD-based design and pre-processing tools for additive manufacturing,' *Journal of Manufacturing Systems*, vol. 52, pp. 227–241, 2019, ISSN: 0278-6125. DOI: 10.1016/j.jmsy.2019.03.005. [Online]. Available: https://www.sciencedirect.com/science/article/pii/S0278612519300160.

[96] A. M. Al-Ahmari, O. Abdulhameed and A. A. Khan, 'An automatic and optimal selection of parts orientation in additive manufacturing,' *Rapid Prototyping Journal*, vol. 24, no. 4, pp. 698–708, 2018, ISSN: 1355-2546. DOI: 10.1108/RPJ-12-2016-0208. [Online]. Available: https://doi.org/10.1108/RPJ-12-2016-0208.

[97] G. Moroni, W. P. Syam and S. Petrò, 'Functionality-based Part Orientation for Additive Manufacturing,' *Procedia CIRP*, vol. 36, pp. 217–222, 2015, ISSN: 2212-8271. DOI: 10.1016/j.procir.2015.01.015. [Online]. Available: http://www.sciencedirect.com/science/article/pii/S2212827115000177.

[98] R. Harik, Y. Shi and S. Baek, 'Shape Terra: mechanical feature recognition based on a persistent heat signature,' *Computer-Aided Design and Applications*, vol. 14, no. 2, pp. 206–218, 2017, ISSN: null. DOI: 10.1080/16864360.2016.1223433. [Online]. Available: https://doi.org/10.1080/16864360.2016.1223433.

[99] M. D. Wilkinson, M. Dumontier, I. J. Aalbersberg, G. Appleton, M. Axton, A. Baak, N. Blomberg, J. W. Boiten, L. B. da Silva Santos, P. E. Bourne, J. Bouwman, A. J. Brookes, T. Clark, M. Crosas, I. Dillo, O. Dumon, S. Edmunds, C. T. Evelo, R. Finkers, A. Gonzalez-Beltran, A. J. Gray, P. Groth, C. Goble, J. S. Grethe, J. Heringa, P. A. t Hoen, R. Hooft, T. Kuhn, R. Kok, J. Kok, S. J. Lusher, M. E. Martone, A. Mons, A. L. Packer, B. Persson, P. Rocca-Serra, M. Roos, R. van Schaik, S. A. Sansone, E. Schultes, T. Sengstag, T. Slater, G. Strawn, M. A. Swertz, M. Thompson, J. Van Der Lei, E. Van Mulligen, J. Velterop, A. Waagmeester, P. Wittenburg, K. Wolstencroft, J. Zhao and B. Mons, 'Comment: The FAIR Guiding Principles for scientific data management and stewardship,' *Scientific Data*, vol. 3, Mar. 2016, ISSN: 2052-4463. DOI: 10.1038/sdata.2016.18.

[100] European Commission, *H2020 Online Manual: Open access & Data management*, 2016. [Online]. Available: https://ec.europa.eu/research/participants/docs/h2020-funding-guide/cross-cutting-issues/open-access-data-management/data-management_en.htm.

[101] T. L. Leirmo and O. Semeniuta, 'Investigating the Dimensional and Geometric Accuracy of Laser-Based Powder Bed Fusion of PA2200 (PA12): Experiment Design and Execution,' *Applied Sciences*, vol. 11, no. 5, p. 2031, 2021, ISSN: 2076-3417. DOI: 10.3390/app11052031. [Online]. Available: https://www.mdpi.com/2076-3417/11/5/2031.

[102] L. Rebaioli and I. Fassi, 'A review on benchmark artifacts for evaluating the geometrical performance of additive manufacturing processes,' *The International Journal of Advanced Manufacturing Technology*, vol. 93, no. 5, pp. 2571–2598, 2017, ISSN: 1433-3015. DOI: 10.1007/s00170-017-0570-0. [Online]. Available: https://doi.org/10.1007/s00170-017-0570-0.

[103] S. Moylan, J. Slotwinski, A. Cooke, K. Jurrens and M. A. Donmez, 'An additive manufacturing test artifact,' *Journal of research of the National Institute of Standards Technology*, vol. 119, pp. 429–459, 2014. DOI: 10.6028/jres.119.017.

[104] ISO/ASTM 52902:2019(E), *Additive manufacturing – Test artifacts – Geometric capability assessment of additive manufacturing systems*, Geneva, 2019.

[105] P. Minetola, L. Iuliano and G. Marchiandi, 'Benchmarking of FDM Machines through Part Quality Using IT Grades,' *Procedia CIRP*, vol. 41, pp. 1027–1032, 2016, ISSN: 2212-8271. DOI: 10.1016/j.procir.2015.12.075. [Online]. Available: https://doi.org/10.1016/j.procir.2015.12.075.

[106] V. Brøtan, 'A new method for determining and improving the accuracy of a powder bed additive manufacturing machine,' *The International Journal of Advanced Manufacturing Technology*, vol. 74, no. 9, pp. 1187–1195, 2014, ISSN: 1433-3015. DOI: 10.1007/s00170-014-6012-3. [Online]. Available: https://doi.org/10.1007/s00170-014-6012-3.

[107] C. F. J. Wu and M. S. Hamada, *Experiments: Planning, Analysis, and Optimization, 2nd Edition*, 2nd. Hoboken, New Jersey, USA: John Wiley & Sons, Inc., 2009, ISBN: 978-0-471-69946-0.

[108] T. L. Leirmo, *Data on dimensional and geometric accuracy for laser-based powder bed fusion of PA12 (PA2200)*, Gjøvik, 2021. DOI: 10.18710/DHACHZ.

[109] W. McKinney, 'Data Structures for Statistical Computing in Python,' in *Proceedings of the 9th Python in Science Conference*, S. van der Walt and J. Millman, Eds., 2010, pp. 56–61. DOI: 10.25080/Majora-92bf1922-00a.

[110] C. R. Harris, K. J. Millman, S. J. der Walt, R. Gommers, P. Virtanen, D. Cournapeau, E. Wieser, J. Taylor, S. Berg, N. J. Smith, R. Kern, M. Picus, S. Hoyer, M. H. van Kerkwijk, M. Brett, A. Haldane, J. del Río, M. Wiebe, P. Peterson, P. Gérard-Marchant, K. Sheppard, T. Reddy, W. Weckesser, H. Abbasi, C. Gohlke and T. E. Oliphant, 'Array programming with NumPy,' *Nature*, vol. 585, pp. 357–362, 2020, ISSN: 1476-4687. DOI: 10.1038/s41586-020-2649-2.

[111] J. D. Hunter, 'Matplotlib: A 2D Graphics Environment,' *Computing in Science & Engineering*, vol. 9, no. 3, pp. 90–95, 2007. DOI: 10.1109/MCSE.2007.55.

[112] M. Waskom, 'seaborn: statistical data visualization,' *Journal of Open Source Software*, vol. 6, no. 60, p. 3021, Apr. 2021, ISSN: 2475-9066. DOI: 10.21105/joss.03021.

[113] P. Virtanen, R. Gommers, T. E. Oliphant, M. Haberland, T. Reddy, D. Cournapeau, E. Burovski, P. Peterson, W. Weckesser, J. Bright, S. J. van der Walt, M. Brett, J. Wilson, K. J. Millman, N. Mayorov, A. R. J. Nelson, E. Jones, R. Kern, E. Larson, C. J. Carey, İ. Polat, Y. Feng, E. W. Moore, J. VanderPlas, D. Laxalde, J. Perktold, R. Cimrman, I. Henriksen, E. A. Quintero, C. R. Harris, A. M. Archibald, A. H. Ribeiro, F. Pedregosa, P. van Mulbregt and Scipy 1.0 contributors, 'SciPy 1.0: Fundamental Algorithms for Scientific Computing in Python,' *Nature Methods*, vol. 17, no. 3, pp. 261–272, 2020, ISSN: 1548-7105. DOI: 10.1038/s41592-019-0686-2.

[114] A. Meurer, C. P. Smith, M. Paprocki, O. Čertík, S. B. Kirpichev, M. Rocklin, A. Kumar, S. Ivanov, J. K. Moore, S. Singh, T. Rathnayake, S. Vig, B. E. Granger, R. P. Muller, F. Bonazzi, H. Gupta, S. Vats, F. Johansson, F. Pedregosa, M. J. Curry, A. R. Terrel, Š. Roučka, A. Saboo, I. Fernando, S. Kulal, R. Cimrman and A. Scopatz, 'SymPy: symbolic computing in Python,' *PeerJ Computer*

Science, vol. 3, e103, Jan. 2017, ISSN: 2376-5992. DOI: 10.7717/peerj-cs.103. [Online]. Available: https://peerj.com/articles/cs-103.

[115] P. Conzett, 'DataverseNO: A National, Generic Repository and its Contribution to the Increased FAIRness of Data from the Long Tail of Research,' *Ravnetrykk*, no. 39, May 2020, ISSN: 0804-4554. DOI: 10.7557/15.5514.

[116] Ø. Bjørke, *Computer-aided tolerancing*, 2nd. New York, U.S.A.: ASME Press, 1989, p. 216, ISBN: 0-7918-0010-5.

[117] R. Paul and S. Anand, 'Optimization of layered manufacturing process for reducing form errors with minimal support structures,' *Journal of Manufacturing Systems*, vol. 36, pp. 231–243, 2015, ISSN: 0278-6125. DOI: 10.1016/j.jmsy.2014.06.014. [Online]. Available: http://www.sciencedirect.com/science/article/pii/S0278612514000806.

[118] G. E. P. Box, 'Science and Statistics,' *Journal of the American Statistical Association*, vol. 71, no. 356, pp. 791–799, 1976.

[119] T. L. Leirmo and O. Semeniuta, 'Minimizing form errors in additive manufacturing with part build orientation - An optimization method for continuous solution spaces,' *Open Engineering*, vol. (Accepted),

[120] T. L. Leirmo, O. Semeniuta, I. Baturynska and K. Martinsen, 'Extracting shape features from a surface mesh using geometric reasoning,' *Procedia CIRP*, vol. 93, pp. 544–549, 2020, ISSN: 2212-8271. DOI: 10.1016/j.procir.2020.02.142. [Online]. Available: http://www.sciencedirect.com/science/article/pii/S2212827120306788.

[121] W. M. Wang, C. Zanni and L. Kobbelt, 'Improved Surface Quality in 3D Printing by Optimizing the Printing Direction,' *Computer Graphics Forum*, vol. 35, no. 2, pp. 59–70, 2016, ISSN: 1467-8659. DOI: 10.1111/cgf.12811. [Online]. Available: http://dx.doi.org/10.1111/cgf.12811.

[122] H. Budinoff and S. McMains, 'Prediction and visualization of achievable orientation tolerances for additive manufacturing,' *Procedia CIRP*, vol. 75, pp. 81–86, 2018, ISSN: 2212-8271. DOI: 10.1016/j.procir.2018.03.315. [Online]. Available: http://www.sciencedirect.com/science/article/pii/S2212827118304967.

[123] J. P. Kruth, G. Levy, F. Klocke and T. H. Childs, 'Consolidation phenomena in laser and powder-bed based layered manufacturing,' *CIRP Annals - Manufacturing Technology*, vol. 56, no. 2, pp. 730–759, 2007, ISSN: 0007-8506. DOI: 10.1016/j.cirp.2007.10.004.

[124] T. L. Leirmo, O. Semeniuta and K. Martinsen, 'Tolerancing from STL data: A Legacy Challenge,' *Procedia CIRP*, vol. 92, pp. 218–223, 2020, ISSN: 2212-8271. DOI: 10.1016/j.procir.2020.05.180. [Online]. Available: http://www.sciencedirect.com/science/article/pii/S221282712030946X.

[125] T. S. Leirmo and K. Martinsen, 'Deterministic part orientation in additive manufacturing using feature recognition,' *Procedia CIRP*, vol. 88, pp. 405–410, 2020, ISSN: 2212-8271. DOI: 10.1016/j.procir.2020.05.070. [Online]. Available: http://www.sciencedirect.com/science/article/pii/S2212827120303899.

Appendix A

Detailed descriptions of geometric features for AM

Based on previous studies and geometric primitives from CSG, the present work consider the five geometric features in figure A.1:

Planes are flat surfaces defined by a normal vector orthogonal to the surface.

Cylinders are surfaces revolved about a single axis. Both circular and elliptical cross-sectional cylinders are considered. The axis of revolution defines the orientation of the surface.

Cones are also revolved about a single axis, but with an apex angle. The axis of revolution defines the orientation of the surface.

Spheres are double-curved surfaces where a center point can be identified. Spheres have no orientation as such, but may be assigned an orientation based for example on the boundaries of the sphere.

Tori are doughnut-shaped surfaces, i.e. double-curved surfaces where the second axis of revolution is a ring around the center point. The orientation of a torus is defined as the orthogonal vector of the peripheral circumference.

Free-form surfaces does not easily fall within any of the surfaces above. These surfaces may be partitioned into small patches resembling the surfaces above, but are more effectively handled as

a free-form surface to reduce the number of geometric features. The orientation of such surfaces follows no set definition but may be determined from the general direction of the surface, or its boundary.

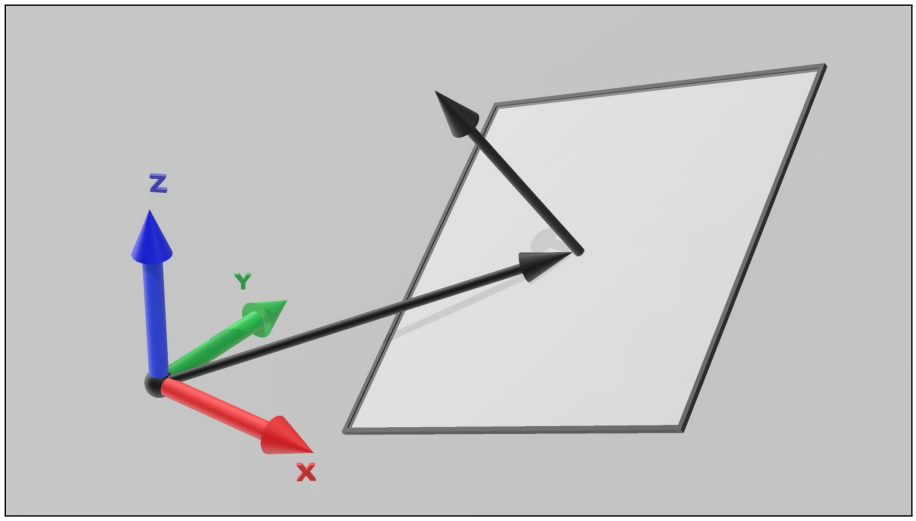

(a) Plane with position and orientation vector

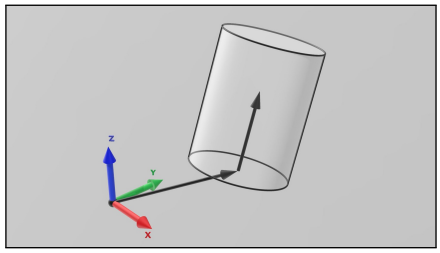

(b) Cylinder with position and orientation vector

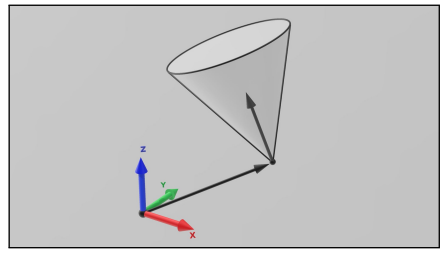

(c) Cone with position and orientation vector

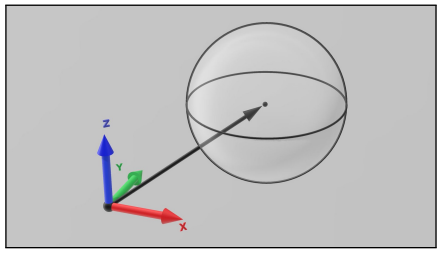

(d) Sphere with only position vector

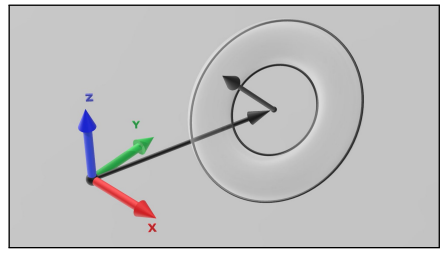

(e) Torus with position and orientation vector

Figure A.1: Shape features with position and orientation vectors. Spheres are not assigned an orientation due to three full degrees of freedom in rotation.

Appendix B

Details on build layout

The build layout of the experiments adopts a matrix structure of $3 \times 3 \times 5$ for the main specimens as described in table B.1. The open spaces between these fixed positions are used for additional specimens. This is done for the purpose of creating a more even slice distribution while also adding value to the experiment by generating more data. Figures B.2 and B.3 are screenshots from the Magics software used for build layout design. Each specimen type is assigned a separate color for visualization purposes. The slice distributions of all builds are visualized in figure B.1.

Table B.1: Detailed description of the build layout.

Index	Position			Coordinates			Orientation		
	x	y	z	x	y	z	Build 1	Build 2	Build 3
1	1	1	1	70	70	50.88	70	85	165
2	2	1	1	170	70	50.88	140	155	140
3	3	1	1	270	70	50.88	-90	-90	-90
4	1	2	1	70	170	50.88	145	180	75
5	2	2	1	170	170	50.88	165	170	95
6	3	2	1	270	170	50.88	120	175	10
7	1	3	1	70	270	50.88	110	130	0
8	2	3	1	170	270	50.88	-90	-90	-90
9	3	3	1	270	270	50.88	35	20	40
10	1	1	2	70	70	150.6	20	5	150
11	2	1	2	170	70	150.6	15	30	20
12	3	1	2	270	70	150.6	55	0	15
13	1	2	2	70	170	150.6	135	150	160
14	2	2	2	170	170	150.6	75	100	170
15	3	2	2	270	170	150.6	115	145	45
16	1	3	2	70	270	150.6	60	135	110
17	2	3	2	170	270	150.6	-90	-90	-90
18	3	3	2	270	270	150.6	40	140	85
19	1	1	3	70	70	250.32	80	115	135
20	2	1	3	170	70	250.32	130	55	50
21	3	1	3	270	70	250.32	-90	-90	-90
22	1	2	3	70	170	250.32	5	65	125
23	2	2	3	170	170	250.32	125	95	180
24	3	2	3	270	170	250.32	0	120	100
25	1	3	3	70	270	250.32	45	10	30
26	2	3	3	170	270	250.32	-90	-90	-90
27	3	3	3	270	270	250.32	100	50	115
28	1	1	4	70	70	350.04	65	25	105
29	2	1	4	170	70	350.04	170	160	65
30	3	1	4	270	70	350.04	95	70	120
31	1	2	4	70	170	350.04	175	80	25
32	2	2	4	170	170	350.04	85	40	55
33	3	2	4	270	170	350.04	30	45	70
34	1	3	4	70	270	350.04	150	15	60
35	2	3	4	170	270	350.04	-90	-90	-90
36	3	3	4	270	270	350.04	90	90	35
37	1	1	5	70	70	449.76	25	110	145
38	2	1	5	170	70	449.76	10	60	80
39	3	1	5	270	70	449.76	-90	-90	-90
40	1	2	5	70	170	449.76	160	125	5
41	2	2	5	170	170	449.76	105	105	155
42	3	2	5	270	170	449.76	155	75	90
43	1	3	5	70	270	449.76	180	35	130
44	2	3	5	170	270	449.76	-90	-90	-90
45	3	3	5	270	270	449.76	50	165	175

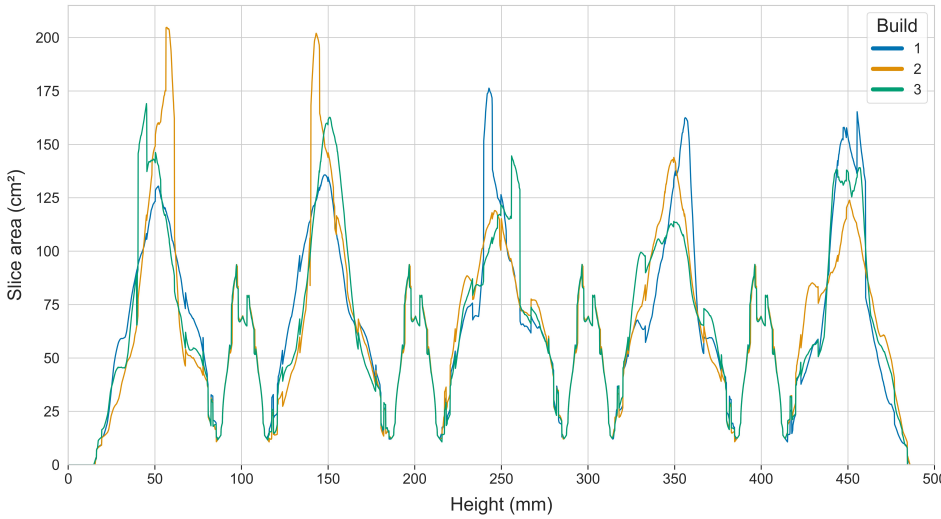

Figure B.1: Slice distributions for each build.

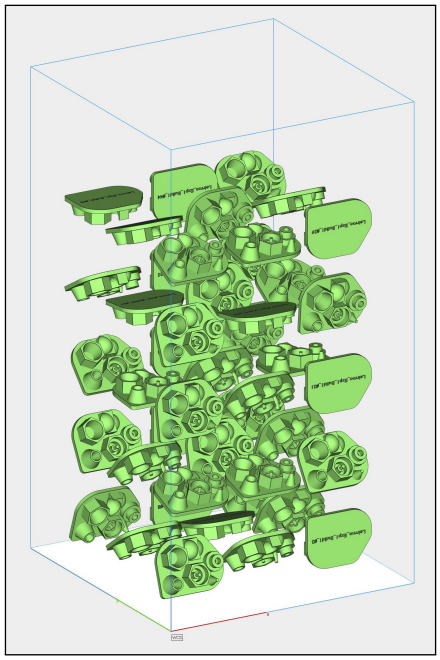

(a) Main specimens of build 1

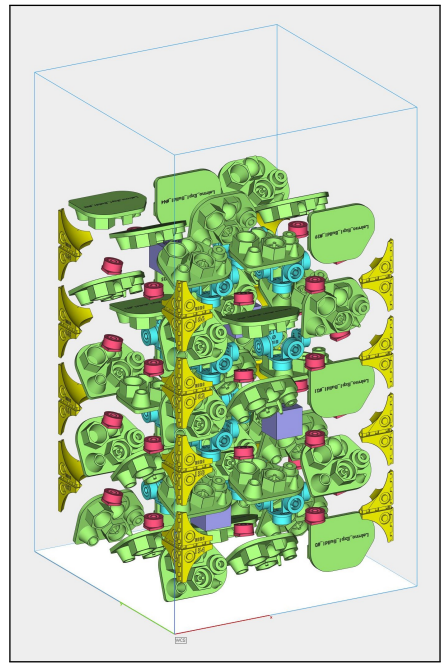

(b) Entire layout of build 1

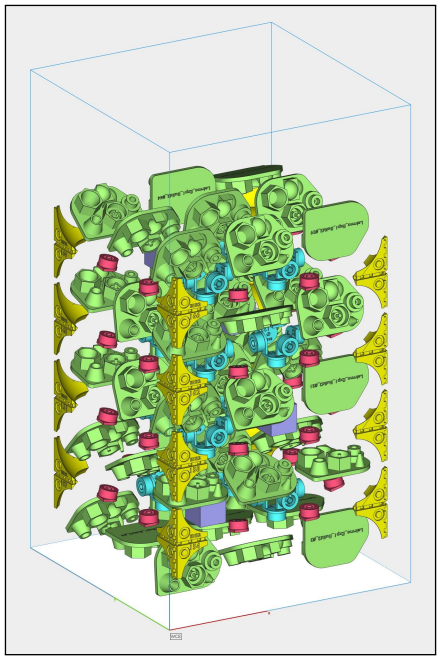

(c) Entire layout of build 2

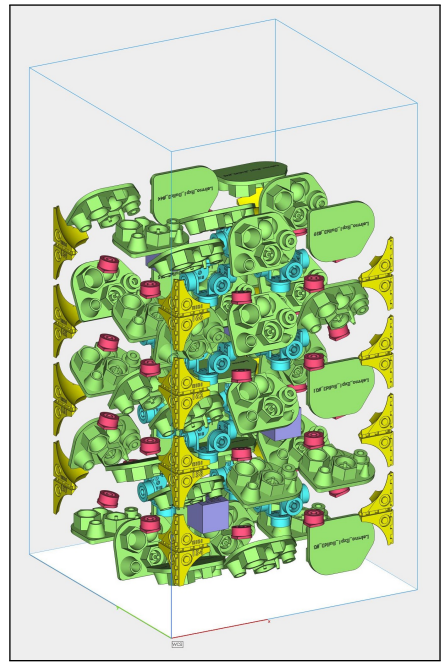

(d) Entire layout of build 3

Figure B.2: Screenshots from Magics showcasing the build layout (part 1)

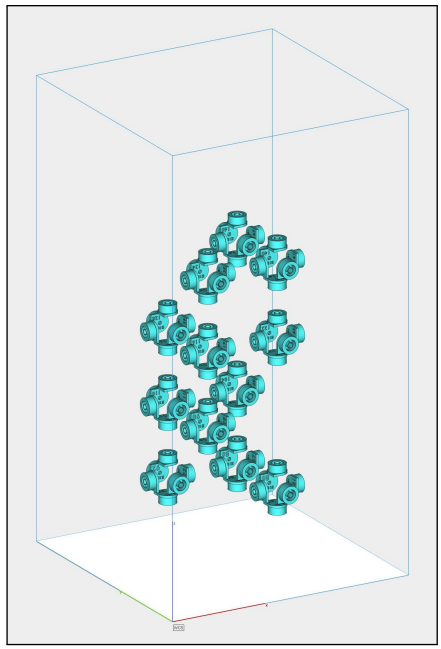

(a) Constellations of CA_F

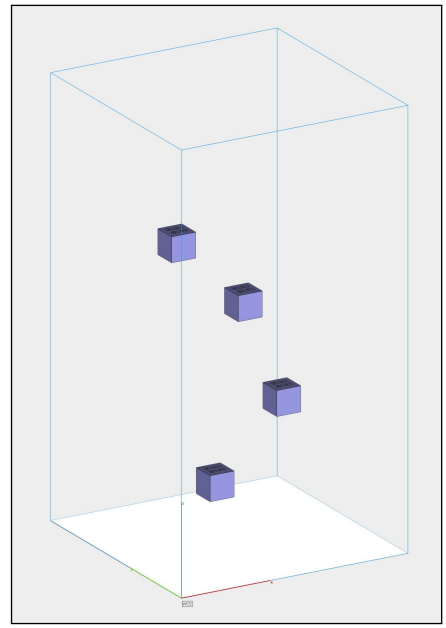

(b) Hollow boxes

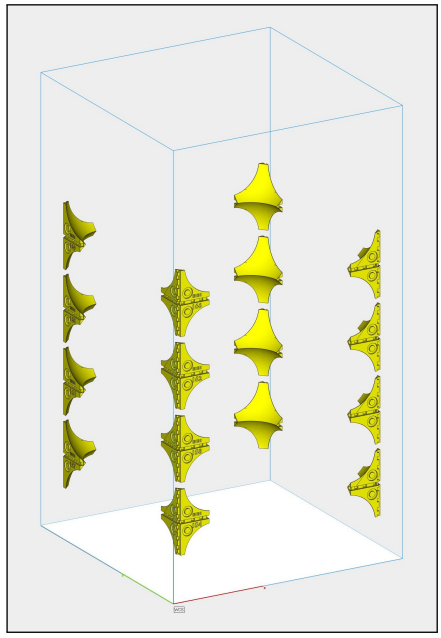

(c) Corner specimens

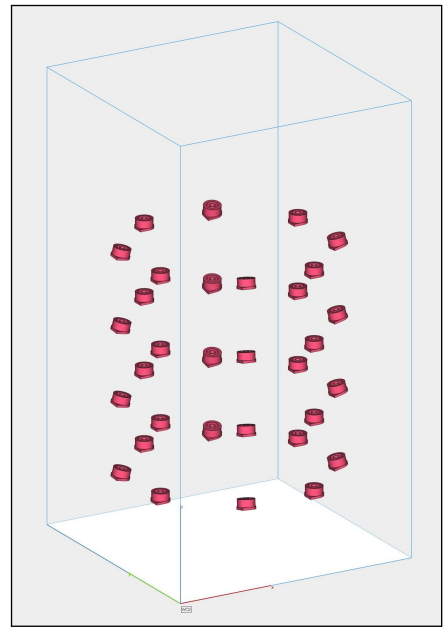

(d) CA_F around the edges

Figure B.3: Screenshots from Magics showcasing the build layout (part 2)

Appendix C

Details on artifact design

The test artifact utilized in the experiment was designed specifically for this project inspired by the design of Minetola, Iuliano and Marchiandi [105]. The artifact encompasses several features on a common base plate where the features are assigned to eight groups as displayed in figure C.1.

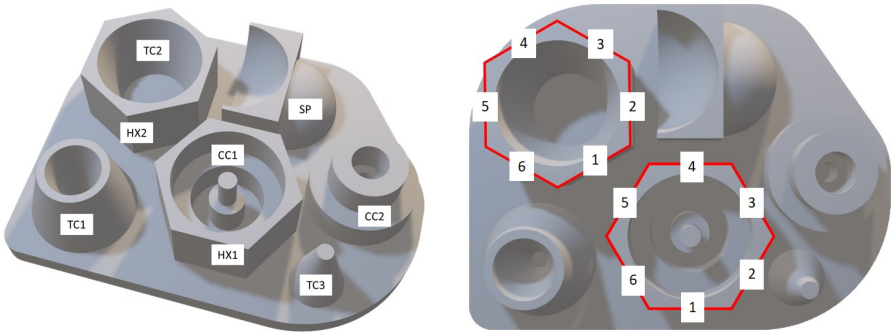

(a) All feature groups **(b)** Numbering within the HX groups

Figure C.1: Rendering of the test artifact where the feature groups are labeled.

Table C.1: Tabular description of artifact design.

Group	Description	Diameter [mm]	Position [mm] x	y	z	Normal vector x	y	z
HX1	plane	N/A	0.00	-13.86	8.00	0	-1	0
	Plane	N/A	12.00	-6.93	8.00	$\cos 30°$	-0.5	0
	Plane	N/A	12.00	6.93	8.00	$\cos 30°$	0.5	0
	Plane	N/A	0.00	13.86	8.00	0	1	0
	Plane	N/A	-12.00	6.93	8.00	$-\cos 30°$	0.5	0
	Plane	N/A	-12.00	-6.93	8.00	$-\cos 30°$	-0.5	0
HX2	plane	N/A	-18.43	13.43	8.00	0.5	$-\cos 30°$	0
	Plane	N/A	-11.50	25.43	8.00	1	0	0
	Plane	N/A	-18.43	37.43	8.00	0.5	$\cos 30°$	0
	Plane	N/A	-32.28	37.43	8.00	-0.5	$\cos 30°$	0
	Plane	N/A	-39.21	25.43	8.00	-1	0	0
	Plane	N/A	-32.28	13.43	8.00	-0.5	$-\cos 30°$	0
CC1	Cylinder	24.00	0.00	0.00	8.00	0	0	1
	Cylinder	16.00	0.00	0.00	0.00	0	0	1
	Cylinder	8.00	0.00	0.00	0.00	0	0	1
	Cylinder	4.00	0.00	0.00	8.00	0	0	1
CC2	Cylinder	24.00	-24.49	18.00	0.00	0	0	1
	Cylinder	16.00	-24.49	18.00	8.00	0	0	1
	Cylinder	8.00	-24.49	18.00	8.00	0	0	1
	Cylinder	4.00	-24.49	18.00	0.00	0	0	1
TC1	Cone	24.00	21.36	-24.38	0.00	0	0	1
	Cone	12.00	21.36	-24.38	16.00	0	0	-1
TC2	Cone	24.00	-9.34	-34.67	16.00	0	0	-1
TC3	Cone	12.00	-2.53	24.86	0.00	0	0	1
SP	Sphere	24.00	-30.84	-10.30	0.00	0	0	0
	Sphere	24.00	-24.34	-21.56	13.00	0	0	0

Appendix D

Details on fixture design

A unique fixture was designed for holding the specimens in place during the inspection. This fixture also ensures that all specimens are inspected under close to identical conditions in the CMM. The fixture was designed in Solidworks 2018, and the schematics are presented in figure D.1.

The internal dimensions of the fixture are marginally larger than the nominal dimensions of the test artifact to facilitate specimen exchange, and also leave room for moderate dimensional variations. The fixture was produced in a Prusa MK2.5 FFF machine and is depicted in figure D.2(b) where a prototype of the artifact is mounted in the fixture. The design is intended for the Zeiss Duramax CMM where M10 bolts are used to attach the fixture to the measurement table.

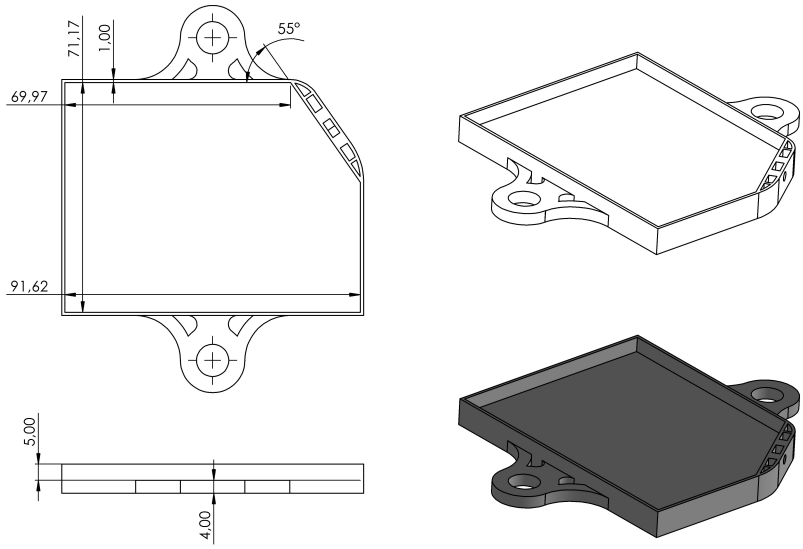

Figure D.1: Drawing and rendering of the designed fixture. The slot in the cut corner is designed to hold an M4 nut in which the bolt for clamping is inserted.

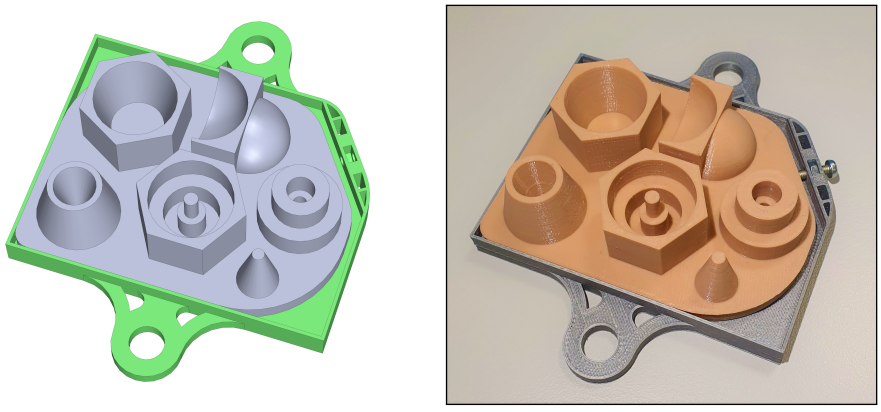

(a) Rendering from Solidworks **(b)** 3D-printed fixture

Figure D.2: Mounting of artifact in the designed fixture.

Part 2: Original papers

Paper P1

T. S. Leirmo and K. Martinsen, 'Evolutionary algorithms in additive manufacturing systems: Discussion of future prospects,' *Procedia CIRP*, vol. 81, pp. 671–676, 2019, ISSN: 2212-8271. DOI: 10.1016/j.procir.2019.03.174. [Online]. Available: http://www.sciencedirect.com/science/article/pii/S2212827119304792

Available online at www.sciencedirect.com

ScienceDirect

Procedia CIRP 81 (2019) 671–676

www.elsevier.com/locate/procedia

52nd CIRP Conference on Manufacturing Systems

Evolutionary algorithms in additive manufacturing systems: Discussion of future prospects

Torbjørn Schjelderup Leirmo[a,]*, Kristian Martinsen[a]

[a]*Department of Manufacturing and Civil Engineering, Norwegian University of Science and Technology, Teknologivegen 22, 2815 Gjøvik, Norway*

* Corresponding author. Tel.: +47 480 88 390. *E-mail address:* torbjorn.leirmo@ntnu.no

Abstract

Additive Manufacturing (AM) as a manufacturing process is increasingly implemented in manufacturing and is thus subjected to the high demands of industry. With the industrialization of AM technologies follows demands regarding not only dimensions and tolerances, but also mechanical properties, processing time and cost. The multi-objective optimization problems arising from AM is just another venue where Evolutionary Algorithms (EAs) are applied. This paper attempts to provide an overview of the current role of EAs in AM in order to make a discussion on the future prospects of EAs in the industry.

© 2019 The Authors. Published by Elsevier Ltd.
This is an open access article under the CC BY-NC-ND license (http://creativecommons.org/licenses/by-nc-nd/3.0/)
Peer-review under responsibility of the scientific committee of the 52nd CIRP Conference on Manufacturing Systems.

Keywords: Evolutionary algorithm; Additive Manufacturing; Optimization; Metaheuristic; Swarm intelligence; Artificial intelligence

1. Introduction

Over the last thirty years, Additive Manufacturing (AM) has developed from a rapid prototyping technology to a broad concept encompassing a variety of manufacturing technologies ranging from desktop 3D-printers for private use, to large industrial machines for high-end metal processing [1, 2]. AM is currently being implemented in industry both as a stand-alone process, as well as in tandem with traditional manufacturing technologies in hybrid manufacturing systems [3]. AM is, however still an immature process and the many challenges has sparked significant efforts in the research community for the optimization of the build process to improve part quality, repeatability and reliability [4, 5]. Mitigating these challenges further enables integration of AM in modern production systems and is vital for the continued growth of AM in manufacturing industry [6, 7].

This paper aims to review the current role of evolutionary algorithms (EAs) in AM systems to get an understanding of the future prospects of EAs in the AM discourse, and possible future developments of EAs in AM industry.

1.1. Additive Manufacturing

Since the first Stereolithography Apparatus (SLA) was patented in 1986 [8], various methods for fabricating three dimensional objects in a layered fashion has been developed, resulting in a total of seven AM process categories as defined by ISO/ASTM 52900:2015 [9]:

- Binder Jetting
- Directed Energy Deposition
- Material Extrusion
- Material Jetting
- Powder Bed Fusion
- Sheet Lamination
- Vat Photopolymerization

The above categorization covers all current AM technologies regardless of build material, and they all involve sequential addition of material with the accompanying benefits and drawbacks [2]. The layered manner of part fabrication results in anisotropic material properties, which is

2212-8271 © 2019 The Authors. Published by Elsevier Ltd.
This is an open access article under the CC BY-NC-ND license (http://creativecommons.org/licenses/by-nc-nd/3.0/)
Peer-review under responsibility of the scientific committee of the 52nd CIRP Conference on Manufacturing Systems.
10.1016/j.procir.2019.03.174

one of the major hurdles to reliability and quality assurance [5]. Other defects and inaccuracies observed in AM includes material failures, stair stepping, surface roughness and dimensional inaccuracies, all of which can be mitigated with proper machine settings and part build orientation [1, 2, 10].

No matter how significant, part properties is only one of several challenges in AM. The long build time of AM compared to its alternative conventional technologies continues to be a compelling argument against the adoption of AM in mass production. On the other hand, has AM large potential for manufacturing of very complex components. The advanced geometries enabled by AM further complicates the already complex problem of part placement in the build chamber [11]. Optimization of geometry, process planning, and layout optimization remains crucial to increase the efficiency and reduce lead time of AM [12]. Such problems are not trivial, and the possibility of mass customization indicates that optimization problems must be solved on a regular basis.

The generic process of additive manufacturing can be decomposed into eight discrete steps from part design to part application as illustrated in Fig. 1 [1]. Depending on the vendor of the AM machine and software, part orientation and placement may be conducted either prior to machine setup, or in the same processing step. The final step of application may not imply end use but could also be additional treatment such as priming or painting, or it could be part of an assembly e.g. in a hybrid manufacturing system.

The need for optimization in AM is perhaps most apparent in the earlier stages of design and process planning, but later stages of the AM process chain are also important and indeed valid for optimization efforts. The development of real-time closed loop feedback control systems for in-build process optimization is an important research area for improved part quality [13].

1.2. Evolutionary Algorithms

In this paper, an EA is defined in accordance with the definition of Dan Simon as "[…] an algorithm that evolves a problem solution over many iterations" [14, p. 3]. This generally includes population-based and bio-inspired metaheuristics and, perhaps more controversial, swarm intelligence. This definition further places EAs under the umbrella of artificial intelligence as a subset of soft computing and related to machine learning [14].

Finding the exact solution to an optimization problem is a complicated task that has been relying on computers for half a century [15]. As the complexity of optimization problems increases, the means to solve them inevitably do the same. One measure to overcome the complexity of optimization problems is to take inspiration from how optimization problems are solved in nature. EAs were originally developed by biologists in the late 50s and early 60s to simulate biological evolution [16]. However, the algorithms turned out to be well suited for optimization problems, and so the Genetic Algorithm (GA) was applied to optimization problems. This created the foundation for other algorithms such as Genetic Programming (GP) and Evolutionary Programming, and also more recent concepts such as Simulated Annealing (SA) and swarm intelligence including Particle Swarm Optimization (PSO) and Ant Colony Optimization [14].

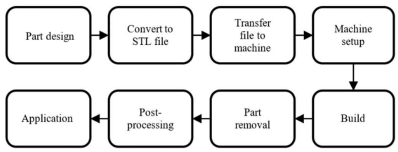

Fig. 1. Typical additive manufacturing processing steps. Adapted from [1].

The basis of any EA is a general architecture inducing certain properties and basic abilities providing wide applicability in problem solving. Yet, the algorithms are adaptable, and it is advised to include problem specific information to improve performance [14].

One of the great contributions of EAs is their ability to maintain a population of candidate solutions, effectively exploring different areas of the solution space simultaneously. When considering multiple contradicting objectives, the complexity of optimization becomes increasingly difficult as a trade-off must be made. This trade-off can either be conducted in one of two ways. The weighted sum method effectively converts a multi-objective problem into a single-objective problem by normalizing the objectives before they are multiplied with a scaling factor. However, the result will be biased by the weights assigned to the objectives and thus the validity of results are questionable.

Another approach strongly advocated in more recent research, is to allow the optimization algorithm to converge to multiple solutions constituting the Pareto front. The Pareto front is the set of non-dominated solutions, i.e. solutions where an improvement in one objective has a negative effect on at least one other objective. An educated selection can then be made among the presented set of non-dominated solutions resulting in a more fitting solution [17].

2. Current situation

EAs have been applied to a number of problems in AM ranging from the design stage through process planning to machine setup [6]. The following section provides a brief overview of current applications of EAs in AM systems.

2.1. Design for Additive Manufacturing

AM relieves designers of traditional manufacturing constraints, and new AM-specific constraints are imposed [2]. This calls for a paradigm shift from traditional design for manufacture and assembly, to design for AM (DfAM) [1, 18].

GAs have been extensively used in engineering design at an early stage outside the AM domain, and a thorough review of early use cases is provided by Renner and Ekárt [19]. The geometric freedom available in AM makes it possible to design cellular structures and topologically optimized (TO) parts unattainable by conventional methods [20]. The complex structures of such designs make EAs a good tool for computer-aided design [21].

Salonitis et al. used a GA to reduce part weight by optimizing the strut diameter in a lattice structure with constraints formulated as maximum displacement [22]. GA can also be found in TO of concrete structures enabled by additive deposition of concrete [21]. Other efforts utilize PSO for design of cellular structures in AM [23, 24], and the performance of PSO is found to exceed that of the Levenberg-Marquardt method which is widely used [24].

EAs can also be used to create the design from scratch with a process known as generative design. Dhokia, Essink, Flynn and Goguelin demonstrates how a termite nest building algorithm inspired by Ant Colony Optimization is used to generate a design given some loading conditions, a build envelope and some general objectives [25, 26]. Yao et al. applied the Non-dominated Sorting Genetic algorithm (NSGA-II) of Deb et al. [27] to aid the designer in selecting proper materials, components, AM technology and dimensional parameters [28]. GAs have also proven useful for assessing design feasibility [29].

AM enables new functionally graded materials, allowing two or more materials to be seamlessly combined in a single part [20]. As the multimodal nature of the solution space makes it difficult for numerical methods to obtain optimal results, EAs are often utilized to determine material distributions. Kou et al. demonstrates the ability of PSO to design functionally graded materials [30], and a case study on functionally graded materials in a dental implant found that GA and SA achieve better results than the more traditional response surface method [31]. Hiller and Lipson reports interesting work on automatic design of soft robots building on functionally graded materials for ductility and applies a GA [32].

2.2. Optimization of part build orientation

The problem of orientation in AM can be traced back to 1994 [33], but it took another ten years before Thrimurthulu, Pandey and Reddy proposed a solution using a GA and the weighted sum method [34]. Later the same year they used the NSGA-II to find the Pareto front [35]. Both of these applications was applied to Fused Deposition Modelling (FDM) considering surface roughness and build time [34, 35].

In addition to FDM [36-39], later applications of EAs also includes other AM technologies such as SLA [40-43], Selective Laser Sintering (SLS) [44, 45], Selective Laser Melting (SLM) [46, 47], and combinations of SLA, SLS and FDM [48, 49]. Furthermore, other objectives are considered for the optimization problem such as material use [44, 46], volumetric error [37, 39, 50-52], support structures [36, 43, 46, 47, 52] and mechanical properties [36, 47]. The objective of minimizing post processing time and cost by GA was proposed by Kim and Lee who considered part height, surface roughness and support structures in SLA [42]. Zhang et al. used a GA to simultaneously optimize the orientation of 16 parts for minimizing build cost in multi-part production with a total of five objectives [41]. A recent optimization scheme also using GA was proposed by Brika et al. where eight objectives was considered in SLM including yield strength, tensile strength and elongation, in addition to typical objectives such as build time, surface roughness and support structures [47].

It is clear that GA is the most widely used EA in the field of part build orientation, but examples of other population based algorithms do exist. Padhye, Deb and Kalia compared the performance of NSGA-II with a multi-objective PSO and found that the latter was outperformed, both in terms of execution time and quality of results [38, 45]. A more recent application of PSO is proposed by Barclift et al. who applied the algorithm to minimize cost in SLM [46].

Other implementations include the unconventional DNA-based EA proposed by Tyagi et al. for minimizing stair stepping and build time [39].

2.3. Placement of parts in the build space

The placement of parts in the AM build space, also known as layout planning, nesting or part packing, is important to reduce build time and improve efficiency. EAs was applied to the packing problem at an early stage with GA being applied to SLA already in 1994 for the sequential packing of boxes in two and three dimensions [53]. A GA directed at SLS was introduced in 1997 working on bounding boxes [54] and later improved to utilize multiple CPUs [55]. GAs was later used in two dimensions for packing parts according to their projections onto the build plane [12, 56, 57].

Some years after the first GA, Dickinson and Knopf applied SA to the packing problem [58, 59] and inspired further applications of SA in the field [60]. More recently, a re-seeding mechanism in SA was proposed by Cao et al. [61]. The re-seeding is a measure to prevent pre-mature convergence to a sub-optimal solution manifested as a local optimum in the solution space.

Zhang et al. [12] argues that orientation should be considered in the packing process to ensure part quality. GAs are used to solve this problem both for two [12, 57] and three dimensions [11, 62-64].

2.4. Build parameter optimization

Rong-Ji et al. used a combination of GA and Artificial Neural Network (ANN) to optimize the process parameters of SLS considering part shrinkage [65]. The relations between seven processing parameters and part shrinkage was described by ANN, and later used as input for the GA which optimized the parameter settings. GA has also been applied in Direct Metal Laser Sintering to optimize hatch direction to improve material properties [66]. The melt pool of Laser Direct Metal Deposition is shown to be predictable by ANN [67], and PSO was proposed by Mozaffari et al. in combination with a Self-organizing Pareto based EA for optimizing process parameters [68]. A modified version of the NSGA-II has also been proposed to optimize final part properties [69].

The tool path in Laminated Object Manufacturing is similar to that in conventional machining operations and can also be optimized by GA [70].

The surface quality of FDM has been optimized by applying ANN in combination with bacterial foraging

optimization algorithm [71], and an improved ANN based on PSO and the Imperialist Competitive Algorithm [72].

Rao and Rai used their Teaching-Learning Based Optimization EA for optimizing the compressive strength in FDM and achieved better performance compared with GA and a PSO algorithm [73]. A non-dominated sorting version of PSO was also applied to a multi-objective problem and performed similarly to NSGA-II.

Vijayaraghavan et al. proposed using GP in FDM to enable offline prediction of final part properties and achieved results comparable to ANN and support vector regression [74]. A similar effort is found in [75] where GP is proposed for modelling characteristics of SLS, and in [76] where GP is used to model the bead size in Wire and Arc AM.

2.5. Other applications in additive manufacturing systems

Ewald et al. used a mixed integer GA to find the most cost effective solution for hybrid manufacturing using wrought material as a basis for Laser Metal Deposition [77]. The single objective GA varied the size, orientation and position of the work piece to obtain the most economical work distribution between conventional milling and additive manufacturing.

Xu et al. applied a GA to the problem of adaptive part slicing for improved surface roughness in SLA. Their algorithm considered horizontal sections of the STL model sequentially and determined the slice thickness for each section independently of neighboring sections. The benefit of an EA became apparent with increasing geometric complexity as the number of local optima increased drastically [78].

3. Trends and future prospects

New and better applications of EAs are still published regularly even 25 years after its initial introduction to the field of AM. Based on the literature presented in the previous section, it is apparent that few variations of EAs are documented in the literature as most efforts focus on GAs. Furthermore, a rather limited range of technologies and materials have been subjected to EAs in the literature except for FDM which is generally quite well covered. Future developments should contribute to closing this gap by testing of new algorithms on different technologies and materials.

3.1. Variations of evolutionary algorithms

The long history of GAs may explain why this is such a popular method even though closely related metaheuristics such as Evolutionary Programming and Evolution Strategies are not to be found anywhere in AM discourse, and GP is only found to be used by a single group of researchers [74-76]. The meta-perspective of these methods facilitates flexibility and might enable a single solution for multiple technologies. This contradicts the recommendation of tailoring EAs to specific problems to improve performance [14].

Other variations of EAs may be introduced in the field of AM as they mature over the years to come. New EAs are proposed with different inspirations, most of which are bio-inspired and draw parallels to natural optimization processes e.g. Ant Colony Optimization and Bacterial Foraging Optimization. An argument could be made that separating the algorithm from its original biological inspiration may be the path to more effective solutions as they relieve the developer from constraints imposed by the biological origins of the algorithm.

History show that increasing computational power enables more complex algorithms with more constraints, objectives and parameters. Part packing is a good example where the problem has been simplified due to computational limitations. With more power, comes more possibilities as it not only facilitates details in optimization, but also enables the consideration of more parameters and constraints. Future applications of EAs in AM are likely to benefit from advancements in computational power and generally produce results of higher quality [6].

3.2. Processes and materials

The literature on EAs in AM is dominated by the plastic processing technologies SLA, FDM and SLS. The large players in industry are however often primarily interested in high value metal applications where mechanical and geometrical tolerances are paramount [7]. The reasons why there are so few use cases in metal AM is surely many, but one major factor is the need for establishing process knowledge and discovery of causal relationships between process parameters and final part properties. With better understanding of the process, better predictions can be made on part properties which enables EAs to be applied to optimize process parameters.

The application of machine learning could play a major role in the optimization of individual AM machines settings. The customization of process parameters for a single machine or even a specific part is made possible through e.g. Artificial Neural Networks. Further advances could be achieved if knowledge gained from one process could be transferred to another. The extraction of process knowledge from one machine to another without human involvement is an interesting area of future research which requires computational intelligence.

3.3. Other prospects

Integration of AM in industrial environments is likely to bring about more hybrid manufacturing solutions where AM is used together with conventional manufacturing technologies. EAs have already been used to aid in process planning for hybrid systems [77]. However, designing for hybrid manufacturing could bring about previously unknown issues where EAs are good problem solvers due to the complex and multimodal nature of real-world problems.

4. Concluding remarks

EAs are popular tools for optimization of complex multi-objective problems in the AM domain related to design, process planning and machine setup. Many applications of GA and PSO are present in the literature, but rather few

variations of EAs are found in use cases. It is expected that future applications derive advantage from increasing computational power which enables new algorithms to be more sophisticated and precise.

EAs are already present in design applications but is likely to become even more important as hybrid manufacturing becomes more common in industry. The complexity induced by combining additive and subtractive technologies inspires for increased exploration of EAs in the AM domain.

Finally, closed loop process control and optimization by machine learning could be of major importance in the effort towards industrialization of AM. Part quality and repeatability is vital to inspire wide spread implementation of AM in the manufacturing industry. EAs are crucial tools in the optimization processes necessary to achieve this goal, and collaboration between academia and industry will be the final step in bridging the gap from research to implementation.

Acknowledgements

This research is funded by the Norwegian Ministry of Research and Education, and is associated with SFI Manufacturing.

References

[1] Gibson I, Rosen DW, Stucker B. Additive manufacturing technologies. 2nd ed. New York: Springer; 2015.
[2] Gao W, Zhang Y, Ramanujan D, Ramani K, Chen Y, Williams CB, et al. The status, challenges, and future of additive manufacturing in engineering. Comput Aided Des. 2015;69:65–89.
[3] Dilberoglu UM, Gharehpapagh B, Yaman U, Dolen M. The Role of Additive Manufacturing in the Era of Industry 4.0. Procedia Manuf. 2017;11:545–54.
[4] Delgado J, Ciurana J, Rodríguez CA. Influence of process parameters on part quality and mechanical properties for DMLS and SLM with iron-based materials. Int J Adv Manuf Technol. 2012;60(5):601–10.
[5] Horn TJ, Harrysson OLA. Overview of current additive manufacturing technologies and selected applications. Sci Prog. 2012;95(3):255–82.
[6] Majewski C. Applications of Evolutionary Computing to Additive Manufacturing. In: Tiwari M, Harding JA, editors. Evolutionary Computing in Advanced Manufacturing. Massachusetts: Scrivener Publishing LCC; 2011. p. 197–234.
[7] Pradel P, Zhu Z, Bibb R, Moultrie J. Investigation of design for additive manufacturing in professional design practice. J Eng Des. 2018;29(4–5):165–200.
[8] Hull CW. Apparatus for production of three-dimensional objects by stereolithography. US patent US4575330 A. 1986.
[9] ISO/ASTM 52900:2015. Standard Terminology for Additive Manufacturing – General Principles – Terminology. ISO/ASTM; 2015.
[10] Baturynska I. Statistical analysis of dimensional accuracy in additive manufacturing considering STL model properties. Int J Adv Manuf Technol. 2018;97:2835–49.
[11] Gogate AS, Pande SS. Intelligent layout planning for rapid prototyping. Int J Prod Res. 2008;46(20):5607–31.
[12] Zhang Y, Gupta RK, Bernard A. Two-dimensional placement optimization for multi-parts production in additive manufacturing. Robot Comput-Integr Manuf. 2016;38:102–17.
[13] Chua ZY, Ahn IH, Moon SK. Process monitoring and inspection systems in metal additive manufacturing: Status and applications. Int J Precis Eng Manuf-Green Technol. 2017;4(2):235–45.
[14] Simon D. Evolutionary optimization algorithms. New Jersey: John Wiley & Sons; 2013.
[15] Dantzig GB. Reminiscences about the origins of linear programming. Operations Research Letters. 1982;1(2):43–8.
[16] Goldberg DE. Genetic Algorithms in Search, Optimization and Machine Learning: Addison-Wesley Longman Publishing Co., Inc.; 1989.
[17] Deb K. Multi-Objective Optimization Using Evolutionary Algorithms. Chichester: John Wiley & Sons; 2008.
[18] Thompson MK, Moroni G, Vaneker T, Fadel G, Campbell RI, Gibson I, et al. Design for Additive Manufacturing: Trends, opportunities, considerations, and constraints. CIRP Annals. 2016;65(2):737–60.
[19] Renner G, Ekárt A. Genetic algorithms in computer aided design. Comput Aided Des. 2003;35(8):709–26.
[20] Rosen DW. A review of synthesis methods for additive manufacturing. Virtual Phys Prototyp. 2016;11(4):305–17.
[21] Duballet R, Gosselin C, Roux P. Additive Manufacturing and Multi-Objective Optimization of Graded Polystyrene Aggregate Concrete Structures. In: Thomsen MR, Tamke M, Gengnagel C, Faircloth B, Scheurer F, editors. Modelling Behaviour: Design Modelling Symposium 2015. Cham: Springer International Publishing; 2015. p. 225–35.
[22] Salonitis K, Chantzis D, Kappatos V. A hybrid finite element analysis and evolutionary computation method for the design of lightweight lattice components with optimized strut diameter. Int J Adv Manuf Technol. 2017;90(9):2689–701.
[23] Chu C, Graf G, Rosen DW. Design for Additive Manufacturing of Cellular Structures. Comput Aided Des Appl. 2008;5(5):686–96.
[24] Chu J, Engelbrecht S, Graf G, Rosen DW. A comparison of synthesis methods for cellular structures with application to additive manufacturing. Rapid Prototyp J. 2010;16(4):275–83.
[25] Essink WP, Flynn JM, Goguelin S, Dhokia V. Hybrid Ants: A New Approach for Geometry Creation for Additive and Hybrid Manufacturing. Procedia CIRP. 2017;60:199–204.
[26] Dhokia V, Essink WP, Flynn JM. A generative multi-agent design methodology for additively manufactured parts inspired by termite nest building. CIRP Annals. 2017;66(1):153–6.
[27] Deb K, Agrawal S, Pratap A, Meyarivan T. A Fast Elitist Non-dominated Sorting Genetic Algorithm for Multi-objective Optimization: NSGA-II. In: Schoenauer M. et al., editors. Parallel Problem Solving from Nature PPSN VI; Paris, France: Springer; 2000.
[28] Yao X, Moon SK, Bi G. Multidisciplinary design optimization to identify additive manufacturing resources in customized product development. J Comput Des Eng. 2017;4(2):131–42.
[29] Hsiao S-W, Chiu F-Y, Lu S-H. Product-form design model based on genetic algorithms. Int J Ind Ergon. 2010;40(3):237–46.
[30] Kou XY, Parks GT, Tan ST. Optimal design of functionally graded materials using a procedural model and particle swarm optimization. Comput Aided Des. 2012;44(4):300–10.
[31] Sadollah A, Bahreininejad A. Optimum gradient material for a functionally graded dental implant using metaheuristic algorithms. J Mech Behav Biomed Mater. 2011;4(7):1384–95.
[32] Hiller J, Lipson H. Automatic Design and Manufacture of Soft Robots. IEEE Trans Robot. 2012;28(2):457–66.
[33] Allen S, Dutta D. On the computation of part orientation using support structures in layered manufacturing. Proceedings of Solid Freeform Fabrication Symposium, University of Texas at Austin; 1994.
[34] Thrimurthulu K, Pandey PM, Reddy NV. Optimum part deposition orientation in fused deposition modeling. Int J Mach Tool Manuf. 2004;44(6):585–94.
[35] Pandey PM, Thrimurthulu K, Reddy NV. Optimal part deposition orientation in FDM by using a multicriteria genetic algorithm. Int J Prod Res. 2004;42(19):4069–89.
[36] Luo Z, Yang F, Dong G, Tang Y, Zhao YF. Orientation Optimization in Layer-Based Additive Manufacturing Process. Computers and Information in Engineering Conference; Charlotte, North Carolina, USA: ASME; 2016.
[37] Ghorpade A, Karunakaran KP, Tiwari MK. Selection of optimal part orientation in fused deposition modelling using swarm intelligence. Proc Inst Mech Eng B J Eng Manuf. 2007;221(7):1209–19.
[38] Padhye N, Kalia S. Rapid prototyping using evolutionary approaches: part 1. In: Raidl G, editor. Proceedings of the 11th Annual Conference Companion on Genetic and Evolutionary Computation Conference: Late Breaking Papers; Montreal, Canada: ACM; 2009.

[39] Tyagi SK, Ghorpade A, Karunakaran KP, Tiwari MK. Optimal part orientation in layered manufacturing using evolutionary stickers-based DNA algorithm. Virtual Phys Prototyp. 2007;2(1):3–19.
[40] Canellidis V, Giannatsis J, Dedoussis V. Genetic-algorithm-based multi-objective optimization of the build orientation in stereolithography. Int J Adv Manuf Technol. 2009;45(7):714–30.
[41] Zhang Y, Bernard A, Harik R, Karunakaran KP. Build orientation optimization for multi-part production in additive manufacturing. J Intell Manuf. 2017;28(6):1393–407.
[42] Kim H-C, Lee S-H. Reduction of post-processing for stereolithography systems by fabrication-direction optimization. Comput Aided Des. 2005;37(7):711–25.
[43] Nezhad AS, Barazandeh F, Rahimi AR, Vatani M. Pareto-Based Optimization of Part Orientation in Stereolithography. Proc Inst Mech Eng B J Eng Manuf. 2010;224(10):1591–8.
[44] Phatak AM, Pande SS. Optimum part orientation in Rapid Prototyping using genetic algorithm. J Manuf Syst. 2012;31(4):395–402.
[45] Padhye N, Deb K. Multi - objective optimisation and multi - criteria decision making in SLS using evolutionary approaches. Rapid Prototyp J. 2011;17(6):458–78.
[46] Barclift M, Armstrong A, Simpson TW, Joshi SB. CAD-Integrated Cost Estimation and Build Orientation Optimization to Support Design for Metal Additive Manufacturing. 43rd Design Automation Conference; Cleveland, Ohio, USA: ASME; 2017.
[47] Brika SE, Zhao YF, Brochu M, Mezzetta J. Multi-Objective Build Orientation Optimization for Powder Bed Fusion by Laser. Journal of Manufacturing Science and Engineering. 2017;139(9):111011-1–9.
[48] Byun HS, Lee KH. Determination of the optimal part orientation in layered manufacturing using a genetic algorithm. Int J Prod Res. 2005;43(13):2709–24.
[49] Ahn D, Kim H, Lee S. Fabrication direction optimization to minimize post-machining in layered manufacturing. Int J Mach Tool Manuf. 2007;47(3):593–606.
[50] Li Y, Zhang J. Multi-criteria GA-based Pareto optimization of building direction for rapid prototyping. Int J Adv Manuf Technol. 2013;69(5):1819–31.
[51] Zhang J, Li Y. A unit sphere discretization and search approach to optimize building direction with minimized volumetric error for rapid prototyping. Int J Adv Manuf Technol. 2013;67(1):733–43.
[52] Jibin Z. Determination of optimal build orientation based on satisfactory degree theory for RPT. In: Martin, DC, editor. Ninth International Conference on Computer Aided Design and Computer Graphics; Hong Kong, China: IEEE; 2005.
[53] Wodziak JR, Fadel GM, Kirschman C. A genetic algorithm for optimizing multiple part placement to reduce build time. Proceedings of the Fifth International Conference on Rapid Prototyping, Ohio: University of Dayton; 1994.
[54] Ikonen I, Biles WE, Kumar A, Wissel JC, Ragade RK. A Genetic Algorithm for Packing Three-Dimensional Non-Convex Objects Having Cavities and Holes. Seventh International Conference on Genetic Algorithms; Michigan State University; 1997.
[55] Lewis JE, Ragade RK, Kumar A, Biles WE. A distributed chromosome genetic algorithm for bin-packing. Robot Comput Integr Manuf. 2005;21(4):486–95.
[56] Canellidis V, Giannatsis J, Dedoussis V. Efficient parts nesting schemes for improving stereolithography utilization. Comput Aided Des. 2013;45(5):875–86.
[57] Canellidis V, Dedoussis V, Mantzouratos N, Sofianopoulou S. Pre-processing methodology for optimizing stereolithography apparatus build performance. Comput Ind. 2006;57(5):424–36.
[58] Dickinson JK, Knopf GK. Serial packing of arbitrary 3D objects for optimizing layered manufacturing. In: Casasent DP, editor. Intelligent Robots and Computer Vision XVII: Algorithms, Techniques, and Active Vision. Boston: SPIE; 1998.
[59] Dickinson JK, Knopf GK. Packing Subsets of 3D Parts for Layered Manufacturing. Int J Smart Eng System Design. 2002;4(3):147–61.
[60] Zhang X, Zhou B, Zeng Y, Gu P. Model layout optimization for solid ground curing rapid prototyping processes. Robot Comput Integr Manuf. 2002;18(1):41–51.
[61] Cao P, Fan Z, Gao RX, Tang J. Harnessing multi-objective simulated annealing toward configuration optimization within compact space for additive manufacturing. Robot Comput Integr Manuf. 2019;57:29–45.
[62] Hur S-M, Choi K-H, Lee S-H, Chang P-K. Determination of fabricating orientation and packing in SLS process. J Mater Process Technol. 2001;112(2–3):236–43.
[63] Wu S, Kay M, King R, Vila-Parrish A, Warsing D. Multi-objective optimization of 3D packing problem in additive manufacturing. In: Guan Y, Liao H, editors. Industrial and Systems Engineering Research Conference; Montréal, Canada: Institute of Industrial and Systems Engineers (IISE); 2014.
[64] Arndt A, Hackbusch H, Anderl R. An algorithm-based method for process-specific three-dimensional nesting for additive manufacturing processes. International Solid Freeform Fabrication Symposium; University of Texas at Austin; 2015.
[65] Rong-Ji W, Xin-hua L, Qing-ding W, Lingling W. Optimizing process parameters for selective laser sintering based on neural network and genetic algorithm. Int J Adv Manuf Technol. 2009;42(11):1035–42.
[66] Ning Y, Wong YS, Fuh JYH. Effect and control of hatch length on material properties in the direct metal laser sintering process. Proc Inst Mech Eng B J Eng Manuf. 2005;219(1):15–25.
[67] Caiazzo F, Caggiano A. Laser Direct Metal Deposition of 2024 Al Alloy: Trace Geometry Prediction via Machine Learning. Materials (Basel). 2018;11(3):444.
[68] Mozaffari A, Fathi A, Khajepour A, Toyserkani E. Optimal design of laser solid freeform fabrication system and real-time prediction of melt pool geometry using intelligent evolutionary algorithms. Appl Soft Comput. 2013;13(3):1505–19.
[69] Möller M, Baramsky N, Ewald A, Emmelmann C, Schlattmann J. Evolutionary-based Design and Control of Geometry Aims for AMD-manufacturing of Ti-6Al-4V Parts. Phys Procedia. 2016;83:733–42.
[70] Wah PK, Murty KG, Joneja A, Chiu LC. Tool path optimization in layered manufacturing. IIE Trans. 2002;34(4):335–47.
[71] Mahapatra SS, Sood AK. Bayesian regularization-based Levenberg–Marquardt neural model combined with BFOA for improving surface finish of FDM processed part. Int J Adv Manuf Technol. 2012;60(9):1223–35.
[72] Ebrahim V, Sadegh R. Improvement of FDM parts' surface quality using optimized neural networks – medical case studies. Rapid Prototyp J. 2017;23(4):825–42.
[73] Rao RV, Rai DP. Optimization of fused deposition modeling process using teaching-learning-based optimization algorithm. Eng Sci Technol Int J. 2016;19(1):587–603.
[74] Vijayaraghavan V, Garg A, Lam JSL, Panda B, Mahapatra SS. Process characterisation of 3D-printed FDM components using improved evolutionary computational approach. Int J Adv Manuf Technol. 2015;78(5):781–93.
[75] Vijayaraghavan V, Garg A, Wong C, Tai K, Regalla SP, Tsai M. Density characteristics of laser-sintered three-dimensional printing parts investigated by using an integrated finite element analysis–based evolutionary algorithm approach. Proc Inst Mech Eng B J Eng Manuf. 2016;230(1):100–10.
[76] Panda B, Shankhwar K, Garg A, Savalani MM. Evaluation of genetic programming-based models for simulating bead dimensions in wire and arc additive manufacturing. J Intell Manuf. 2019;30(2):809–20.
[77] Ewald A, Sassenberg T, Schlattmann J. Evolutionary-based optimization strategy in a hybrid manufactured process using LMD. Procedia CIRP. 2018;74:163–7.
[78] Xu F, Wong YS, Loh HT, Fuh JYH, Miyazawa T. Optimal orientation with variable slicing in stereolithography. Rapid Prototyp J. 1997;3(3):76–88.

Paper P2

T. S. Leirmo and K. Martinsen, 'Deterministic part orientation in additive manufacturing using feature recognition,' *Procedia CIRP*, vol. 88, pp. 405–410, 2020, ISSN: 2212-8271. DOI: 10.1016/j.procir.2020.05.070. [Online]. Available: http://www.sciencedirect.com/science/article/pii/S2212827120303899

Available online at www.sciencedirect.com

ScienceDirect

Procedia CIRP 88 (2020) 405–410

www.elsevier.com/locate/procedia

13th CIRP Conference on Intelligent Computation in Manufacturing Engineering, CIRP ICME '19

Deterministic part orientation in additive manufacturing using feature recognition

Torbjørn Schjelderup Leirmo[a,*], Kristian Martinsen[a]

[a]*Department of Manufacturing and Civil Engineering, Norwegian University of Science and Technology, Teknologivegen 22, 2815 Gjøvik, Norway*

* Corresponding author. Tel.: +47 480 88 390. *E-mail address:* torbjorn.leirmo@ntnu.no

Abstract

Additive Manufacturing (AM) is becoming an integral part of modern manufacturing systems and therefore, the AM technologies needs to adhere to strict quality demands. Due to the layered nature of AM, the part build orientation has a major influence on final part properties. Previous efforts to optimize the part orientation largely utilizes evolutionary algorithms, which are stochastic in nature. This paper argues for a deterministic solution to facilitate automation and standardization, and proposes a method utilizing feature recognition for faster computation. A case study for selective lase sintering is presented to demonstrate the feasibility of the proposed method.

© 2020 The Authors. Published by Elsevier B.V.
This is an open access article under the CC BY-NC-ND license (http://creativecommons.org/licenses/by-nc-nd/4.0/)
Peer review under the responsibility of the scientific committee of the 13th CIRP Conference on Intelligent Computation in Manufacturing Engineering, 17-19 July 2019, Gulf of Naples, Italy.

Keywords: Additive Manufacturing; Optimization; Surface; Quality; Computer Automated Process; Part Orientation

1. Introduction

The concept of additive manufacturing (AM) had its genesis in 1986 when the stereolithography apparatus (SLA) was first patented by Hull and later commercialized by 3D Systems [1, 2]. Since then, AM has developed from manufacturing of physical (but non-functional) prototypes reducing time-to-market, to an entire family of technologies [3]. The AM concept encompass processes capable of producing anything from multicolored models to functional parts for end use in a variety of materials [4]. These versatile areas of application make AM increasingly popular in manufacturing industry. From 2010 to 2015, an annual growth of approximately 30% was recorded, and the industry show no signs of regressing any time soon [5].

As the industrial sector continues to embrace the technology, the need for efficiency is increasing. Subsequently, this necessitates research in several areas of AM, one of which is the automatic optimization of part orientation [6]. The orientation of the part during additive manufacture affects not only the build height, which in turn affects the build time [7], but also surface quality [8], part accuracy [9] and mechanical properties [10]. For technologies that require support structures, the need for such structures can also be reduced by a proper part build orientation [11]. This means that a suitable orientation can save time, material, and energy – all of which ultimately contributes to a reduction of total cost [12].

Existing solutions to the orientation problem extensively utilizes evolutionary algorithms (EAs) to converge to a solution. The stochastic nature of EAs introduces variability to the manufacturing process, which in the spirit of standardization and automation is a suboptimal solution. This paper proposes a novel non-stochastic method for determining the part build orientation using the basic geometric features of a part.

2. Related work

Since the middle of the 1990s, researchers have developed methods for optimizing part orientation in AM [13]. Frank and Fadel [7] developed an expert system for SLA that guided the user to the orientation with minimal staircase effect and additionally minimized build time and support structures. Cheng, et al. [9] developed a multi-objective optimization method for finding the orientation

2212-8271 © 2020 The Authors. Published by Elsevier B.V.
This is an open access article under the CC BY-NC-ND license (http://creativecommons.org/licenses/by-nc-nd/4.0/)
Peer review under the responsibility of the scientific committee of the 13th CIRP Conference on Intelligent Computation in Manufacturing Engineering, 17-19 July 2019, Gulf of Naples, Italy.
10.1016/j.procir.2020.05.070

for a single part in SLA and fused deposition modelling (FDM). The authors considered part accuracy and build time by comparing all orientations yielding a planar surface that could be used as a base for beginning the build process. Xu, et al. [14] ensured part stability in SLA by proper orientation, and further improved part accuracy by working directly on the CAD (Computer Aided Design)-model and introduced an adaptive variable thickness slicer. The authors later considered build cost as the main objective for the technologies SLA, FDM, selective laser sintering (SLS), and layered object manufacturing (LOM) [12].

Masood, et al. [15] introduced volumetric error as an estimation of volumetric difference between the STL-file and the final part assuming sharp edges in FDM. The concept was applied to cones and pyramids [16], before more complex parts were investigated by rotation at certain increments about user specified axes [17, 18]. Because of the difficulties of correctly modelling the edge of each layer, several proposals are found in the literature. As an alternative to volumetric error, Lin, et al. [19] developed a mathematical model for comparing layered process error imposed by the staircase effect of several candidate orientations.

Byun and Lee [20] proposed average weighted surface roughness as another measure of surface quality assuming round edges. The authors used a genetic algorithm (GA) to optimize the weighted objective function considering surface roughness and build time. Later, the authors included build cost and variable slicing in the consideration [21], and also made recommendations on what technology to use for fabrication [22].

Paul and Anand [23] introduced tolerances to the optimization objectives by including cylindricity error. Later, Geometric Dimensioning and Tolerancing (GD&T) was further investigated as cylindricity and flatness error was considered together with support volume [24]. Das, et al. [11] utilized unit spheres to visualize how tolerances and support volume was affected by part orientation, and later used a combination of an exhaustive search and GA to solve the optimization problem [6].

Zhang and Bernard [25] proposed using AM features as the foundation for part orientation before a multi-attribute decision making method is applied to arrive at the final solution [26]. The authors further develop the method to rotate 16 parts simultaneously by applying a GA [27], and optimize orientation in FDM for continuous fibers [28]. Furthermore, the authors developed a facet clustering method as an alternative to feature recognition for accelerating subsequent computation [29, 30]. Quite recently, Delfs, et al. [10] utilized an exhaustive search by 5-degree intervals for predicting surface roughness in SLS with build height as a secondary objective. The method used the STL file as input and calculated the roughness values for every single facet as the part was rotated about the x- and y-axis. This effort represents one of few deterministic solutions to the orientation problem in AM.

The work of Zhang et al. [25-30] is promising, and the application of feature recognition in non-stochastic optimization schemes for orientation in AM is at this point an unexplored combination – the potential of which is currently unknown.

3. Theoretical background

3.1. The STL file format

With the first AM technology, a new file format emerged for transferring data for three-dimensional (3D) geometries. The STereoLithography (STL) file format was adopted by other processes as they were introduced, and soon became the de facto industry standard for communicating part geometry in AM [31]. The abbreviation is also described as Standard Triangulation Language or Standard Tessellation Language [32].

As indicated by the more popular abbreviations, the STL file describes a part by a tessellation of triangles constituting the surface of the part. All triangles (facets) are defined by the three coordinates of each corner (vertex), and the unit normal vector of the surface as illustrated in Fig. 1 (left). The file contains a list of all facets with their twelve coordinates as displayed in Fig. 1 (right). The facet unit normal is always pointing outwards, and the vertices are listed in a counter clockwise fashion making the notation of a facet unambiguous [33].

3.2. Feature recognition

Automatic identification of machining features is by no means a new concept, and the literature describes several areas of application [34, 35], however the use of feature recognition in the AM domain is limited. In early research, there are a few occurrences of features being used as a foundation for basic design rules in AM and implicitly considered in orientation [7, 9].

More recently, feature recognition was used in the work of Zhang, et al. [26] who also proposed an alternative facet clustering method as previously mentioned [29, 30]. There are, however currently only stochastic applications of feature recognition to the orientation problem reported in the literature. Feature recognition has the potential to accelerate calculations due to the reduced number of elements compared to all facets of the entire STL-file.

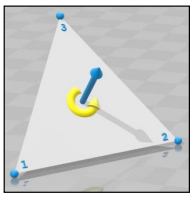


```
solid <name>
  facet normal <x> <y> <z>
    outer loop
      vertex <x> <y> <z>
      vertex <x> <y> <z>
      vertex <x> <y> <z>
    endloop
  endfacet
.....
(Repeats for each facet)
.....
endsolid <name>
```

Fig. 1 Illustration of a triangular facet with normal vector and vertices (left) and the syntax of an STL file in ASCII format (right).

3.3. Surface quality

The surface quality influences not only the physical properties of the part in interaction with its surroundings, but also the visual and haptic perception of the part [36]. Layered manufacturing technologies are prone to the staircase effect inherent in the build process as illustrated in Fig. 2 [2]. Additionally, powder bed fusion processes leave residual particles on the part surface that contributes to increased surface roughness [10]. Finally, processes where support structures are required suffers from poor surface quality in areas where the supports have been removed due to burrs and residue [6]. Water soluble filament for support structures has however been introduced to eliminate this influence in FDM [20].

Of the three influencing factors previously outlined, it is known that part orientation is crucial to control the intensity of the staircase effect [37] and the volume and location of support structures [38]. As supports are redundant in SLS, this paper focus on surface roughness and the staircase effect in particular.

In addition to proper orientation, the staircase effect can also be prevented by reducing the layer thickness [37]. Some AM processes are in fact capable of higher resolution in the z-direction than the x-y plane [39]. Thinner layers will however prolong the build time, and thus methods have been developed for adaptive layer thickness based on the local topography of the part [14]. Adaptive layer thickness can be applied in combination with proper part orientation, but problems arise when multiple parts are manufactured simultaneously as the layer thickness is uniform throughout the build space [40].

While Padhye and Deb [41] predicted surface roughness in SLS based on the orientation of every single facet, the present work utilizes a simplified objective function to facilitate faster computation of optimal orientation. It is however noted that such predictive functions may replace the simple function applied in the present work to incorporate more factors and provide other insights. Such adaptations are however outside the scope of this paper and thus left for future research.

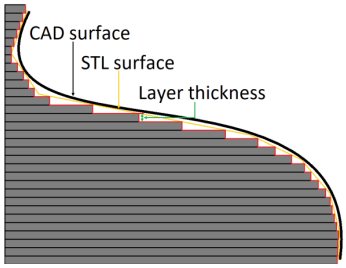

Fig. 3. Illustration of staircase effect and conversion errors.

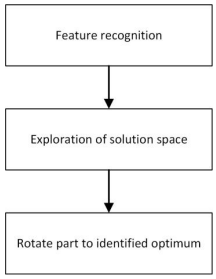

Fig. 2. Flowchart for part orientation.

4. Proposed method

The task of optimizing part orientation is divided in two separate modules as displayed in Fig. 3; the first being feature recognition where geometric features of the STL file are identified, and the second being an exhaustive exploration of the solution space. The objective of the optimization scheme is to find the part build orientation where the staircase effect has the least effect on final surface quality.

In the following it is assumed that every part is made up of a combination of primitive surfaces (plane, cylinder, sphere, cone and torus), and that these features has been successfully extracted from the STL data. This categorization implies that it is possible to represent any freeform surface by a combination of these geometric features. This could however prove to be impractical as the number of features could be tremendous – especially for topologically optimized designs and organic structures. A solution to this challenge could be to disregard freeform surfaces, or to approximate them to one of the basic features.

Furthermore, it is assumed that each feature is accompanied with a vector denoting the orientation of the feature, and that the surface area of the feature is known. Based on this, a function can be designed to evaluate the fitness of different feature types. An exhaustive search for the global optimum is then conducted by rotating the part about the x- and y-axes in increments of one degree. For every increment, a score is aggregated based on the fitness of each feature as

$$S_{tot} = \sum_{i=1} F_i \tag{1}$$

Where S_{tot} is the aggregated total score for all features in the given orientation, and F is the score of a single feature for the same orientation.

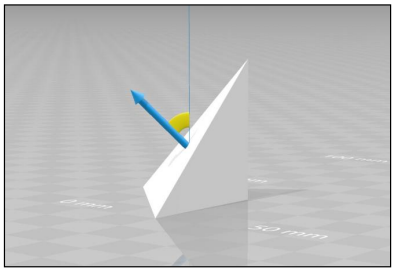

Fig. 4. The angle between the feature normal and the build direction.

The fitness of a given orientation with regards to a specific feature is evaluated as a function of the angle between the feature normal and the build direction as displayed in Fig. 4. Each feature factor should be weighted to prioritize certain features over others. It is here proposed to multiply the fitness factor with the surface area of the feature to give weight to larger features. It is also possible to exclude features smaller than a certain threshold to accelerate computations and avoid the influence of insignificant features.

In the present work, two versions of a simple trigonometric expression is proposed to evaluate the fitness of features with regards to a given orientation:

$$S_{plane} = A \cdot \cos^2\left(2\left(\theta_x + \alpha_x\right)\right) \cdot \cos^2\left(2\left(\theta_y + \alpha_y\right)\right) \quad (2)$$

$$S_{cylinder} = A \cdot \cos^2\left(\theta_x + \alpha_x\right) \cdot \cos^2\left(\theta_y + \alpha_y\right) \quad (3)$$

Where S_{plane} and $S_{cylinder}$ is the score of a plane and a cylinder respectively, A is the surface area of the feature, θ_x and θ_y is the evaluated rotation about the x- and y-axis respectively, and similarly α_x and α_y is the initial offset of the feature about both x- and y- axis.

5. Case study

The method was applied to 19 test parts of varying geometries and origins to investigate the viability of the developed method (see Fig. 5). Three computers were used to eliminate any problems related to a specific unit, and the method was executed three times on each computer to reduce any variability currently present in the computer system. All computers gave identical results considering the proposed solution varying only in execution time.

Table 1 contains a summary of the method's performance on all 19 test parts including the number of recognized features, execution time (in seconds), and qualitative evaluation of end solution. The portrayed performances are the average results of a computer with 8 GB RAM and a 2.30 GHz processor running on 64-bit Windows 10 operating system. No measures (i.e. terminating background processes) were taken to reduce execution time during the trials. The following subsections presents three representative parts (part numbers 2, 6 and 17 of Fig. 5).

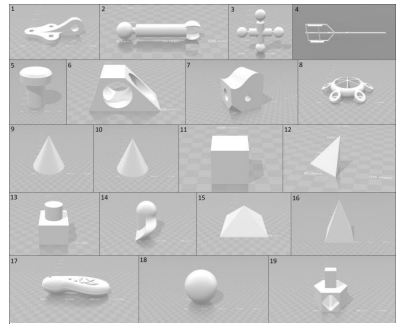

Fig. 5. Overview of all test parts involved in the study.

Table 1. Run time and quality of solutions for 19 test parts.

Part #	Facets	Features	Avg. run time [s]	Quality of solution
1	1 064	9	0.813	Good
2	11 752	96	8.222	Good
3	17 208	77	6.610	Poor
4	7 564	77	6.573	Good
5	900	5	0.414	Good
6	844	9	0.826	Good
7	692	9	0.786	Good
8	59 922	274	23.194	Good
9	70	1	0.088	OK
10	112	1	0.087	OK
11	12	6	0.531	Good
12	4	4	0.331	Good
13	174	7	0.591	Good
14	12 699	326	27.878	Poor
15	6	5	0.410	Good
16	6	5	0.416	Good
17	43 130	905	77.491	Good
18	5 852	5	0.425	N/A
19	80	17	1.405	Good

5.1. Low geometric complexity

Part number 6 is a reconstruction derived from Cheng, et al. [9] where eight distinct features can be identified; six planar sides, and two cylindrical holes. The deviations observed in Table 1 is due to the division of cylinders into multiples, and imprecise data in the STL file.

The method yields a solution where all planar features are oriented either parallel or perpendicular to the build direction thus minimizing the staircase effect on these

surfaces. Furthermore, one of the cylindrical holes is oriented parallel to the build direction. This solution is identical to those found in literature [9, 22, 26, 40, 42, 43], thus demonstrating the validity for simple geometries.

5.2. Medium geometric complexity

Part number 2 is a ball joint arm retrieved from literature [44]. The part consists of a cylindrical shaft with a convex sphere on one end, and the concave counterpart on the other. Because the feature recognition module is incapable of recognizing spherical features, both ends of the part is identified as a series of cylinder segments. The effect of this is twofold; (i) the number of features passed on to the orientation algorithm is artificially inflated, and (ii) the dispersed cylinders have contradicting feature vectors that in turn could throw off the orientation algorithm. However, because of the relatively small surface area of the individual segments, the larger features that are correctly identified as cylinders and planes dominates the search.

The proposed solution orients the part parallel to the build orientation minimizing the staircase effect on the large cylinder. The spherical features are not influenced by the build orientation in terms of the staircase effect and can thus be neglected in this assessment.

5.3. High geometric complexity

Part number 17 is a remote control also constructed according to [44]. The part is an assembly of the buttons (all connected in one shell), and the top- and bottom covers. The surface is curved in a free form fashion that introduce significant difficulties for feature recognition resulting in 905 identified features.

Despite the large number of features, the aggregation of many small feature normals of similar orientation makes it possible for the method to propose a valid solution where the remote is oriented in its upright position, with the main surfaces parallel to the build direction. This orientation minimizes the influence of the staircase effect on the largest surfaces, but unavoidably sacrifice some surfaces for the benefit of others.

6. Discussion

The proposed method is developed with an emphasis on consistency and speed. An optimal solution cannot be guaranteed with this method because the accuracy of the results cannot exceed the resolution of the search grid. As the rotational increments are reduced, the execution time grows exponentially and will soon become too time-consuming to be viable. Rotational increments of 1 degree is suggested, but not verified as a neither necessary, nor sufficient interval.

The solutions of the case study is generally believed to be good, but it is clear that the inability of the feature recognition module to identify sphere, cone and torus is a major obstacle for the subsequent search for the optimal orientation. However, it is observed that when features of a certain magnitude are correctly recognized, the validity of the final solution increases dramatically. Proper recognition would however have a major impact on the execution time of the method, which increases linearly with the number of features in the neighborhood of 0.085–0.095 seconds per feature.

The case study demonstrates the method's capability to give stable output given no change in input files. The ability to provide a stable output facilitates standardization and automation, which are key factors in modern industry. With industry 4.0 and mass customization, the need for stable processes may be considered more important than ever. Eliminating variability in complex manufacturing processes facilitates the adoption of AM in industry, and the modernization of manufacturing systems.

There are developments towards direct manufacturing of CAD models without the intermediate STL (or AMF/3MF) file format. Avoiding a tessellated model means increased accuracy because the surface is no longer approximated by triangles. However, such solutions are often application specific and thus generality is lost. The proposed method will in this case become obsolete in its current form, but the concept of utilizing shape features for non-stochastic optimization of orientation in AM remains relevant as this also applies to CAD files.

7. Conclusions

This paper proposed a novel method for optimizing part orientation based on part features without utilizing stochastic techniques. The method will provide the same solution every time given no changes in input, which facilitates automation in industry through elimination of variation. The case study demonstrates the method's feasibility considering execution time and general quality of solutions.

Currently, mitigation of the staircase effect is the sole purpose of the method, and thus the integration of additional objectives is a relevant area of future development, especially objectives contributing to further adaptation by industry such as mechanical properties and accuracy. Furthermore, the algorithm for feature recognition needs to be improved and expanded to handle sphere, cone and torus as these feature types currently may inflict errors in the results.

The developed method is intended for SLS, but the concept can generally be applied to any AM process prone to the staircase effect. An interesting path of future research entails adaptation to other technologies, also outside the powder bed domain.

Acknowledgements

This research is funded by the Norwegian Ministry of Research and Education and is associated with SFI Manufacturing. The authors would like to acknowledge the contributions of Julie Langedahl and Harald Grønvold for contributing with test parts for the case study.

References

[1] Hull CW. Apparatus for production of three-dimensional objects by stereolithography. US patent no. US4575330 A. 1986.

[2] Gibson I, Rosen DW, Stucker B. Additive manufacturing technologies. 2nd ed. New York: Springer; 2015.

[3] Joshi PC, Dehoff RR, Duty CE, Peter WH, Ott RD, Love LJ, et al. Direct digital additive manufacturing technologies: Path towards hybrid integration. In: Future of Instrumentation International Workshop (FIIW); 2012.

[4] Thompson MK, Moroni G, Vaneker T, Fadel G, Campbell RI, Gibson I, et al. Design for Additive Manufacturing: Trends, opportunities, considerations, and constraints. CIRP Ann Manuf Technol. 2016;65(2):737–60.

[5] Bourell DL. Perspectives on Additive Manufacturing. Annu Rev Mater Res. 2016;46(1):1–18.

[6] Das P, Mhapsekar K, Chowdhury S, Samant R, Anand S. Selection of build orientation for optimal support structures and minimum part errors in additive manufacturing. 2017. DOI: 10.1080/16864360.2017.1308074.

[7] Frank D, Fadel G. Expert system-based selection of the preferred direction of build for rapid prototyping processes. J Intell Manuf. 1995;6(5):339–45.

[8] Li Y, Zhang J. Multi-criteria GA-based Pareto optimization of building direction for rapid prototyping. Int J Adv Manuf Technol. 2013;69(5):1819–31.

[9] Cheng W, Fuh JYH, Nee AYC, Wong YS, Loh HT, Miyazawa T. Multi - objective optimization of part - building orientation in stereolithography. Rapid Prototyp J. 1995;1(4):12 – 23.

[10] Delfs P, Tows M, Schmid HJ. Optimized build orientation of additive manufactured parts for improved surface quality and build time. Addit Manuf. 2016;12:314–20.

[11] Das P, Chandran R, Samant R, Anand S. Optimum Part Build Orientation in Additive Manufacturing for Minimizing Part Errors and Support Structures. Procedia Manuf. 2015;1:343–54.

[12] Xu F, Loh HT, Wong YS. Considerations and selection of optimal orientation for different rapid prototyping systems. Rapid Prototyp J. 1999;5(2):54–60.

[13] Allen S, Dutta D. On the computation of part orientation using support structures in layered manufacturing. In: Proceedings of Solid Freeform Fabrication Symposium; University of Texas at Austin, Austin, TX; 1994.

[14] Xu F, Wong YS, Loh HT, Fuh JYH, Miyazawa T. Optimal orientation with variable slicing in stereolithography. Rapid Prototyp J. 1997;3(3):76–88.

[15] Masood SH, Rattanawong W, Iovenitti P. Part Build Orientations Based on Volumetric Error in Fused Deposition Modelling. Int J Adv Manuf Technol. 2000;16(3):162–8.

[16] Rattanawong W, Masood SH, Iovenitti P. A volumetric approach to part-build orientations in rapid prototyping. J Mater Process Technol. 2001;119(1):348–53.

[17] Masood SH, Rattanawong W. A Generic Part Orientation System Based on Volumetric Error in Rapid Prototyping. Int J Adv Manuf Technol. 2002;19(3):209–16.

[18] Masood SH, Rattanawong W, Iovenitti P. A generic algorithm for a best part orientation system for complex parts in rapid prototyping. J Mater Process Technol. 2003;139(1):110–6.

[19] Lin F, Sun W, Yan Y. Optimization with minimum process error for layered manufacturing fabrication. Rapid Prototyp J. 2001;7(2):73–82.

[20] Byun HS, Lee KH. Determination of the optimal part orientation in layered manufacturing using a genetic algorithm. Int J Prod Res. 2005;43(13):2709–24.

[21] Byun HS, Lee KH. Determination of optimal build direction in rapid prototyping with variable slicing. Int J Adv Manuf Technol. 2006;28(3):307–13.

[22] Byun HS, Lee KH. Determination of the optimal build direction for different rapid prototyping processes using multi-criterion decision making. Robot Comput Integr Manuf. 2006;22(1):69–80.

[23] Paul R, Anand S. Optimal part orientation in Rapid Manufacturing process for achieving geometric tolerances. J Manuf Syst. 2011;30(4):214–22.

[24] Paul R, Anand S. Optimization of layered manufacturing process for reducing form errors with minimal support structures. J Manuf Syst. 2015;36:231–43.

[25] Zhang Y, Bernard A. Using AM feature and Multi-attribute decision making to orientate part in Additive Manufacturing. In: International Conference on Advanced Research in Virtual and Rapid Prototyping; Leiria, Portugal; 2013.

[26] Zhang Y, Bernard A, Gupta RK, Harik R. Feature based building orientation optimization for additive manufacturing. Rapid Prototyp J. 2016;22(2):358–76.

[27] Zhang Y, Bernard A. A Parallel 2D Nesting Method for Machine's Work Space Planning in Additive Manufacturing. In: 14ème Colloque National: Produits, Procédés, Systèmes Intelligents et Durables; 2015.

[28] Zhang Y, De Backer W, Harik R, Bernard A. Build Orientation Determination for Multi-material Deposition Additive Manufacturing with Continuous Fibers. Procedia CIRP. 2016;50:414–9.

[29] Zhang Y, Harik R, De Backer W, Bernard A. A facet cluster-based method for alternative build orientation generation in additive manufacturing. In: Proceedings of Solid Freeform Fabrication Symposium; University of Texas at Austin, Austin, TX; 2016.

[30] Zhang Y, Harik R, Fadel G, Bernard A. A statistical method for build orientation determination in additive manufacturing. Rapid Prototyp J. 2019;25(1):187–207.

[31] Zwier MP, Wits WW. Design for Additive Manufacturing: Automated Build Orientation Selection and Optimization. 2016;55:128–33.

[32] ISO/ASTM 52900:2015. Standard Terminology for Additive Manufacturing – General Principles – Terminology. 2015.

[33] Hull CW, Spence ST, Albert DJ, Smally DR, Harlow RA, Steinberg P, et al. Cad/cam stereolithographic data conversionno. 1989.

[34] Henderson MR, Anderson DC. Computer recognition and extraction of form features: A CAD/CAM link. Comput Ind. 1984;5(4):329-39.

[35] Subrahmanyam S, Wozny M. An overview of automatic feature recognition techniques for computer-aided process planning. Comput Ind. 1995;26(1):1–21.

[36] Wang WM, Zanni C, Kobbelt L. Improved Surface Quality in 3D Printing by Optimizing the Printing Direction. Comput Graph Forum. 2016;35(2):59–70.

[37] Kulkarni P, Marsan A, Dutta D. A review of process planning techniques in layered manufacturing. Rapid Prototyp J. 2000;6(1):18–35.

[38] Chowdhury S, Mhapsekar K, Anand S. Part Build Orientation Optimization and Neural Network-Based Geometry Compensation for Additive Manufacturing Process. J Manuf Sci Eng. 2018;140(3).

[39] Chen Y, Lu J. RP part surface quality versus build orientation: when the layers are getting thinner. Int J Adv Manuf Technol. 2013;67(1):377–85.

[40] Canellidis V, Giannatsis J, Dedoussis V. Genetic-algorithm-based multi-objective optimization of the build orientation in stereolithography. Int J Adv Manuf Technol. 2009;45(7):714–30.

[41] Padhye N, Deb K. Multi - objective optimisation and multi - criteria decision making in SLS using evolutionary approaches. Rapid Prototyp J. 2011;17(6):458 – 78.

[42] Pham DT, Dimov SS, Gault RS. Part Orientation in Stereolithography. Int J Adv Manuf Technol. 1999;15(9):674–82.

[43] Pandey PM, Thrimurthulu K, Reddy NV. Optimal part deposition orientation in FDM by using a multicriteria genetic algorithm. Int J Prod Res. 2004;42(19):4069–89.

[44] Tran P. SolidWorks 2014. Part I. Basic Tools. Mission, Kansas: SDC Publications; 2013.

Paper P3

T. L. Leirmo, O. Semeniuta and K. Martinsen, 'Tolerancing from STL data: A Legacy Challenge,' *Procedia CIRP*, vol. 92, pp. 218–223, 2020, ISSN: 2212-8271. DOI: 10.1016/j.procir.2020.05.180. [Online]. Available: http://www.sciencedirect.com/science/article/pii/S221282712030946X

Available online at www.sciencedirect.com

ScienceDirect

Procedia CIRP 92 (2020) 218–223

www.elsevier.com/locate/procedia

16th CIRP Conference on Computer Aided Tolerancing (CIRP CAT 2020)

Tolerancing from STL data: A Legacy Challenge

Torbjørn Langedahl Leirmo[a]*, Oleksandr Semeniuta[a], Kristian Martinsen[a]

[a]*Department of Manufacturing and Civil Engineering, Norwegian University of Science and Technology, Teknologivegen 22, 2815 Gjøvik, Norway*

* Corresponding author. Tel.: +47 480 88 390. *E-mail address:* torbjorn.leirmo@ntnu.no

Abstract

Part representation in additive manufacturing (AM) is dominated by the stereolithography (STL) file format as a universal mode for communicating and transferring part geometry from one system to another. However, when the CAD model is converted to the triangle mesh constituting the STL file the topology is no longer explicitly defined hence the design intent is lost together with any tolerancing information. Computer aided tolerancing of actual part geometry is hindered by the sparse information about the nominal geometry directly available in STL data, therefore the feature information is often assumed or recreated through reverse engineering methods. This paper investigates how nominal geometry can be deduced from STL data to support quality control by the identification of geometric elements from a triangle mesh. We further discuss how vectorial tolerancing can extend the scope of feature recognition to tolerancing and quality assessment. A method for automatic extraction and tolerancing of features from STL files is described and an application example is provided. The outlined method enables the automation of tolerancing activities and facilitates the integration of STL files into the digital pipeline of modern manufacturing systems.

© 2020 The Authors. Published by Elsevier B.V.
This is an open access article under the CC BY-NC-ND license (http://creativecommons.org/licenses/by-nc-nd/4.0/)
Peer-review under responsibility of the scientific committee of the CIRP CAT 2020

Keywords: Tolerancing; Additive Manufacturing; Geometry.

Nomenclature

AM	Additive Manufacturing
CAD	Computer Aided Design
CAM	Computer Aided Manufacturing
CAT	Computer Aided Tolerancing
FCS	Feature Coordinate System
FFF	Fused Filament Fabrication
GD&T	Geometric Dimensioning and Tolerancing
STL	Stereolithography (file format)
VT	Vectorial Tolerancing
WCS	Workpiece Coordinate System

1. Introduction

Since its conception in the late 1980s [1], Additive Manufacturing (AM) has evolved from a rapid prototyping process to a family of technologies capable of manufacturing functional parts. In the meantime, the file format originally developed to accommodate the limited computational power at the time has remained unchanged and is still widely used in the AM industry and the AM community at large [2].

As AM is embraced by the industry for the manufacture of end-use and near-net-shape parts, the quality requirements of industry are inevitably imposed on the products. Requirements for geometrical accuracy were originally developed to moderate defects from traditional manufacturing technologies and was later formalized in the standards ISO 1101 [3] and ASME Y14.5 [4] for geometric dimensioning and tolerancing (GD&T), and ISO 286 [5] for linear sizes.

If a component is exported as a stereolithography (STL) file from computer aided design (CAD) software, the design intent is lost together with any tolerancing information since the topology is no longer explicitly defined [6, 7]. The task of recognizing features from a triangle mesh is a simple job for the human brain but turns out to be a complex problem for a computer. The automatic extraction of shape features from mesh data is still an active field of research after several decades [8, 9]. Computer aided tolerancing (CAT) heavily relies on the availability of feature information, but in a situation where the original CAD file is unavailable, this

2212-8271 © 2020 The Authors. Published by Elsevier B.V.
This is an open access article under the CC BY-NC-ND license (http://creativecommons.org/licenses/by-nc-nd/4.0/)
Peer-review under responsibility of the scientific committee of the CIRP CAT 2020
10.1016/j.procir.2020.05.180

information must then either be assumed or recreated through reverse engineering.

The geometrical accuracy of functional surfaces is of vital importance when manufacturing end-use products – especially when the manufactured component is part of an assembly. As AM is finding its way into modern manufacturing systems, the components are also increasingly used in assemblies where the interfaces need tolerancing. This is, however, a challenge when dealing with STL files because information about the position and orientation of shape features is not readily available. Closed loop tolerance engineering is enabled by the integration of all manufacturing operations in a digital pipeline to which the STL file constitutes a major obstacle [10, 11].

The current work describes how the functional surfaces extracted from STL files may be described by vectors in accordance with vectorial tolerancing (VT) practices. This representation scheme directly enables VT of extracted features, and by extension the automation of quality inspection. Furthermore, the vectorial representation offers a link back to the STL file which enables proactive manipulation of the geometry to accommodate process inaccuracies.

2. Related work

2.1. Geometric inaccuracies in additive manufacturing

The different technologies in the AM family introduce a myriad of variations in actual geometry. The observed geometric deviations may, however, be traced back to four distinct origins as indicated by Dantan, et al. [12]:

- File format and resolution;
- Process planning and parameters;
- Machine specific errors and inaccuracies; and
- Material properties and environmental effects.

The low resolution of STL files may cause distinguishable triangles on the part surface, and numerical imprecisions introduces errors that may cause any downstream process to fail. Process planning includes the placement and orientation of the part in the build space which inevitably impose imprecisions due to raster patterns and layer thickness – a phenomenon commonly referred to as the staircase effect [13]. Moreover, machine imprecisions due to loose components and rounded edges cause deviations from nominal to actual geometry, and finally, the material may introduce variations and could react to environmental factors by shrinking and warping. A comprehensive discussion on the challenges related to tolerancing in AM is presented in [6].

2.2. Achievable tolerances in additive manufacturing

Budinoff and McMains [14] performed a theoretical analysis of achievable tolerances in AM considering the geometric deviations due to the layered approximation. The authors further described a tool for identifying feasible orientation zones given a part with accompanying tolerances.

Minetola, et al. [15] investigated the achievable geometric tolerances of fused filament fabrication (FFF) and mapped them to the international tolerancing grades. Dimitrov, et al. [16] achieved the same objective for binder jetting, and Hanumaiah and Ravi [17] investigated direct metal laser sintering and the stereolithography process for tooling purposes. Geometric accuracy for SLA was also mapped out in [18], but with simplifications with regards to feature orientation. Studies similar to [15] but for dimensional tolerances has been conducted by Lieneke, et al. [19] for FFF and for material jetting by Kitsakis, et al. [20]. A study by Ippolito, et al. [21] compared the accuracy of five AM processes and evaluated them relative to traditional manufacturing technologies.

The optimization of process parameters with respect to achievable tolerances complements the studies mentioned above. Arni and Gupta [13] presented a method for constructing build orientation feasibility regions for flatness tolerances in AM, while the cylindricity error was investigated by Paul and Anand [22] who later combined the two methods and included support structures [23]. Building on this previous work, Das, et al. [24] developed an optimization scheme for minimizing the volume of support structures while satisfying GD&T callouts, and later also considered the accessibility of support structures for post-processing [25]. The input of these optimization methods is described as a CAD file with embedded tolerance callouts.

2.3. Extracting shape features from STL files

Many applications would benefit from the topological information no longer present after converting to STL file format, and thus the task of extracting topological information from STL data has received major research interest. This already troublesome task is made more complicated by export defects such as occasional holes and intersecting triangles corrupting the STL file [8].

Two distinct categories may be identified in the literature: (i) feature recognition where information is extracted for manufacturing purposes [26, 27], and (ii) mesh segmentation which is primarily geared towards computer graphics [28, 29]. The different intended uses result in a pivotal difference in how these methods work. While the former strives to describe the geometry as precisely as possible to enable direct manufacturing, the latter is concerned with the partition of geometries for identification purposes. A mix of the two can be found in reverse engineering applications where a combination of methods may be utilized [30]. For the purpose of tolerancing, we argue that the successful extraction of geometric primitives from STL data is of higher importance than partitioning of freeform surfaces because of their use as functional surfaces.

Moroni, et al. [31] proposed a methodology for estimating the accuracy of cylindrical features in FFF based on STL data. The authors proposed an algorithm effectively slicing the part along all three axes to identify cylindrical features of the part. The method enables the comparison of actual dimensions to nominal data but provided no means to store or communicate the information.

3. Theoretical foundations

3.1. The STL file format

The stereolithography file format originally got its name from the AM process it was intended to serve [2, 32]. Later, the acronym has also been explained as Standard Tessellation (or Triangulation) Language [33]. In addition to the simplicity of the format, the STL files are being used largely due to its availability for import and export in CAD/CAM applications.

The STL file contains an unordered list of triangles (facets) with their unit normal vectors (facet normals) and the coordinates of the three corners (vertices). This requires 12 floating point numbers stored for each facet where the facet normals point towards the exterior.

3.2. Defining coordinate systems

Any coordinate system is defined from the origin O fixed at (0, 0, 0). The Cartesian coordinate system (x, y, z) is defined by three basic unit vectors representing the axes of the coordinate system: $\mathbf{i} = [1,0,0]$, $\mathbf{j} = [1,0,0]$ and $\mathbf{k} = [1,0,0]$. Alternative coordinate systems include the spherical polar coordinates (r, θ, φ), and cylindrical coordinates (r, θ, z). The choice of coordinate system depends on the application as this influences the complexity of computation. Cartesian coordinates are used for the remainder of this paper.

Regardless of the coordinate system, the position of any point in space can be represented by a position vector $\overrightarrow{OP}$ which defines the location of the point P with reference to the origin. In manufacturing applications, separate coordinate systems may be defined for each manufacturing feature or functional surface to facilitate local process planning such as machining operations. The feature coordinate system (FCS) is defined with respect to the workpiece coordinate system (WCS) and may be oriented differently as displayed in Fig. 1.

3.3. Vector representation and manipulation

The location of a directional vector in $\mathbb{R}^3$ is typically defined by a translation vector $\mathbf{t} \in \mathbb{R}^3$, while the orientation may be represented as a 3×3 special orthogonal matrix ($\mathbf{R} \in SO(3)$). It is common to combine the rotation matrix $\mathbf{R}$ and the translation vector $\mathbf{t}$ in a single homogeneous transformation matrix $\mathbf{T} \in SE(3)$:

$$\mathbf{T} = \begin{bmatrix} \mathbf{R} & \mathbf{t} \\ 0_{1\times3} & 1 \end{bmatrix} = \begin{bmatrix} \vdots & \vdots & \vdots & t_x \\ r_x & r_y & r_z & t_y \\ \vdots & \vdots & \vdots & t_z \\ 0 & 0 & 0 & 1 \end{bmatrix} \quad (1)$$

The representation of a vector in $\mathbb{R}^3$ may thus be condensed into a representation in the form of $(r_x, r_y, r_z, t_x, t_y, t_z)$. The rotation components are typically denoted A, B and C for the counterclockwise rotation about the x-, y- and z-axis respectively and are formalized for AM in ISO/ASTM 52921:2013(E) [34].

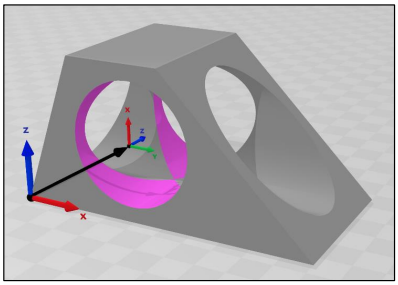

Fig. 1. A part with Workpiece Coordinate System (WCS) and a Feature Coordinate System (FCS) for a cylinder.

3.4. Vectorial definitions of geometric primitives

Martinsen [35] describes how the location and orientation of geometric primitives can be represented vectorially. This gives rise to six degrees of freedom which can be used to classify the fixed and open dimensions of geometric primitives as displayed in Table 1.

Table 1. Degrees of freedom. F = Fixed, O = Open. Adapted from [35].

Surface type	Translations			Rotations		
	X	Y	Z	A	B	C
Plane	O	O	F	F	F	O
Cylinder	F	F	O	F	F	O
Sphere	F	F	F	O	O	O
Cone	F	F	F	F	F	O
Torus	F	F	F	F	F	O

Similarly, a scheme for vectorial representation may be constructed to define the position, orientation, and size of geometric primitives as shown in Table 2. Relevant sizes comprise the radius of cylinders, spheres, and tori (R), as well as the apex angle of cones (ω).

Table 2. Vectorial surface description with location vector **P**, orientation vector **E**, radius Adapted from [35].

Surface type	Location vector P_0			Orientation vector E			Sizes	
Plane	X_0	Y_0	Z_0	E_x	E_y	E_z		
Cylinder	X_0	Y_0	Z_0	E_x	E_y	E_z	R	
Sphere	X_0	Y_0	Z_0				R	
Cone	X_0	Y_0	Z_0	E_x	E_y	E_z	ω	
Torus	X_0	Y_0	Z_0	E_x	E_y	E_z	R1	R2

The location vector in Table 2 points to the origin of the surface which may be explicitly defined if all translation of the surface type is fixed with regards to every dimension with reference to Table 1. This leaves out planes and cylinders which require additional rules for an unambiguous definition of surface origin. Whenever the exact point of origin is without importance, a random point satisfying the fixed dimension(s) may be selected [35].

3.5. Vectorial tolerancing

The description of geometric primitives by vectors gave rise to the concept of VT in the late 1980s. While traditional tolerancing methodology is based on the premise of 1-dimensional measurements, VT enables the unambiguous representation of nominal part geometry in three dimensions [36]. The application of tolerances on the surface descriptions of Table 2 makes it possible to rigorously quantify the location and orientation of shape features in 3D space. The tolerances can then easily be tabulated as displayed in Table 3 [37]. The table states the nominal location vector **P** and the nominal orientation vector **E** with their respective deviation tolerances $\mathbf{T_P}$ and $\mathbf{T_E}$. Furthermore, the size **S** (if relevant), and form may be specified in the table.

4. Proposed method

The proposed method entails a stepwise transition from a triangle mesh, to a vectorial representation of constituent geometric primitives to which tolerances may be applied. This framework also makes it possible for other processing stages to access higher-order information from the STL file by maintaining the digital thread of CAD/CAM processing. A stepwise description is provided in the following subsections.

4.1. Vectorial representation of geometric primitives

When geometric primitives are extracted from STL data, the jump to vectorial representation is quite short. The current work assumes the preceding feature recognition module to be capable of identifying the feature type and location of surface points in a stable manner. The feature origin may be defined in accordance with the VT paradigm based on these surface points by following predefined rules according to the number of degrees of freedom associated with the surface type (see Table 1). The location vector will then be the vector from the WCS to the feature origin.

The relevant sizes of a feature may also be extracted from STL data by different methods. The apex angle ω of cones are easily deduced from the normal vectors of member facets, and the radius may be calculated as the distance of vertices to a common center.

In consequence, the basic geometric primitives may be automatically extracted from STL data and represented as vectors where the WCS, including its origin, is adopted from the STL file. By directly transferring the WCS, the link back to the STL file is left uncorrupted which facilitates later adjustments for manufacturing optimization at various processing stages including build preparation and quality inspection.

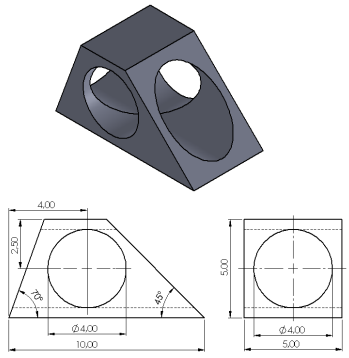

Fig. 2. Drawing of sample part with six planes and two cylinders. Recreated from [20].

4.2. Vectorial part representation

By extending the reasoning from the previous subsection, all primitives of a part may be unambiguously defined and tabulated as displayed in Table 3. This table may be the direct output from automatic feature recognition providing an overview of the constituent primitives of the part, as well as a starting point for tolerance analysis. Depending on the sophistication of the feature recognition module, the resulting table may include an unknown number of features not relevant for tolerancing purposes. Hence, the judgment of an engineer may be required to transform the automatically generated table to a suitable configuration.

5. Application example

To demonstrate the approach described in the previous section, a simple part geometry recreated from [38] is used as a case study (Fig. 2). The STL file contains a list of 860 facets which may be reduced to the 8 constituent features as displayed in Table 4. The table directly enables the specification of the vectorial tolerances associated with the part features.

Table 3. Tolerance table for vectorial tolerances of n shape features. **P** is the nominal location vector and **E** is the nominal orientation unit vector.

#	Location						Orientation						Size		Form	
	Nominal			Limit deviation (±) [mm]			Nominal			Limit deviation (±) ×0.001			Nominal	Limit dev. (±)	Nominal	Limit deviation
	P_x	P_y	P_z	T_{Px}	T_{Py}	T_{Pz}	E_x	E_y	E_z	T_{Ex}	T_{Ey}	T_{Ez}	S[mm]	T[mm]	[type]	[mm]
1	…	…	…	…	…	…	…	…	…	…	…	…	…	…	…	…
2	…	…	…	…	…	…	…	…	…	…	…	…	…	…	…	…
|	|	|	|	|	|	|	|	|	|	|	|	|	|	|	|	|
n	…	…	…	…	…	…	…	…	…	…	…	…	…	…	…	…

To conduct a proper case study, the part should be assigned a function. Since the true purpose of the part is unknown, two assumptions are made about the design intent:

- The component is a standardized part of an assembly where it is intended to connect two or more shafts; and
- One possible application of the component requires support on the angled planes.

Based on the assumptions above, the main emphasis of tolerancing is on the cylindrical holes (features 1 and 2 in Table 4) because they are regarded as functional surfaces. Of secondary importance, the accuracy of the angled planes should be within certain limits (features 3 and 4 in Table 4). Certainly, additional tolerances can easily be added to the table as additional columns or supplementary rows beneath the relevant feature. The table enables the tolerancing of all identified features, but this is not deemed appropriate for this case study.

Table 4 can later be used to evaluate the feasibility of an AM process, quality assessment, or as a tool for process planning if combined with process-specific knowledge.

6. Discussion

6.1. Digital continuity

The era of industry 4.0 calls for digital integration of all manufacturing processes to establish a two-way connection between upstream and downstream operations [11]. Closed loop tolerance engineering provides a framework for this integration in modern manufacturing systems [10] which greatly benefits from CAT [39]. However, this integration is impeded by intermediate file formats such as STL [6].

The vectorial representation of geometric primitives offers a two-way link between the STL file and the subsequent processes. This link may be utilized to improve the accuracy of the realized geometry by manipulation of the STL file to mitigate inaccuracies for the specific part in the next iteration of manufacturing. Over time, the aggregated data on vectorial deviations enables the utilization of intelligent computation methods such as machine learning to make predictive changes to the STL file towards first-time-right manufacturing.

A major benefit of VT is how it facilitates the automatic integration of tolerance considerations in CAD/CAM applications. Increased automation and digital integration improve the traceability of tolerances in the manufacturing system which in turn facilitates intelligent process planning.

6.2. Quantification of inaccuracies

The STL file format introduces certain inaccuracies brought about by round off errors as well as the discretization of smooth curves resulting in the characteristic tessellated surface. Due to these errors, some uncertainty regarding the true size and position of features is inevitable when extracting information from STL data.

One solution to this problem is to discretize the coordinate space and move vertices to their closest valid values. This approach is however invalid as it assumes that the coordinate system of the STL file is the same as the one utilized in the design phase, while it may have been subjected to several file manipulations including translation, rotation, and scaling.

Another solution to file inaccuracies is to allow the user to do corrections after the features are extracted. This approach requires a cost analysis to determine what is most costly: the time spent by an engineer to correct the data or the problems caused by these errors. Most likely, the errors will be negligible and not significantly affect the final product. Consideration of the entire tolerance chain should reveal the necessity of addressing this issue for each case.

6.3. Freeform surfaces

While primitive geometries may be easily defined by standard sizes, freeform surfaces require a flexible scheme to be accurately described. The proposed method is geared towards primitive geometric shapes and is not directly applicable to freeform surfaces such as the organic structures that characterize topology optimized designs. The current work is believed to provide a basis for future work which could include freeform surfaces, as well as integration with other methods for assigning quality measures to design features. Future research could entail complimenting the current work with representation and specification of organic structures and internal geometries with other relevant quality requirements such as mechanical properties or graded material specifications.

Table 4. Tolerance table for sample part. Nominal location vector **P**, nominal orientation unit vector **E** and nominal sizes extracted from STL file.

#	Location						Orientation						Size		Form	
	Nominal			Limit deviation (±) [mm]			Nominal			Limit deviation (±) ×0.001			Nominal	Limit dev. (±)	Nominal	Limit deviation
	P_x	P_y	P_z	T_{Px}	T_{Py}	T_{Pz}	E_x	E_y	E_z	T_{Ex}	T_{Ey}	T_{Ez}	S [mm]	T [mm]	[type]	[mm]
1	4.0	0	2.5	0.1	0.1	0.1	0	1	0	5	5	5	4	0.05	Cylinder	0.05
2	0.18	2.5	2.5	0.1	0.1	0.1	1	0	0	5	5	5	4	0.05	Cylinder	0.10
3	0	0	0	0.2	0.2	0.2	-sin(70)	0	cos(70)	10	10	10	-	-	Plane	0.15
4	5.0	0	5	0.2	0.2	0.2	sin(45)	0	cos(45)	10	10	10	-	-	Plane	0.15
5	1.82	0	5.0	-	-	-	0	0	1	-	-	-	-	-	Plane	-
6	0	5.0	0	-	-	-	0	0	-1	-	-	-	-	-	Plane	-
7	0	5.0	0	-	-	-	0	1	0	-	-	-	-	-	Plane	-
8	0	0	0	-	-	-	0	-1	0	-	-	-	-	-	Plane	-

7. Summary

The industrialization of AM entails tolerancing of AM products. The continued use of legacy file formats such as the STL file brings about novel challenges especially in maintaining the digital thread throughout the product life cycle. When a product geometry is converted to STL file format, any tolerancing information is lost along with the design intent. To perform a tolerance analysis for the product, this information must then either be assumed or recreated through reverse engineering.

This paper described how functional surfaces of STL files may be converted to vectorial representations which directly enables VT of shape features. A case study demonstrated a practical application of the method with an accompanying tolerancing table. It is argued that the proposed method fits well into the digital pipeline of contemporary manufacturing systems, and constitutes a meaningful approach to the tolerancing of AM products.

Acknowledgments

This research is funded by the Norwegian Ministry of Research and Education and is associated with SFI Manufacturing funded by the Norwegian Research Council.

References

[1] Hull CW. Apparatus for production of three-dimensional objects by stereolithography. US patent no. US4575330 A. 1986.
[2] Gibson I, Rosen DW, Stucker B. Additive manufacturing technologies. 2nd ed. New York: Springer; 2015.
[3] ISO 1101:2017(E). Geometrical product specifications (GPS) – Geometrical tolerancing – Tolerances of form, orientation, location and run-out. 2017.
[4] ASME Y14.5M-2018. Dimensioning and Tolerancing. 2018.
[5] ISO 286-1:2010(E). Geometrical product specifications (GPS) – ISO code system for tolerances on linear sizes – Part 1: Basis of tolerances, deviations and fits. 2010.
[6] Ameta G, Lipman R, Moylan S, Witherell P. Investigating the Role of Geometric Dimensioning and Tolerancing in Additive Manufacturing. J Mech Des N Y. 2015;137(11):111401–10.
[7] Moroni G, Petrò S, Polini W. Geometrical product specification and verification in additive manufacturing. CIRP Ann Manuf Technol. 2017;66(1):157–60.
[8] Szilvśi-Nagy M, Mátyási G. Analysis of STL files. Math Comput Model. 2003;38(7):945–60.
[9] Shi Y, Zhang Y, Baek S, De Backer W, Harik R. Manufacturability analysis for additive manufacturing using a novel feature recognition technique. Comput Aided Des Appl. 2018;15(6):941–52.
[10] Krogstie L, Martinsen K. Closed Loop Tolerance Engineering – A Relational Model Connecting Activities of Product Development. Procedia CIRP. 2012;3:519–24.
[11] Schleich B, Wärmefjord K, Söderberg R, Wartzack S. Geometrical Variations Management 4.0: towards next Generation Geometry Assurance. Procedia CIRP. 2018;75:3–10.
[12] Dantan J-Y, Huang Z, Goka E, Homri L, et al. Geometrical variations management for additive manufactured product. CIRP Ann Manuf Technol. 2017;66(1):161–4.
[13] Arni R, Gupta SK. Manufacturability analysis of flatness tolerances in solid freeform fabrication. J Mech Des N Y. 2001;123(1):148–56.
[14] Budinoff H, McMains S. Prediction and visualization of achievable orientation tolerances for additive manufacturing. Procedia CIRP. 2018;75:81–6.
[15] Minetola P, Iuliano L, Marchiandi G. Benchmarking of FDM Machines through Part Quality Using IT Grades. Procedia CIRP. 2016;41:1027–32.
[16] Dimitrov D, van Wijck W, Schreve K, de Beer N. Investigating the achievable accuracy of three dimensional printing. Rapid Prototyp J. 2006;12(1):42–52.
[17] Hanumaiah N, Ravi B. Rapid tooling form accuracy estimation using region elimination adaptive search based sampling technique. Rapid Prototyp J. 2007;13(3):182–90.
[18] Lynn-Charney C, Rosen DW. Usage of accuracy models in stereolithography process planning. Rapid Prototyp J. 2000;6(2):77–87.
[19] Lieneke T, Denzer V, Adam GAO, Zimmer D. Dimensional Tolerances for Additive Manufacturing: Experimental Investigation for Fused Deposition Modeling. Procedia CIRP. 2016;43:286–91.
[20] Kitsakis K, Kechagias J, Vaxevanidis N, Giagkopoulos D. Tolerance Analysis of 3d-MJM parts according to IT grade. IOP Conf Ser Mater Sci Eng. 2016;161:012024.
[21] Ippolito R, Iuliano L, Gatto A. Benchmarking of Rapid Prototyping Techniques in Terms of Dimensional Accuracy and Surface Finish. CIRP Ann Manuf Technol. 1995;44(1):157–60.
[22] Paul R, Anand S. Optimal part orientation in Rapid Manufacturing process for achieving geometric tolerances. J Manuf Syst. 2011;30(4):214–22.
[23] Paul R, Anand S. Optimization of layered manufacturing process for reducing form errors with minimal support structures. J Manuf Syst. 2015;36:231–43.
[24] Das P, Chandran R, Samant R, Anand S. Optimum Part Build Orientation in Additive Manufacturing for Minimizing Part Errors and Support Structures. Procedia Manuf. 2015;1:343–54.
[25] Das P, Mhapsekar K, Chowdhury S, Samant R, Anand S. Selection of build orientation for optimal support structures and minimum part errors in additive manufacturing.Comput Aided Des Appl. 2017;14(sup1):1–13.
[26] Zhang J, Li Y. Region segmentation and shape characterisation for tessellated CAD models. Int J Comput Integr Manuf. 2016;29(8):907–15.
[27] Sunil VB, Pande SS. Automatic recognition of features from freeform surface CAD models. Comput Aided Des. 2008;40(4):502–17.
[28] Shamir A. A survey on Mesh Segmentation Techniques. Comput Graph Forum. 2008;27(6):1539–56.
[29] Rodrigues RSV, Morgado JFM, Gomes AJP. A contour-based segmentation algorithm for triangle meshes in 3D space. Comput Graph. 2015;49:24–35.
[30] Mejia D, Ruiz-Salguero O, Sánchez JR, Posada J, et al. Hybrid geometry/topology based mesh segmentation for reverse engineering. Comput Graph. 2018;73:47–58.
[31] Moroni G, Syam WP, Petrò S. Towards Early Estimation of Part Accuracy in Additive Manufacturing. Procedia CIRP. 2014;21:300–5.
[32] Hull CW, Spence ST, Albert DJ, Smally DR, et al. Cad/cam stereolithographic data conversion. US patent no. US182830. 1989.
[33] ISO/ASTM 52900:2015(E). Standard Terminology for Additive Manufacturing – General Principles – Terminology. 2015.
[34] ISO/ASTM 52921:2013(E). Standard terminology for additive manufacturing – Coordinate systems and test methodologies. 2013.
[35] Martinsen K. Vectorial tolerancing for all types of surfaces. In: Advances in Design Automation; Albuquerque, USA: ASME; 1993.
[36] Britten W, Weber C. Transforming ISO 1101 Tolerances into Vectorial Tolerance Representations — A CAD-Based Approach. In: van Houten, F, Kals, H, editors. Global Consistency of Tolerances; Dordrecht: Springer Netherlands; 1999.
[37] Bialas S, Humienny Z, Kiszka K. Relations Between ISO 1101 Geometrical Tolerances and Vectorial Tolerances—Conversion Problems. In: ElMaraghy, HA, editor. Geometric Design Tolerancing: Theories, Standards and Applications: Springer; 1998. p. 88–99.
[38] Cheng W, Fuh JYH, Nee AYC, Wong YS, et al. Multi-objective optimization of part-building orientation in stereolithography. Rapid Prototyp J. 1995;1(4):12–23.
[39] Schleich B, Wartzack S. How can Computer Aided Tolerancing Support Closed Loop Tolerance Engineering? Procedia CIRP. 2014;21:312–7

Paper P4

T. L. Leirmo, O. Semeniuta, I. Baturynska *et al.*, 'Extracting shape features from a surface mesh using geometric reasoning,' *Procedia CIRP*, vol. 93, pp. 544–549, 2020, ISSN: 2212-8271. DOI: 10.1016/j.procir.2020.02.142. [Online]. Available: http://www.sciencedirect.com/science/article/pii/S2212827120306788

Available online at www.sciencedirect.com

ScienceDirect

Procedia CIRP 93 (2020) 544–549

www.elsevier.com/locate/procedia

53rd CIRP Conference on Manufacturing Systems

Extracting shape features from a surface mesh using geometric reasoning

Torbjørn Langedahl Leirmo[a,*], Oleksandr Semeniuta[a], Ivanna Baturynska[a], Kristian Martinsen[a]

[a]*Department of Manufacturing and Civil Engineering, NTNU – Norwegian University of Science and Technology, Teknologivegen 22, 2815 Gjøvik, Norway*

* Corresponding author. Tel.: +47 480 88 390. *E-mail address:* torbjorn.leirmo@ntnu.no

Abstract

Mesh data is extensively used in CAD/CAM applications to approximate three-dimensional (3D) solid models. The STL file format is one of the key file formats for 3D data transfer in modern manufacturing systems. STL files, however, retain no topological information, which would have been beneficial for subsequent file analysis and manipulation. The ability to extract geometric features from mesh data enables automation and facilitates process planning. This paper describes how geometric primitives may be reconstructed from mesh data by simple heuristics. A case study is presented, and a discussion is made on possible applications.

© 2020 The Authors. Published by Elsevier B.V.
This is an open access article under the CC BY-NC-ND license (http://creativecommons.org/licenses/by-nc-nd/4.0/)
Peer-review under responsibility of the scientific committee of the 53rd CIRP Conference on Manufacturing Systems

Keywords: Geometric modelling; Computer-Aided Design (CAD); Feature recognition

1. Introduction

Computer-aided technologies such as computer-aided design (CAD), computer-aided manufacturing (CAM) and computer automated process planning (CAPP) have had a drastic influence on manufacturing systems over the last forty years. The CAD models of components are central in modern manufacturing systems and holds important information with regards to intellectual property, manufacturing processes and capabilities, and quality control and assurance. Because of the widespread use of digital models, a large number of file formats for the representation of part geometries and related properties exist both in open format and software specific formatting.

The STL file format was originally developed to accommodate the specific process planning needs of early additive manufacturing technology with the computational capabilities at that time [1]. The format was made accessible to all and was soon utilized for transferring 3D data between platforms across the computer-aided processes [2]. While the original CAD model retains information about the geometric features of the design which would be useful in subsequent processing stages, this information is not explicit in the STL file [3]. Regaining the lost information about the nominal geometry is necessary whenever the CAD model is unavailable, and the design is needed for operations such as optimizing build preparation in additive manufacturing.

While tessellating a computer model to create an STL file is simple enough, the reverse engineering of shape features from STL data is a much more difficult task. Existing solutions make use of complex mathematical analysis and metaheuristics for mesh segmentation and feature classification, both of which are computationally expensive. As an alternative of low computational complexity, we demonstrate how geometric reasoning may be applied to identify shape features from a triangle mesh as described in the STL file format in four steps:

1. Establish connections to neighboring triangles
2. Identify coplanar facets
3. Identify curved segments
4. Merge curved features to create double-curved surfaces

The important difference from the existing body of knowledge is the deduction of regional geometry based on local topology without engaging in computationally extensive

2212-8271 © 2020 The Authors. Published by Elsevier B.V.
This is an open access article under the CC BY-NC-ND license (http://creativecommons.org/licenses/by-nc-nd/4.0/)
Peer-review under responsibility of the scientific committee of the 53rd CIRP Conference on Manufacturing Systems
10.1016/j.procir.2020.02.142

mathematical analysis. The method described herein assumes that the STL file is valid and free from noise, preferably originating from CAD software.

First, a literature review is presented before the fundamentals of the STL file format and relevant geometric methods are provided. Next, the method for extracting shape features using geometric reasoning is described and an example implementation demonstrates the application. Finally, a discussion is made on the prospects of the method before a summary and future work.

2. Literature review

The gap from design to manufacturing operations was recognized at an early stage, hence a number of research efforts have been directed at problems such as the CAD/CAM gap. The work of Henderson and Anderson [4] constitutes an early approach to the problem where machining features such as slots, holes, and pockets were automatically extracted from CAD data and a feature graph was created. Marefat and Kashyap [5] introduced a cavity graph approach to the same problem where prismatic depressions were identified through geometric reasoning. Both [4] and [5] took the CAD model as input and therefore cannot be directly applied to STL files.

Krysl and Ortiz [6] describe a set of algorithms for converting a tessellated surface into boundary representation (B-Rep) where the geometry is described by patches defining the boundary between the interior and the exterior with the use of faces, edges, and vertices. While the STL file is exclusively composed of triangular planar faces, the patches of a B-Rep model are represented by splines and may, therefore, take any form [7]. The authors, however, provide no means to identify any shape features of the part, merely to describe its boundary. A B-Rep model was also created by Chappuis, et al. [8] who demonstrated a diffuse integration method for recognizing features in a surface mesh by calculating the local curvature. More recently, Bénière, et al. [9] proposed a method to reconstruct B-Rep models by fitting primitives based on curvature characteristics of the area around vertices.

Moroni, et al. [10] sliced the STL model with three orthogonal planes and identified cylinders by analyzing closed loops in the resulting contour. The same goal was achieved by Qu and Stucker [11] who presented a method based on the edges between facets to construct closed loops which, after an elimination procedure, constitutes the drilled holes of the part.

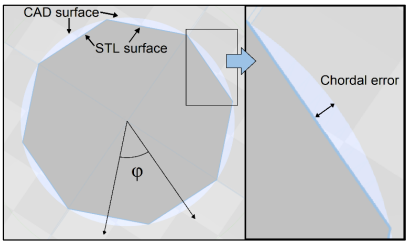

Fig. 1. Illustration of chordal error from STL conversion and the dihedral angle φ.

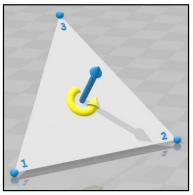


```
solid <name>
  facet normal <x> <y> <z>
    outer loop
      vertex <x> <y> <z>
      vertex <x> <y> <z>
      vertex <x> <y> <z>
    endloop
  endfacet
.....
(Repeats for each facet)
.....
endsolid <name>
```

Fig. 2. Illustration of a triangular facet with normal vector and vertices (left) and the syntax of an STL file in ASCII format (right).

A somewhat similar method was proposed by Sunil and Pande [12] who identified feature edges by calculating dihedral angles and bounded the identified feature regions. Eight feature types relevant for sheet metal parts could be identified by Gauss and mean curvature calculations. Dihedral angles are widely used in literature for mesh segmentation, and occasionally, they are also utilized for the classification of feature types [13-16].

Hao, et al. [16] demonstrates how the estimation of curvature may be utilized for extracting feature boundaries, but not the feature type. Zhang and Li [17] performed mesh segmentation with regards to local convexity and identified the feature type by analyzing the gaussian image – a technique also applied in [9, 12] where the facet normals are projected on a unit sphere.

3. Theoretic foundations

3.1. Triangle tessellations

Converting a prismatic surface to a triangle tessellation such as the ones present in STL files is unproblematic with regards to accuracy. However, as soon as a curved surface is involved, a deviation known as a chordal error between the original design and the STL model will arise from surface approximations, i.e. the distance from the curved surface of the CAD model to the plane surface of the triangle (Fig. 1) [18]. The magnitude of the chordal errors depends on the resolution of the constructed STL file, i.e. the number of triangles used to represent the part. Typically, the CAD software enables the user to set tolerances for the conversion in terms of maximal chordal error and maximum dihedral angle φ used to represent curved surfaces.

3.2. The STL file format

The STL file contains an unordered list of all the triangles (facets) composing the part, where every facet is represented by a unit normal vector and the coordinates of all three corners. To unambiguously delimit the interior from the exterior, the facet normal points outwards, and the vertices are listed in counterclockwise order as seen from the outside as displayed in Fig. 2 [1, 19].

All facets have three adjacent facets which are referred to as neighbors, however, the file contains no information about adjacency relations. In other words, we know that any given facet must have three neighbors, but there is no straight forward way of finding these facets in the file. The three neighbors of a

facet are collectively referred to as the neighborhood of the facet in the remainder of this paper and is illustrated in Fig. 4.

The STL file may originate from different sources that influence the contents of the file: (i) export from CAD software generally produces valid files with minimal noise; and (ii) scanned geometries often introduces noise from environmental factors and invalid files are commonplace. Invalid files typically contain intersecting triangles, inverted normal vectors or holes. Moreover, processed meshes may have unpredictable effects on the STL data due to smoothing or simplifications which further complicates file processing.

3.3. Geometric primitives

There are five distinguishable geometric primitives as illustrated in Fig. 3, plane, cylinder, cone, sphere and torus. In constructive solid geometry, these basic shapes constitute the foundation for all designs through Boolean operations such as union and intersection. These primitives are also central in mechanical parts for creating interfacing and functional surfaces which is why it is desired to extract these primitives from the triangle mesh. The orientation of a primitive surface is defined by a feature vector that is perpendicular to plane surfaces and parallel to the axis of single curved surfaces. Note that some surface types are subject to ambiguous feature vectors due to the degrees of freedom associated with the surface type [20]. E.g. a sphere has no identifiable feature orientation without being supplemented with additional information or rules for determining its feature vector.

3.4. Calculating dihedral angles

In the context of a surface mesh, the dihedral angle φ is defined as the angle between the normal vectors of two adjacent facets as illustrated in Fig. 1. The angle θ between two vectors $\mathbf{v}$ and $\mathbf{p}$ in $\mathbb{R}^3$ may generally be calculated as:

$$\theta = \arccos\left(\frac{\mathbf{p}\cdot\mathbf{v}}{|\mathbf{p}|\cdot|\mathbf{v}|}\right) \tag{1}$$

Because the normal vectors of STL files are unit vectors, the denominator will always be one and therefore insignificant. Based on Eq. 1, the dihedral angle may be calculated simply as:

$$\varphi = \arccos(\mathbf{p}\cdot\mathbf{v}) \tag{2}$$

The dihedral angle φ is positive for all normal vectors and will not give any indication of convexity.

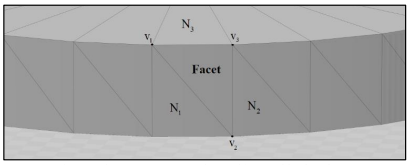

Fig. 4. A facet with vertices v_1, v_2 and v_3 and its neighborhood (N_1, N_2, N_3).

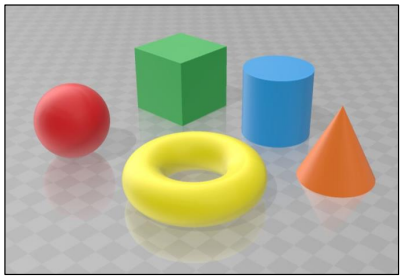

Fig. 3. Illustration of the five geometric primitives: plane (green), cylinder (blue), cone (orange), sphere (red) and torus (yellow).

3.5. Analysis of a triangle neighborhood

The relationship between two neighboring facets may be categorized with respect to the dihedral angle φ based on assumptions regarding the tessellation process. Firstly, it is assumed that any round off errors present in the STL file may be contained within a relatively narrow margin of error denoted as ε. Secondly, it is assumed that a limit γ exists for the maximum dihedral angle φ for curved surfaces regardless of which geometric primitive it represents. Finally, it is assumed that ε is small enough to avoid confusion with curved surfaces. These values enable classification of the angular relationship between the facets as displayed in Table 1. We denote the three angular ranges case *A*, *B* and *C* for the remainder of this paper.

Table 1. Ranges of dihedral angles with edge descriptions.

Case	Dihedral angle φ	Description
A	$\varphi \le \varepsilon$	The facets are coplanar
B	$\varepsilon < \varphi \le \gamma$	The edge represents a curved surface
C	$\varphi > \gamma$	The facets are members of separate features

Because each triangle has three neighbors, all of which may represent any of the cases in Table 1, the number of possible combinations constitutes a problem of k-combinations with repetition [21]. This can be expressed as a multiset coefficient as:

$$\left(\binom{n}{k}\right) = \binom{n+k-1}{k} = \binom{3+3-1}{3} = \binom{5}{3} = \frac{5\times4}{2\times1} = 10 \tag{3}$$

where n is the number of neighbors and k is the number of possible relations (n multichoose k).

The ten possible combinations of neighborhood relations calculated in Eq. 3 correspond to certain local characteristics and may be used in the identification of shape features as tabulated in Table 2. The order of N_1, N_2, and N_3 is irrelevant for this purpose as the number of neighbors corresponding to a surface type is the only information of interest in this regard.

Table 2. Possible combinations of neighborhood relations.

#	N_1	N_2	N_3	Description
1	*A*	*A*	*A*	All neighbors are part of a single large plane
2	*A*	*A*	*B*	All but one neighbor are coplanar
3	*A*	*A*	*C*	All but one neighbor are coplanar
4	*A*	*B*	*B*	One coplanar neighbor and two curved edges
5	*A*	*B*	*C*	One of each category
6	*A*	*C*	*C*	One coplanar facet and two irrelevant neighbors
7	*B*	*B*	*B*	All three edges are curved
8	*B*	*B*	*C*	Two curved edges and one irrelevant neighbor
9	*B*	*C*	*C*	Only one curved edge and two irrelevant neighbors
10	*C*	*C*	*C*	No relevant neighbors (triangular plane detected)

4. Proposed method applying geometric reasoning

The proposed method involves the following four steps:

1. Establish connections to neighboring triangles
2. Identify coplanar facets
3. Identify curved segments
4. Merge curved features to create double-curved surfaces

Establishing the connection between triangles is pivotal for the efficient handling of the triangles in subsequent operations. The details of the data structure created in the first step are not central in the current work and are outside the scope of this paper. The interested reader is referred to [7, 22] for details on possible data structures. The remaining steps are however explained in detail in the following subsections.

4.1. Identifying planes

The first step of feature recognition is to identify all plane surfaces composed of more than one facet. In practice, each facet must be evaluated with respect to the dihedral angles to its neighbors. From Table 2 this would cover all combinations 1–6. Additionally, case 10 indicates a triangular plane surface that needs only a single facet for its representation and hence requires no further processing.

If two facets are found to be coplanar, a recursive neighborhood search is conducted to identify other facets potentially belonging to the same plane. This region-growing continues until the entire plane is identified. If more than two connected facets are coplanar, the feature type may be confirmed as a plane because no other feature type would yield more than two coplanar connected facets.

4.2. Identifying curved surfaces

Curved surfaces appear in many forms in STL files and require a much more thorough analysis compared to the planar surfaces. The candidate list for curved surfaces includes all single facets remaining after step 1 except those subject to case 10. Additionally, all plane surfaces composed of only two facets must be considered because pairs of coplanar triangles are sometimes present on curved surfaces (see Fig. 5).

Another useful piece of information for guiding the identification of curved surfaces is that they are often represented by triangles of roughly the same dimensions. Consequently, if a neighboring triangle is much larger or smaller than the facet of interest, the chance of the neighbor belonging to a different feature is substantial. However, the area of facets should only be used to guide the feature growing, not to determine membership. This is because facets may be of similar size without necessarily belonging to the same feature.

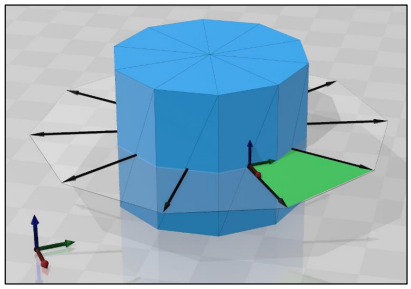

Fig. 5. Illustration of how all facet unit normal vectors lie in the same plane to which the axis of the cylinder is perpendicular.

When two neighboring facets are candidates for a curved surface (i.e. a relationship of case *B*, and roughly the same size), the first step is to check if the facets are part of a cylindrical surface. This is accomplished by identifying the direction of the axis of the potential cylinder and then testing the hypothesis on the next neighbors for validation. The direction of the axis of the potential cylinder may be defined as a vector perpendicular to the normal vectors of both facets as illustrated in Fig. 5. The hypothesis is tested by simply checking for perpendicularity between the cylinder axis and the facet normal vectors of the next neighboring facets. Note that because of possible numerical imprecisions in the STL file, all calculations must consider a margin of error.

If none of the next neighbors meet the criteria for cylinders, a similar test is performed to check for cone. This test requires a third facet that must be acquired from the neighborhood with a unique facet normal vector. Because the unit normal vectors are of equal length, the endpoints of the vectors may be used to define a plane that will have a normal vector parallel to the axis of the cone, thus defining the direction of the cone axis as illustrated in Fig. 6. The axis of the cone may be defined as the normal vector of the plane defined by the endpoint of all three facet normal vectors. The apex angle can easily be calculated as twice the angle between the facet normals and the axis. The hypothesis is confirmed if a fourth facet is found that is connected to the existing members with a dihedral angle within the range of case *B* and complies with the apex angle. If the surface is confirmed as a cylinder or cone, a recursive neighborhood search is conducted to collect all member facets.

4.3. Merging from single- to double-curved features

Because of the discretization of continuous surfaces, all surfaces have been decomposed into planes, cylinders, and cones after the previous section. The tessellation process turns

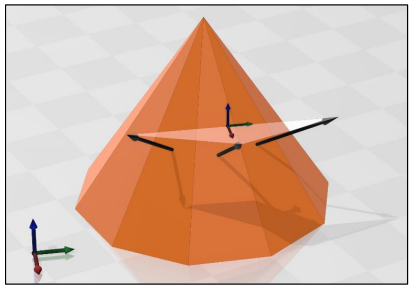

Fig. 6. Illustration of how the endpoints of the facet unit normal vectors may define a plane to which the axis of the cone is perpendicular.

spherical and toric surfaces into segments of connected cones and cylinders (Fig. 7). Hence, the identification of spheres and tori may be accomplished by checking if adjacent cones are coaxial and with apex angles deviating from each other with an angle within the tolerance of curved surfaces, i.e. same as case *B* for dihedral angles (Fig. 7a). Likewise, adjacent cylindrical segments with axes deviating with an angle within the range of case *B* may also be combined to form spheres or tori as illustrated in Fig. 7b and c. To avoid the features merging into unrelated connected surfaces, the direction of axial offset should be constrained. One solution to this problem is to define a plane on which the axes of potential candidate cylinders should lie. For spheres and tori alike, an extra check for the sizes of triangles within candidate features should be conducted to avoid features growing out of bounds.

5. Example implementation

To demonstrate the feasibility of the proposed method, the approach is exemplified on a ball joint which is a simple geometry that embodies several of the geometric primitives. Fig. 8a depicts a plain representation of the triangle mesh, and Fig. 8b illustrates the geometric primitives comprising the ball joint with the color scheme introduced in Fig. 3. The component is designed in SolidWorks 2018 and exported as an STL file with the resolution option “fine” which resulted in 8044 triangles. Due to the rounded edges of the part, no connected triangles form dihedral angles large enough to clearly distinguish separate features. With reference to Table 1, this means that only cases *A* and *B* are present in the mesh which consequently leaves only combinations 1, 2, 4 and 7 from Table 2.

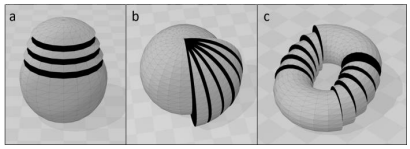

Fig. 7. Segmentations of double curved surfaces. a) cones of a sphere, b) cylinders of a sphere, and c) cylinders of a torus.

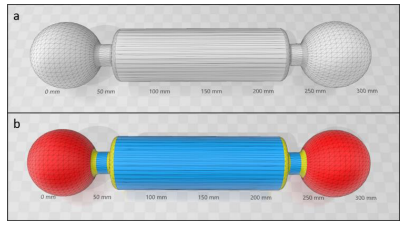

Fig. 8. Ball joint represented as a) raw STL file, b) with color coded surfaces with respect to the geometric primitives.

After the adjacency relations have been established, the first step is to extract coplanar adjacent facets by pairwise comparison of facet normals. Following Table 2, no regions correspond to neighborhood combination 1. Combination 2 is present only in the planar sections visible in Fig. 9. Because three connected coplanar facets may be found by investigating the neighbors of a single facet, the sections are immediately recognized as planar features. Combination 4 is present in most of the mesh. In fact, apart from the planar features already identified, all but the outermost sections of the spheres are classified as combination 4. All instances of combination 4 are included in the subsequent search for curved surfaces.

The second step identifies cylinders and cones by investigating the facet neighborhood. Consider the large cylinder in the middle of the part. The curved surface is prevented from growing into the filleted edges because of the proportional size difference. However, the normal vectors of all the triangles constituting the cylinder lie in the y-z-plane and thus the axis of the cylinder must be parallel with the x-axis as exemplified in Fig. 5). As soon as this knowledge is obtained, the remainder of the cylinder is identified by finding the dihedral angle of the next neighbor recursively and making sure it is perpendicular to the axis of the cylinder. Similarly, segments of the toric and spherical surfaces are identified in this step. Note that depending on the particular implementation and order of facets in the list, the exact results from this step may vary. However, with perfectly defined threshold values and a thorough exploration of cylinders before going forth with identifying cones, one would end up with the cylindrical segments displayed in Fig. 9a. A similar implementation with an emphasis on cones would give the results in Fig. 9b.

Finally, adjacent single curved segments are compared with respect to the orientation of their axes. Again, the relative sizes of the facets constituting the surfaces may be used as a guide for avoiding features growing out of bounds. If two surfaces

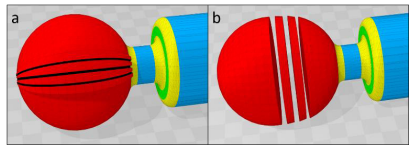

Fig. 9. Ball joint with a) cylindric segments, and b) segments of conic form.

are found to be compatible, they are joined to form the relevant double-curved surface (sphere or torus).

6. Discussion

There are some prerequisites for the proposed method to be feasible in an industrial setting. Firstly, the STL file must be free from holes and intersecting triangles for the adjacency relations to be established correctly. This is important because the method relies on the neighboring triangles being readily available for efficient execution. Next, the method assumes smooth surfaces in the sense that no shape feature contains surface areas deviating from the shape primitive more than the errors induced by the tessellation and numerical imprecision. In practice, this means that the method is not suitable for processing 3D scanned surfaces without preprocessing such as smoothing operations to reduce the inherent noise. Such operations should, however, be used with care, especially in automatic applications, as they can easily distort the geometry.

The presented method is geared towards STL files originating from CAD software without any form of re-meshing and may, therefore, be infeasible in many real-world applications. Certain adaptations must be considered before the method may be successfully applied to organic geometries and alternative file origins. However, the reasoning described in the current work constitutes a logic foundation that is viable for extracting shape features from valid STL files. The proposed method may provide a starting point or otherwise support more advanced feature recognition techniques.

A current trend in manufacturing is the increasing geometric complexity of components, motivated by sustainability in terms of cost savings as well as environmental concerns [23]. Additive manufacturing promises complexity for free, but despite the organic shapes created through topology optimization, the functional surfaces are still primitive. Naturally, the proposed method will perform poorly on freeform surfaces because only small pieces of primitive shapes will be recognized.

7. Summary and further work

The current work described how geometric reasoning may be applied to extract geometric primitives from a triangle mesh. The presented method involves four steps; (i) establishing adjacency relations, (ii) identifying planes, (iii) recognizing single curved segments, and (iv) joining single curved segments to double-curved surfaces. An example implementation was presented to demonstrate the progression of the method. Further validation and demonstration by application on industrial components is planned for future work and a C++ implementation is being developed.

The current work constitutes a computationally inexpensive framework that establishes a foundation for rule-based geometric analysis. The logic presented may be used as a starting point for more advanced feature recognition methods, or as support for computer-aided operations such as process planning, quality assessment, and design optimization. Future work should include the integration of the method with computer-aided technologies. Furthermore, the reverse engineering of solid models from STL data is a possible extension of the current work along with the identification of solid features.

Acknowledgments

This research is funded by the Norwegian Ministry of Research and Education and is associated with SFI Manufacturing funded by the Norwegian Research Council.

References

[1] Hull CW, Spence ST, Albert DJ, Smally DR, et al. Cad/cam stereolithographic data conversion. US patent no. US182830. 1989.
[2] Gibson I, Rosen DW, Stucker B. Additive manufacturing technologies. 2nd ed. New York: Springer; 2015.
[3] Moroni G, Petrò S, Polini W. Geometrical product specification and verification in additive manufacturing. CIRP Ann Manuf Technol. 2017;66(1):157–60.
[4] Henderson MR, Anderson DC. Computer recognition and extraction of form features: A CAD/CAM link. Comput Ind. 1984;5(4):329–39.
[5] Marefat M, Kashyap RL. Geometric reasoning for recognition of three-dimensional object features. IEEE Trans Pattern Anal Mach Intell. 1990;12(10):949–65.
[6] Krysl P, Ortiz M. Extraction of boundary representation from surface triangulations. Int J Numer Methods Eng. 2001;50(7):1737–58.
[7] Bærentzen JA, Gravesen J, Anton F, Aanæs H. Guide to Computational Geometry Processing: Foundations, Algorithms, and Methods. Springer, London; 2012.
[8] Chappuis C, Rassineux A, Breitkopf P, Villon P. Improving surface meshing from discrete data by feature recognition. Eng Comput. 2004;20(3):202–9.
[9] Bénière R, Subsol G, Gesquière G, Le Breton F, Puech W. A comprehensive process of reverse engineering from 3D meshes to CAD models. Comput Aided Des. 2013;45(11):1382–93.
[10] Moroni G, Syam WP, Petrò S. Towards Early Estimation of Part Accuracy in Additive Manufacturing. Procedia CIRP. 2014;21:300–5.
[11] Qu X, Stucker B. Circular hole recognition for STL-based toolpath generation. Rapid Prototyp J. 2005;11(3):132–9.
[12] Sunil VB, Pande SS. Automatic recognition of features from freeform surface CAD models. Comput Aided Des. 2008;40(4):502–17.
[13] Yang S, Shu S. Robust Feature Extraction for the Composite Surface Mesh from STL File. In: The 9th International Conference for Young Computer Scientists: IEEE; 2008:1373–8.
[14] Shamir A. A survey on Mesh Segmentation Techniques. Comput Graph Forum. 2008;27(6):1539–56.
[15] Bespalov D, Shokoufandeh A, Regli WC, Sun W. Local Feature Extraction Using Scale-Space Decomposition. In: Computers and Information in Engineering Conference; Salt Lake City, Utah, USA: ASME; 2004:1–10.
[16] Hao J, Fang L, Williams RE. An efficient curvature-based partitioning of large-scale STL models. Rapid Prototyp J. 2011;17(2):116–27.
[17] Zhang J, Li Y. Region segmentation and shape characterisation for tessellated CAD models. Int J Comput Integr Manuf. 2016;29(8):907–15.
[18] Zha W, Anand S. Geometric approaches to input file modification for part quality improvement in additive manufacturing. J Manuf Process. 2015;20:465–77.
[19] Szilvśi-Nagy M, Mátyási G. Analysis of STL files. Math Comput Model. 2003;38(7):945–60.
[20] Martinsen K. Vectorial tolerancing for all types of surfaces. In: Advances in Design Automation; Albuquerque, USA: ASME; 1993.
[21] Stanley RP. Enumerative Combinatorics. Springer, Boston, MA; 1986.
[22] Guo K-B, Zhang L-C, Wang C-J, Huang S-H. Boolean operations of STL models based on loop detection. Int J Adv Manuf Technol. 2007;33(5):627–33.
[23] Thompson MK, Moroni G, Vaneker T, Fadel G, et al. Design for Additive Manufacturing: Trends, opportunities, considerations, and constraints. CIRP Ann Manuf Technol. 2016;65(2):737–60.

Paper P5

T. L. Leirmo and O. Semeniuta, 'Investigating the Dimensional and Geometric Accuracy of Laser-Based Powder Bed Fusion of PA2200 (PA12): Experiment Design and Execution,' *Applied Sciences*, vol. 11, no. 5, p. 2031, 2021, ISSN: 2076-3417. DOI: 10.3390/app11052031. [Online]. Available: https://www.mdpi.com/2076-3417/11/5/2031

applied sciences

MDPI

Article

Investigating the Dimensional and Geometric Accuracy of Laser-Based Powder Bed Fusion of PA2200 (PA12): Experiment Design and Execution

Torbjørn Langedahl Leirmo * and Oleksandr Semeniuta

Department of Manufacturing and Civil Engineering, Faculty of Engineering, NTNU—Norwegian University of Science and Technology, 2815 Gjøvik, Norway; oleksandr.semeniuta@ntnu.no
* Correspondence: torbjorn.leirmo@ntnu.no; Tel.: +47-480-88-390

Featured Application: The present paper describes the execution of an experiment and the resulting data to facilitate the reuse of experiment results and open research.

Abstract: Variation management in additive manufacturing (AM) is progressively more important as technologies are implemented in industrial manufacturing systems; hence massive research efforts are focused on the modeling and optimization of process parameters and the effect on final part quality. These efforts are, however, hampered by the very problem they are seeking to solve, as conclusions are weakened by poor validity, reliability, and repeatability. This paper details an elaborate experiment design and the subsequent execution with the aim of making the research data available without loss of validity. Test artifacts were designed and allocated to fixed positions and orientations in a grid pattern within the build chamber to facilitate rigid analysis between different builds and positions in the build chamber. A total of 507 specimens were produced over three builds by laser sintering PA12 before inspection with a coordinate measuring machine. This research demonstrates the inherent variations of laser-based powder bed fusion of polymers (LB-PBF/P) that must be considered in experiment designs to account for noise factors. In particular, the results indicate that the position in the xy-plane has a major influence on the geometric accuracy, while the position in the z-direction appears to be less influential.

Keywords: additive manufacturing; geometric tolerancing; part build orientation; powder bed fusion; selective laser sintering; PA12; PA2200

check for updates

Citation: Leirmo, T.L.; Semeniuta, O. Investigating the Dimensional and Geometric Accuracy of Laser-Based Powder Bed Fusion of PA2200 (PA12): Experiment Design and Execution. *Appl. Sci.* **2021**, *11*, 2031. https://doi.org/10.3390/app11052031

Academic Editor: Wilma Polini

Received: 29 January 2021
Accepted: 20 February 2021
Published: 25 February 2021

Publisher's Note: MDPI stays neutral with regard to jurisdictional claims in published maps and institutional affiliations.

Copyright: © 2021 by the authors. Licensee MDPI, Basel, Switzerland. This article is an open access article distributed under the terms and conditions of the Creative Commons Attribution (CC BY) license (https://creativecommons.org/licenses/by/4.0/).

1. Introduction

As additive manufacturing (AM) is increasingly used for the manufacture of functional components and assemblies, requirements are imposed on the AM processes with regards to dimensional and geometric accuracy [1]. In the manufacturing industry, quality requirements are formalized in standards, such as ISO 1101 [2] for geometric product specifications (GPS) and ASME Y14.5 [3] for geometric dimensioning and tolerancing (GD&T). These standards provide measures of geometric accuracy—commonly referred to as characteristics—that are crucial to secure a good fit of an assembly and the proper functioning of a product. The ability of AM to achieve tolerances comparable to conventional manufacturing technologies is vital for the continued expansion of AM technologies into the commercial manufacturing industry.

ISO/ASTM 52900:2015 [4] distinguishes seven process categories of AM, all characterized by widely different properties and peculiarities; hence generalization between the technologies is difficult. Due to the inherent differences of the processes, research efforts are often directed towards a single process or a small selection of processes. Although still under rapid development, powder bed fusion (PBF) is one of the more industrialized AM processes and is, therefore, already subjected to the requirements of industry

at a larger scale. Further classification of PBF is made by specifying the energy source and material type, i.e., electron beam or laser as the energy source, and metal, polymer, or ceramics as materials, as illustrated in Figure 1 [5]. The current work reports on experiments on laser-based PBF of polymers (LB-PBF/P), popularly known as selective laser sintering (SLS).

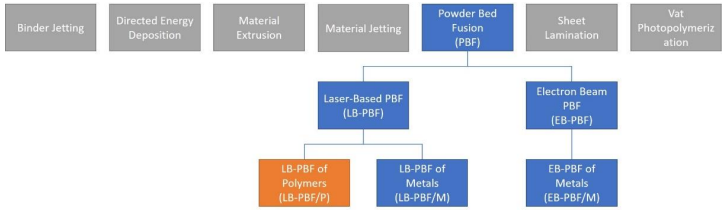

Figure 1. Process categories in additive manufacturing as defined in ISO/ASTM 52900:2015 and 52911:2019.

Layered manufacturing processes are generally prone to the so-called staircase effect arising from the discretization of a 3D surface into 2.5D layers. This inevitably affects the surface topography and accuracy [6]; hence the phenomena have been modeled in terms of both flatness [7] and cylindricity [8]. Because the severity of the staircase effect depends on the angle of the surface, the surface type plays a major role in how the staircase effect manifests, and therefore, also how the part builds orientation influences the geometric accuracy. In this context, a surface type may be any of the five geometric primitives—plane, cylinder, cone, sphere, and torus—and an occurrence of a surface type on a 3D-model is referred to as a shape feature. Because surface types are influenced differently by part build orientation, the shape features can be used to optimize part build orientation and to predict geometric deviations [9,10].

Previous research has shown that PBF is a complex process with many variables affecting the product in terms of mechanical properties [11–15], surface quality [14–19], and geometric and dimensional accuracy [15,20–22]. The part build orientation is known to have a significant effect on final quality with regards to all of these areas in addition to its contribution to build time and cost [23]. Consequently, numerous studies include part build orientation as an experimental factor to gauge and model its effect on various measures [24]. While studies on surface roughness in various AM technologies have investigated part build orientations with 10- and 15-degree intervals [19], the effect on dimensional and geometric accuracy is typically not researched with the same level of detail. Baturynska [21] performed a statistical analysis of dimensional accuracy in LB-PBF/P, where four orientations were utilized. Senthilkumaran et al. [25] conducted an experiment in LB-PBF/P with a central composite design where the effect of orientation on flatness and cylindricity was investigated in five levels from 0 to 90 degrees alongside several other factors. Similar studies on other AM technologies are also reported in literature where orientation is typically investigated in 2–5 levels of an experiment design [26–29].

The driving hypothesis of the present experiment is that the relationship between part build orientation and geometric accuracy is more complex than what can be derived from traditional experiment designs, and more thorough analysis is required. Therefore, the current paper describes an elaborate experiment that is designed and executed to enable a closer analysis of the effects of part build orientation on geometric accuracy.

2. Materials and Methods

The experiment was conducted in five distinct steps as described in the following subsections. First, a test artifact was designed to incorporate the features of interest for the current project. Next, the build layout of three builds was created before the build

process started. When the build process was completed, data collection was conducted by employing a coordinate measuring machine (CMM) for accurate and reliable measurements. Finally, the data from the CMM were exported and analyzed.

2.1. Experimental Factors and Strategies

The repeatability of AM experiments is a challenge because the experiments are not only affected by the processing parameters, but studies also indicate that there are major differences between machine types and even between machines of the same make [30,31]. Furthermore, the variations may occur between builds in the same machine and even different positions in the same build [21,32]. It is, therefore, of paramount importance to design rigid experiments by utilizing blocking strategies, or at the very least enable some characterization of such variations. The current experiment applies both blocking and randomizing strategies and replicates all specimens of the main study three times to enable the characterization of variation.

The main purpose of the experiment is to investigate the effect of part build orientation on dimensional and geometric accuracy. In order to obtain data points of adequate density, part build orientations from 0 to 180 degrees are investigated at five-degree intervals around a single axis. To minimize unwanted variations (noise) in the experiment, all variables are kept constant or handled with blocking and randomization strategies, as displayed in Table 1.

Table 1. Experiment variables with their designated type/strategy and number of levels.

Variable	Strategy/Type	Levels	Values
Part build orientation (φ)	Experimental	37	$\varphi \in \{0, 5, \ldots, 180\}$
Placement in build (P)	Blocking/randomization	45	$P(i,j,k)$ where $i \in \{1, 2, 3\}$, $j \in \{1, 2, 3\}$, *and* $k \in \{1,2,\ldots,5\}$
Build ID (B)	Blocking/randomization	3	$B \in \{1, 2, 3\}$
Feature type (F)	Experimental	4	F ∈ {plane, cylinder, cone, sphere}
Feature size (S)	Experimental	1–4	$S_{cylinder} \in \{4, 8, 16, 24\}$ $S_{cone} \in \{12, 24\}$ $S_{sphere} \in \{24\}$
Laser power	Constant	1	*
Scan speed	Constant	1	*
Raster pattern	Constant	1	*
Layer thickness	Constant	1	120 µm *
Build chamber temperature	Constant	1	180 °C
Room temperature	Regulated	1	20–21 °C †
Humidity	Regulated	1	40–50% †
Material	Constant	1	PA2200 (PA12)
Postprocessing	Constant	1	Air blasting
STL file resolution	Constant	1	Tolerances 0.01 mm and 2°

* given by EOS parameter profile "Balanced", † approximate range with natural variation. Supplementary data are available in the online repository at GitHub: https://github.com/TheThorb/Leirmo_Exp1_Publication1, accessed on 29 January 2021.

In addition to the experimental variable (part build orientation), four variables from Table 1 stand out: (i) placement in build, (ii) build ID, (iii) feature type, and (iv) feature size. It is necessary to produce several specimens simultaneously to complete the experiment within a reasonable time and keep the cost at an acceptable level. A blocking strategy is implemented with regards to the part location in the build to enable linear comparison along the axes of the machine by defining fixed positions in the build space where specimens may be fabricated. The details of the build layout are presented in Section 2.3.

Because the build space is too small to fit three replications of all 37 levels of the experimental variable "part build orientation" in a single build, the experiment must be completed through three separate builds. The variation between builds is handled with a blocking strategy by replicating all part build orientations in every build. Moreover, the three builds were completed in as close succession as possible without interfering with other activities in the laboratory. The environmental conditions were comparable, and the material came from the same batch without any refilling of the powder bins between builds. Details about the build process are presented in Section 2.4, and details on temperature, precipitation and humidity are available in the online repository.

The size of any shape may affect the results of the experiments, especially in AM, where the ratio between the feature size and the layer thickness could significantly affect the deviations of the manufactured surface from the designed surface. It is desired to incorporate shape features of different sizes to investigate how the accuracy varies with feature size; hence several different dimensions are incorporated in the test artifact as described in the following Section 2.2.

2.2. Designing the Test Artifact

Many benchmark artifacts have been proposed over the years, but few are widely used. For a comprehensive overview of geometric benchmarks for AM, the interested reader is referred to [33]. For the current research, the artifact proposed in [34] was adapted by eliminating redundant features and adding a few elements. The artifact is designed specifically to enable inspection with a CMM and can be manufactured in its original orientation by any current AM technology without the need for support structures. Moreover, the design process was guided by the dimensions of the build space available for the experiment, thus restricting the allowable dimensions of the design. Specifically, it was desired to fit three specimens in their initial build orientation on the same plane in the build space, while maintaining a safe distance between all specimens, as well as between the specimens and the boundaries of the build space (the details on the build layout is presented in Section 2.3.). The feature types selected for the design serve the purpose of gauging the quantitative accuracy of the process rather than the qualitative capabilities. Several dimensions of cylinders and cones are present to enable the analysis of how different feature sizes are affected by the build orientation. The resulting artifact is displayed in Figure 2, where all features are labeled in line with the naming convention of [34], where the elements are assigned a short name based on the surface type and numbered if there are more than one (e.g., CC1 for the first truncated cylinders and SP for the spheres). The artifact was designed in the computer-aided design (CAD) software SolidWorks 2018 and exported as an STL (Stereolithography) file in ASCII-format using deviation tolerances of 0.01 mm and 2°. The artifact was inspected and reoriented to aligned with Cartesian orthogonal axes using Microsoft 3D Builder and converted to binary format. The interested reader is referred to [35] and [36] for details on STL files and the challenges they impose on AM and tolerancing. The artifact is available online, along with all supplementary data.

Following the specifications given in [34], the spherical features (SP) are both 24 mm in diameter, and CC1 and CC2 comprise cylindrical features of the four diameters 4 mm, 8 mm, 16 mm, and 24 mm in both concave and convex form. All cylinders are 8 mm in height to enable inspection with CMM while keeping the dimensions of the artifact at a minimum. The cones in TC1, TC2, and TC3 are all 16 mm tall, with an apex angle of 30 degrees and larger diameters of 12 and 24 mm convex and concave. The HX1 and HX2 are both hexagons extruded 16 mm from the base plate, angled 15 degrees relative to each other, yielding 12 vertical planes in unique orientations evenly distributed from 0 to 275 degrees. All features protrude from a 5 mm thick base plate with rounded corners to minimize the volume of the design. The bounding box of the design is 89.67 mm × 69.24 mm × 21 mm, and the volume of the design is 53,230 mm^3. Details on all the elements of the design are available in Table 2.

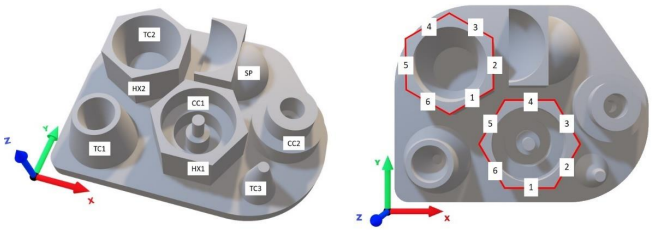

(**a**) (**b**)

Figure 2. The test artifact designed for the experiment. (**a**) The computer-aided design (CAD) model with labeled features in perspective; (**b**) top view of the CAD model showing the numbering of planes in HX1 and HX2.

Table 2. Details on all shape features of the designed artifact.

Group	Description	Diameter (mm)	Position * (mm)			Normal Vector		
			x	y	z	x	y	z
HX1	First plane	*N/A*	0.00	−13.86	8	0	−1	0
	Second plane	*N/A*	12.00	−6.93	8	cos(30°)	−0.5	0
	Third plane	*N/A*	12.00	6.93	8	cos(30°)	0.5	0
	Fourth plane	*N/A*	0.00	13.86	8	0	1	0
	Fifth plane	*N/A*	−12.00	6.93	8	−cos(30°)	0.5	0
	Sixth plane	*N/A*	−12.00	−6.93	8	−cos(30°)	−0.5	0
HX2	First plane	*N/A*	−18.43	13.43	8	0.5	−cos(30°)	0
	Second plane	*N/A*	−11.50	25.43	8	1	0	0
	Third plane	*N/A*	−18.43	37.43	8	0.5	cos(30°)	0
	Fourth plane	*N/A*	−32.28	37.43	8	−0.5	cos(30°)	0
	Fifth plane	*N/A*	−39.21	25.43	8	−1	0	0
	Sixth plane	*N/A*	−32.28	13.43	8	−0.5	−cos(30°)	0
CC1	Largest cylinder	24	0	0	8	0	0	1
	Second largest cylinder	16	0	0	0	0	0	1
	Third largest cylinder	8	0	0	0	0	0	1
	Smallest cylinder	4	0	0	8	0	0	1
CC2	Largest cylinder	24	−24.49	18	0	0	0	1
	Second largest cylinder	16	−24.49	18	8	0	0	1
	Third largest cylinder	8	−24.49	18	8	0	0	1
	Smallest cylinder	4	−24.49	18	0	0	0	1
TC1	Convex cone	24	21.36	−24.38	0	0	0	1
	Concave cone	12	21.36	−24.38	16	0	0	−1
TC2	Concave cone	24	−9.34	−34.67	16	0	0	−1
TC3	Convex cone	12	−2.53	24.86	0	0	0	1
SP	Convex sphere	24	−30.84	−10.3	0	0	0	0
	Concave sphere	24	−24.34	−21.56	13	0	0	0

* the positions of all elements are based on a local origin defined as the center of CC1 for the xy-plane and the top of the base plate in the z-direction. The position of a plane is defined by its center point.

2.3. Build Layout

The build layout is designed to reduce the required number of builds to conduct the experiment while ensuring acceptable validity. With this in mind, the experiment was designed in three phases as follows:

1. Build space segmentation to define fixed positions for specimens in the build space;
2. Part location assignment to ensure best validity and repeatability of results; and
3. Controlling slice distribution to improve temperature distribution and reduce the risk of failure.

2.3.1. Build Space Segmentation

The build space is first segmented to allow re-orientation of all specimens without violating the required distance between parts. The segmentation serves to define fixed positions in the build space to facilitate comparisons between the different positions and builds in the experiment as this is a known source of variation. This experiment is conducted on an EOSINT P395 with a build volume of 340 × 340 × 620 mm. Due to temperature gradients along the edges of the build envelope, it is recommended to keep a safe distance of 20 mm to the edge, effectively reducing the available build space to a 300 × 300 mm square in the xy-plane. Similarly, it is advisable to keep a certain distance to the bottom of the build space to allow the environment to stabilize (both in terms of temperature and power distribution) before the sintering begins. For this experiment, a safe distance of 6 mm was applied.

To avoid cross-contamination between specimens in the same build, all specimens should be located at a safe distance from each other. For this experiment, a 10 mm safe zone is considered around all specimens in all directions. The test artifact is designed to fit a grid of three by three specimens in any orientation without violating the safe zone. The first step of build space segmentation is presented as two 2D-projections with a top view in Figure 3a and a front view in Figure 3b. The green discs represent the area potentially occupied by specimens, and red rings encapsulating each disc represent the safe zone. Additionally, the red square frame demarks the safe distance from the edges of the build envelope. The coordinates in the figure are center coordinate components relative to the machine coordinate system [37]. The positions are defined based on the center point at (170, 170), from which the remaining positions are located at the extremes of (170 ± 100, 170 ± 100), i.e., an orthogonal grid with 100 mm distance from center to center. This grid is repeated five times in the z-direction, as illustrated in Figure 3b, yielding a total of 45 defined positions in the build space. These positions may formally be described by three components $\{i, j, k\}$ where $i \in \{1, 2, 3\}$, $j \in \{1, 2, 3\}$ and $k \in \{1, 2, \ldots, 5\}$. The five layers in the z-direction are distributed to account for the required safe distance and adjusted to the closest multiple of the layer thickness (120 µm), resulting in a distance of 99.72 mm from center to center. The lowest center point is determined by finding the lowest viable position that does not violate the 6 mm safe distance from the bottom and then rounding up to the closest multiple of the layer thickness.

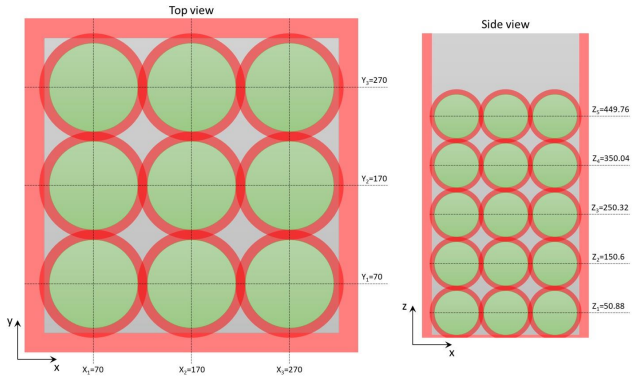

(**a**) (**b**)

Figure 3. The first step of build space segmentation. (**a**) The build space as seen from the top; (**b**) the build space as seen from the front of the machine.

2.3.2. Part Location Assignment

To mitigate systematic errors arising from the position in the build chamber, each specimen is randomly assigned to one of the defined locations in the build space. However, because 45 positions are defined for each build, and only 37 specimens should be produced, a plan must be derived for the remaining eight positions. First, the positions cannot be left open because this could disturb the temperature distribution throughout the build; hence something should be produced in all 45 positions. To ensure that an equal amount of energy is applied to all positions, the same specimen will, therefore, be used to fill this space. Furthermore, these specimens shall not be part of the main study, and they should, therefore, be differentiated from the main group somehow, and it was decided to make the part build orientation 270 degrees about the x-axis—an orientation outside the scope of the main study, while still being somewhat comparable. This allows using these specimen as a control group to further facilitate comparative analyses across builds and positions. In order to keep the variation between the specimens to a minimum, the superfluous positions were restricted to eight defined positions in the build space to be duplicated in all three builds. The rear-center position at (170, 270) for all z-layers was selected because of the assumed similarity to the front-center position (170, 70) and also had the benefit of not being first or last relative to the recoater for any layer. The final three positions excluded from the main study are located in the front-right corner at z-layers 1, 3, and 5. These positions should be similar to the other corners and are evenly distributed along the z-layers to provide evenly distributed data points along this dimension of the build space. The specimens produced at eight extra positions are referred to as "anchor" specimens inspired by their function as fixed data points in the experiment design.

The randomization was conducted in Microsoft Excel by applying the RAND function to assign a floating-point number in the range of [0, 1) to every orientation and then sorting the list with respect to the random number. The list of orientations was then aligned with the list of available positions in the build space, effectively using the list index to determine the position in the build according to the numbering of Figure 4. The assignment of orientations to positions is available in Table A1 in the Appendix A.

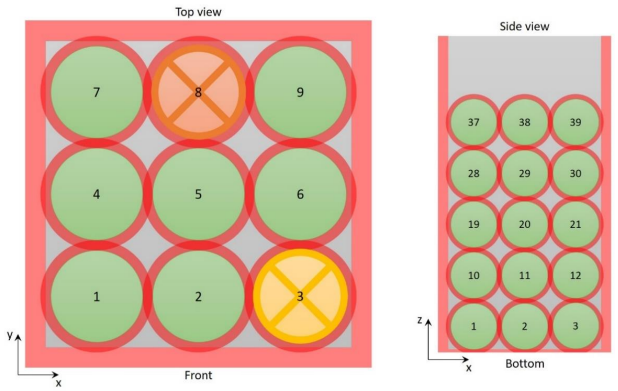

(**a**) (**b**)

Figure 4. Numbered positions for the specimens and the positions of the "anchor" specimens. (**a**) The bottom layer of specimens numbered 1 through 9. Position 3 is reserved anchor specimens for z-layers 1, 3, and 5, while position 8 is reserved anchor specimens for all z-layers; (**b**) a front view showing the first three numbers of each layer (the front row).

The build layout was prepared in the software Materialise Magics 23.01, where the artifact design was imported as a binary STL file, and the mass labeling-function was utilized to create 45 duplicates with the appropriate labeling as displayed in Figure 5. The labeled models were translated to their predetermined position in accordance with the build space segmentation by center coordinates (note that Magics defines the center point of a part as the geometric center of the bounding box). Finally, the models are reoriented into their predetermined part build orientation by counterclockwise rotation about the x-axis.

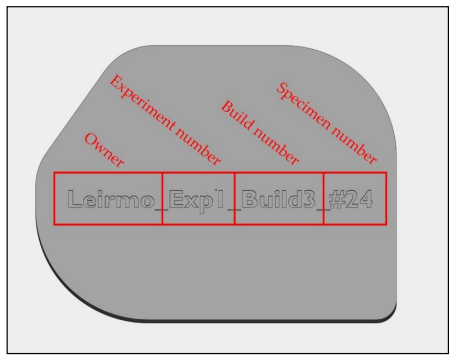

Figure 5. Illustration of the labeling scheme applied in the experiment. The writing is imprinted and embedded in the stereolithography (STL) file during layout preparation in Magics 23.01.

2.3.3. Controlling Slice Distribution

To minimize the risk of machine failure, it is generally recommended to achieve relatively smooth transitions between layers in terms of energy density, i.e., the amount of energy applied to one layer should not deviate too much from the amount of energy applied to the adjacent layers. In practice, this means that parts should preferably be evenly distributed along the build direction or optimally have a uniform intersection area. The cross-sectional area of slices at user-defined intervals can be exported from Magics as an Excel file, effectively yielding the sintered area of each layer. The slice distribution achieved from inserting the specimens of build 1 from Table A1 into the build space yields the graph in Figure 6a, which exhibits large portions without any energy input. These portions without energy input originate from the safe distance between specimens in the z-direction and cannot be eliminated without the introduction of additional specimens. This is demonstrated in Figure 6b, which shows the slice distribution for spheres of 90 mm diameter inserted at the positions of the specimens.

While Figure 6 displays some minor gaps in the slice distribution, the actual layouts of the three builds would be significantly worse because the true geometry of the artifact is much more complex than a perfect sphere, leading to large portions in z-direction without any energy input at all. To counteract the risk associated with the energy fluctuations, one could either change the previously determined positions, or objects could be added to the low-energy volumes to even out the slice distribution. The second option enables additional information to be collected from the experiment by adding useful objects to the unused volumes marked in green in Figure 7.

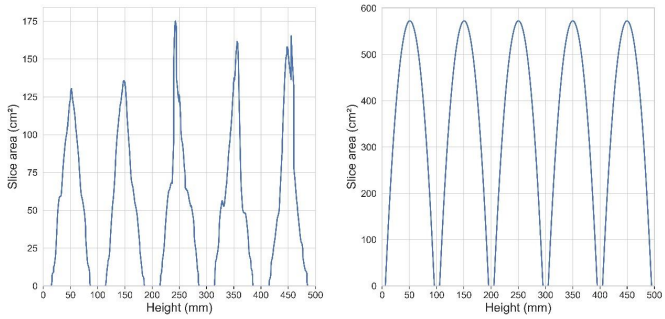

(**a**) (**b**)

Figure 6. Slice distribution graphs showing the sintered area per layer. (**a**) Slice distribution for build 1 without additional specimens; (**b**) slice distribution for perfect spheres of 90 mm diameter in all positions.

The object inserted in the additional space should be massive enough to significantly contribute to an even slice distribution but also provide additional information that contributes to the validity and reliability of the experiment. The recently developed standard for test artifacts in additive manufacturing ISO/ASTM 52902:2019 [38] provides several candidates in STEP format. The circular artifact CA_F (Figure 8) was selected due to its appropriate size, volume, and feature type. The model was loaded to SolidWorks, exported as a binary STL file, and later duplicated and reoriented in Magics.

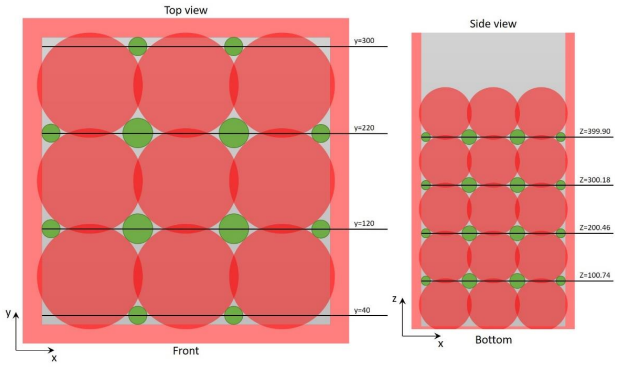

(**a**) (**b**)

Figure 7. Open volumes available to even out the slice distribution. (**a**) Top view of available spaces in the xy-plane; (**b**) front view of the available spaces along the z-axis.

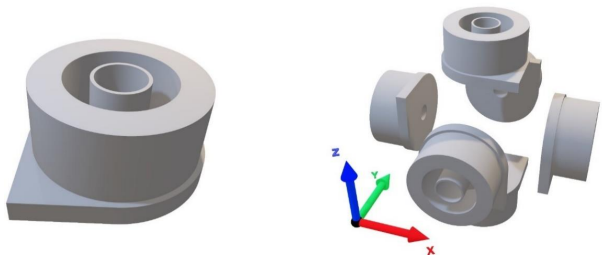

(**a**) (**b**)

Figure 8. Cylindrical test artifact CA_F collected from ISO/ASTM 52902:2019(E). (**a**) 3D-model; (**b**) constellation of six samples in orthogonal orientations.

With reference to Figure 7, the green areas on the edges of the build volume fit one sample of CA_F each. Therefore, these volumes are used to investigate the effect of the laser angle (as opposed to the build direction), which is shown to be a decisive factor for surface roughness in LB-PBF/M [39]. On each side of the build space, one sample is fabricated with the cylinder orthogonal to the layers, and one sample is adjusted, so the axis of the cylinder points directly towards the laser origin (the last deflection point, i.e., the last mirror before the laser beam enters the build volume). For any point on the powder bed, the laser angle ξ can be expressed as:

$$\xi = \cos^{-1}\left(\frac{\vec{p}\cdot\vec{l}}{\|\vec{p}\|\cdot\|\vec{l}\|}\right) \quad (1)$$

where $\vec{p}$ is the vector from the center of the powder bed to the point, $\vec{l}$ is the vector from the laser origin to the point, and $\|\vec{p}\|$ and $\|\vec{l}\|$ are the magnitudes of the respective vectors. This adjustment assumes that the last mirror is installed 600 mm above the powder bed and precisely in the center, ultimately adjusting the orientation by 13.1 degrees. Table 3 tabulates the positions and re-orientations.

Table 3. Location and re-orientation of specimen CA_F at edge positions. Rotations A and B signify the counterclockwise rotation about the x- and y-axis, respectively.

Center x	Center y	Rotation A	Rotation B
120	40	−12.2251	4.763642
220	40	0	0
300	120	−4.76364	−12.2251
300	220	0	0
220	300	12.22512	−4.76364
120	300	0	0
40	220	4.763642	12.22512
40	120	0	0

The four empty volumes indicated by green circles in the interior of the build space in Figure 7 are large enough to fit six samples of CA_F pointing in six orthogonal directions each. All specimens of the constellation are located 26.5 mm away from a shared center point to uphold the 10 mm safe zone. This setup is demonstrated in Figure 8b and allows for the investigation of the variations across the build space and between the different builds for a limited number of orientations. This constellation is inserted three of the four volumes, leaving the fourth spot available for a hollow box used to collect powder samples from inside the build. The position of the box is rotated counterclockwise by one-step for each part layer, as displayed in Figure 9.

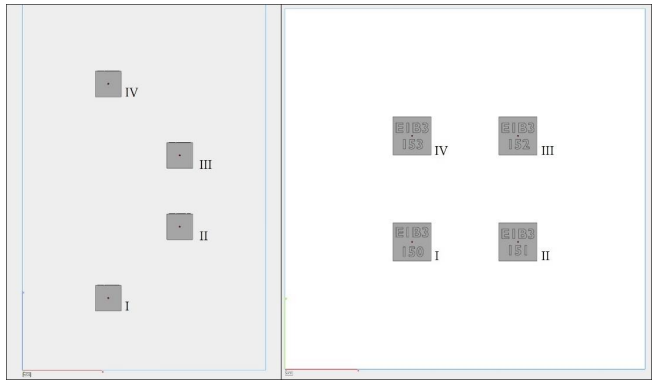

(**a**) (**b**)

Figure 9. Locations for powder sample boxes. Roman numerals (I–IV) indicate the positions of specimens 150–153. (**a**) Front view; (**b**) top view showing the labeling of the boxes.

However, the design and constellations are not dense enough to have much of an impact on the slice distribution; hence, yet another artifact was introduced to the layout.

At this point, the only viable spaces left in the build volume are the corners of Figure 7, i.e., each of the five layers of main specimens. In order to maximize the utility of the space, an artifact was designed in Microsoft 3D Builder based on the shape of the available volume. This design had the potential to add further value to the experiment, and shapes were, therefore, added to the planar faces of the workpiece. First, the linear artifact LA from ISO/ASTM 52902:2019 [38] is imported and used as a pattern to create imprints in the design. The pattern leaves notches in the back of the specimen of certain intervals along all three axes and allows for measuring the dimensional accuracy on the corners of the build envelope. The remaining area was utilized to add cylinders of 8 and 15 mm in diameter, completing the design in Figure 10. These specimens are inserted at the four z-levels indicated in Figure 7 with four specimens on each level—one in each corner rotated, so the large planar surfaces are parallel with the walls of the build chamber, only leaving the safe distance of 20 mm.

The final layout includes a total of 169 specimens per build: 45 replications of the main specimen, of which 37 replicates are part of the main study and the remaining eight are anchor specimens, 104 replicates of CA_F, of which 72 are part of constellations, and 32 replicates are located along the edges of the build space, 16 duplicates of the corner artifacts and four hollow boxes for powder samples. When the layout design was completed, the Magics "fix" function was utilized to automatically detect and repair STL file errors, such as inverted normals, holes, and intersecting triangles. The slice distributions of all three builds after insertion of the additional parts are shown in Figure 11, the labeling scheme for the additional parts is displayed in Figure 12, and the three builds are displayed in Figure 13.

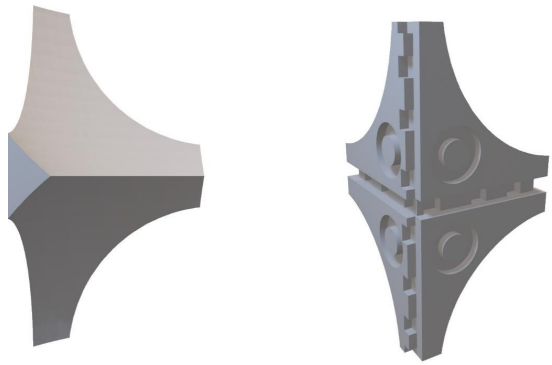

(**a**) (**b**)

Figure 10. Artifact designed for the corners of the build space to even out the slice distribution. (**a**) Spherical surfaces towards the interior of the build space; (**b**) flat surfaces towards the exterior.

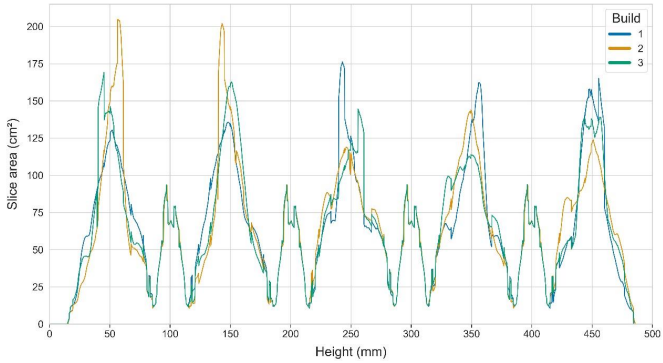

Figure 11. Slice distribution for all three builds.

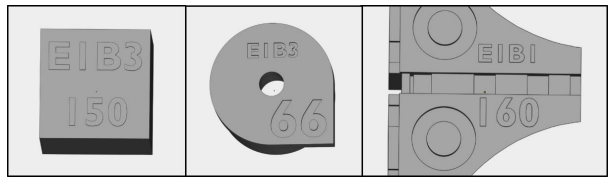

Figure 12. Labeling of additional models where "E1B3" signifies "experiment 1, build 3" and the final number corresponds to the specimen's number in the current build.

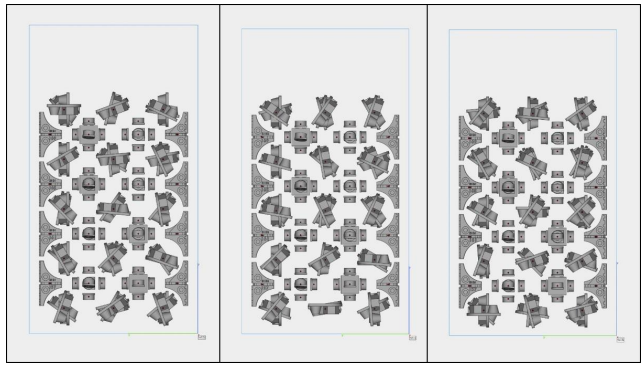

(**a**) (**b**) (**c**)

Figure 13. Build layout in Magics 23.01 for all three builds as seen from the left. (**a**) Build 1; (**b**) build 2; (**c**) build 3.

2.4. Build Process

The specimens were manufactured through three runs with an EOSINT P395 situated at AddLab at NTNU in Gjøvik. The layout described in Section 2.3 was exported to the EOS process software (PSW), where the parameter profile "balanced" was selected with a layer thickness of 120 µm as a typical tradeoff between build time and quality. The powder bins were filled with EOS powder PA2200 (PA12). All virgin powder originated from the same batch, and the machine was fed with a 50/50 blend of virgin and recycled powder. The specifics are summarized in Table 4. The build cycle took roughly 36 h to complete and needed another 36 h to cool before the part cake could be extracted. All specimens were removed from the part cake by hand before pressurized air was used to remove excess powder. After treatment, the specimens are stored in a container in the posttreatment facility to ensure minimum environmental influence.

Table 4. Build process specifications.

Parameter	Value
Machine manufacturer	EOS GmbH—Electro Optical Systems
Machine model	EOSINT P395
Parameter profile	Balanced
Layer height	120 µm
Hatch distance	0.3 mm
Build chamber temperature	180 °C
Material	PA2200 (PA12)
Bulk density	>0.430 *
Mean grain size	d50 = 58 * d10 = 40 * d90 = 90 *
Material blend	50% recycled

* from the material datasheet.

2.5. Data Collection

This section describes the data collection related to the main study and, therefore, only considers the main specimen while the additional specimens are left for future work. For maximum precision, the specimens were inspected with a Zeiss DuraMax CMM with a measurement accuracy of 2.9 µm + L/200 at 18–30 °C where L is the measurement length in mm. A fixture was designed and 3D-printed to automate the inspection, ensure specimens were measured under the same conditions, and make the changeover from one specimen to the next as simple as possible. The fixture was printed with PLA using a Prusa MK2.5 fused-filament fabrication (FFF) printer with a layer thickness of 0.1 mm. The fixture makes use of a small bolt to secure the specimen against the opposite corner, and the force is carefully exerted on the specimen to avoid deflection, which could influence the results. The fixture was tested with a prototype of the specimen 3D-printed with PLA filament prior to the fabrication of the actual test specimens. This preliminary test displayed negligible deflection when the bolt was tightened by hand and was, therefore, considered appropriate for the current experiment. This decision is further substantiated by the material properties as PLA is significantly more flexible than PA12 and, therefore, more prone to deflection. Figure 14 shows the CAD-design of the fixture (a) and the fixture with the prototype in place (b). The two ears allow the fixture to be bolted to the measurement table with M10 bolts.

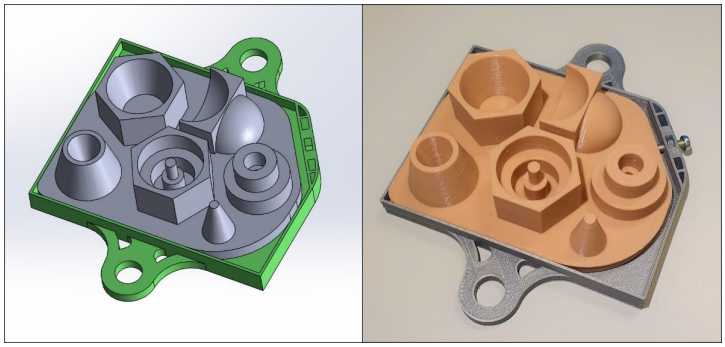

(**a**) (**b**)

Figure 14. Fixture design for test artifact. (**a**) Assembled CAD-drawing. (**b**) The fixture with a prototype of the test artifact in place.

2.5.1. Establishing a Base Alignment

Before the measurement can start, an inspection plan must be devised and programmed. This step was completed at the CMM with the accompanying computer running the Zeiss proprietary software Calypso 6.6. The CAD-model is first imported as a STEP file for efficient feature extraction before a base alignment is established to determine the position and rotation of the specimen in space. The base alignment is necessary to teach the CMM where the specimen is located so that it can continue an inspection in automatic mode. In fact, the base alignment lay the foundation for all machine movement in CNC-mode, potentially causing the probe to crash if not correctly defined. The base alignment is typically determined based on the part function and/or the production method using the so-called 3–2–1 principle where a plane (defined by a minimum of three points), a line (minimum two points), and a point is used to define the spatial translation and rotation of a part. However, because the test artifact has no real purpose and the nature of the process inaccuracies are unknown, the following considerations are made regarding which features to utilize: (i) the features should be contained within a single surface/element (i.e., a line stretching across several planes are not recommended); (ii) the features should be located close to the center of the part to counter dimensional accuracies; and (iii) planar features are preferred because they are generally easier to clean and residual powder is more easily detectable. Consequently, the base plate was selected as the plane for base alignment and also defined the origin for the z-axis, a line is drawn on the second plane of HX2, which also defines the origin for the x-axis, and finally, a point is taken on the fourth plane of HX1, which also defines the origin for the y-axis. Figure 15 illustrates the probing points used for the manual alignment conducted at the beginning of every inspection. Because this is a manual task, variation is inevitable, and the red discs of Figure 15 differ in size to reflect the area available for the manual probing. After the manual alignment, the CMM switches to CNC-mode and repeats the alignment before the inspection is automatically completed.

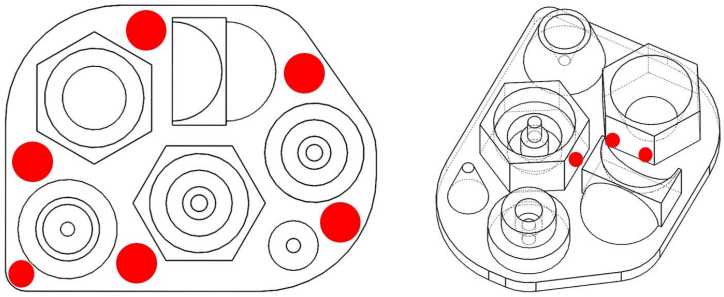

(**a**) (**b**)

Figure 15. Manual probing points for base alignment are indicated with red areas. (**a**) Top view of points on the base plate; (**b**) a perspective view showing points on HX1 and HX2.

2.5.2. Defining the Inspection Strategy

When the base alignment is established, the features of interest may be extracted from the CAD-model to define tolerance characteristics and determine inspection strategies. The entire inspection is conducted with a single stylus of 3 mm diameter, effectively filtering out surface roughness and other minor surface imperfections. The inspection makes use of scanning strategies where the stylus tip is dragged along the surface while taking points at a high-frequency without compromising the accuracy. This allows a high number of points to be registered, which increases the resolution of the measurements and, therefore, also the reliability of the results. Furthermore, the path of the stylus is designed to cross the build layers of the specimen regardless of part build orientation, which enables detection of defects arising from the layered nature of LB-PBF and is of particular importance for the current experiment. Among all the points collected from a scanned surface, the first points are disregarded to safeguard against inertia and any lingering vibrations. Consequently, it is preferred to inspect each feature with a single undisrupted path covering the largest possible surface area. Naturally, a tradeoff must be made between execution time and the accuracy/resolution of the inspection. For continuity, all features belonging to the same group are treated equally with regards to the stylus path, even though the number of points or the measurement speed must be corrected to make up for the dimensional differences.

The base plate is inspected by a single path starting in the bottom left corner, moving along the edge in a counterclockwise manner, as displayed in Figure 16. When returning to the start point, the path trails off towards the interior of the specimen to make sure any warping towards the middle is included in the base alignment for, which this feature is crucial. Next, the line on HX2_Plane2 is repeated as a scanned line before the point on HX1_Plane4 concludes the CMM's confirmation of the base alignment.

The cylinders are inspected with a helical scanning path starting at the base of convex cylinders (top of concave cylinders) at the extreme point in the x-direction, moving counterclockwise in 3 revolutions before reaching the other end, as shown in Figure 17a. The spheres are inspected by three lateral paths at 15, 45, and 75 degrees from the horizontal, as illustrated in Figure 17b, and the cones are inspected by helical paths in the same way as cylinders (Figure 17c). Finally, the planes are inspected by a continuous path, as illustrated in Figure 17d, where three square paths are connected and inspected as one.

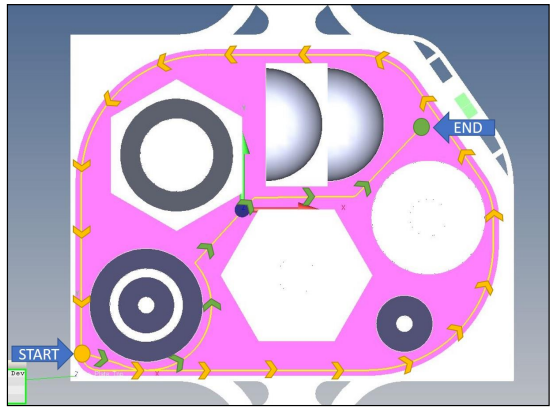

Figure 16. Inspection strategy for the base plate. A single path follows the edge of the base plate before trailing off towards the interior.

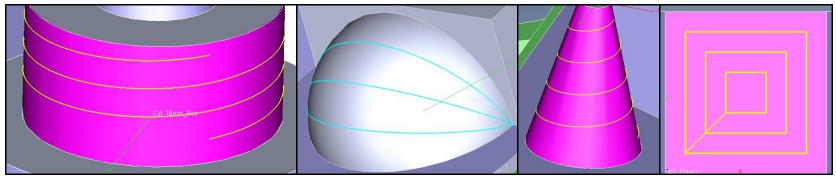

(**a**) (**b**) (**c**) (**d**)

Figure 17. Illustrations of inspection paths for the different geometries. (**a**) Helical inspection path for cylinders; (**b**) three lateral paths for spheres; (**c**) a helical path for cones; (**d**) a single continuous path for planes.

2.5.3. Defining Characteristics

When all features are extracted and assigned an inspection strategy, the characteristics must be defined for the software to calculate the results and generate reports. The flatness of all planes in HX1 and HX2 is calculated, and a pairwise comparison is conducted to check parallelism and distance between opposing planes, i.e., plane 1 vs. plane 4, plane 2 vs. plane 5, and plane 3 vs. plane 6. For the cylinders, the cylindricity is calculated along with diameter and position. Additionally, pairwise comparison is done to check coaxiality between stacked cylinders, e.g., the convex 24 mm cylinder is compared with the 16 mm convex cylinder on top, and the convex 4 mm cylinder is compared to the 8 mm convex cylinder below it. The cones are checked for position, apex angle, and diameter at three altitudes. Unfortunately, the measurement strategy was ineffective in measuring apex angle and diameter, and the calculated results appear to be overfitted. The spherical shape features are assigned roundness characteristics along with diameter for each of the inspection paths. Moreover, a position is calculated (based on the estimated center of the sphere), and a profile characteristic is assigned. An overview is tabulated in Table 5, along with the scheme used for naming the characteristics.

Table 5. Characteristics with accompanying naming scheme.

Groups	Characteristic	Characteristic Name
HX1 HX2	Flatness	Flatness_<Group>_Plane<#> [1,2]
	Parallelism	Parallelism_<Group>_<#a>-<#b> [1,2,3]
	Distance	Dist_<Group>_<#a>-<#b> [1,2,3]
CC1 CC2	Cylindricity	Cylindricity_Cyl_<dimension>_<curvature> [4,5]
	Diameter	Diameter_Cyl_<dimension>_<curvature> [4,5]
	Coaxiality	Coaxiality_<Group>_<dim-a>-<dim-a> [1,3,5]
	Position	Position_Cyl_<dimension>_<curvature> [4,5]
TC1 TC2 TC3	Position	Position_Cone_<dimension>_<curvature> [4,5]
	Apex angle	Cone_Angle_<dimension>_<curvature> [4,5]
	Diameter	Diameter_Cone_<dimension>_<curvature>_<altitude> [4,5,6]
SP	Roundness	Roundness_SP_<curvature>_<altitude> [5,6]
	Position	Position_SP_<curvature> [5]
	Profile	Profile_SP_<curvature> [5]
	Diameter	Diameter_SP_<curvature>_<altitude> [5,6]

[1] <Group> is the group ID, e.g., "HX1"; [2] <#> is the plane number, e.g., "Plane1"; [3] <a> and <b> refer to the first and last feature in a comparison, respectively; [4] <dimension> and <dim> both refer to the dimension of the feature, e.g., "4 mm" (NB! no space); [5] <curvature> is either "Pos" for convex or "Neg" for concave; [6] <altitude> is "Low", "Mid" or "Hi"/"Top" where measurements are available at different levels.

2.5.4. Conducting the Inspection

The inspection is initialized from the computer, and a unique name is created for each inspection in accordance with the unique name of the specimen under consideration. All inspections are repeated three times, including the fixing and removal of the specimen from the fixture to enable the analysis of any variations that may occur from any manual operations. Even though the fixture ensures that the CMM is aware of the position of the specimen, a manual alignment is still completed at the beginning of the inspection. This because a manual alignment must be done for each specimen to account for variations between specimens, and therefore, this action should also be repeated to enable the analysis of variation arising from manual operations.

When the manual alignment is completed as described in Section 2.5.1., the CMM switches to CNC-mode and repeats the base alignment before continuing to the inspection. One repetition of the inspection took a minimum of 9 min and 20 s. Variations in elapsed time occur when deviations from nominal geometry cause the measurement to be executed with wrong measurement pressure, causing the CNC to repeat the measurement with adjusted parameters to account for the inaccuracy. This adjustment includes changing the measurement speed and thereby prolonging the inspection considerably, as outlined in Table 6. Moreover, a safety feature requires a restart of the entire inspection if the stylus collides with an obstruction. Due to the small dimensions of the smallest concave cylinder, this blind hole is difficult to properly clean and caused the inspection to fail at this shape feature multiple times. Measures were taken to secure the completion of future inspections by mechanically removing the residual powder from this hole, but this, unfortunately, renders all results from this cylinder invalid. The machine stops are not considered in Table 6 as the timer also was reset in these instances.

Every inspection is finalized by calculations of all defined features and characteristics, and a report is generated for the operator. The results are stored in a database queried by another proprietary software called PiWeb reporting that visualizes the results and offers a simple analysis of the results.

Table 6. A statistical overview of elapsed inspection time for successful inspections.

Statistic	Elapsed Time (mm:ss)
Minimum	09:20
Median	10:25
Average	11:42
Standard deviation	02:41
Maximum	18:15

2.6. Data Analysis

This paper briefly reports on a preliminary high-level analysis whose purpose is to investigate the variation between the different blocks of the experiment. It is crucial for the validity of the experiment that the variation between the different blocks can be characterized and attributed to natural variation. This analysis is conducted in Python 3 utilizing SciPy, Numpy, and Pandas and visualized with Matplotlib and Seaborn in a Jupyter Notebook environment. The source code is available in the online repository together with the data and all relevant documentation.

The brief analysis described herein considers the results for diameter, cylindricity, and flatness. When a feature is measured by a series of points, the location of the actual surface is estimated by least-squares approximation. The diameter is hence a measure of this estimated surface, and the cylindricity is the difference between the largest positive and negative deviation from the estimated surface. Similarly, flatness is defined as the difference between the largest positive and negative deviations from the estimated plane.

3. Results

While the database contains the information on every single measurement point, the data extracted from the database are restricted to the aggregate measures defined for each characteristic, such as flatness, cylindricity, etc. All data were exported as a 257 kB comma-separated values (CSV) file for each specimen and is freely available online. The following subsections provide a brief description of the data in terms of what data are available and further perform a brief analysis of the results to characterize variation within and between a selection of variables.

3.1. Contents of CSV Files

All files are exported with the same parameters, yielding a table with the same 52 columns for all specimens, although many of these are not in use. The columns of interest are outlined in Table 7.

Table 7. Column descriptions for comma-separated values (CSV) files.

Column Name	Format	Description
Uuid	64 hexadecimals + separators	A unique ID for each measurement
Characteristic	String	The name of the characteristic
K1 measured value	Floating-point number	The measured value
K4 time/date	mm/dd/yyyy hh:mm:ss AM/PM	Time and date the inspection was completed
K14 part ident	Integer	Repetition number *
K53 order number	String	The name of the specimen
K2001 characteristic number	Integer	Integer ID for characteristic
K2101 nominal value	Floating-point number	The nominal value
K2540 direction X	Floating-point number	x-component of the normal vector
K2541 direction Y	Floating-point number	y-component of the normal vector
K2542 direction Z	Floating-point number	z-component of the normal vector
K2543 position X	Floating-point number	x-component of the position
K2544 position Y	Floating-point number	y-component of the position
K2545 position Z	Floating-point number	z-component of the position

* measurements are repeated three times. The column "K53 order number" designates, which repetition the measurement represents.

3.2. Variation between Repeated Measurements

The entire inspection was repeated three times for each specimen, which enables a characterization of the variation of measurements and, therefore, the reliability of measurements. The three repeated inspections were conducted in sequence and included the mounting and demounting of the specimen in the fixture, hence enabling the analysis of this variation in the study. In addition to the natural random variations of the measurement setup, the experiment is also prone to variations arising from the minuscule deviations from one mounting in the CMM to the next, effectively offsetting the inspection path. Figure 18 plots the three repeated inspections of HX1_Plane1 from specimen #6 from build 3 (Build3_#6_HX1_Plane1). Some minor variations are apparent in the figure, and even though the measured surface topology is close to identical, the minor deviations give rise to the three measured error values 0.062, 0.058, and 0.059 mm, respectively.

The preliminary analysis indicates that there is indeed some variation between repeated measurements as introduced in Figure 18 and further detailed in Table 8. This preliminary analysis considers the measurements of cylindricity, diameter, and flatness of all the relevant features except for the 4mm concave cylinder omitted due to residual powder not removable by pressurized air. With 7 cylindricity-, 7 diameter- and 12 flatness measurements for all 135 specimens, we obtain a total of 3510 data points for each repeated inspection. To analyze the variation between measurements, we compute the mean value of the three repeated measurements and—more importantly—the difference between the highest and the lowest value among the repeated measurements (Δ). The characteristics of this data set are described in Table 8, where Rep 1–3 corresponds to the measured error of the first, second and third repeated inspections, respectively, Rep Mean is the mean value of the three repeated measurements and Δ is the difference between the highest and lowest measured error. The negative values originate from deviations where the measured diameters are smaller than the nominal values. Form errors (i.e., cylindricity and flatness) may only take positive values since this is the distance between the most extreme positive and negative deviations from a perfect geometry.

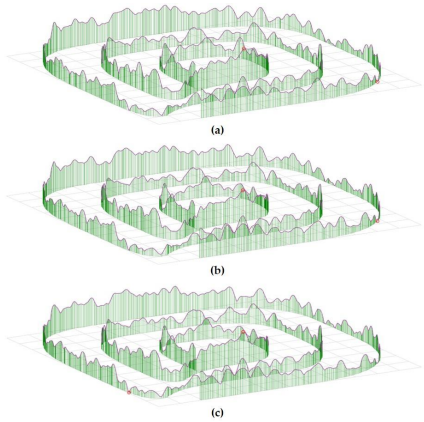

Figure 18. Plotted results for three repeated inspections for the flatness of Build3_#6_HX1_Plane1 of scale 500:1. Maximum and minimum points for each plot are highlighted with red circles. (**a**) 1st inspection: 0.062 mm; (**b**) 2nd inspection: 0.058 mm; (**c**) 3rd inspection: 0.059 mm.

Table 8. Aggregated data for repeated measurements.

	Rep 1	Rep 2	Rep 3	Rep Mean	Δ
n	3510	3510	3510	–	–
$\bar{x}$	0.088577	0.084998	0.083011	0.085529	0.008634
σ	0.122123	0.118936	0.117179	0.119282	0.011865
Min	−0.544659	−0.540020	−0.537463	−0.540714	0.000022
25%	0.068541	0.066567	0.065653	0.066977	0.002682
50%	0.090128	0.087218	0.086086	0.087838	0.005521
75%	0.132110	0.127516	0.124374	0.127606	0.009823
Max	0.626687	0.576267	0.542467	0.559931	0.256032

Table 8 reveals a general declining trend in measured error through the repeated inspections, which can be explained by the removal of some residual powder during and between the inspections. This effect may be amplified by the fact that the probe is following the same path and might leave a trail or a slight indentation on the surface. Figure 19 contains a scatterplot where Δ is plotted for the different characteristics, and outliers are clearly visible. These outliers contribute to a higher variance, which makes unfiltered data difficult to analyze graphically; hence, Figure 19b only includes the data points below five standard deviations (5σ). The width of the groups reflects the number of points.

The plots of Figure 19 show a high-density of points close to zero, which indicates that the observed variations do not follow a normal distribution but rather a lognormal distribution where a higher density is observed close to zero. Figure 20 briefly explores this observation by fitting a lognormal distribution to the data and comparing this to normalized histograms of the distributions. These plots do indeed indicate that the distribution roughly follows a lognormal distribution where the measurements of diameter stand out as slightly less repeatable compared to the distributions of flatness and cylindricity. This discrepancy may be explained by the diameter being estimated by the least-squares method and hence consider all the measured values, while the geometric errors of flatness and cylindricity are solely dependent on the extremes of the measured points.

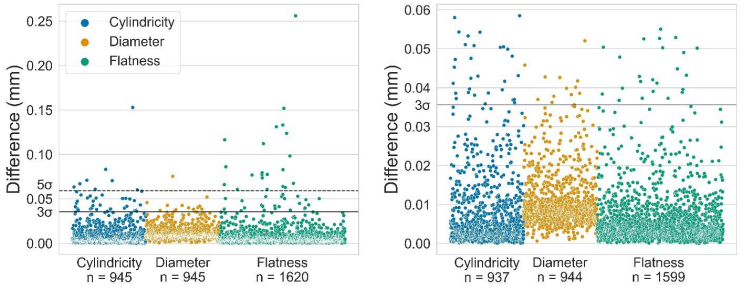

(**a**) (**b**)

Figure 19. Difference between repeated measurements (Δ) of cylindricity, diameter, and flatness. (**a**) Scatterplot, including all data points; (**b**) scatterplot only, including data points within five standard deviations (5σ).

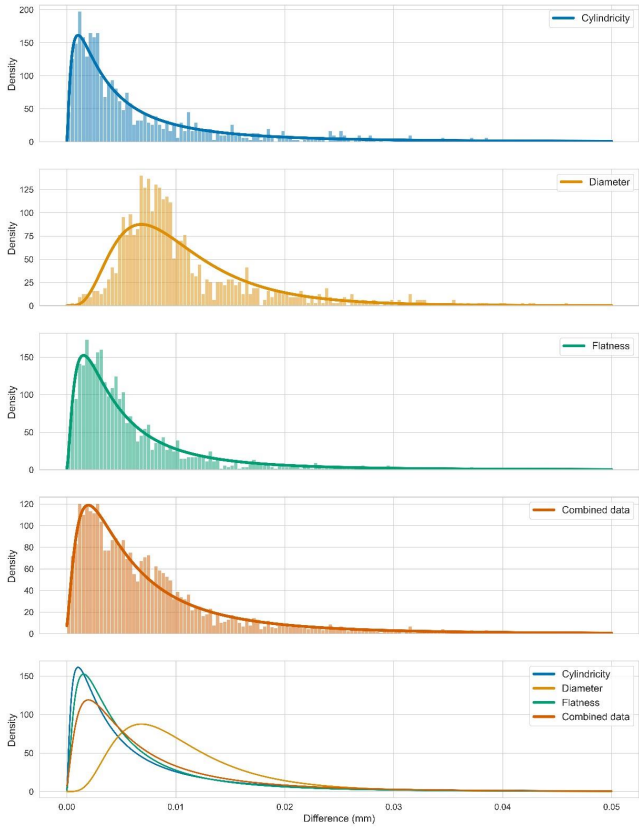

Figure 20. Lognormal probability distributions fitted to the measured data for selected features.

3.3. *Variation between Builds*

The build layout of the experiment enables the comparison of the different builds by inspecting the anchor specimens, which are in the exact same position and orientation for every build. Furthermore, another possibility to compare the builds is provided by the geometry of the artifact and the fact that all specimens are rotated about a single axis, effectively leaving Planes 2 and 5 of HX2 vertical for all orientations. This means that there are comparable data points available for all positions in the build space for all three builds.

Figure 21 display the variation between the three builds when considering the mean value of the three repeated measurements for the vertical planes in all locations in the build space. While some variations are present, the data appears to be quite consistent between builds, with a few outliers disrupting the homogeneity of the distributions. The kernel

density estimation of Figure 21b indicates quite similar distributions between the three builds, again with some influence from outliers. A statistical description is presented in Table 9 for both planes, where the difference is the difference between the minimum and maximum measured flatness error of a plane in the same position in the three builds.

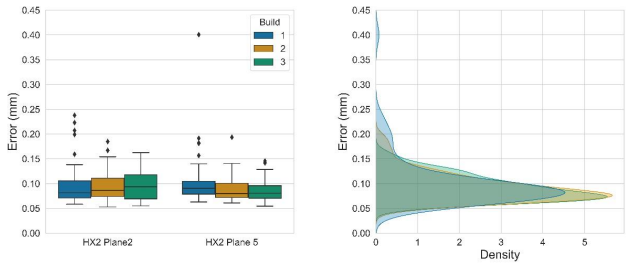

(**a**) (**b**)

Figure 21. Comparison of measured error between builds considering vertical planes. (**a**) A boxplot visualizing the measured flatness error; (**b**) kernel density estimation of the measured values.

Table 9. Statistical description of measured flatness error of planes 2 and 5 from HX2 and the difference between the three builds.

	Build 1	Build 2	Build 3	Mean	Difference
n	90	90	90	–	–
$\bar{x}$	0.100579	0.091916	0.091149	0.094548	0.040117
σ	0.049281	0.028711	0.025326	0.026291	0.040889
Min	0.058330	0.052950	0.054538	0.065753	0.002214
25%	0.074281	0.072488	0.070237	0.075634	0.019272
50%	0.084530	0.083260	0.085130	0.086795	0.027337
75%	0.105167	0.103796	0.107094	0.103580	0.049757
Max	0.400476	0.193571	0.162345	0.211045	0.301388

3.4. Variation between Positions in the Build Chamber

The designed build layout facilitates the comparison of discrete positions in the build chamber in the z-direction as well as in the xy-plane. A slight trend towards tighter tolerances in the higher end of the build may be observed in Figure 22a, but the statistical significance of this trend is inconclusive from the current analysis. Except for one extreme outlier at the lowest level, the distributions among the different z-levels are quite similar, as seen in the kernel density estimation of Figure 22b. The statistical description of the data is tabulated in Table 10, where the columns correspond to the five levels of z-positions, the mean value for all z-levels of a specific position considered across all three builds, and the difference is calculated as the difference between the minimum and the maximum value from the same population.

A more distinct variation may be found within each z-level as the position in the xy-plane appears to be of significant influence on the geometric accuracy and the observed variation. This discrepancy is apparent in all the preliminary analyses but exemplified here by diametrical error due to the clear results for this particular characteristic. When comparing the diametrical error of cylinders fabricated in the front-right corner to the ones fabricated at the rear center, it is clear that the position in the front-right is far more accurate than the rear positions, as shown in Figure 23.

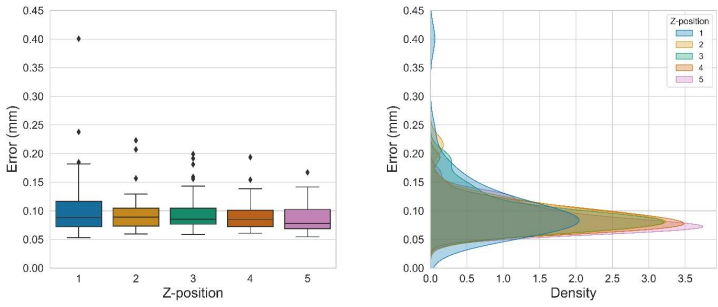

(**a**) (**b**)

Figure 22. Comparison of flatness error at different z-positions in the build chamber. (**a**) Boxplot of all five z-levels; (**b**) kernel density estimations for the levels of z-positions.

Table 10. Statistical description of measured flatness error of planes 2 and 5 from HX2 and the difference between the five z-levels.

	Level 1	Level 2	Level 3	Level 4	Level 5	Mean	Difference
n	54	54	54	54	54	–	–
$\bar{x}$	0.104644	0.093710	0.096776	0.089911	0.087698	0.094548	0.054769
σ	0.055572	0.031782	0.033028	0.025317	0.024961	0.024226	0.050230
Min	0.052950	0.059441	0.058330	0.060803	0.054538	0.063893	0.011309
25%	0.071951	0.073234	0.076536	0.072325	0.068809	0.078640	0.025433
50%	0.088348	0.088711	0.084912	0.084803	0.078242	0.087961	0.041132
75%	0.116436	0.104522	0.104658	0.101218	0.102372	0.110861	0.063584
Max	0.400476	0.222995	0.199056	0.193571	0.167091	0.176043	0.328619

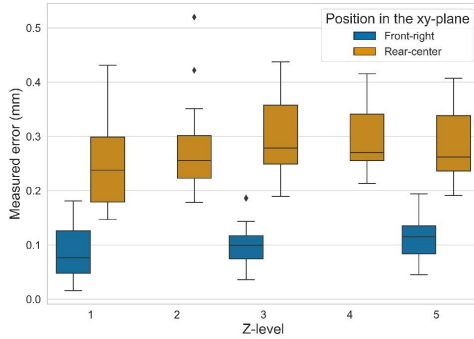

Figure 23. Boxplot for diametrical error for the anchor specimens across all three builds.

Recall that the anchor specimens are only fabricated in the front-right position at layers 1, 3, and 5, hence the gaps in the above observation. A more holistic analysis may be conducted by comparing the vertical planes, i.e., planes 2 and 5 of HX2, which enables the

comparison of all positions in the build space. The boxplot of Figure 24 shows the measured variations considering the specimens' position along the x- and y-axes. While Figure 24a displays quite uniform distribution between the three rows in the x-direction, Figure 24b exhibits a rather clear discrepancy in the third position, i.e., the rear of the build chamber.

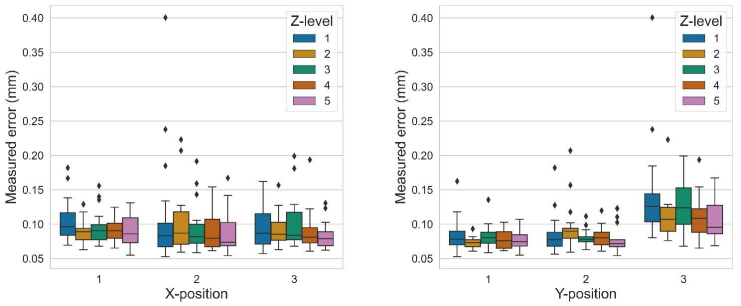

Figure 24. Boxplot for measured flatness error of vertical planes at different positions. (**a**) The rows along the x-axis at different z-levels; (**b**) the rows along the y-axis at different z-levels.

4. Discussion

The described experiment is designed, planned, and executed to produce repeatable and valid results. By developing a rigid methodology and performing automated data acquisition with a CMM, the obtained data should be of high-quality. At present, however, there are many unknown factors and even a couple of minor discrepancies discovered in the analysis. The following subsections contain declarations of the known discrepancies, as well as the known unknowns, accompanied by a short discussion of the possible consequences of these factors. Finally, a discussion is made on the implications of underlying assumptions and the scope of the current study with possible directions for further work.

4.1. Hitherto Discovered Discrepancies

At the time of publication, all discovered discrepancies are considered minor inconveniences with marginal effect on the validity of the current study. The most noteworthy deviation from the original plan is the issues related to the smallest concave cylinder (CC2), where the residual powder was difficult to remove due to the blind hole. Because the CMM inspection was impaired, the scan strategy for this particular feature was altered, and the remaining powder was removed mechanically effectively, rendering all results related to this feature invalid, including the roundness, cylindricity, and position of this feature as well as its relation to other features (i.e., coaxiality). The problem of residual powder is omnipresent in LB-PBF/P partly due to the material being prone to static electricity, which impedes the proper removal of powder. This study aims at investigating the as-build geometry and, therefore, avoided mechanical removal of powder, which could mitigate the problem of adhering particles but could also damage the surface and obscure the results.

Although a full analysis of the collected data has not yet been conducted, potential issues were observed during the inspections related to cones and spheres as the calculated diameter and apex angle were identical to nominal values. This is obviously not the reality and probably a result of inappropriate inspection strategies and evaluation methods for the features in question. Consequently, the use of these measurements should be used with extra care but does not affect the overall inspection in any way.

Additional discrepancies are limited to naming errors where corner specimens of the third build are labeled as build 1, and inspection results for select characteristics are labeled incorrectly. The mislabeling of the corner specimens has a marginal impact as this error was detected during postprocessing, and the specimens from the three builds are kept separate, thus preventing cross-contamination. Naming errors from the inspections of the main specimens are limited to typographical errors, which may cause some issues in automatic data processing but are easily handled in data preparation when they are known in advance. These naming errors are explicitly disclosed in the online repository.

4.2. External Factors

All experiments are subject to external factors that cannot be controlled. One such factor is the weather conditions that influence the experiment, especially in terms of humidity, which may influence the powder during sintering. Moreover, while the AM machine is situated in a room with thorough climate control, the CMM and the areas between are not subject to the same level of control. Hence, the specimens were stored in the areas of climate control and transported to the CMM in batches to minimize exposure to uncontrolled environments. Weather data for the relevant days are available in the online repository.

Due to restricted access to build parameters, the "Balanced" profile was chosen for the machine settings of the EOSINT P395, which is assumed to constitute a reasonable tradeoff between accuracy and speed. Note that finer settings are available, which could yield more accurate results than what is reported in the present study. However, the goal is not to achieve the best possible results but rather to investigate the influence of other factors (e.g., part build orientation); hence keeping the machine settings constant is sufficient to fulfill the purpose of this study without compromising its validity.

4.3. Implications of Assumptions and Boundaries

The current work assumes that the utilized technologies are able to fabricate and detect the targeted deviations with sufficient accuracy to yield valid results. This is especially relevant for the choice of probe size for the CMM, which acts as a filter for the surface roughness [40]. A probe diameter of 3 mm was selected not only for practical reasons but also to facilitate the analysis of geometric deviation without the noise imposed by surface roughness. A smaller probe could enable the analysis of narrow grooves, thus potentially exposing additional surface variations and defects, while the filtering could still be conducted numerically to enable an analysis of larger variations. Such inspections and analyses could be compared to the collected data but are—for now—left for future work.

The present study was limited to external geometric and dimensional accuracy where the CMM was the measuring instrument of choice. Investigations of surface roughness, mechanical properties, and internal structures are outside the scope of this study and are left for future work. While these areas are the subject of many research efforts, the preliminary results of the current study, as well as results of related research, suggest that the variations between positions in the build space are substantial and cannot be neglected in the design of experiments for LB-PBF/P. Closer examination of these effects in other AM technologies constitutes an avenue of future research—first of all for LB-PBF/M, but perhaps also other powder bed systems.

5. Conclusions

This paper described the design and execution of an elaborate experiment to generate valid and reproducible data on dimensional and geometric accuracy in LB-PBF/P. The following conclusions can be drawn from the analysis:

- The experiment design described herein enabled the analysis and characterization of variation between the different builds and between various positions in the build chamber;

- The variation between the builds appears to be negligible, and the three builds can be compared without loss of validity;
- There is a slight trend of higher accuracy towards the higher levels of the builds (higher z-coordinates), but this trend is not found to be statistically significant;
- The variation in the xy-plane is significant, with considerably larger geometric and dimensional errors towards the rear of the machine. No efforts are made to explain this discrepancy.

The current research warrants further investigations into variation management in LB-PBF and especially the control of noise factors to ensure valid and reliable results in future experiments. The analysis presented in the current paper is merely scraping the surface of the data generated from the experiment, and thorough analysis is left for future work. Moreover, the data enables the development of numerical models for the prediction of geometric and dimensional accuracy. The next step of the current project involves further analysis of the data to construct predictive models for geometric and dimensional accuracy. The additional specimens produced through the described experiment have not been inspected and, therefore, constitute a major source of unrevealed data that can be utilized to further improve the understanding of LB-PBF/P.

Author Contributions: Conceptualization, T.L.L., and O.S.; methodology, T.L.L., and O.S.; formal analysis, T.L.L.; investigation, T.L.L.; data curation, T.L.L.; writing—original draft preparation, T.L.L.; writing—review and editing, O.S.; visualization, T.L.L.; supervision, O.S.; project administration, T.L.L. All authors have read and agreed to the published version of the manuscript.

Funding: This research is funded by the Norwegian Ministry of Research and Education through the PhD-scholarship of Torbjørn Langedahl Leirmo.

Institutional Review Board Statement: Not applicable.

Informed Consent Statement: Not applicable.

Data Availability Statement: Data, artifacts, and all code for analysis are available online through a repository at GitHub: https://github.com/TheThorb/Leirmo_Exp1_Publication1.

Acknowledgments: The authors would like to acknowledge the contributions of Ivanna Baturynska in the planning of the experiment and Pål Erik Endrerud for facilitating the experiment execution.

Conflicts of Interest: The authors declare no conflict of interest.

Abbreviations

3D	Three dimensional
AM	Additive manufacturing
ASCII	American Standard Code for Information Interchange
CAD	Computer-aided design
CMM	Coordinate measuring machine
CNC	Computer numerical control
CSV	Comma-separated values
FFF	Fused-filament fabrication
GD&T	Geometric dimensioning and tolerancing
GPS	Geometric product specifications
LB-PBF	Laser-based powder bed fusion
LB-PBF/M	Laser-based powder bed fusion of metals
LB-PBF/P	Laser-based powder bed fusion of polymers
PA12	Polyamide 12
PBF	Powder bed fusion
PLA	Polylactic acid
SLS	Selective laser sintering
STEP	Standard for the exchange of product model data
STL	Stereolithography (file format)

Appendix A

Table A1. Overview of all defined positions in the build space and the orientation fabricated in each position and for each build. The anchor positions are highlighted for clarity.

Position							Rotation about x-Axis (Degrees)		
Index	Relative			Center Point (mm)			Build 1	Build 2	Build 3
	x	y	z	x	y	z			
1	1	1	1	70	70	50.88	70	70	70
2	2	1	1	170	70	50.88	140	140	140
3	3	1	1	270	70	50.88	−90	−90	−90
4	1	2	1	70	170	50.88	145	145	145
5	2	2	1	170	170	50.88	165	165	165
6	3	2	1	270	170	50.88	120	120	120
7	1	3	1	70	270	50.88	110	110	110
8	2	3	1	170	270	50.88	−90	−90	−90
9	3	3	1	270	270	50.88	35	35	35
10	1	1	2	70	70	150.6	70	70	70
11	2	1	2	170	70	150.6	140	140	140
12	3	1	2	270	70	150.6	−90	−90	−90
13	1	2	2	70	170	150.6	145	145	145
14	2	2	2	170	170	150.6	165	165	165
15	3	2	2	270	170	150.6	120	120	120
16	1	3	2	70	270	150.6	110	110	110
17	2	3	2	170	270	150.6	−90	−90	−90
18	3	3	2	270	270	150.6	35	35	35
19	1	1	3	70	70	250.32	70	70	70
20	2	1	3	170	70	250.32	140	140	140
21	3	1	3	270	70	250.32	−90	−90	−90
22	1	2	3	70	170	250.32	145	145	145
23	2	2	3	170	170	250.32	165	165	165
24	3	2	3	270	170	250.32	120	120	120
25	1	3	3	70	270	250.32	110	110	110
26	2	3	3	170	270	250.32	−90	−90	−90
27	3	3	3	270	270	250.32	35	35	35
28	1	1	4	70	70	350.04	70	70	70
29	2	1	4	170	70	350.04	140	140	140
30	3	1	4	270	70	350.04	−90	−90	−90
31	1	2	4	70	170	350.04	145	145	145
32	2	2	4	170	170	350.04	165	165	165
33	3	2	4	270	170	350.04	120	120	120
34	1	3	4	70	270	350.04	110	110	110
35	2	3	4	170	270	350.04	−90	−90	−90
36	3	3	4	270	270	350.04	35	35	35
37	1	1	5	70	70	449.76	70	70	70
38	2	1	5	170	70	449.76	140	140	140
39	3	1	5	270	70	449.76	−90	−90	−90
40	1	2	5	70	170	449.76	145	145	145
41	2	2	5	170	170	449.76	165	165	165
42	3	2	5	270	170	449.76	120	120	120
43	1	3	5	70	270	449.76	110	110	110
44	2	3	5	170	270	449.76	−90	−90	−90
45	3	3	5	270	270	449.76	35	35	35

References

1. Wohlers Associates Inc. *Wohlers Report 2019*; Wohlers Associates Inc.: Fort Collins, CO, USA, 2019.
2. ISO 1101:2017(E). *Geometrical Product Specifications (GPS)—Geometrical Tolerancing—Tolerances of Form, Orientation, Location And Run-Out*; International Organization for Standardization: Geneva, Switzerland, 2017.
3. ASME Y14.5M-2018. *Dimensioning and Tolerancing*; ASME: New York, NY, USA, 2018.

4. ISO/ASTM 52900:2015(E). *Standard Terminology for Additive Manufacturing—General Principles—Terminology*; ISO/ASTM: West Conshohocken, PA, USA, 2015.
5. ISO/ASTM 52911:2019(E). *Additive Manufacturing—Design—Part 2: Laser-Based Powder Bed Fusion of Polymers*; ISO/ASTM: Geneva, Switzerland, 2019.
6. Delfs, P.; Tows, M.; Schmid, H.J. Optimized build orientation of additive manufactured parts for improved surface quality and build time. *Addit. Manuf.* **2016**, *12*, 314–320. [CrossRef]
7. Arni, R.; Gupta, S.K. Manufacturability analysis of flatness tolerances in solid freeform fabrication. *J. Mech. Des.* **2001**, *123*, 148–156. [CrossRef]
8. Paul, R.; Anand, S. Optimal part orientation in Rapid Manufacturing process for achieving geometric tolerances. *J. Manuf. Syst.* **2011**, *30*, 214–222. [CrossRef]
9. Zhang, Y.; Bernard, A.; Gupta, R.K.; Harik, R. Feature based building orientation optimization for additive manufacturing. *Rapid Prototyp. J.* **2016**, *22*, 358–376. [CrossRef]
10. Cheng, W.; Fuh, J.Y.H.; Nee, A.Y.C.; Wong, Y.S.; Loh, H.T.; Miyazawa, T. Multi-objective optimization of part-building orientation in stereolithography. *Rapid Prototyp. J.* **1995**, *1*, 12–23. [CrossRef]
11. Salmoria, G.V.; Leite, J.L.; Vieira, L.F.; Pires, A.T.N.; Roesler, C.R.M. Mechanical properties of PA6/PA12 blend specimens prepared by selective laser sintering. *Polym. Test.* **2012**, *31*, 411–416. [CrossRef]
12. Caulfield, B.; McHugh, P.E.; Lohfeld, S. Dependence of mechanical properties of polyamide components on build parameters in the SLS process. *J. Mater. Process. Technol.* **2007**, *182*, 477–488. [CrossRef]
13. Baturynska, I. Application of Machine Learning Techniques to Predict the Mechanical Properties of Polyamide 2200 (PA12) in Additive Manufacturing. *Appl. Sci.* **2019**, *9*, 1060. [CrossRef]
14. Beitz, S.; Uerlich, R.; Bokelmann, T.; Diener, A.; Vietor, T.; Kwade, A. Influence of Powder Deposition on Powder Bed and Specimen Properties. *Materials* **2019**, *12*, 297. [CrossRef] [PubMed]
15. Pavan, M.; Faes, M.; Strobbe, D.; Van Hooreweder, B.; Craeghs, T.; Moens, D.; Dewulf, W. On the influence of inter-layer time and energy density on selected critical-to-quality properties of PA12 parts produced via laser sintering. *Polym. Test.* **2017**, *61*, 386–395. [CrossRef]
16. Kundera, C.; Kozior, T. Evaluation of the influence of selected parameters of Selective Laser Sintering technology on surface topography. *J. Phys. Conf. Ser.* **2019**, *1183*, 012002. [CrossRef]
17. Sachdeva, A.; Singh, S.; Sharma, V.S. Investigating surface roughness of parts produced by SLS process. *Int. J. Adv. Manuf. Technol.* **2013**, *64*, 1505–1516. [CrossRef]
18. Mavoori, N.K.; Vekatesh, S.; M, M.H. Investigation on surface roughness of sintered PA2200 prototypes using Taguchi method. *Rapid Prototyp. J.* **2018**, *25*, 454–461. [CrossRef]
19. Reinhardt, T.; Martha, A.; Witt, G.; Köhler, P. Preprocess-Optimization for Polypropylene Laser Sintered Parts. *Comput.-Aided Des. Appl.* **2014**, *11*, 49–61. [CrossRef]
20. Pavan, M. *CT-Based Optimization of Laser Sintering of Polyamide-12*; KU Leuven: Brussels, Belgium, 2018.
21. Baturynska, I. Statistical analysis of dimensional accuracy in additive manufacturing considering STL model properties. *Int. J. Adv. Manuf. Technol.* **2018**, 2835–2849. [CrossRef]
22. Ha, S.; Ransikarbum, K.; Han, H.; Kwon, D.; Kim, H.; Kim, N. A dimensional compensation algorithm for vertical bending deformation of 3D printed parts in selective laser sintering. *Rapid Prototyp. J.* **2018**, *24*, 955–963. [CrossRef]
23. Di Angelo, L.; Di Stefano, P.; Guardiani, E. Search for the Optimal Build Direction in Additive Manufacturing Technologies: A Review. *J. Manuf. Mater. Process.* **2020**, *4*, 71. [CrossRef]
24. Taufik, M.; Jain, P.K. Role of build orientation in layered manufacturing: A review. *Int. J. Manuf. Technol. Manag.* **2013**, *27*, 47–73. [CrossRef]
25. Senthilkumaran, K.; Pandey, P.M.; Rao, P.V.M. Statistical modeling and minimization of form error in SLS prototyping. *Rapid Prototyp. J.* **2012**, *18*, 38–48. [CrossRef]
26. Sood, A.K.; Ohdar, R.K.; Mahapatra, S.S. Improving dimensional accuracy of Fused Deposition Modelling processed part using grey Taguchi method. *Mater. Des.* **2009**, *30*, 4243–4252. [CrossRef]
27. Rizzuti, S.; De Napoli, L.; Ventra, S. The Influence of Build Orientation on the Flatness Error in Artifact Produced by Direct Metal Laser Sintering (DMLS) Process. In Proceedings of the International Joint Conference on Mechanics, Design Engineering & Advanced Manufacturing, Cham, Switzerland, 14–16 September 2019; pp. 463–472.
28. Nidagundi, V.B.; Keshavamurthy, R.; Prakash, C.P.S. Studies on Parametric Optimization for Fused Deposition Modelling Process. *Mater. Today: Proc.* **2015**, *2*, 1691–1699. [CrossRef]
29. Ollison, T.; Berisso, K. Three-Dimensional Printing Build Variables That Impact Cylindricity. *J. Ind. Technol.* **2010**, *26*, 2–10.
30. Minetola, P.; Calignano, F.; Galati, M. Comparing geometric tolerance capabilities of additive manufacturing systems for polymers. *Addit. Manuf.* **2020**, *32*, 101103. [CrossRef]
31. Fahad, M.; Hopkinson, N. Evaluation and comparison of geometrical accuracy of parts produced by sintering-based additive manufacturing processes. *Int. J. Adv. Manuf. Technol.* **2017**, *88*, 3389–3394. [CrossRef]
32. Brøtan, V. A new method for determining and improving the accuracy of a powder bed additive manufacturing machine. *Int. J. Adv. Manuf. Technol.* **2014**, *74*, 1187–1195. [CrossRef]

33. Rebaioli, L.; Fassi, I. A review on benchmark artifacts for evaluating the geometrical performance of additive manufacturing processes. *Int. J. Adv. Manuf. Technol.* **2017**, *93*, 2571–2598. [CrossRef]
34. Minetola, P.; Iuliano, L.; Marchiandi, G. Benchmarking of FDM Machines through Part Quality Using IT Grades. *Procedia Cirp.* **2016**, *41*, 1027–1032. [CrossRef]
35. Szilvśi-Nagy, M.; Mátyási, G. Analysis of STL files. *Math. Comput. Model.* **2003**, *38*, 945–960. [CrossRef]
36. Leirmo, T.L.; Semeniuta, O.; Martinsen, K. Tolerancing from STL data: A Legacy Challenge. *Procedia Cirp.* **2020**, *92*, 218–223. [CrossRef]
37. ISO/ASTM 52921:2013(E). *Standard Terminology for Additive Manufacturing—Coordinate Systems and Test Methodologies*; ISO/ASTM: Geneva, Switzerland, 2013.
38. ISO/ASTM 52902:2019(E). *Additive Manufacturing—Test Artifacts—Geometric Capability Assessment of Additive Manufacturing Systems*; ISO/ASTM: Geneva, Switzerland, 2019.
39. Rott, S.; Ladewig, A.; Friedberger, K.; Casper, J.; Full, M.; Schleifenbaum, J.H. Surface roughness in laser powder bed fusion—Interdependency of surface orientation and laser incidence. *Addit. Manuf.* **2020**, *36*, 101437. [CrossRef]
40. Lou, S.; Brown, S.B.; Sun, W.; Zeng, W.; Jiang, X.; Scott, P.J. An investigation of the mechanical filtering effect of tactile CMM in the measurement of additively manufactured parts. *Measurement* **2019**, *144*, 173–182. [CrossRef]

Paper P6

T. L. Leirmo and O. Semeniuta, 'Minimizing form errors in additive manufacturing with part build orientation - An optimization method for continuous solution spaces,' *Open Engineering*, vol. (Accepted),

DE GRUYTER Open Eng. 2021; aop

Research Article

Torbjørn L. Leirmo* and Oleksandr Semeniuta

Minimizing form errors in additive manufacturing with part build orientation

An optimization method for continuous solution spaces

https://doi.org/..., Received ...; accepted ...

Abstract: For Additive Manufacturing (AM) to be successfully implemented in manufacturing systems, the geometric accuracy of components must be controlled in terms of form, fit, and function. Because the accuracy of AM products is greatly affected by the part build orientation, this factor dictates the achievable tolerances and thereby the ability to incorporate AM technologies in large-scale production. This paper describes a novel optimization method for minimizing form errors based on the geometric features of the part. The described method enables the combination of separate expressions for each feature to create a continuous solution space. Consequently, the optimal part build orientation can be precisely determined based on a mathematical description of the effect of build direction on each surface type. The proposed method is demonstrated in two case studies with step-by-step descriptions including discussions on viability and possible extensions. The results indicate good performance and enable flexible prioritization and trade-offs between tolerance characteristics.

Keywords: Additive Manufacturing (AM); Part build orientation; Quality; Accuracy; Build direction; Optimization

AM Additive Manufacturing
EA Evolutionary Algorithm
FFF Fused Filament Fabrication
GA Genetic Algorithm
PCS Part Coordinate System
STL STereoLithography file format
VE Volumetric Error
WCS World Coordinate System

1 Introduction

Additive Manufacturing (AM) holds the potential to revolutionize the manufacturing industry through topology-optimized lightweight structures and mass-customized designs. However, the full potential of the technology remains largely unexploited due to cost restrictions and quality issues. While AM is utilized in medical, aerospace, and automotive industries for small production volumes, this is only possible because every component is carefully engineered and validated through an iterative process before production is initiated.

***Corresponding author: Torbjørn L. Leirmo,** Department of Manufacturing and Civil Engineering, Faculty of Engineering, NTNU – Norwegian University of Science and Technology, Gjøvik, Norway, e-mail: torbjorn.leirmo@ntnu.no
Oleksandr Semeniuta, Department of Manufacturing and Civil Engineering, Faculty of Engineering, NTNU – Norwegian University of Science and Technology, Gjøvik, Norway

Open Access. © 2021 T. L. Leirmo and O. Semeniuta, published by De Gruyter. This work is licensed under the Creative Commons Attribution 4.0 License

For mass customization to truly reach its potential in agile manufacturing, automated process planning for AM must be developed to ensure quality and consistency in production.

While AM offers design freedom to create innovative free form surfaces previously unattainable by conventional manufacturing methods, traditional shape features will still be present in novel designs, such as the interfaces between components of an assembly. The interconnection between AM and conventional manufacturing technologies in manufacturing systems warrants the control of geometric accuracy in terms of traditional tolerancing features.

To enable consistent production of unique components while meeting quality requirements, it is necessary to develop valid models and methods for predicting, mitigating, and adapting to variation in the build process. One of the major determining factors for geometric accuracy in AM is the part build orientation, i.e. the direction in which material is added to the substrate to realize the geometry [1]. This paper describes a method for the precise determination of optimal part build orientation to minimize the deviations from nominal to actual geometry by considering the geometric features of the part.

The accuracy of an additively manufactured surface partly depends on its curvature (or lack thereof). Therefore, the proposed method enables separate mathematical models to be applied to each surface type. These models are then populated with data from the CAD-model, and combined into a single expression of quality as a function of part build orientation. The result is a continuous objective function for the entire solution space which enables the identification of optimal part build orientations, or feasible regions for secondary objectives.

The remainder of this paper is structured as follows: First, the theoretic foundations and previous work are outlined in section 2 before the method is described in section 3. In section 4, two case studies are presented to demonstrate the method step-by-step before a brief discussion on the viability and possible extensions is presented in section 5. Finally, section 6 summarizes the paper and provides directions for future work.

2 Theoretic background

In general, AM techniques successively add layers of material to create an object [1]. This layered manner of fabrication is a decisive factor in how accuracy errors occur in the AM process. Dantan et al. [2] identifies a range of defect modes in Fused Filament Fabrication (FFF), many of which can be extended to other AM technologies. Defect modes relating to the direction of material deposition, as well as errors in machine/tool movement influence the accuracy of the produced surface regardless of technology and material. Apart from the various surface defects and inaccuracies present in most AM processes, the products also exhibit anisotropic mechanical properties where the behavior depends on the build direction [3]. Consequently, the part build orientation is a decisive factor in the final part quality both in terms of accuracy and mechanical properties.

The staircase effect is perhaps the most illustrative example of how part build orientation is vital in AM. The layered manufacturing approach inevitably leaves a characteristic pattern on inclined surfaces. This pattern emerges when the contours of two subsequent layers cannot align perfectly. The result is a stepped surface as displayed in figure 1, commonly referred to as the staircase effect.

The staircase effect can be modeled in two dimensions as the cusp height h_{cusp}, i.e. the shortest distance from the inner corner of a step, to the hypotenuse of the right triangle of figure 1 [4]. The cusp height h_{cusp} may be calculated from the layer thickness h_{layer} and surface angle θ which is the angle between the build direction $\hat{z} = \begin{bmatrix} 0 & 0 & 1 \end{bmatrix}$ and the surface normal vector $\vec{n}$ as described by Alexander, Allen, and Dutta [5]:

$$h_{cusp} = \begin{cases} h_{layer} |\cos\theta| & \text{if } |\cos\theta| \neq 1 \\ 0 & \text{if } |\cos\theta| = 1 \end{cases} \tag{1}$$

Another measure of the staircase effect is the Volumetric Error (VE) introduced by Masood, Rattanawong, and Iovenitti [6] which corresponds to the volumetric difference between the CAD model and the realized geometry. This solution soon becomes quite complex when extended from two to three dimensions. Figure 1 illustrates the deviations due to the staircase effect where the area below the dashed line is lost. The VE is the

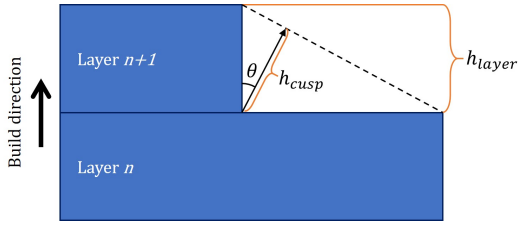

Fig. 1: Illustration of the staircase effect and the cusp height introduced by layered manufacturing.

result of integrating this area along the perimeter of the layer. Complex surfaces drastically complicate the computation of VE, and simplifications are often necessary.

The obvious solution for mitigating the staircase effect is to make sure all surfaces are oriented either parallel or perpendicular to the build direction. However, when a part consists of several features in different directions (which is the case for most functional components), there will be no part build orientation in which all surfaces are either parallel or perpendicular to the build direction. Furthermore, curved surfaces do not benefit from perpendicular orientations as this will maximize the staircase effect. Therefore, a trade-off must be made in order to converge on a globally optimal solution where the staircase effect is minimized. The orientation problem for accuracy is however comprised of many more failure modes other than the staircase effect, all of which matters in modeling the final geometry.

While the part build orientation should be considered in the design stage, this is not always possible. Consequently, the information available when deciding the part build orientation may differ from full CAD-model with tolerances, to the tessellated STereoLithography file format (STL) commonly used in the final stages of process planning for AM. Naturally, methods for dealing with the orientation problem with these varying knowledge levels have been proposed in literature – some relying on computational methods, and others on a human expert. Additionally, some may focus on finding a minimal solution fast, while others may prefer to spend more time to find the optimal orientation. The many possible combinations of methods, objectives, and limitations have resulted in a plethora of approaches ranging from the general to the highly specific. However, the crux of the orientation problem remains to achieve the best possible result with the information at hand, within a reasonable time.

2.1 Related work

Part build orientation is a key factor in AM as it is easily manipulated and has a clear influence on final properties. The effect of part build orientation has been the subject of many research efforts but remains an open issue [7]. Methods for determining the optimal part build orientation can largely be divided into two groups: (i) those evaluating a set of candidate solutions with respect to an objective function, and (ii) those mathematically describing the solution space in order to explore this continuous space for the optimal solution. A selection of the most relevant related methods is showcased in table 1. The interested reader may refer to [7] and [8] for recent reviews on the orientation problem.

The first group is the most common and starts by identifying candidate orientations. This process is either based on a set of rules (e.g. flat surfaces of the convex hull) or by discretization of the solution space, i.e. certain intervals of rotation about one or more predefined axes. In the next step, either an exhaustive search is performed where all candidates are considered, or a guided search is conducted e.g. by a Genetic Algorithm (GA). These discrete methods have certain advantages, but they inherently fail to consider the

Tab. 1: Characteristics of related work in chronological order.

Reference	Candidate orientations	Search method
Cheng et al. [9]	Flat surfaces	ES
Alexander, Allen, and Dutta [5]	Flat surfaces + user defined	ES
Masood, Rattanawong, and Iovenitti [10]	Discretized solution space	ES
Byun and Lee [11]	Faces of convex hull	ES
Padhye and Deb [12]	**All**	EAs
Zhang and Li [13]	Discretized unit sphere	ES and EA
Li and Zhang [14]	Discretized unit sphere	EA
Das et al. [15]	**All**	GBM
Zhang et al. [16]	Discretized unit sphere	ES
Das et al. [17]	**All**	GBM
Budinoff and McMains [18]	Discretized unit sphere	ES
Chowdhury, Mhapsekar, and Anand [19]	**All**	GBM
Zhang et al. [20]	Facet clusters	ES
Qin et al. [21]	Facet clusters	ES

ES = Exhaustive Search, EA = Evolutionary Algorithm, GBM = Gradient-Based Method

entire (continuous) solution space and therefore risk missing good orientations. Additionally, any attempt to refine the search space by including more candidate orientations inevitably increases the computation time.

The second group, on the other hand, grants access to the entire solution space, where the complexity of this solution space generally correlates with the complexity of the geometry. This category is not as well explored, perhaps due to the simplicity of discrete solution spaces, or the ability of discrete approaches to handle discontinuous functions. Nevertheless, a continuous solution space may facilitate more nuanced objective functions and complex solution spaces. Continuous solution spaces can be explored by Evolutionary Algorithms (EAs), but also enables gradient-based methods where knowledge of the topology of the solution space is exploited in an iterative search for the global optimum.

The approach described herein constitutes a hybrid of the two methods outlined above: The solution space is described with a differentiable function which is used to identify critical points. The critical points will then constitute the candidate orientations in the final evaluation which identifies the global optimum. The novelty of this approach lies in the combination of simplicity from generalizing surface types, and the flexibility brought forward by the general framework that can be populated with any objective function.

Cheng et al. [9] considered all flat surfaces as candidates for determining the optimal part build orientation and evaluated every candidate orientation with respect to the accuracy, build time, and stability. A similar approach was proposed for the minimization of cost by Alexander, Allen, and Dutta [5] who included the cost of post-processing and build time in the cost calculations. Zhang et al. [16] generated a set of candidate orientations from every shape feature and evaluated them for several attributes including surface roughness and support volume. Similar methods have also been proposed with facet clustering where groups of facets are considered collectively based on how they are affected by part build orientation [20, 22, 21]. All these methods benefit from the generalization of how different surfaces are affected by the build direction. While various methods are employed in these studies in the search for an optimal solution, none of them consider a continuous solution space generated from the geometry.

Zhang and Li [13] proposed a discretization of the solution space (i.e. a unit sphere) and let each facet of the STL file promote the two orientations parallel to the facet normal, as well as the great circle corresponding to the perpendicular of the normal vector. The authors describe methods to make the selection using an exhaustive search for minimizing VE, as well as a GA for combined optimization of VE and part height [13, 14]. The authors argue for the use of GA over exhaustive search when the number of discretized points becomes large due to time concerns. Discretization allows for controlling the resolution of the solution space, and therefore also the computational cost. However, the approach remains oblivious to any effects other than those of the predefined points in the solution space.

Das et al. [15, 17] proposed a method for minimizing form errors and support structures by formulating a minimization problem to be solved in MATLAB with gradient-based optimization. The method is based on the 1-dimensional tolerance maps of Paul and Anand [23, 24] for cylindricity, and Arni and Gupta [25] for flatness – both theoretically derived from the staircase effect. A similar approach was proposed by Chowdhury, Mhapsekar, and Anand [19] who continued to compensate the geometry for any expected deviations still present after optimization. However, both of these proposed methods involve a risk of convergence to local optima due to the gradient-based approach. The convergence to local optima is avoided in the work of Budinoff and McMains [18] who performs an exhaustive search of one-degree increments to identify feasible regions from which the final orientation may be selected.

The existing body of literature describes various approaches to the orientation problem with various benefits and drawbacks. Exploiting higher-level information about local topology facilitates the generation of candidate orientations. This information can also be used to construct continuous solution spaces for achievable tolerances and other objectives. The method presented herein benefits from the generalization of part geometry to reduce the number of parameters in optimization, while also accessing the entire solution space for mathematical analysis.

2.2 Mathematical foundations

There is no shortage of mathematical formulations of the orientation problem in academic literature. The plethora of formulations arises from the subtle differences in AM technologies which have varying parameters with different effects. The number of formulations is further amplified by the deviating scope and objectives of previous works. For instance, the VE is a common measure of accuracy in AM. However, the calculation of VE is based on fundamental assumptions regarding the surface profile, typically assuming right-angled steps. However, the real surface will be filleted as various effects will round off the corners and hence throw off the theoretical models [26, 27].

Nevertheless, the effect of part build orientation on surface accuracy is indisputable in current AM systems, although of less concern when the layers are thinner [28]. Therefore, the modeling of quality as a function of part build orientation is warranted, and mathematical descriptions of orientations are necessary.

According to Euler's rotation theorem, any orientation of a rigid body in $\mathbb{R}^3$ can be described as a sequence of three basic rotations (α, β, γ) where no two subsequent rotations are performed about the same axis. The basic rotations are performed about the x-, y-, and z-axis individually, and a rotation of θ degrees about the respective axes can be calculated using the 3×3 rotation matrices $\boldsymbol{R}_x$, $\boldsymbol{R}_y$ and $\boldsymbol{R}_z$ where

$$\boldsymbol{R}_x(\theta) = \begin{bmatrix} 1 & 0 & 0 \\ 0 & \cos\theta & -\sin\theta \\ 0 & \sin\theta & \cos\theta \end{bmatrix} \tag{2}$$

$$\boldsymbol{R}_y(\theta) = \begin{bmatrix} \cos\theta & 0 & \sin\theta \\ 0 & 1 & 0 \\ -\sin\theta & 0 & \cos\theta \end{bmatrix} \tag{3}$$

$$\boldsymbol{R}_z(\theta) = \begin{bmatrix} \cos\theta & -\sin\theta & 0 \\ \sin\theta & \cos\theta & 0 \\ 0 & 0 & 1 \end{bmatrix} \tag{4}$$

The rotation matrices of equations 2, 3 and 4 will rotate any column vector about the respective axis by the angle θ. The direction of the rotation is determined by the right-hand rule, i.e. counterclockwise as seen from the positive end towards the origin. According to Euler, any orientation can be achieved by three successive rotations. However, because matrix multiplication is non-commutative, the sequence of rotations influences the final orientation of the body. Consequently, when three rotations are performed in succession following Euler's rules, there are still twelve possible combinations divided into two distinct groups:

Tab. 2: Possible rotation sequences.

Proper Euler angles	Tait-Bryan angles
$X_1Y_2X_3$	$X_1Y_2Z_3$
$X_1Z_2X_3$	$X_1Z_2Y_3$
$Y_1X_2Y_3$	$Y_1X_2Z_3$
$Y_1Z_2Y_3$	$Y_1Z_2X_3$
$Z_1X_2Z_3$	$Z_1X_2Y_3$
$Z_1Y_2Z_3$	$Z_1Y_2X_3$

1. Proper Euler angles where the first and last rotations are performed about the same axis; and
2. Tait-Bryan angles where all three rotations are performed about unique axes.

In the current work, the notation for rotation sequence is simply the axes in the order of which the rotations are performed with a subscript further emphasizing the sequence. For instance, the most common rotation following a proper Euler angle sequence is $Z_1X_2Z_3$, which means first rotation about the z-axis, second rotation about the (new) x-axis, and finally another rotation about the (now current) z-axis. Table 2 tabulates all twelve rotation sequences following this notation.

The range of rotations is limited to the unit circle as rotations of more than 2π radians make little sense. Hence, the range of α and γ can be restricted to $[0, 2\pi)$. Conversely, the range of β need not exceed π radians because larger rotations will only repeat previous spaces, hence the range of β can be reduced to $[0, \pi)$. In consequence, the orientation problem in AM is bound to the finite space where $(\alpha, \gamma) \in [0, 2\pi)$ and $\beta \in [0, \pi)$.

3 Proposed method

The proposed optimization method is based on shape features to facilitate implementation in traditional tolerancing schemes. In this context, a shape feature is defined as either a geometric primitive, i.e. plane, cylinder, cone, sphere, or torus (figure 2), or a free-form surface. These feature types are affected by the build direction in different ways and are also subject to different tolerance characteristics such as flatness, cylindricity, etc. Therefore, these features should be used in the construction of the objective function.

The current method requires information about the feature types and the relative orientation of the features. This information is readily available in many 3D-file formats such as STEP, however, when the geometry is converted to the popular intermediate STL format, the information about local topology is lost. For such tessellated file formats, the geometry may be deduced by feature recognition algorithms as described elsewhere [29, 30, 31].

Due to the ability to parameterize geometric primitives (e.g. height and diameter of a cylinder), these shape features may be generalized and are considered in the remainder of this paper. The free-form surfaces on the other hand are more complex and therefore necessitate closer analysis and will only be discussed briefly. This prioritization is based on the assumption that surfaces that require tolerancing are functional surfaces that predominantly are primitive in shape. The problem of free-form surfaces is left for future work.

Vectorial characterization of shape features enables the description of the relative location and orientation of shape features. Consider that each feature F is described by a location vector $\vec{p}$ and an orientation vector $\vec{v}$ with respect to a Part Coordinate System (PCS) where $\vec{p}, \vec{v} \in \mathbb{R}^3$. This is demonstrated in figure 3 where the PCS is located at the bottom left of the design and the black arrow represents the location vector for the highlighted horizontal through-hole. The location vector points to the center of the hole where a feature coordinate system signifies the orientation of the feature, i.e. with the z-axis of the cylinder parallel to the y-axis of the PCS.

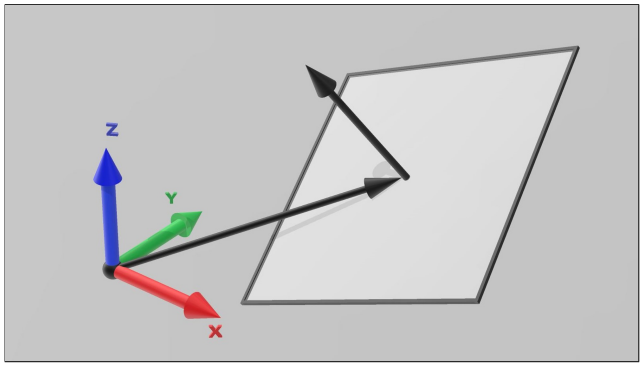

(a) Plane with position and orientation vector

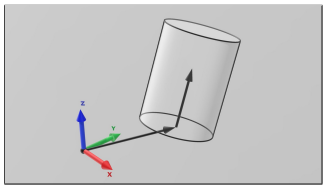

(b) Cylinder with position and orientation vector

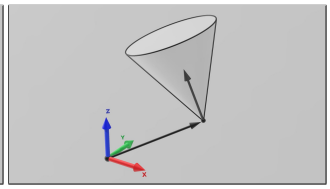

(c) Cone with position and orientation vector

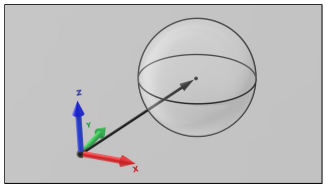

(d) Sphere with only position vector

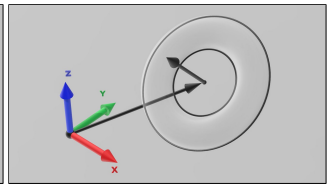

(e) Torus with position and orientation vector

Fig. 2: Shape features with position and orientation vectors. Spheres are not assigned an orientation due to three full degrees of freedom in rotation.

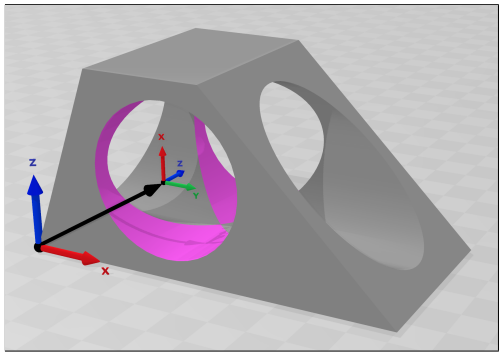

Fig. 3: Sample part 1 recreated from Cheng et al. [9] with coordinate frames.

When all features are described vectorially, the entire part P may be described as a set of all these features $P = \{F_1, F_2, \ldots, F_n\}$. The geometry of figure 3 is recreated from Cheng et al. [9] and will be used as a sample part for a simple geometry in this paper.

3.1 Mathematical description of part build orientation

Consider a part $P = \{F_1, F_2, \ldots, F_n\}$. These features may be of different sizes and feature types, i.e. planes, cylinders, spheres, cones, and tori. The quality of each feature type can be modeled as a function of some parameters $Q_F = f(x_1, x_2, \ldots, x_n)$. If a consistent measure of quality is applied (e.g. surface roughness Ra), the mean quality of the entire part Q_{part} may be calculated as:

$$Q_{part} = \frac{\sum_{i=1}^{n} Q_i A_i}{A_{part}} \tag{5}$$

where n is the number of features, Q_i and A_i is the quality and area of the ith feature respectively, and A_{part} is the total surface area of the part.

While the area may be a suitable weight factor in many cases, it is also possible to introduce a separate weight factor that enables the prioritization of features. This weight factor can be applied on any level, e.g. certain feature types may be ignored, or individual features may attain a higher priority. Furthermore, the fundamental assumption is made that the quality of an additively manufactured surface can be described as a function of its orientation with respect to the build direction.

The orientation of a feature F with respect to the build direction $\hat{z}$ may be described as two Euler angles (α, β) necessary for the rotational transformation of $\hat{z}$ to $\vec{v}$ where $\vec{v}$ is the feature vector of F. In the current work, (α, β) represents rotations about the x- and y-axis respectively, both with reference to the original reference frame (i.e. Tait-Brian angles $X_1Y_2Z_3$).

The angle θ between two arbitrary vectors $\vec{u}$ and $\vec{v}$ is found by:

$$\theta = \arccos\left(\frac{\vec{u} \cdot \vec{v}}{|\vec{u}| \cdot |\vec{v}|}\right) \tag{6}$$

By utilizing unit vectors, $|\vec{u}| \cdot |\vec{v}|$ evaluates to 1 and reduces the expression to

$$\theta = \arccos\left(\vec{u} \cdot \vec{v}\right) \tag{7}$$

By inserting $\hat{z} = \begin{bmatrix} 0 & 0 & 1 \end{bmatrix}$ for $\vec{u}$, the above expression can be further reduced because

$$\begin{bmatrix} 0 & 0 & 1 \end{bmatrix} \cdot \begin{bmatrix} x \\ y \\ z \end{bmatrix} = z \tag{8}$$

In this context, z will be the z-component of the feature vector $\vec{v}$, denoted $\vec{v}_z$. However, we want to express the angle θ as a function of the part's orientation in 3D space to enable optimization of orientation. For this purpose, the orientation vector can be expressed in terms of Tait-Bryan angles ($Z_1Y_2X_3$). These rotations are commonly referred to as yaw, pitch, and roll in engineering applications, and describes the orientation of a rigid body with respect to the World Coordinate System (WCS). The feature vector can then be derived from the rotation matrices in equations 2, 3 and 4, and the sequential rotations about the x-, y-, and z-axis can then be performed in a single operation by multiplying the matrices as follows:

$$\begin{aligned} \boldsymbol{R} &= \boldsymbol{R}_z \cdot \boldsymbol{R}_y \cdot \boldsymbol{R}_x \\ &= \begin{bmatrix} \cos\beta\cos\gamma & \sin\alpha\sin\beta\cos\gamma - \sin\gamma\cos\alpha & \sin\alpha\sin\gamma + \sin\beta\cos\alpha\cos\gamma \\ \sin\gamma\cos\beta & \sin\alpha\sin\beta\sin\gamma + \cos\alpha\cos\gamma & -\sin\alpha\cos\gamma + \sin\beta\cos\gamma\cos\alpha \\ -\sin\beta & \sin\alpha\cos\beta & \cos\alpha\cos\beta \end{bmatrix} \end{aligned} \tag{9}$$

This means that the orientation vector $\vec{v}$ of a feature may be expressed as:

$$\vec{v} = \begin{bmatrix} x\cos\beta\cos\gamma + y(\sin\alpha\sin\beta\cos\gamma - \sin\gamma\cos\alpha) + z(\sin\alpha\sin\gamma + \sin\beta\cos\alpha\cos\gamma) \\ x\sin\gamma\cos\beta + y(\sin\alpha\sin\beta\sin\gamma + \cos\alpha\cos\gamma) + z(-\sin\alpha\cos\gamma + \sin\beta\cos\gamma\cos\alpha) \\ -x\sin\beta + y\sin\alpha\cos\beta + z\cos\alpha\cos\beta \end{bmatrix} \tag{10}$$

which means

$$\vec{v}_z = -x\sin\beta + y\sin\alpha\cos\beta + z\cos\alpha\cos\beta \tag{11}$$

When $\vec{v}_z$ from equation 11 is inserted in equation 7, the final expression simply becomes

$$\theta = \arccos(-x\sin\beta + y\sin\alpha\cos\beta + z\cos\alpha\cos\beta) \tag{12}$$

To enable the mathematical description of the entire geometry in a single expression, the orientation of each feature is described relative to a common coordinate frame, i.e. the WCS. The geometry may be regarded as a rigid body, which means that the relation between the surfaces remains constant and any transformation acts on all surfaces equally. In consequence, the orientation of all surfaces may be collectively calculated from the same values of α, β, and γ using equation 10 where x, y and z are the components of the feature's initial orientation vector. Accordingly, equation 12 is valid for all surfaces with α and β as the only variables.

3.2 Finding the optimal part build orientation

Based on the theory above, it is possible to determine the optimal part build orientation mathematically by evaluating the critical points of the objective function. The critical points of a function $f(x, y)$ are found where

$$\frac{\partial f}{\partial x} = \frac{\partial f}{\partial y} = 0 \text{ or undefined} \tag{13}$$

Typically, there will be several solutions to equation 13, and each solution needs to be evaluated separately. These solutions will represent points, edges, and perhaps even entire areas in the 2D solution space. Provided the formalization in the previous section, the part build orientation can be described as a set of two rotations α and β. If a function is based on these two rotations, α and β will replace x and y in equation 13 in the search for critical points. The solution space will be the surface of a unit sphere where $\alpha \in [0, 2\pi)$ and $\beta \in [0, \pi)$. A point on this surface will correspond to a single unique orientation, while a line will correspond to a range of

orientations. Note that the entire unit sphere is accessible already with only half a rotation of β, still, a full rotation of β is used in the visualizations of this paper to make their analysis more intuitive.

The fundamental assumption remains that the quality of a surface can be modeled as a function of its orientation with respect to the build orientation and that this function is differentiable. A conditional function (such as the one in equation 1) introduces certain challenges to this method. However, such discontinuities would represent edges and areas in the 2D solution space that could be added to the list of candidate orientations.

Each feature of the geometry will add a term to the objective function, and each term will typically add one or more candidate orientations to the list. The exact number of additional candidates depends on the mathematical model as higher-order functions will yield more candidates. It is therefore beneficial to limit or minimize the number of terms to avoid excessive computations. A simple way to minimize the number of terms is to join similar terms, e.g. two features of the same type and orientation can be combined into a single term of the objective function. Other measures include a manual selection of significant features and automatic filtering of features based on type, size, etc.

As surfaces are affected differently by build direction, separate models for each feature type are necessary to enable proper evaluation. This is easily implemented by inserting the appropriate expression for $F_{Quality}$ in equation 5 for each feature.

4 Case study

Two case studies are presented to demonstrate the proposed method:

1. A simple geometry to enable a step-by-step demonstration of the approach and all calculations; and
2. A slightly more complex geometry to illustrate the applicability to more complex parts

Simple mathematical models of quality are constructed for the illustrative purpose of this study. The implementation of empirical models is left for future work as this would obscure the central elements of this paper. Before the case studies are presented, the construction of these mathematical models is detailed to provide the necessary foundations for the subsequent illustrations.

4.1 Constructing the mathematical models

The following models are based on the orientation rules described by Frank and Fadel [32], stating that cylinders should be oriented with the axis parallel to the build direction, while planes can be oriented both parallel or perpendicular to the build direction. Up-facing and down-facing surfaces are treated equally in the examples in order to keep the objective functions simple. This can naturally be incorporated in the objective function to account for any additional effects, e.g. overcure, support structures, etc.

The central assumption in the current work is that the accuracy of a feature can be modeled as a function of its angle to the build direction (θ) which in turn is a function of the part's orientation as described in equation 12. Also, we are modeling deviations from nominal geometry which can be considered a cost, hence a low cost indicates a high fitness of a given orientation. However, the angle will not be sufficient to evaluate the fitness of a certain orientation. Consider for instance a cylinder oriented at a 45° angle from the build direction ($\theta = 45^\circ$). The same cylinder oriented at $\theta = 135^\circ$ would yield the same result, but the angle θ is quite different. Clearly, the objective function should be more sophisticated to incorporate this behavior.

Because the angle θ always will be in the interval $[0^\circ, 180^\circ]$, the sine of the angle will provide three desirable properties of an objective function: (i) the result is always a number between 0 and 1, (ii) the function is minimized at vertical orientations and maximized at horizontal orientations, and (iii) the function is periodic and symmetric. This study employs this function as an expression for the quality of cylinders:

$$Q_{cylinder}(\theta) = \sin\theta \tag{14}$$

Tab. 3: Numeric description of part features for sample part 1.

		Position			Orientation			Area	
#	Type	P_x	P_y	P_z	E_x	E_y	E_z	(mm^2)	(%)
1	Plane	4.55	0.00	1.80	0.00	-1.00	0.00	20	9.3
2	Plane	5.00	2.50	0.00	0.00	0.00	-1.00	50	22.8
3	Plane	3.41	2.50	5.00	0.00	0.00	1.00	16	7.3
4	Plane	4.55	5.00	1.80	0.00	1.00	0.00	20	9.3
5	Plane	0.91	2.50	2.50	-0.90	0.00	0.45	13	6.0
6	Plane	7.50	2.50	2.50	0.81	0.00	0.59	18	8.0
7	Cylinder	4.00	0.00	2.50	0.00	1.00	0.00	31	14.0
8	Cylinder	0.18	2.50	2.50	1.00	0.00	0.00	51	23.1

where θ is the angle between the feature normal vector and the build direction. This can be formulated as a function of (α, β) by inserting equation 12 for θ. With this substitution for θ, equation 14 may be written as:

$$Q_{cylinder}(\alpha, \beta) = \sqrt{1 - (-x \sin\beta + y \sin\alpha \cos\beta + z \cos\alpha \cos\beta)^2} \tag{15}$$

Planes, on the other hand, require some additional configurations as we must consider both vertical and horizontal orientations as positive. To incorporate this new behavior, equation 14 is multiplied by $\cos^2\theta$. This term ensures that planes are positively evaluated at both vertical and horizontal orientations. Additionally, the function is more sensitive to minor changes when a plane is horizontal than when the plane is vertical. This fit well together with the VE being large when the plane is close to horizontal, while not being as prominent in close-to-vertical orientations.

Finally, the function is normalized to facilitate comparison with other feature types, etc. The normalization is achieved by introducing a divisor equal to the maximum of the function. The maximum is easily obtained by derivation and reveals a normalization factor of 2.598 when rounded to three decimal points. This yields the following expression for the quality of planes:

$$Q_{plane}(\theta) = 2.598 \sin\theta \cos^2\theta \tag{16}$$

where θ is the angle between the feature normal vector and the build direction. As with equation 14, the expression for planes may also be rewritten as a function of (α, β) by inserting equation 12 for θ. The result may be formulated as:

$$\begin{aligned} Q_{plane}(\alpha, \beta) = 2.598 &\sqrt{1 - (-x \sin\beta + y \sin\alpha \cos\beta + z \cos\alpha \cos\beta)^2} \\ &\times \left(-x \sin(\beta) + y \sin(\alpha)\cos(\beta) + z \cos(\alpha)\cos(\beta)\right)^2 \end{aligned} \tag{17}$$

The solution spaces of equations 15 and 17 are illustrated in figure 4 where a 3D graph and a contour plot are presented for each of the equations.

4.2 Case 1: A simple geometry

The first case study is the simple geometry reconstructed from Cheng et al. [9] and presented in figure 3. This geometry provides a gentle introduction to the method by enabling a step-wise analysis of the geometry and the accuracy model. The first step of the method is to obtain a numeric description of the geometry in the appropriate format. Table 3 provides the positions and orientations of the features defined relative to the PCS as illustrated in figure 3.

The data from table 3 is inserted into equations 15 and 17 one row at a time as follows:

1. The feature type determines which equation to use (equation 15 for cylinders or 17 for planes)
2. The variables x, y and z are substituted with E_x, E_y, and E_z from table 3

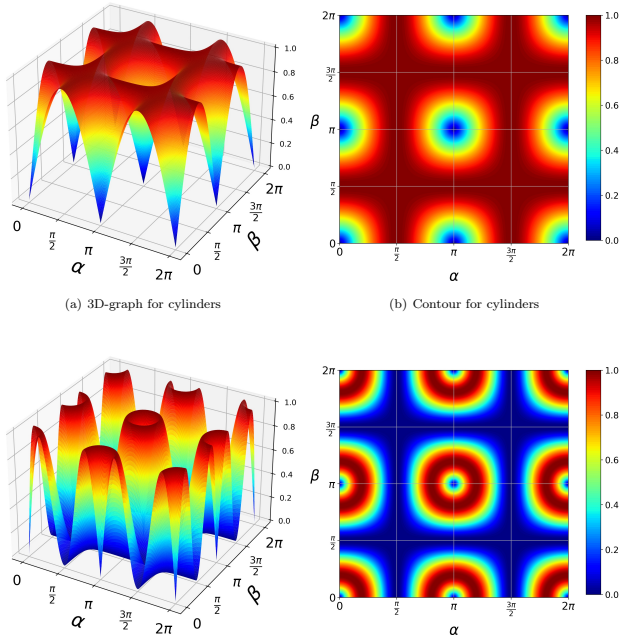

(a) 3D-graph for cylinders

(b) Contour for cylinders

(c) 3D-graph for planes

(d) Contour for planes

Fig. 4: Solution spaces for planes and cylinders $\alpha, \beta \in [0, 2\pi]$ from equations 15 and 17 respectively.

3. The expression is multiplied with the relative surface area of the feature (final column of table 3)

Following the progression above, we start with the first row from table 3 and perform the following steps: (1) The feature is identified as a planar type and we, therefore, use equation 17. (2) The values of E_x, E_y, and E_z are inserted for x, y and z. For the first feature, this means that 0 is inserted for x and z, while 1 is inserted for y. (3) Finally, the weight factor is introduced by multiplying by the relative surface area as found in the final column of table 3, namely 0.093 (9.3%). These steps are displayed in the calculations of equation 18.

$$\begin{aligned} Q_{F_1}(\alpha,\beta) &= 2.598A\sqrt{1-(-x\sin\beta+y\sin\alpha\cos\beta+z\cos\alpha\cos\beta)^2} \\ &\quad\times(-x\sin(\beta)+y\sin(\alpha)\cos(\beta)+z\cos(\alpha)\cos(\beta))^2 \\ &= 2.598A\sqrt{1-(-\mathbf{0}\sin\beta+\mathbf{1}\sin\alpha\cos\beta+\mathbf{0}\cos\alpha\cos\beta)^2} \\ &\quad\times(-\mathbf{0}\sin(\beta)+\mathbf{1}\sin(\alpha)\cos(\beta)+\mathbf{0}\cos(\alpha)\cos(\beta))^2 \\ &= 2.598\times\mathbf{0.093}\sqrt{1-\sin^2(\alpha)\cos^2(\beta)}\sin^2(\alpha)\cos^2(\beta) \\ &= 0.24\sqrt{1-\sin^2(\alpha)\cos^2(\beta)}\sin^2(\alpha)\cos^2(\beta) \end{aligned} \tag{18}$$

When all the data from table 3 is inserted into equations 15 and 17, all the equations may be collected in a single expression for the entire geometry as follows:

$$\begin{aligned} P_{Quality}(\alpha,\beta) = {} & 0.23\sqrt{1-\sin^2(\beta)} \\ & + 0.14\sqrt{1-\sin^2(\alpha)\cos^2(\beta)} \\ & + 0.48\sqrt{1-\sin^2(\alpha)\cos^2(\beta)}\sin^2(\alpha)\cos^2(\beta) \\ & + 0.78\sqrt{1-\cos^2(\alpha)\cos^2(\beta)}\cos^2(\alpha)\cos^2(\beta) \\ & + 0.10\sqrt{1-0.5(-\sin(\beta)+\cos(\alpha)\cos(\beta))^2}(-\sin(\beta)+\cos(\alpha)\cos(\beta))^2 \\ & + 0.14\sqrt{1-0.88(\sin(\beta)+0.36\cos(\alpha)\cos(\beta))^2}(\sin(\beta)+0.36\cos(\alpha)\cos(\beta))^2 \end{aligned} \tag{19}$$

This yields the solution space illustrated in figure 5. The solution space reflects the symmetry and regularity of the geometry as the orientations where feature vectors align with the build direction are clear.

In the next step, the partial derivatives are calculated and evaluated according to equation 13. Figure 6 shows the graphs of the partial derivatives where the dashed lines of figures 6(a) and 6(b) correspond to the contour lines where the derivative evaluates to zero or are undefined.

The critical points are found where both derivatives either evaluate to zero or are undefined. This can be displayed graphically by plotting the dashed lines of figures 6(a) and 6(b) in a single figure as shown in figure 7. Finally, individual evaluation of these points and edges must be conducted to identify the global optimum as tabulated in table 4.

The evaluation of $\alpha,\beta\in[0,2\pi)$ reveals four solutions with equal cost. However, these four solutions are pairwise identical, i.e. (270°, 180°) is the same as (90°, 0°), and (90°, 180°) is the same as (270°, 0°). Moreover, these two unique orientations are polar opposites, corresponding to the object lying on its left or right side as exemplified in figure 8(a). This evaluation of the optimal orientation is also consistent with previous assessments of the same geometry [9, 11, 16].

Another orientation achieving a low cost is the upright position which is achieved for any value of α when β is 90° or 270°. This constitutes two edges in the solution space with identical solutions. These orientations correspond to the front or the back facing upwards which aligns the largest cylinder with the build direction as displayed in figure 8(b). Note that the up-facing and down-facing surfaces are not differentiated by the objective function. Incorporating this behavior would yield different results where repetition of the solution space is avoided.

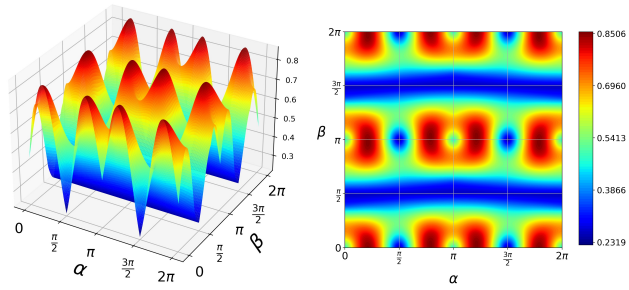

(a) 3D-graph for case 1 (b) Contour for case 1

Fig. 5: Solution space for case 1 based on equation 19.

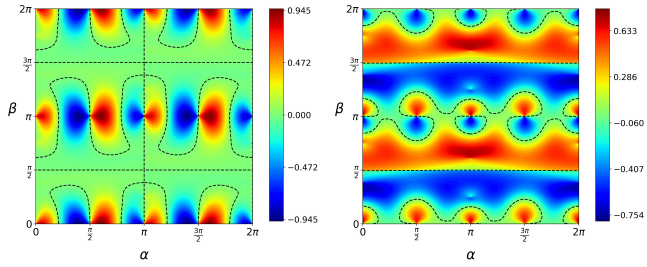

(a) Contour for $\frac{\partial}{\partial \alpha}$ (b) Contour for $\frac{\partial}{\partial \beta}$

Fig. 6: Graphs displaying the partial derivatives of equation 19.

Tab. 4: Evaluation of critical points for case 1. Lower value indicates higher accuracy. Lowest value in bold.

$(0° \leq \alpha < 45°)$		$(45° \leq \alpha < 180°)$		$(180° \leq \alpha < 225°)$		$(225° \leq \alpha < 360°)$	
Orientation	**Cost**	**Orientation**	**Cost**	**Orientation**	**Cost**	**Orientation**	**Cost**
(0, 0)	0.46	(87, 40)	0.53	(180, 0)	0.46	(267, 140)	0.53
(0, 28)	0.71	(87, 220)	0.53	(180, 28)	0.69	(267, 320)	0.53
(0, 90)	0.26	**(90, 0)**	**0.23**	(180, 90)	0.26	**(270, 0)**	**0.23**
(0, 152)	0.69	(90, 90)	0.26	(180, 152)	0.71	(270, 90)	0.26
(0, 180)	0.46	**(90, 180)**	**0.23**	(180, 180)	0.46	**(270, 180)**	**0.23**
(0, 208)	0.71	(90, 270)	0.26	(180, 208)	0.69	(270, 270)	0.26
(0, 270)	0.26	(93, 140)	0.53	(180, 270)	0.26	(273, 40)	0.53
(0, 332)	0.69	(93, 320)	0.53	(180, 332)	0.71	(273, 220	0.53
(38, 176)	0.85	(142, 4)	0.85	(218, 4)	0.85	(322, 176)	0.85
(38, 356)	0.85	(142, 184)	0.85	(218, 184)	0.85	(322, 356)	0.85

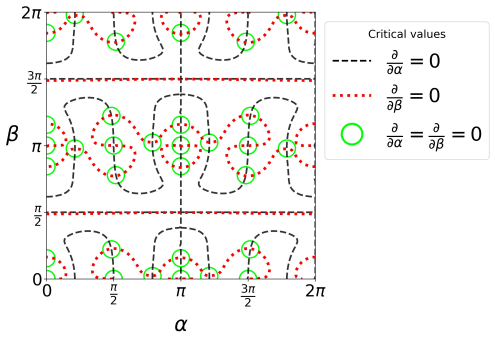

Fig. 7: Contour lines for the partial derivatives of equation 19.

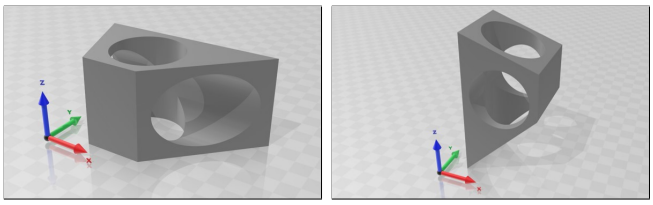

(a) Identified optimum (90°, 0°)

(b) Second-best orientation (0°, 90°)

Fig. 8: Optimal orientations identified for case 1.

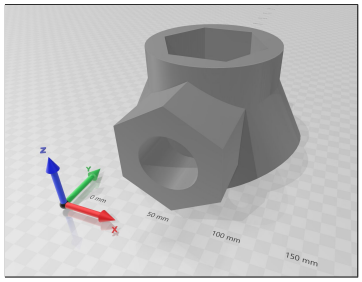

Fig. 9: The joint designed for case 2.

4.3 Case 2: Example with more complex geometry

The second case is an original design created for the sole purpose of demonstrating the applicability of the proposed method on a slightly more complex geometry. The part displayed in figure 9 is a joint with connectors in various directions. 44 features may be identified where 15 are cylindrical, and the remaining 29 are planes. A numeric description of the geometry is presented in table 5.

Using the functions for planes and cylinders from equations 15 and 17 populated with the data of table 5, the solution space of figure 10 is obtained. Because many features share orientation vectors, the overall objective function can be simplified to contain a minimal number of terms:

$$
\begin{aligned}
P_{Quality}(\alpha,\beta) = {} & 0.18\sqrt{\cos^2(\beta)}\sin^2(\beta) \\
& + 0.09\sqrt{1-\cos^2(\alpha)\cos^2(\beta)} \\
& + 0.09\sqrt{1-\sin^2(\alpha)\cos^2(\beta)} \\
& + 0.25\sqrt{1-\sin^2(\alpha)\cos^2(\beta)}\sin^2(\alpha)\cos^2(\beta) \\
& + 0.10\sqrt{1-\cos^2(\alpha)\cos^2(\beta)}\cos^2(\alpha)\cos^2(\beta) \\
& + 0.13\sqrt{1-0.8(\sin(\beta)-0.5\cos(\alpha)\cos(\beta))^2} \\
& + 0.12\sqrt{1-0.8(\sin(\beta)+0.5\cos(\alpha)\cos(\beta))^2} \\
& + 0.14\sqrt{1-0.8(\sin(\beta)-0.5\cos(\alpha)\cos(\beta))^2}(\sin(\beta)-0.5\cos(\alpha)\cos(\beta))^2 \\
& + 0.05\sqrt{1-0.8(\sin(\beta)+0.5\cos(\alpha)\cos(\beta))^2}(\sin(\beta)+0.5\cos(\alpha)\cos(\beta))^2 \\
& + 0.14\sqrt{1-0.8(\sin(\beta)+0.5\cos(\alpha)\cos(\beta))^2}(\sin(\beta)+0.5\cos(\alpha)\cos(\beta))^2 \\
& + 0.03\sqrt{1-0.75(0.58\sin(\alpha)\cos(\beta)-\sin(\beta))^2}(0.58\sin(\alpha)\cos(\beta)-\sin(\beta))^2 \\
& + 0.06\sqrt{1-0.75(0.58\sin(\alpha)\cos(\beta)+\sin(\beta))^2}(0.58\sin(\alpha)\cos(\beta)+\sin(\beta))^2 \\
& + 0.05\sqrt{1-0.8(-\sin(\beta)+0.5\cos(\alpha)\cos(\beta))^2}(\sin(\beta)-0.5\cos(\alpha)\cos(\beta))^2 \\
& + 0.06\sqrt{1-0.75(0.58\sin(\beta)-\cos(\alpha)\cos(\beta))^2}(0.58\sin(\beta)-\cos(\alpha)\cos(\beta))^2 \\
& + 0.12\sqrt{1-0.75(0.58\sin(\beta)+\cos(\alpha)\cos(\beta))^2}(0.58\sin(\beta)+\cos(\alpha)\cos(\beta))^2 \\
& + 0.03\sqrt{1-0.75(-0.58\sin(\alpha)\cos(\beta)+\sin(\beta))^2}(0.58\sin(\alpha)\cos(\beta)-\sin(\beta))^2 \\
& + 0.06\sqrt{1-0.75(-0.58\sin(\beta)+\cos(\alpha)\cos(\beta))^2}(0.58\sin(\beta)-\cos(\alpha)\cos(\beta))^2
\end{aligned}
\tag{20}
$$

The solution space for the second case is also quite regular as demonstrated in figure 11 where the partial derivatives of equation 20 are displayed. The regularity of these plots reflects the redundancy in the domain $\alpha, \beta \in [0, 2\pi]$.

Tab. 5: Numeric description of features for sample part 2.

		Position			Orientation			Area	
#	Type	P_x	P_y	P_z	E_x	E_y	E_z	(mm^2)	(%)
1	Plane	32.14	0.00	-64.83	0.89	0.00	-0.45	6 176	6.26
2	Plane	-32.14	0.00	-64.83	-0.89	0.00	-0.45	6 176	6.26
3	Plane	0.00	0.00	25.00	0.00	0.00	1.00	3 697	3.75
4	Plane	0.00	84.64	-25.00	0.00	1.00	0.00	2 900	2.94
5	Plane	0.00	-84.64	-25.00	0.00	-1.00	0.00	2 900	2.94
6	Plane	15.56	0.00	-17.22	-0.89	0.00	0.45	2 324	2.35
7	Plane	-15.56	0.00	-17.22	0.89	0.00	0.45	2 324	2.35
8	Plane	0.00	34.64	2.41	0.00	-1.00	0.00	1 800	1.82
9	Plane	0.00	-34.64	2.41	0.00	1.00	0.00	1 800	1.82
10	Plane	34.64	62.85	-24.18	1.00	0.00	0.00	1 735	1.76
11	Plane	34.64	-62.85	-24.18	1.00	0.00	0.00	1 735	1.76
12	Plane	-34.64	62.85	-24.18	-1.00	0.00	0.00	1 735	1.76
13	Plane	-34.64	-62.85	-24.18	-1.00	0.00	0.00	1 735	1.76
14	Plane	18.32	64.93	4.43	0.50	0.00	0.87	1 560	1.58
15	Plane	18.32	-64.93	4.43	0.50	0.00	0.87	1 560	1.58
16	Plane	-18.32	64.93	4.43	-0.50	0.00	0.87	1 560	1.58
17	Plane	-18.32	-64.93	4.43	-0.50	0.00	0.87	1 560	1.58
18	Plane	17.43	66.74	-54.94	0.50	0.00	-0.87	1 430	1.45
19	Plane	17.43	-66.74	-54.94	0.50	0.00	-0.87	1 430	1.45
20	Plane	-17.43	66.74	-54.94	-0.50	0.00	-0.87	1 430	1.45
21	Plane	-17.43	-66.74	-54.94	-0.50	0.00	-0.87	1 430	1.45
22	Plane	29.52	18.15	7.38	-0.87	-0.50	0.00	1 400	1.42
23	Plane	29.52	-18.15	7.38	-0.87	0.50	0.00	1 400	1.42
24	Plane	-29.52	18.15	7.38	0.87	-0.50	0.00	1 400	1.42
25	Plane	-29.52	-18.15	7.38	0.87	0.50	0.00	1 400	1.42
26	Plane	14.47	24.49	-28.94	0.89	0.00	-0.45	314	0.32
27	Plane	14.47	-24.49	-28.94	0.89	0.00	-0.45	314	0.32
28	Plane	-14.47	24.49	-28.94	-0.89	0.00	-0.45	314	0.32
29	Plane	-14.47	-24.49	-28.94	-0.89	0.00	-0.45	314	0.32
30	Cylinder	0.00	0.00	-7.68	0.00	0.00	1.00	7 590	7.69
31	Cylinder	0.00	0.00	-25.00	-0.89	0.00	-0.45	6 804	6.89
32	Cylinder	0.00	0.00	-25.00	0.89	0.00	-0.45	6 804	6.89
33	Cylinder	0.00	50.00	-25.00	0.00	1.00	0.00	4 518	4.58
34	Cylinder	0.00	-50.00	-25.00	0.00	-1.00	0.00	4 518	4.58
35	Cylinder	14.47	24.49	-28.94	0.89	0.00	-0.45	2 513	2.55
36	Cylinder	14.47	-24.49	-28.94	0.89	0.00	-0.45	2 513	2.55
37	Cylinder	-14.47	24.49	-28.94	-0.89	0.00	-0.45	2 513	2.55
38	Cylinder	-14.47	-24.49	-28.94	-0.89	0.00	-0.45	2 513	2.55
39	Cylinder	0.00	0.00	-25.00	0.00	0.00	1.00	449	0.45
40	Cylinder	0.00	0.00	-25.00	0.00	0.00	1.00	449	0.45
41	Cylinder	0.00	0.00	-25.00	-0.89	0.00	-0.45	411	0.42
42	Cylinder	0.00	0.00	-25.00	-0.89	0.00	-0.45	411	0.42
43	Cylinder	0.00	0.00	-25.00	0.89	0.00	-0.45	411	0.42
44	Cylinder	0.00	0.00	-25.00	0.89	0.00	-0.45	411	0.42

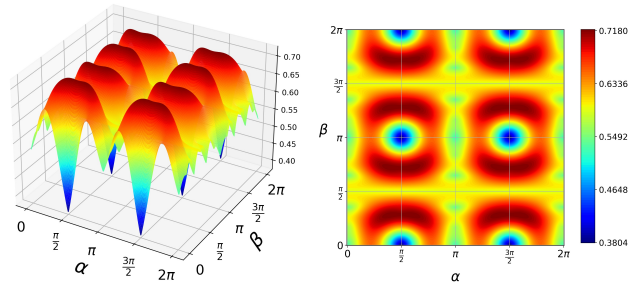

(a) 3D-graph for case 2 (b) Contour for case 2

Fig. 10: Solution space for case 2 based on equation 20.

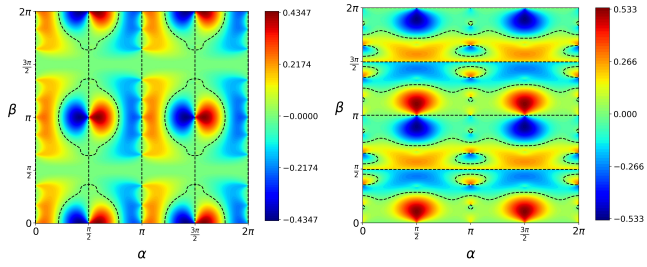

(a) Contour for $\frac{\partial}{\partial \alpha}$ (b) Contour for $\frac{\partial}{\partial \beta}$

Fig. 11: Graphs displaying the partial derivatives of equation 20.

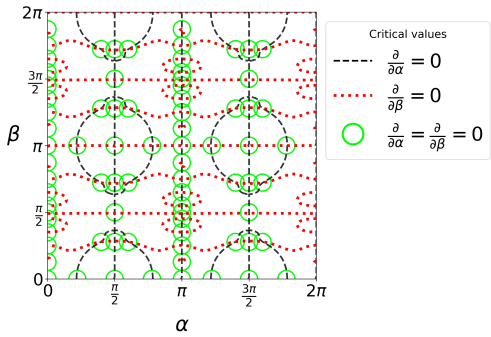

Fig. 12: Contour lines for the partial derivatives of equation 20.

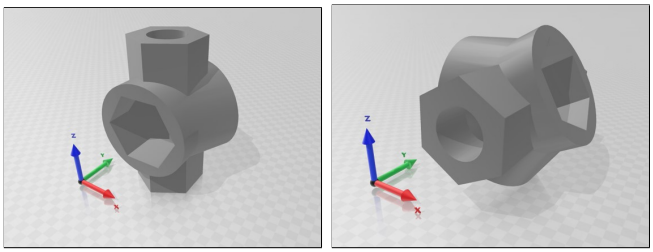

(a) Identified optimum (90°, 0°)

(b) Alternative orientation (0°, 63°)

Fig. 13: Optimal orientations identified for case 2.

As demonstrated in case 1, the critical points are found where both partial derivatives are either zero or undefined, which corresponds to the intersections of red and black lines in figure 12. All critical points are tabulated in table 6 where the minima are highlighted in bold text.

For the second case study, the optimal orientation is achieved by 90° rotation about the x-axis as displayed in figure 13(a). The same cost is also observed for three other combinations of rotations as displayed in table 6. Due to redundancy in the solution space, these four combinations of rotations only correspond to two unique orientations in exactly opposite directions. With the hexagonal protrusions oriented parallel to the build direction, 25 out of the 29 planes are in a favorable orientation, while only two of the 15 cylinders are vertical.

Clearly, the large number of planes favors the orientation at (90°, 0°). However, if cylinders are given a higher priority than planes, this orientation may no longer be as favorable. Figure 14 compares the effect of assigning a weight factor to cylindrical features for three orientations. A point of intersection is identified at a weight factor of 3.4, where the orientation (0°, 63°) becomes more favorable than the previous best at (90°, 0°) (see figure 13(b)). This analysis indicates that for this part, cylinders should be at least 3.4 times as important relative to planes before the orientation at (0°, 63°) is selected.

Tab. 6: Evaluation of critical points for case 2. Lower value indicates higher accuracy. Lowest values highlighted in bold.

$(\alpha = 0°)$		$(0° < \alpha < 180°)$		$(\alpha = 180°)$		$(180° < \alpha < 360°)$	
Orientation	**Cost**	**Orientation**	**Cost**	**Orientation**	**Cost**	**Orientation**	**Cost**
(0, 0)	0.53	(40, 0)	0.65	(180, 0)	0.53	(220, 0)	0.65
(0, 23)	0.57	(40, 180)	0.65	(180, 23)	0.57	(220, 180)	0.65
(0, 45)	0.60	(72, 50)	0.72	(180, 45)	0.60	(252, 50)	0.72
(0, 63)	0.54	(72, 130)	0.72	(180, 63)	0.54	(252, 130)	0.72
(0, 81)	0.60	(72, 230)	0.72	(180, 81)	0.60	(252, 230)	0.72
(0, 90)	0.59	(72, 310)	0.72	(180, 90)	0.59	(252, 310)	0.72
(0, 99)	0.60	**(90, 0)**	**0.37**	(180, 99)	0.60	**(270, 0)**	**0.37**
(0, 117)	0.54	(90, 50)	0.72	(180, 117)	0.54	(270, 50)	0.72
(0, 135)	0.60	(90, 90)	0.59	(180, 135)	0.60	(270, 90)	0.59
(0, 157)	0.57	(90, 130)	0.72	(180, 157)	0.57	(270, 130)	0.72
(0, 180)	0.53	**(90, 180**	**0.37**	(180, 180)	0.53	**(270, 180**	**0.37**
(0, 203)	0.57	(90, 230)	0.72	(180, 203)	0.57	(270, 230)	0.72
(0, 225)	0.60	(90, 270)	0.59	(180, 225)	0.60	(270, 270)	0.59
(0, 243)	0.54	(90, 310)	0.72	(180, 243)	0.54	(270, 310)	0.72
(0, 261)	0.60	(108, 50)	0.72	(180, 261)	0.60	(288, 50)	0.72
(0, 270)	0.59	(108, 130)	0.72	(180, 270)	0.59	(288, 130)	0.72
(0, 279)	0.60	(108, 230)	0.72	(180, 279)	0.60	(288, 230)	0.72
(0, 297)	0.54	(108, 310)	0.72	(180, 297)	0.54	(288, 310)	0.72
(0, 315)	0.60	(140, 0)	0.65	(180, 315)	0.60	(320, 0)	0.65
(0, 337)	0.57	(140, 180)	0.65	(180, 337)	0.57	(320, 180)	0.65

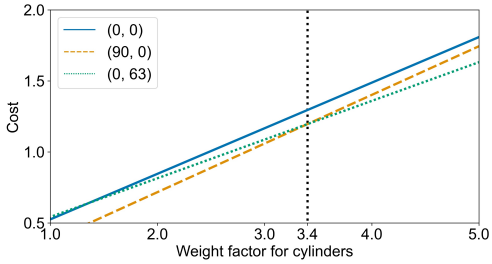

Fig. 14: Comparison of three orientations for case part 2 when an additional weight factor is introduced for cylinders.

Both case studies exhibit repetitive symmetric patterns in the evaluation table. This symmetry arises from two sources: (i) as stated in section 2.2, the domain of β can be constrained to $[0, \pi)$ as rotations exceeding this range will only repeat previous solutions, and (ii) the objective function of these case studies takes no regard of the difference between up-facing and down-facing surfaces. One may also question the alignment of many critical points with right-angle orientations. This is however a result of the initial orientation of the part which originates from the design phase. If the initial orientation was different, the patterns observed in the plots would change due to the projection but the solution space would remain unaltered.

A more complex geometry with more features would yield a solution space with more local extremes where the complexity of the solution space reflects the complexity of the geometry. Naturally, the objective functions for each surface type also contribute towards the topology of the solution space. Consequently, different objective functions, e.g. those obtained through experiments, would give different results to those reported above.

5 Discussion

A mathematical description of the solution space provides a range of possibilities for finding the optimal orientation. What approach is best suited to solve the optimization problem depends on the purpose of the optimization as well as the complexity of the part. As the geometry becomes more complex, function evaluations are increasingly expensive. Hence, complex geometries may benefit from intelligent methods where an effort is made to accelerate the computations. The simplicity of an exhaustive search may have certain advantages for simple geometries but may be ineffective for complex geometries.

The continuous solution space facilitates gradient-based methods as a qualified decision can be made concerning the next iteration of the search sequence. However, unless all critical points are investigated, the risk of getting stuck in local optima is ever-present. A stochastic component or a larger population of solutions may counter this problem, as is typically the case of evolutionary algorithms.

When the solution space is clearly defined, it is possible to identify feasible regions in line with previous works [25, 18]. These regions are defined from requirements and represent ranges of feasible orientations where tolerance requirements are met. Consequently, these regions can make up the boundaries for subsequent optimizations, e.g. with respect to mechanical properties. Adding steps to the optimization process will inevitably complicate and prolong the process, but interactive methods may be useful when the objectives are fuzzy or when flexibility is required.

Practical implementations of the proposed method would entail the formulation of objective functions for all relevant surface types. The relevant types and their definition may differ as long as they can be formulated as orientation vectors with accompanying objective functions. Furthermore, a solution for obtaining information on the orientation of the surfaces is required to automate the optimization process. An alternative implementation enables the identification of feasible regions for subsequent optimization. This would imply the integration of the method in a larger system with capabilities beyond what can be expressed by surfaces and their orientations.

The proposed optimization method has the benefit of being stable (i.e. no stochastic components), has no limitations with regards to search grid resolution, and provides the flexibility to incorporate separate expressions for each feature. Moreover, by considering the features of the part rather than every facet of a tessellated file, the effect of build direction may be generalized for each surface type. This drastically reduces the number of function evaluations. The feature-based approach also enables feature dimensions to be included in the objective function which may affect the outcome.

The proposed method is not applicable to free-form surfaces due to the inability to formulate proper objective functions to handle the unknown. At present, this is not an issue for assembly features. However, as the potential of AM is unlocked, more complex surfaces may become widely used in industrial design. The development of flexible formulations to handle this challenge is left for future work, along with the appropriate parametrization of such surfaces.

6 Conclusions and outlook

The approach described in this paper provides the mathematical foundations for both deterministic and stochastic solutions to the orientation problem. By describing the solution space as a continuous function in a closed domain, the optimization can be performed mathematically. More importantly, this approach enables the determination of feasible orientation zones for the optimization of secondary objectives. Under the assumption that quality can be described as a function of build direction, the proposed method can be populated with any mathematical description of the relationship between quality and part build orientation.

The development of accurate mathematical models is crucial for optimization in process planning. AM technologies comprise many different processes that require separate models for predicting final part properties. Future research entails developing and validating prediction models that can be utilized in optimization processes. Practical implementation in a system with capabilities beyond the described method constitutes an interesting avenue for future research. Furthermore, the integration of all processing stages into a digital pipeline – from design and process planning to quality assessment and verification – will enable traceability throughout the manufacturing system, and ultimately the entire product life cycle.

Acknowledgment: The authors appreciate the support from colleagues at the Department of Manufacturing and Civil Engineering.

Funding: This research is funded by the Norwegian Ministry of Research and Education through the PhD-grant of Torbjørn Langedahl Leirmo.

Conflict of Interest: The authors declare no competing interests.

References

1. Gibson I, Rosen D, Stucker B, and Khorasani M. Additive Manufacturing Technologies. 3rd ed. Cham: Springer Nature Switzerland AG, 2021. DOI: https://doi.org/10.1007/978-3-030-56127-7
2. Dantan JY, Huang Z, Goka E, Homri L, Etienne A, Bonnet N, and Rivette M. Geometrical variations management for additive manufactured product. CIRP Annals 2017; 66:161–4. DOI: https://doi.org/10.1016/j.cirp.2017.04.034. Available from: http://www.sciencedirect.com/science/article/pii/S0007850617300343
3. Thompson MK, Moroni G, Vaneker T, Fadel G, Campbell RI, Gibson I, Bernard A, Schulz J, Graf P, Ahuja B, and Martina F. Design for Additive Manufacturing: Trends, opportunities, considerations, and constraints. CIRP Annals 2016; 65:737–60. DOI: https://doi.org/10.1016/j.cirp.2016.05.004. Available from: http://www.sciencedirect.com/science/article/pii/S0007850616301913
4. Dolenc A and Mäkelä I. Slicing procedures for layered manufacturing techniques. Computer-Aided Design 1994; 26:119–26. DOI: https://doi.org/10.1016/0010-4485(94)90032-9. Available from: https://www.sciencedirect.com/science/article/pii/0010448594900329
5. Alexander P, Allen S, and Dutta D. Part orientation and build cost determination in layered manufacturing. Computer-Aided Design 1998; 30:343–56. DOI: https://dx.doi.org/10.1016/S0010-4485(97)00083-3. Available from: http://www.sciencedirect.com/science/article/pii/S0010448597000833
6. Masood SH, Rattanawong W, and Iovenitti P. Part Build Orientations Based on Volumetric Error in Fused Deposition Modelling. The International Journal of Advanced Manufacturing Technology 2000; 16:162–8. DOI: https://doi.org/10.1007/s001700050022. Available from: https://doi.org/10.1007/s001700050022
7. Di Angelo L, Di Stefano P, and Guardiani E. Search for the Optimal Build Direction in Additive Manufacturing Technologies: A Review. Journal of Manufacturing and Materials Processing 2020; 4:71. DOI: https://doi.org/10.3390/jmmp4030071. Available from: https://www.mdpi.com/2504-4494/4/3/71
8. Qin Y, Qi Q, Shi P, Scott PJ, and Jiang X. Status, issues, and future of computer-aided part orientation for additive manufacturing. The International Journal of Advanced Manufacturing Technology 2021 May. DOI: 10.1007/s00170-021-06996-6
9. Cheng W, Fuh JYH, Nee AYC, Wong YS, Loh HT, and Miyazawa T. Multi-objective optimization of part-building orientation in stereolithography. Rapid Prototyping Journal 1995; 1:12–23. DOI: https://doi.org/10.1108/13552549510104429

10. Masood SH, Rattanawong W, and Iovenitti P. A generic algorithm for a best part orientation system for complex parts in rapid prototyping. Journal of Materials Processing Technology 2003; 139:110–6. DOI: https://doi.org/10.1016/S0924-0136(03)00190-0. Available from: http://www.sciencedirect.com/science/article/pii/S0924013603001900
11. Byun HS and Lee KH. Determination of the optimal build direction for different rapid prototyping processes using multi-criterion decision making. Robotics and Computer-Integrated Manufacturing 2006; 22:69–80. DOI: https://doi.org/10.1016/j.rcim.2005.03.001. Available from: http://www.sciencedirect.com/science/article/pii/S0736584505000232
12. Padhye N and Deb K. Multi-objective optimisation and multi-criteria decision making in SLS using evolutionary approaches. Rapid Prototyping Journal 2011; 17:458–78. DOI: https://doi.org/10.1108/13552541111184198. Available from: http://www.emeraldinsight.com/doi/abs/10.1108/13552541111184198
13. Zhang J and Li Y. A unit sphere discretization and search approach to optimize building direction with minimized volumetric error for rapid prototyping. The International Journal of Advanced Manufacturing Technology 2013; 67:733–43. DOI: https://doi.org/10.1007/s00170-012-4518-0. Available from: http://dx.doi.org/10.1007/s00170-012-4518-0
14. Li Y and Zhang J. Multi-criteria GA-based Pareto optimization of building direction for rapid prototyping. The International Journal of Advanced Manufacturing Technology 2013; 69:1819–31. DOI: https://doi.org/10.1007/s00170-013-5147-y. Available from: http://dx.doi.org/10.1007/s00170-013-5147-y
15. Das P, Chandran R, Samant R, and Anand S. Optimum Part Build Orientation in Additive Manufacturing for Minimizing Part Errors and Support Structures. Procedia Manufacturing 2015; 1:343–54. DOI: https://doi.org/10.1016/j.promfg.2015.09.041. Available from: http://www.sciencedirect.com/science/article/pii/S2351978915010410
16. Zhang Y, Bernard A, Gupta RK, and Harik R. Feature based building orientation optimization for additive manufacturing. Rapid Prototyping Journal 2016; 22:358–76. DOI: https://doi.org/10.1108/rpj-03-2014-0037
17. Das P, Mhapsekar K, Chowdhury S, Samant R, and Anand S. Selection of build orientation for optimal support structures and minimum part errors in additive manufacturing. Computer-Aided Design and Applications 2017. DOI: https://doi.org/10.1080/16864360.2017.1308074. Available from: https://doi.org/10.1080/16864360.2017.1308074
18. Budinoff H and McMains S. Prediction and visualization of achievable orientation tolerances for additive manufacturing. Procedia CIRP 2018; 75:81–6. DOI: https://doi.org/10.1016/j.procir.2018.03.315. Available from: http://www.sciencedirect.com/science/article/pii/S2212827118304967
19. Chowdhury S, Mhapsekar K, and Anand S. Part Build Orientation Optimization and Neural Network-Based Geometry Compensation for Additive Manufacturing Process. English. Journal of Manufacturing Science and Engineering 2018; 140. DOI: https://doi.org/10.1115/1.4038293
20. Zhang Y, Harik R, Fadel G, and Bernard A. A statistical method for build orientation determination in additive manufacturing. Rapid Prototyping Journal 2019; 25:187–207. DOI: https://doi.org/10.1108/RPJ-04-2018-0102. Available from: https://doi.org/10.1108/RPJ-04-2018-0102
21. Qin Y, Qi Q, Shi P, Scott PJ, and Jiang X. Automatic determination of part build orientation for laser powder bed fusion. Virtual and Physical Prototyping 2021; 16:29–49. DOI: 10.1080/17452759.2020.1832793. Available from: https://doi.org/10.1080/17452759.2020.1832793
22. Qin Y, Qi Q, Shi P, Scott PJ, and Jiang X. Automatic generation of alternative build orientations for laser powder bed fusion based on facet clustering. Virtual and Physical Prototyping 2020; 15:307–24. DOI: 10.1080/17452759.2020.1756086. Available from: https://doi.org/10.1080/17452759.2020.1756086
23. Paul R and Anand S. Optimal part orientation in Rapid Manufacturing process for achieving geometric tolerances. Journal of Manufacturing Systems 2011; 30:214–22. DOI: https://doi.org/10.1016/j.jmsy.2011.07.010. Available from: http://www.sciencedirect.com/science/article/pii/S0278612511000665
24. Paul R and Anand S. Optimization of layered manufacturing process for reducing form errors with minimal support structures. Journal of Manufacturing Systems 2015; 36:231–43. DOI: https://dx.doi.org/10.1016/j.jmsy.2014.06.014. Available from: http://www.sciencedirect.com/science/article/pii/S0278612514000806
25. Arni R and Gupta SK. Manufacturability analysis of flatness tolerances in solid freeform fabrication. Journal of Mechanical Design 2001; 123:148–56. DOI: https://doi.org/10.1115/1.1326439
26. Byun HS and Lee KH. Determination of optimal build direction in rapid prototyping with variable slicing. The International Journal of Advanced Manufacturing Technology 2006; 28:307–13. DOI: https://doi.org/10.1007/s00170-004-2355-5. Available from: https://doi.org/10.1007/s00170-004-2355-5
27. Bacchewar PB, Singhal SK, and Pandey PM. Statistical modelling and optimization of surface roughness in the selective laser sintering process. Proceedings of the Institution of Mechanical Engineers, Part B: Journal of Engineering Manufacture 2007; 221:35–52. DOI: 10.1243/09544054jem670. Available from: http://journals.sagepub.com/doi/abs/10.1243/09544054JEM670
28. Chen Y and Lu J. RP part surface quality versus build orientation: when the layers are getting thinner. The International Journal of Advanced Manufacturing Technology 2013; 67:377–85. DOI: https://doi.org/10.1007/s00170-012-4491-7. Available from: https://doi.org/10.1007/s00170-012-4491-7

29. Sunil VB and Pande SS. Automatic recognition of features from freeform surface CAD models. Computer-Aided Design 2008; 40:502–17. DOI: https://doi.org/10.1016/j.cad.2008.01.006. Available from: http://www.sciencedirect.com/science/article/pii/S0010448508000195
30. Moroni G, Syam WP, and Petrò S. Towards Early Estimation of Part Accuracy in Additive Manufacturing. Procedia CIRP 2014; 21:300–5. DOI: https://doi.org/10.1016/j.procir.2014.03.194. Available from: http://www.sciencedirect.com/science/article/pii/S2212827114007604
31. Leirmo TL, Semeniuta O, Baturynska I, and Martinsen K. Extracting shape features from a surface mesh using geometric reasoning. Procedia CIRP 2020; 93:544–9. DOI: https://doi.org/10.1016/j.procir.2020.02.142. Available from: http://www.sciencedirect.com/science/article/pii/S2212827120306788
32. Frank D and Fadel G. Expert system-based selection of the preferred direction of build for rapid prototyping processes. Journal of Intelligent Manufacturing 1995; 6:339–45. DOI: https://doi.org/10.1007/bf00124677. Available from: http://dx.doi.org/10.1007/BF00124677